A new painkiller nanomedicine to by-pass the blood-brain-barrier and the use of morphine

Jiao Feng

université PARIS-SACLAY

NNT : 2018SACLS502

Thèse de doctorat

Développement de nanomédicaments innovants pour vaincre la douleur: une alternative à la morphine

Thèse de doctorat de l'Université Paris-Saclay
Préparée à l'Université Paris-Sud

École doctorale n°569 Innovation Thérapeutique, du fondamental à l'appliqué (ITFA)
Spécialité de doctorat: Pharmacotechnie et Biopharmacie

Thèse présentée et soutenue à Châtenay-Malabry, 14/12/2018, par

Jiao FENG

Composition du Jury:

Elias FATTAL Professeur, Université Paris-Sud	Président
Maria-José BLANCO PRIETO Professeur, Universidad de Navarra	Rapporteur
Juergen SIEPMANN Professeur, Université de Lille	Rapporteur
Philippe KAROYAN Professeur, Université Pierre-et-Marie-Curie	Examinateur
Michel HAMON Professeur, Université Paris Descartes	Examinateur
Patrick COUVREUR Professeur, Université Paris-Sud	Directeur de thèse
Sinda LEPETRE-MOUELHI Maître de Conférences, Université Paris-Sud	Co-Directeur de thèse

DÉVELOPPEMENT DE NANOÉDICAMENTS INNOVANTS POUR VAINCRE LA DOULEUR: UNE ALTERNATIVE À LA MORPHINE

A NEW PAINKILLER NANOMEDICINE TO BYPASS THE BLOOD-BRAIN-BARRIER AND THE USE OF MORPHINE

Thèse de doctorat de l'Université Paris-Saclay

Préparée à l'Université Paris-Sud

École doctorale n°569 Innovation Thérapeutique, du fondamental à l'appliqué (ITFA)

Spécialité de doctorat: Pharmacotechnie et Biopharmacie

Thèse présentée et soutenue à Châtenay-Malabry, 14/12/2018, par

Jiao FENG

Composition du Jury:

Elias FATTAL Professeur, Université Paris-Sud	Président
Maria-José BLANCO PRIETO Professeur, Universidad de Navarra	Rapporteur
Juergen SIEPMANN Professeur, Université de Lille	Rapporteur
Philippe KAROYAN Professeur, Université Pierre-et-Marie-Curie	Examinateur
Michel HAMON Professeur, Université Paris Descartes	Examinateur
Patrick COUVREUR Professeur, Université Paris-Sud	Directeur de thèse
Sinda LEPETRE-MOUELHI Maître de Conférences, Université Paris-Sud	Co-Directeur de thèse

Acknowledgements

I warmly thank Pr. Patrick COUVREUR, my teacher and my supervisor, who have given me the chance to work on this PhD project under his supervision. Many thanks for his kindness in the team and the scientific discussions throughout this thesis work.

I would also like to express my deep gratitude to Dr. Sinda LEPETRE for her enthusiasm, her rigor and her supervision during these years of thesis. Thanks for her great availability and her scientific and managerial skills and her kind helps with my life.

I am also grateful to Pr. Michel HAMON and Dr. Anne GAUTIER who helped me so much with the *in vivo* pharmacological study. I also want to thank Dr. Simona MURA for her kind helps about all the biological studies; our discussions and her enthusiasm were always motivating.

I thank all the other members of the laboratory Institut Galien. Extra thanks go to Dr. Catherine CAILLAUD and Dr. VARNA-PANNEREC Mariana for their professional support in the biodistribution and toxicity studies.

Ms. Julie Mougin (UMR 8612) and Mrs. Ghislaine Frébourg (Electron Microscopy Facility/FR 3631-CNRS-UPMC) are acknowledged for their contribution to Cryo-TEM. Ms. Camille Dejean (BioCIS: Châtenay-Malabry) is acknowledged for help with the NMR interpretations.

Special thanks to my family for their constant support and encouragement; without them it would not have been possible. Thanks to my friends who always stood by my side.

Part of this work was supported by the RBUCE-UP grant agreement (#00001002483/78) between the ERC and Université Paris-Sud, by the ERC under the Framework Program FP7/2007–2013 (Grant Agreement N°249835) and by the Centre National de la Recherche Scientifique. The author acknowledges the financial support from China Scholarship Council (CSC).

Table of contents

Abbreviations

ACE	Angiotensin converting enzymes
ACN	Acetonitrile
AcOEt	Ethyl acetate
ACs	Adenylyl cyclases
Ad-SQ	Adenosine-squalene
ALT	Alanine transaminase
AOA	Acyloxyalkoxy
APN	Aminopeptidase N
AST	Aspartate transaminase
ATP	Adenosine triphosphate
AUC	Area under the curve
BBB	Blood-brain-barriers
BDNF	Brain-derived neurotropic factor
BNB	Blood-nerve-barriers
BSCB	Blood-spinal cord barrier
CA	Coumarinic acid
CAs	Contrast agents
cAMP	Cyclic adenosine monophosphate
CED	Convection-enhanced delivery
CNS	Central nervous system
CRF	Corticotropin-releasing factor
cryo-TEM	Cryogenic transmission electron microscopy
CXCL2/3	Chemokines
DADLE	[D-Ala^2, D-Leu^5]-Enkephalin
DALA	[D-Ala^2]-Met-enkephalin amide
DCC	Dicyclohexylcarbodiimide
dCK	Deoxycytidine kinase
DCM	Dichloromethane
ddA-TP	Dideoxyadenosine triphosphate
ddC	2′,3′-Dideoxycytidine
ddC-SQ	2′,3′-Dideoxycytidine-squalene
ddC-SQ-MP	2′,3′-Dideoxycytidine-squalene monophosphate
ddI	2′,3′-Dideoxyinosine
ddI-SQ	2′,3′-Dideoxyinosine-squalene
DMF	Dimethylformamide
DLS	Dynamic light scattering
DHA	Docosahexaenoic acid
DMAP	4-Dimethylaminopyridine
DOTA	1,4,7,10-Tetrakis(carboxymethyl)-1,4,7,10-tetraazacyclododecane
DOX-SQ	Doxorubicin-squalene
DPP III	Dipeptidyl peptidase III
DRG	Dorsal root ganglion
EDCI	1-Ethyl-3-(3-dimethylaminopropyl)carbodiimide

EM	Endomorphin
EPR	Enhanced permeation and retention
EtOH	Ethanol
FFEM	Electron microscopy after freeze-fracture
Fpx	Fondaparinux
HPLC	High performance liquid chromatography
HSV-1	Herpes simplex virus 1
5-HT	5-Hydroxytryptamine
IASP	International Association for the Study of Pain
IR	Infrared
isoCA-4	Isocombretastatin A-4
GDP	Guanosine 5'-diphosphate
Gem-SQ	Gemcitabine-squalene
Gem-SQ-MP	Gemcitabine-squalene monophosphate
GI	Gastrointestinal
GPCR	G-protein-coupled receptors
GTP	Guanosine-5'-triphosphate
LDC	Lipid-drug conjugates
LDL	Low density lipoproteins
LENK	Leu-enkephalin
LENK-SQ	Leu-enkephalin-squalene
LENK-SQ-Diox	Leu-enkephalin-squalene with dioxycarbonyl linker
LENK-SQ-Dig	Leu-enkephalin-squalene with diglycolic linker
LENK-SQ-Am	Leu-enkephalin-squalene with amide linker
MCAo	Middle cerebral artery occlusion
MeOH	Methanol
MIC	Minimum inhibitory concentration
MRI	Magnetic resonance imaging
MPS	Mononuclear phagocyte system
MS	Mass spectrometry
MTC	Maximum tolerated concentration
MTD	Maximum tolerance doses
NA	Noradrenaline
Nal	Naloxone
Nal-M	Naloxone methiodide
NAs	Nanoassemblies
NDDS	Novel drug delivery system
NEP	Neutral endopeptidase
NHS	N-hydroxysuccinimide
NMR	Nuclear magnetic resonance
NO	Nitric oxide
N/OFQ	Nociceptin/orphanin FQ
NPs	Nanoparticles
NSAIDs	Nonsteroidal anti-inflammatory drugs
14-O-MeM6SU	14-O-methylmorphine-6-O-sulfate
ORL	Opioid receptor-like

OMCA	Oxymethyl-modified coumarinic acid
PBCA	Poly (butylcyanoacrylate)
PCa	Prostate cancer
PDI	polydispersity index
PEG	Polyethylene glycol
PG	Prostaglandins
PG-M	Hyperbranched polyglycerol
PNG	Penicillin G
PNG-SQ	Penicillin G-squalene
PNG-SQsens	Penicillin G-squalene with sensitive bond
PPA	Phenylpropionic acid
ProDyn	Pro-dynorphin
ProENK	Pro-enkephalin
POMC	Pro-opiomelanocortin
PTSA	p-Toluenesulfonic acid
PTX	Paclitaxel
PWL	paw withdrawal latency
RES	Reticuloendothelial system
SAXS	Small angle X-ray scattering
SQ	Squalene
TES	Triethylsilane
TEA	Triethylamine
THF	Tetrahydrofuran
7-TM receptors	7-Transmembrane receptors
TrKA	Tyrosine kinase receptor type 1
TRP channels	Transient receptor potential-generating channels
TRPV1	Transient receptor potential cation channel subfamily V member 1
T-SQ	Thymidine-squalene
USPIO	Ultrasmall superparamagnetic iron oxide particles
VLDL	Very low density lipoproteins
WAXS	Wide-angle X-ray scattering

List of figures

Introduction

Review article: Design, Preparation and Characterization of Modular Squalene-based Nanosystems for Controlled Drug Release

Research article: A new painkiller nanomedicine to bypass the blood-brain-barrier and the use of morphine

Supplementary experiments:

List of tables

General introduction

Pain management is a major public health issue, a criterion for the quality and evolution of the health system, producing a significant social and economic burden. Above all, it responds to humanistic, ethical purposes and human dignity aims, because of the physical and psychological implications. It induces a disability among patients and excludes them gradually or suddenly from society. Physical pain and emotional suffering experienced at all stages of life, weakens even more people made vulnerable by illness. Rebel chronic pain is source of disability, handicap, disability and major alterations in quality of life. Medical advances allowed the healing of many serious diseases, but also favored the transformation of acute into chronic diseases. This result is an increase in life expectancy which can be accompanied by chronic pain. Estimates suggest that 20% of adults suffer from pain globally and 10% are newly diagnosed with chronic pain each year (*1*). It was also reported that 30 to 50% of patients with chronic pain also struggle with mood disorders, such as depression and anxiety (*2, 3*). Relieving pain is now an essential priority based on medical ethics (*4*). Currently, the most powerful and frequently used drugs for killing pain are **morphine** and synthetic opioids which interact with opioid receptors, located in the CNS (central nervous system) and peripheral organs. However, their chronic use could be associated with serious drawbacks, such as respiratory depression, tolerance and dependence, addiction, constipation, sedation, etc.... Therefore, there is an important need for efficient drugs active on moderate pain that can fill the gap between the narcotic and non-narcotic drugs. In spite of recent progress in the development of new compounds, there is yet no marketed drug fulfilling these properties (*5*).

Endogenous neuropeptides such as Enkephalins, produce natural analgesia by activating opioid receptors located on central and peripheral neuronal cell membranes. They represent a promising way to alleviate the pain using natural analgesics devoid of morphine side effects. However, their fast enzymatic metabolism after injection and their inefficient permeability through the blood-brain-barriers (BBB) or blood-nerve-barriers (BNB) restrict their clinical use.

The aim of this project is to **develop novel nanomedicine approach allowing the specific delivery of Enkephalin neuropeptide into inflamed tissues for pain control, using "squalenoylation" concept**. It consists in the chemical linkage of enkephalin with squalene, **a biocompatible and biodegradable lipid**, in order to form amphiphilic prodrug which has the ability to self-assemble in water in nanoparticles of hundred nanometers of diameter. This nanoparticular formulation allow the enkephalins protection from rapid metabolism and thereby also enable them to reach safely opioid receptors.

The **introduction part** will first give general informations concerning **peripheral mechanisms of pain and analgesia**. Then, the **recent strategies** aiming at **optimizing the pharmacological profile of natural opioid peptides** will be presented. A particular attention will be accorded to the strategies allowing the **efficient delivery of opioid peptides to their site of action**. Finally, the new concept of **"squalenoylation"** will be presented as well as an overview of recent advances in the development of **squalene-based nanomedicines** and their application to promising drug candidates with unfavorable pharmacokinetics and biodistribution profiles.

The **main part** will first include the **synthesis** of **bioconjugates** of **Leu-enkephalin** (LENK) using squalenoylation approach. LENK neuropeptide will be coupled to squalene using **three different chemical linkers**, i.e., **dioxycarbonyl**, **diglycolate**, **amide bond**, and then **formulated** into **nanoparticles** (NPs). Their characterization and their ability to release *in vitro* the enkephalin will

also be adressed. A significant part of the research work will also be dedicated to the evaluation of **analgesic effect** of these LENK-SQ NPs on **carrageenan-induced pain model** using a **thermal nociception test** (Hargreaves). Pain sensitivity will be rated in response to a hot stimulus on the inflamed hind paw of rats. In addition, the **biodistribution** of NPs in mice using ***in vivo* fluorescence imaging** in order to assess their ability to target the inflamed tissue will be depicted.

Through this study, we describe here a new nano-formulation based on the bioconjugation of LENK to squalene, capable of precise and efficient delivery of LENK for pain control associated with inflammatory events.

Reference

1. D. S. Goldberg, S. J. McGee, Pain as a global public health priority. *BMC Public Health* **11**, 770 (2011).
2. A. Tsang, M. Von Korff, S. Lee, J. Alonso, E. Karam, M. C. Angermeyer, G. L. G. Borges, E. J. Bromet, G. de Girolamo, R. de Graaf, O. Gureje, J.-P. Lepine, J. M. Haro, D. Levinson, M. A. Oakley Browne, J. Posada-Villa, S. Seedat, M. Watanabe, Common Chronic Pain Conditions in Developed and Developing Countries: Gender and Age Differences and Comorbidity With Depression-Anxiety Disorders. *The Journal of Pain* **9**, 883-891 (2008).
3. D. A. Fishbain, M. Goldberg, B. Robert Meagher, R. Steele, H. Rosomoff, Male and female chronic pain patients categorized by DSM-III psychiatric diagnostic criteria. *Pain* **26**, 181-197 (1986).
4. A. Serrie, [Chronic pain management: societal impact]. *Bull Acad Natl Med* **199**, 555-565 (2015).
5. F. Noble, B. P. Roques, Protection of endogenous enkephalin catabolism as natural approach to novel analgesic and antidepressant drugs. *Expert Opinion on Therapeutic Targets* **11**, 145-159 (2007).

Introduction

I. GENERAL INFORMATION ON PAIN

"**Pain** is an unpleasant sensory and emotional experience associated with actual or potential tissue damage, or described in terms of such damage", as defined by the International Association for the Study of Pain (IASP). This highly disagreeable sensation results from an extraordinarily complex and interactive series of mechanisms integrated at all levels of the neuroaxis, from the periphery, via the dorsal horn to higher cerebral structures (*1, 2*).

Pain typically involves a **noxious stimulus** (e.g., cutting, crushing, or burning stimuli) that activates **nociceptors** (specialized peripheral sensory neurons distributed throughout the body) that convey signals to the central nervous system (*3*), where they are processed and generate multiple responses, including the "**unpleasant sensation of pain**".

1. Nociceptors

"A high-threshold sensory receptor of the peripheral somatosensory nervous system that is capable of transducing and encoding noxious stimuli", according to IASP. The term "nociceptor" comes from Latin "nocere" which means to harm or to damage. Charles Sherrington introduced it for the first time in 1906 to redefine the neural apparatus responsible for detecting a **noxious stimulus**.

Nociceptors are **sensory nerve endings** responsible for detecting **noxious** stimuli which can be **mechanical** (painful pressure, squeezing or cutting the tissue), **thermal** (extreme heat or extreme cold) or **chemical** (stimulation by inflammatory mediators). These nerve cells are constituted by a body (located in the dorsal root ganglion (DRG)) and 2 axons: peripheral and central. The peripheral axon innervates tissues such as skin and whose terminals react to sensory stimuli. The central axon enters the spinal cord in order to transfer information to the central nervous system (CNS) by synaptic communication. These nociceptors are frequently in close contact with small distal blood vessels, lymphatic vessels, and mast cells (*4*).

These sensory neurons **convert** external noxious stimuli into internal **electrical impulses**. Indeed, the noxious stimulus **generates a graded potential in** axons **that if strong enough,** causes the sensory neuron to produce an **action potential** that is relayed into the central nervous system (CNS), where it is integrated with other sensory informations to become a conscious perception of that stimulus.

There are two major classes of nociceptors that respond to different modalities of noxious stimuli: **C-fibers** and **Aδ-fibers**.

C-fibers are the most common group of nociceptors with **unmyelinated axons**, which have a small diameter and conduct slowly. They respond to noxious thermal, mechanical, or chemical stimulation (*5*). Via detectors located in their membrane at their ends, these nociceptors convert the stimulus energy into electrical impulses, which in turn are propagated throughout the nervous system. C-fibers represent the majority of sensory neurons in the peripheral nervous system. **Aδ-fibers** are nociceptors with thinly **myelinated axons**. These nociceptors are slightly larger in diameter, conduct more rapidly than do unmyelinated C-fibers and likely convey "fast" (or sharp) momentary pain, as opposed to slow, diffuse pain, which is transmitted by the C-fibers. Aδ fibers typically respond to a discrete type

of stimulus, such as mechanical stimuli or damaging hot or cold temperatures. They are also sensitized to tissues injury. They are less likely to be polymodal receptors than are C fibers which respond to mechanical, thermal, chemical stimuli (*6*, *7*).

In addition to the **Aδ-** and **C-fibres** that carry noxious sensory information, there are primary afferent **Aβ-fibres** that carry non-noxious stimuli. **Aβ-fibres** are highly **myelinated** and of large diameter, therefore allowing rapid signal conduction. They have a low activation threshold and are normally not involved in pain transmission but usually respond to light touch and convey tactile information (**Table. 1**).

Table 1. Characteristics of different types of sensory fibres

	C-fibres	**Aδ-fibers**	**Aβ-fibres**
Diameter	Smallest <2 µm	Small 2-5 µm	Large
Myelination	unmyelinated	Thinly myelinated	Highly myelinated
Conduction velocity	<2 ms^{-1}	5-15 ms^{-1}	>40 ms^{-1}
Receptor activation thresholds	High	High and low	Low
Sensation on stimulation	Slow, diffuse, dull pain	Rapid, sharp, localized pain	Proprioception, ligh touch, non-noxious

Of note, in addition to sending the information to the cerebral cortex, nociceptor systems have a vital role in triggering reflexes that protect the body from the source of pain, such as the withdrawal reflexes.

2. Nociception and Pain

Nociception and **pain** are distinct concepts. Sherrington coined the term "**nociception**" to describe the detection of a noxious event by nociceptors, which includes the peripheral and central nervous system (CNS) processing of information about the internal or external environment (*8*). However, it is important to note that the responses of neurons to noxious stimuli do not necessarily lead to pain. Indeed, noxious stimulation triggers multiple physiological and behavioral responses, such as increases in blood pressure and heart rate, withdrawal reflexes, etc., and pain sensation is not necessarily implied. Indeed, the threshold for eliciting pain must be high enough to allow the achievement of most activities largely pain-free, but sensitive enough to immediately alert if an injury is impending.

Typically, noxious stimuli, including tissue injury, activate nociceptors that are present in peripheral structures and that transmit information to the spinal cord dorsal horn or its trigeminal homologue, the nucleus caudalis. From there, the information continues to the brainstem and ultimately the cerebral cortex, where the perception of pain is generated (**Fig. 1**) (*9*).

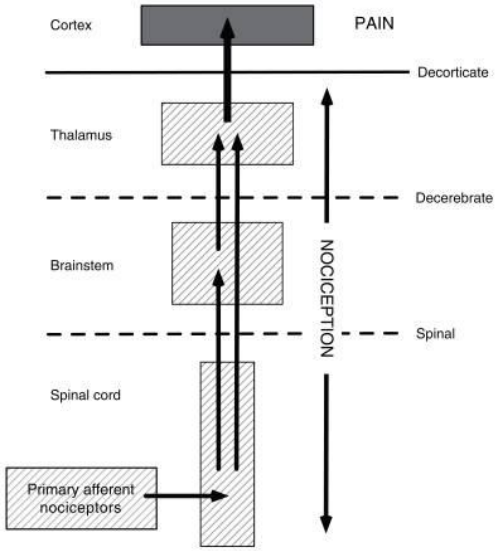

Fig. 1. Anatomical distribution of nociception and pain.

3. Pain classification

Pain can be defined simply as the subjective experience of harm in a part of one's body. In reality, however, pain is a multidimensional phenomenon with sensory, physiological, cognitive, affective, behavioural and spiritual components. Indeed, there are multiple forms of pain, which involve a variety of distinct biological processes. Several ways are used to categorize pain, according to the causes, or the duration and pattern of occurrence, or the regions of body involved, etc.

According to their **mechanisms**, Clifford J. Woolf et al. suggested the classification of pain as **nociceptive pain**, **inflammatory pain** and **pathological pain** (**Fig. 2**) (*1*, *10*).

- **Nociceptive pain**

Nociceptive pain is an early-warning physiological protective system, essential to detect and minimize contact with damaging or noxious stimuli. It involves activation of pain receptors by a noxious stimulus such as exposure to heat or cold, extreme physical pressure, etc. It is a highthreshold pain only activated in the presence of intense stimuli.

- **Inflammatory pain**

It resulted from activation and sensitization of the nociceptive pain pathway by a variety of mediators released at a site of tissue inflammation, involving the release of cytokines and the infiltration of immune cells. Inflammatory pain occurs subsequent to injury, but can be triggered independently by bacterial infections.

Both nociceptive pain and inflammatory pain are physiological **adaptive** and **protective** systems. While the former is essential to minimize contact with noxious stimuli, the later tends to reduce further risk of damage and promotes recovery.

- **Pathological pain**

Unlike nociceptive pain, pathological pain is caused by nerve hypersensitivity due to (i) peripheral or central nerve damage (Neuropathic pain) or (ii) its abnormal function such as phantom limb pain,

diabetic neuropathy (Dysfunctional pain).

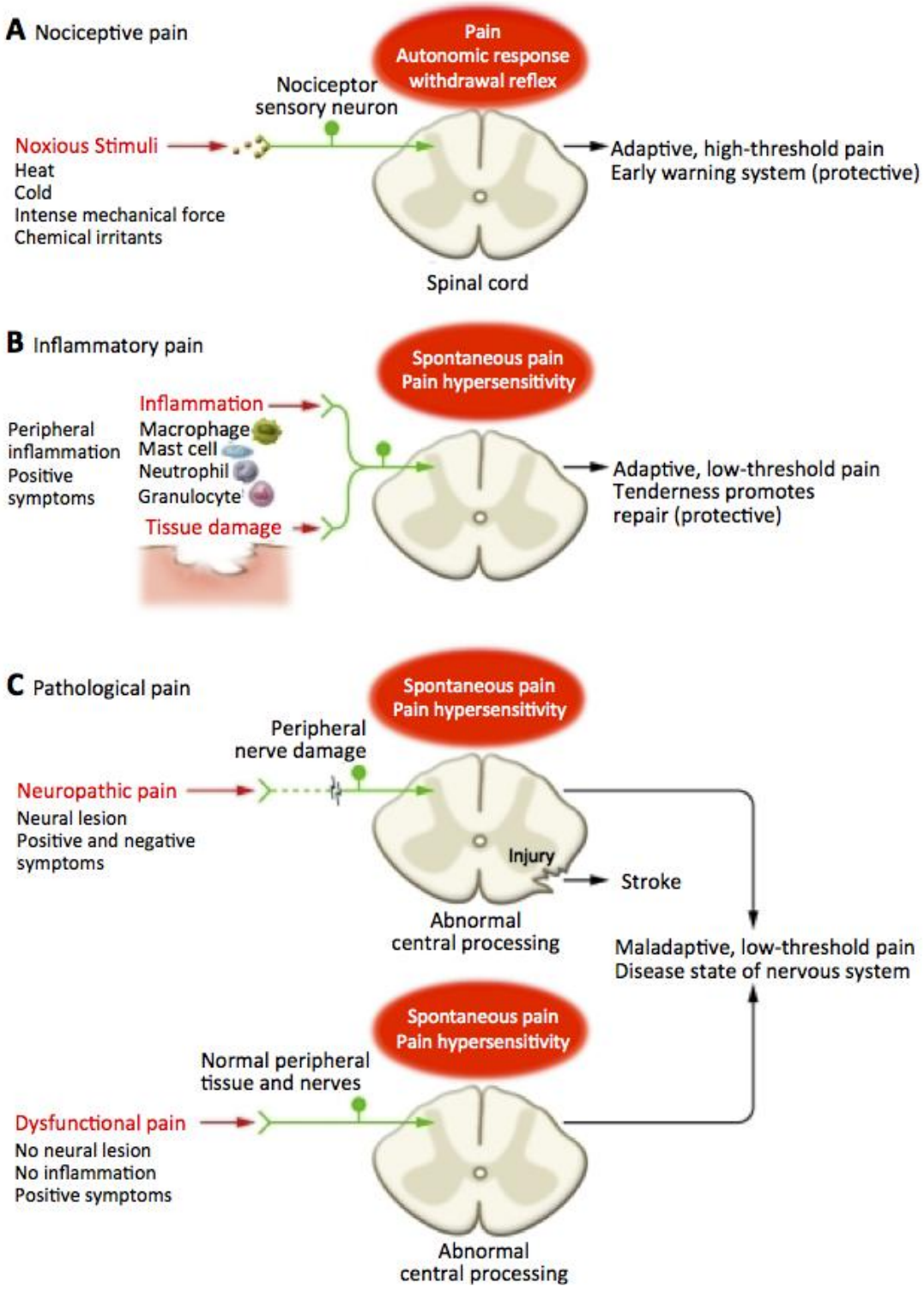

Fig. 2. Pain classification. © 2010 American Society for Clinical Investigation.(*1*)

It should be noted that **pathological pain** is not protective, but **maladaptive.** Physiological pain may progress to a pathological condition itself if persistent, in which case pain does not represent anymore a symptom of disease but rather abnormal sensory processing. Unfortunately, many pathological pain conditions remain poorly understood and resist currently available treatments (*11*). Nociceptive pain is not a clinical problem, except in the specific context of surgery and other clinical

procedures that necessarily involve noxious stimuli, where it must be suppressed by local and general anesthetics or high-dose opioids. Indeed, under inflammatory pain or pathological pain condition, the sensitivity to noxious stimuli may increase, causing **hyperalgesia**, or pain is triggered from stimuli that do not normally provoke pain (innocuous stimuli), inducing **allodynia** (**Fig. 3**)(*12*). Hyperalgesia and allodynia are the result of changes in either the peripheral or central nervous systems, referred to as peripheral or central **sensitization**, respectively.

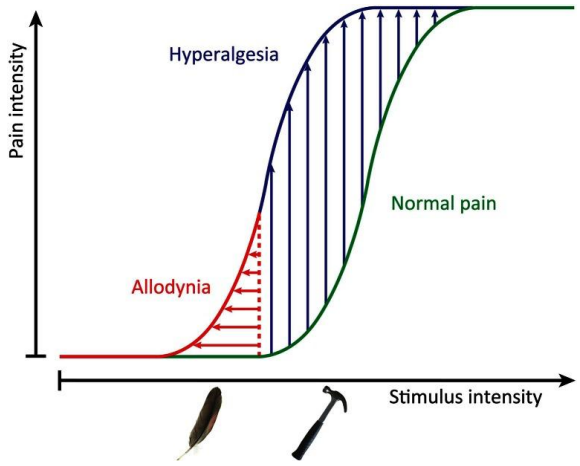

Fig. 3. Sensitization to pain. This graphical representation of the shift in pain thresholds during a pain state shows both enhanced response to noxious, normally painful, stimuli (hyperalgesia) and pain triggered by non-noxious stimuli (allodynia) like the gentle brush of the skin. These two painful states do not always coexist, and it is increasingly apparent that they are driven by distinct mechanisms in different sets of sensory neurons. © Stéphane Lolignier, Niels Eijkelkamp, and John N. Wood, 2014. (*12*)

Depending on their **durations**, pain can be categorized as **acute pain** and **chronic pain**. **Acute pain** typically comes on suddenly and lasts a short time while chronic or persistent pain is of longer duration (3 months or more). Acute pain is frequently provoked by a specific disease or injury, serving a useful biologic purpose. This type of pain usually settles as the tissues heal. In some cases acute pain does not settle and persists, becoming thus chronic. **Chronic pain**, in contrast, may be considered as a disease state. This kind of pain that persists after the normal time of healing, if associated with a disease or injury (*13*).

4. Pain pathway

The pain system is normally described in a simplified way, as described in **Fig. 4**. Generally, pain is generated by activation of peripheral nociceptors (**stimulation**) in response to a noxious stimulus. Then, these nociceptors transform this stimulus into electrical signals (**transduction**) which are conducted to the brain through the spinal cord (**transmission**). At this level, signals are processed and generate multiple responses, including the "unpleasant sensory and emotional experience" (**perception**). Then, within the cerebral structure, some neurons by descending nociceptive pathway (neurotransmitters) modulate the activity of spinal cord nociceptive neurons (**modulation**) (*5*).

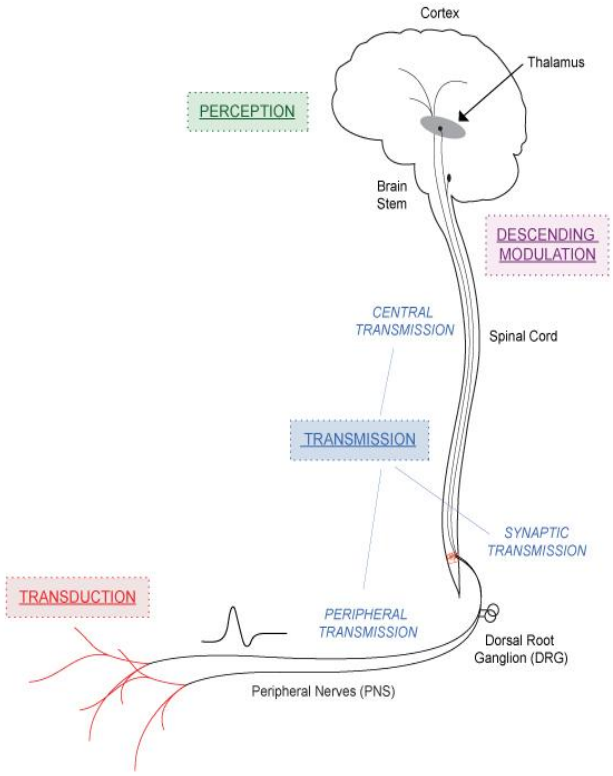

Fig. 4. Ascending pathways of pain perception. ©Copyright 2010 Board of Regents of the University of Wisconsin System

- **Primary sensation**

All sensory systems must convert incoming environmental stimulus information into **electrochemical signals**. Pain occurs when nociceptors are stimulated by thermal, mechanical, or chemical stimulation. The physiochemical properties of noxious stimuli are converted to electrical activity by the detectors located on the terminals of sensory neurons, for example, the transient receptor potential-generating channels (TRP channels) and purinergic channels (**Fig. 5**). The electrical activity formed is then amplified by sodium, potassium, and calcium channels to elicit action potentials that travel to the central nervous system (*5*, *14*).

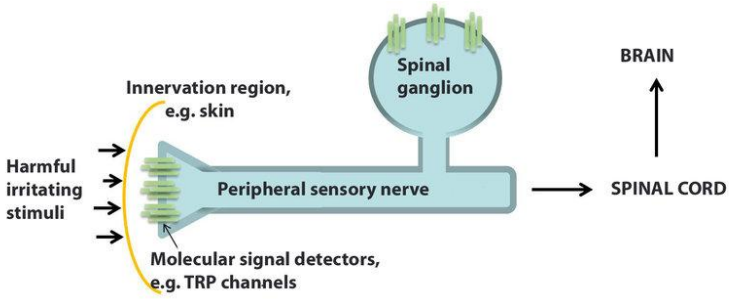

Fig. 5. Highly simplified diagram of the "pain axis". Activation of molecular signal detectors such as TRP channels in the membranes of peripheral sensory nerves by harmful or irritating stimuli generates an electrical pulse that is converted into an action potential in neurons. The action potential, in turn, induces still other membrane proteins to trigger complex signal transduction cascades in the spinal ganglion and subsequently in the spine. The information is then transmitted to various areas of the brain that are ultimately responsible for the perception of pain. © Max Planck Institute of Experimental Medicine/Schmidt.

- **Pain signal transmission**

When peripheral sensory fibers (primary afferent fibers) respond to noxious stimuli, they transmit this information as electrical signals (**action potentials)** via axons by **depolarizing** the presynaptic membrane and inducing the opening of voltage-sensitive calcium channels when it reaches the presynaptic knob. Diffusion of Ca^{2+} ion in the presynaptic knob causes the movement of synaptic vesicles that carry the neurotransmitters to the surface of the knob. Synaptic vesicles then fuse with the presynaptic membrane and get rupture to discharge its content (ie. neurotransmitters) into synaptic cleft. **Neurotransmitters**, such as **glutamate SP**, **CGRP**, nitric oxide (**NO**), prostaglandins (**PG**), and brain-derived neurotropic factor (**BDNF**), bind with specific protein receptors on the postsynaptic membrane of the second-order neuron and change its membrane potential. The depolarization of the postsynaptic membrane then opens the sodium and calcium channel, causing respective influx of Na^{+} and Ca^{2+} ions. In this way, the nerve signal gets transmitted to next neuron along the synapse. The transmission of nociceptive information at the spinal level is modulated by interneurons (mainly inhibitory) through the release of opioid pepides and GABA and also by supraspinal descending neurons ("Descending pathways") through the release of 5-hydroxytryptamine (5-HT) and noradrenaline (NA). Descending pathways may inhibit or enhance nociceptive transmission from the spinal cord. (**Fig. 6**)

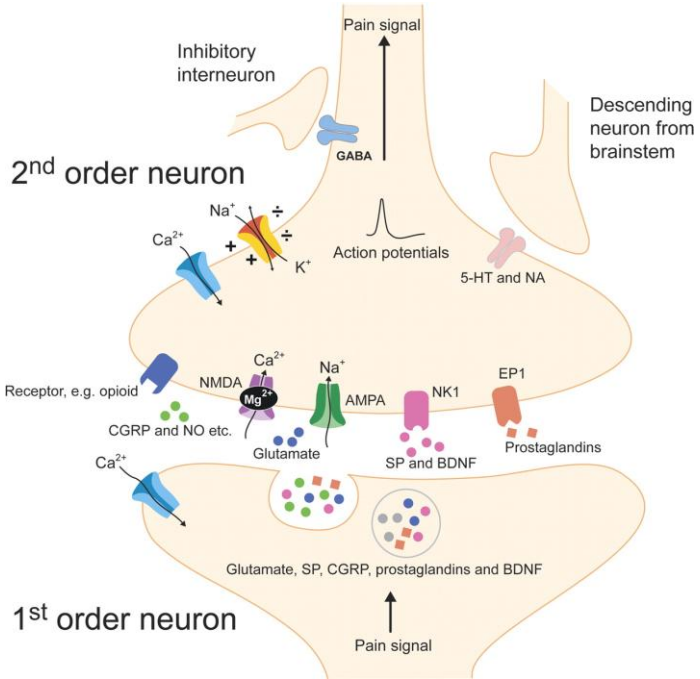

Fig. 6. Simplified representation of the spinal transmission. © The American Society for Pharmacology and Experimental Therapeutics, 2012. (*5*)

- **Inflammatory pain and hyperalgesia**

Inflammation produces a condition known as **hyperalgesia**, which is characterized by enhanced pain sensation and reduced pain threshold. It is the result of exposure to **inflammatory mediators** released at the site of injury (*15*). Indeed, tissue damage lead to the local formation and release of numerous chemicals around the primary afferent nerve endings due to disruption of cells and activation of various specialized cells including mast cells, macrophages, T-cells, neutrophils and other immune cells. Mast cells play a key role in non-neural inflammation (*16*). Mediators released

include bradykinin (BK), interleukins (e.g. IL-1β), serotonin (=5-hydroxytrytamine, 5-HT), histamine (Hi), prostaglandins (e. g. PGE2), protons (H^+), purines (e. g. adenosine triphosphate, ATP), nerve growth factor (NGF), and tumor necrosis factor (TNF). Together these (and other) mediators constitute the **inflammatory soup**. They contribute to the increased sensitivity of peripheral nociceptors by coupling to membrane-bound ion channels (including transient receptor potential (TRP) channels (e.g. TRPV1), acid-sensitive ion channels (ASICs) and purinergic (P2X) receptors) and kinase linked receptors (e.g. NGF-, TNF-α and IL-1β receptors) and G protein-coupled receptors (e. g. bradykinin2- and prostaglandin-receptors), through the action of receptor-initiated second messenger cascades. These mechanisms can lead to depolarization and excitation of the neuron as well as long term **alteration of gene regulation** (e.g. NGF and bradykinin increasing the expression of TRPV1 and prostaglandins increasing the expression of voltage gated sodium channels (VGSC). Increased synthesis of TRPs and VGSC represents another mechanism for the development and maintenance of inflammatory hyperalgesia (*17, 18*). In addition peripheral nociceptor terminals may themselves release substance P (SP) and calcitonin gene related peptide (CGRP), which cause vasodilatation and plasma extravasation at the injury site (*19*).

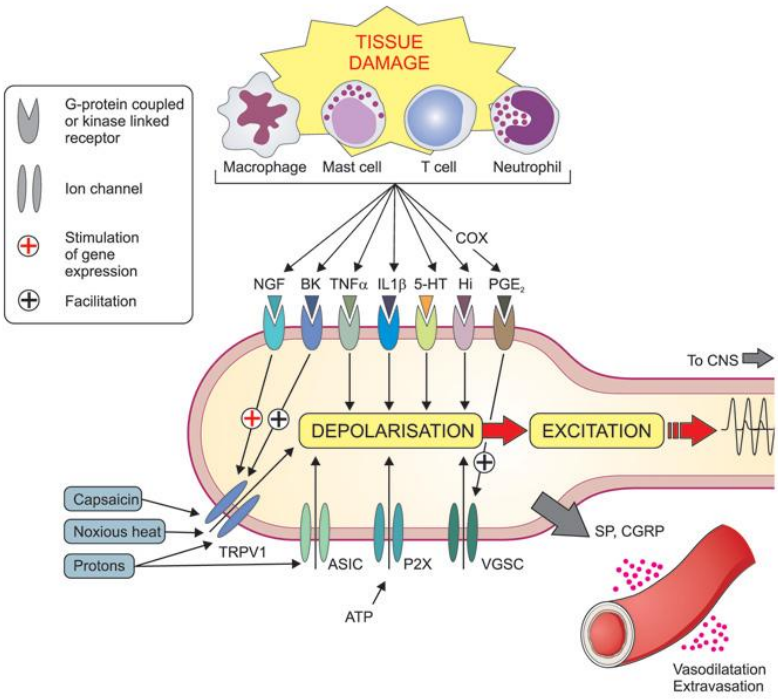

Fig. 7. Mechanisms involved in of peripheral sensitization during inflammation (*19*).

II. OPIOID SYSTEM

Over the past two centuries, opium and its derivatives have become the most widely used analgesics for severe pain. Morphine, as the major active ingredient of opium, was isolated in 1805 by the German pharmacist Wilhelm Sertürner and subsequently named after the Greek god of dreams, Morpheus. In 1973, three independent teams showed that opiates bind to membrane receptors in the brain (*20-22*). In 1976, Martin's group proposed distinctive classes of opioid binding sites: mu (*m*orphine), sigma (SKF 10047, N-allylnormetazocine) and kappa (*k*etocyclazocine)(*23*). Lord and colleagues, in 1977, discovered a binding site in the isolated mouse *vas deferens* with high affinity for

enkephalins and named it the delta (deferens) receptor (*24*). The three opioid receptors, μ, δ and κ have been cloned and the recombinant receptors shown to have binding and functional characteristics consistent with their endogenous counterparts (*21, 25-27*). In that respect, the authentification of specific receptors for opiate alkaloid and related synthetic drugs led to a search for specific endogenous ligands and the discovery of the enkephalins (*28*), β-endorphin (*29*), and dynorphins (*30*). A search for related receptors by homology cloning led to the identification of a receptor which displays 60% substantial sequence identity in comparison with the "classical" opioid receptors. As none of the known endogenous opioid peptides could interact with this receptor, it was named opioid receptor-like (ORL-1). This receptor was considered as "orphan" until the formal identification of its endogenous ligand (nociceptin/orphanin FQ (N/OFQ)) (*31*).

Thus the **opioid receptor**s and their **endogenously produced ligands** compose the innate pain-relieving system, the **opioid system**.

1. Opioid receptors and their ligands

• Opioid receptors

Opioid receptors belong to the group of inhibitory **G-protein coupled receptor** (**GPCR**), a vast family of membrane-traversing proteins, also known as 7-transmembrane receptors (7-TM receptors) (*21, 32, 33*). The GPCRs are essential to the ability of eukaryotic life to detect and mount an intracellular response to a diverse range of extracellular stimuli. They are by far the most abundant class of cell-surface receptors, which are the targets of about 35% of the approved/marketed drugs (*34*).

Opioid receptors are mainly found in various brain regions, the dorsal horn of the spinal cord, on peripheral nerve terminals, in peripheral tissues including the gastrointestinal tract and on immune cells (*35, 36*). In the periphery, opioid receptors are widely distributed in neuronal and non-neuronal cells, including neuroendocrine, immune and ectodermal cells (*32, 37*). In the gastrointestinal tract tract they are present in smooth muscle cells and at the terminals of sympathetic and sensory peripheral neurons (*38*).

• Endogenous opioids

Terenius (*39*) and Hughes (*40*) reported for the first time, in 1975, the existence of endogenous factor in the brain acting as an agonist on opiate receptor in neural tissues. Then Hughes characterized two morphine-like material as pentapeptides and termed them methionine enkephalin (Met-enkephalin) and leucine enkephalin (Leu-enkephalin) (*28, 41*). In addition to **enkephalins**, two other classes of endogenous opioid peptides have been identified afterwards, such as **endorphins** (*42*) and **dynorphins** (*30, 43, 44*). Each opioid peptide is derived from a large **precursor protein**. There are three such large precursors in mammals: **pro-enkephalin (ProEnk)**, **pro-dynorphin (ProDyn)** and **pro-opiomelanocortin (POMC)**. Met-enkephalin is generated after the proteolyic cleavage of proenkephalin, while Leu-enkephalin is produced predominantly from prodynorphin and with less copy from proenkephalin. β-Endorphin generated by pro-opiomelanocortin is the longest opioid peptide (31 amino acids) and shows highly potent and long-lasting analgesic properties. Endogenous peptides derived from these precursors share a common N-terminal sequence (**Tyr-Gly-Gly-Phe-Leu/Met)** and they have varied affinity for μ, δ and κ receptors. Enkephalin can activate both μ- and δ-opioid receptors, with significantly higher (10-fold) affinity for the later, but with negligible affinity

for κ receptors (*45*). β-Endorphin preferentially binds to the μ-opioid receptor while dynorphins prefers κ-opioid receptors. Nociceptin or orphanin FQ (N/OFQ) originating from pro-nociceptin, binds to ORL-1 receptors. Finally, endomorphins (EMs), including EM-1 and EM-2 amide tetrapeptides, display a high binding affinity and selectivity to the μ-opioid receptors. (**Table 2**)

Endogenous opioid peptides are produced and often released together with other neurotransmitter molecules in the **brain**, **pituitary gland**, and **adrenal gland** as well as by **single neurons** in the central and peripheral nervous systems (*46*). Additionally, opioid peptides are also synthesized and secreted by **immune cells** in response to stressful stimuli or stimulation by corticotropin-releasing factor (CRF), formyl peptides and chemokines (CXCL2/3).

Table 2. Mammalian endogenous peptide (adapted from (*45*) with permission).

Precursor	Endogenous peptide	Amino acid sequence	Affinity for opioid receptors
Pro-enkephalin	[Met]enkephalin	Tyr-Gly-Gly-Phe-Met	δ, μ
	[Leu]enkephalin	Tyr-Gly-Gly-Phe-Leu	(δ >> μ)
		Tyr-Gly-Gly-Phe-Met-Arg-Phe	
		Tyr-Gly-Gly-Phe-Met-Arg-Gly-Leu	
	Metorphamide	Tyr-Gly-Gly-Phe-Met-Arg-Arg-Val-NH2	
Pro-opiomelanocortin	β-endorphin	Tyr-Gly-Gly-Phe-Met-Thr-Ser-Glu-Lys-Ser-Gln-Thr-Pro-Leu-Val-Thr-Leu-Phe-Lys-Asn-Ala-Ile-Ile-Lys-Asn-Ala-Tyr-Lys-Lys-Gly-Glu	μ, δ (δ = μ)
Pro-dynorphin	Dynorphin A	Tyr-Gly-Gly-Phe-Leu-Arg-Arg-Ile-Arg-Pro-Lys-Leu-Lys-Trp-Asp-Asn-Gln	κ, μ, δ (κ >> μ = δ)
	Dynorphin A (1-8)	Tyr-Gly-Gly-Phe-Leu-Arg-Arg-Ile	
	Dynorphin B	Tyr-Gly-Gly-Phe-Leu-Arg-Arg-Gln-Phe-Lys-Val-Val-Thr	
	α-Neoendorphin	Tyr-Gly-Gly-Phe-Leu-Arg-Lys-Tyr-Pro-Lys	
	β-Neoendorphin	Tyr-Gly-Gly-Phe-Leu-Arg-Lys-Tyr-Pro	
	[Leu]enkephalin	Tyr-Gly-Gly-Phe-Leu	
Pro-nociceptin	Nociceptin	Phe-Gly-Gly-Phe-Thr-Gly-Ala-Arg-Lys-Ser-Ala-Arg-Lys-Leu-Ala-Asn-Gln	ORL
Unknown	Endomorphin-1	Tyr-Pro-Trp-Phe-NH_2	μ
	Endomorphin-2	Tyr-Pro-Phe-Phe-NH_2	

- **Distribution of enkephalins**

Concerning Enkephalins, they are widely distributed throughout the brain and the spinal cord, the highest concentrations being in the hypothalamus, anterior pituitary, reticular formation, caudate, hippocampus, amygdala, periaqueductal gray, substantia nigra, and neocortex. Although similar ratios of the methionine- and leucine-enkephalins are seen in whole brain extracts, the ratio varies considerably in different brain regions and from one sepecies to another. It was stipulated that methionine- and leucine-enkephalin may exist in two separate neurotransmitter systems with possibly diverse functions **(*47*)**. As with other brain peptides, appreciable quantities of enkephalins are also found in the intestine and in small amounts in other peripheral tissues such as peripheral ganglia and postganglionic neurons. It was also reported that enkephalin activity in sympathetic ganglia and in the vagus nerve suggests that the enkephalins may have a widespread role in the control of peripheral autonomic activity **(*47*)**.

2. Mechanism of opioid analgesic activity

The binding of endogenous ligands to their opioid receptors results in conformational changes of these receptors allowing thus intracellular coupling of heterotrimeric G proteins (consisting of G_{α}, G_{β} and G_{γ} subunits) to the C terminus of the receptor. The activated receptor promotes exchange of GTP for GDP on G_{α} protein by dissociation of the GDP-bound in favour of GTP-bound. This results in the activation of the trimeric G-protein complex, which dissociates into G_{α} (binded to GTP) and $G_{\beta\gamma}$ subunits (**Fig. 8**). Then, G_{α}·GTP inhibits **adenylyl cyclases** (ACs) and consequently cyclic adenosine monophosphate cAMP production, which in turn inhibits the cAMP-dependent calcium influx, resulting in attenuated excitability of neurons and/or reduced neurotransmitter release. Regarding to Gβγ, it directly interacts with different **ion channels** of the membrane, facilitating the opening of potassium channels (efflux of potassium), while inhibiting the opening of calcium channels. The **inhibition of calcium entry,** as well as, the **efflux of potassium** causes the **hyperpolarization** which **inhibits transmitter's release**, therefore blocking **the transmission of the pain** (**Fig. 9**) (*32, 48*). At the postsynaptic membrane, opioid receptors mediate **hyperpolarization** by opening K^+ channels, thereby **preventing excitation and/or propagation of action potentials** (*49, 50*).

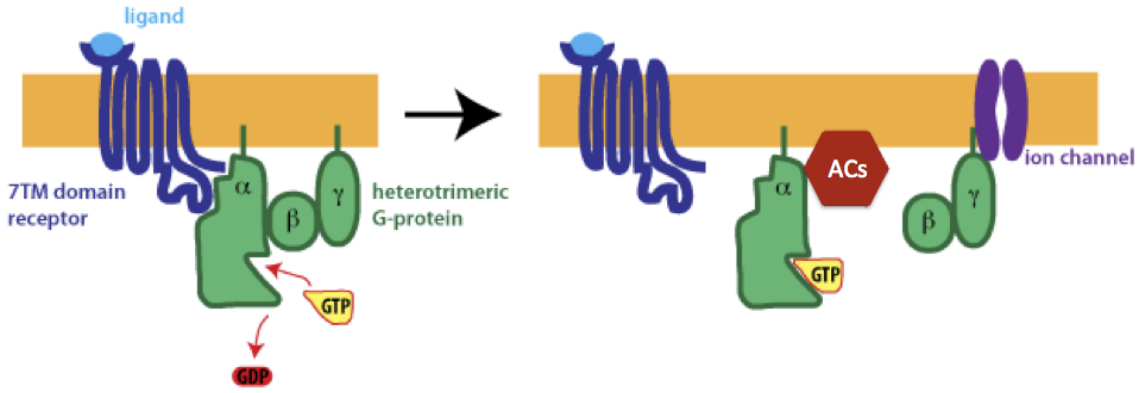

Fig. 8. General principle of the GPCR signaling system.

Morphine and other opiates are widely used in clinical practice for alleviation of the most severe pain syndromes or for anesthetic purposes. Morphine is primarily an agonist ligand for the μ receptor (*51*). Endogenous peptides, for their part, share similar mechanism with morphine in blocking pain transmission (**Fig. 9).** However, morphine application is usually associated with many severe side effects including nausea, constipation, drowsiness, sedation, and even more severe as respiratory depression, development of tolerance and addiction, which relate to the overstimulation of central opioid receptors (*52*).

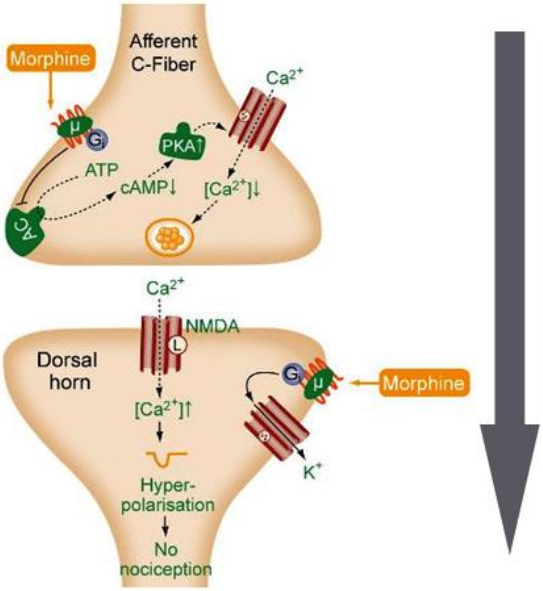

Fig. 9. Mechanism of morphine on blocking pain process.

3. Peripheral analgesia and inflammation

Since a long time, anti-nociceptive effects of opiates were often associated with the activation of central nervous system opioid receptors. The discovery of the anti-nociceptive effects mediated by the opioid receptors on **peripheral** nerve endings at the primary afferent neurons, opened new perspectives for the treatment of pain (*36, 53-55*). Indeed, the activation of peripheral opioid receptors was found to produce a potent analgesia, devoided of **centrally mediated unwanted effects** (*56, 57*), such as respiratory depression and dependence, etc.

The injury of the body (infection, wound, burn or damage by chemical irritants) triggers the body's defense system inducing the inflammatory response. This process is orchestrated by the release of a wide range of chemical factors into the extracellular space by recruited immune cells, damaged tissue and even by the sensory fibres (*58*). These inflammatory mediators are believed to play a key role in the development of the inflammatory pain (*59*) which results in the **up-regulation** of peripheral opioid receptors (*60*). Opioid receptors are first synthesized in the dorsal root ganglion (DRG) and then transported along the intra-axonal microtubules into the periphery of the primary afferent neuron (*61*). The inflammation process can also disrupt the perineural barrier surrounding the neurons, facilitating the access of opioid ligands to the receptors (*62, 63*). The peripheral opioid receptors can then interact with exogenous or endogenous opioid ligands. Endogenous opioid ligands are found in sensory neurons, as well as, in immune cells (*49*). Their secretion is stimulated by the inflammatory soup. Once released from immune cells the opioid peptides activate the up-regulated opioid receptors on sensory nerve terminals thus generating analgesia (**Fig. 10**) (*49, 56, 64, 65*).

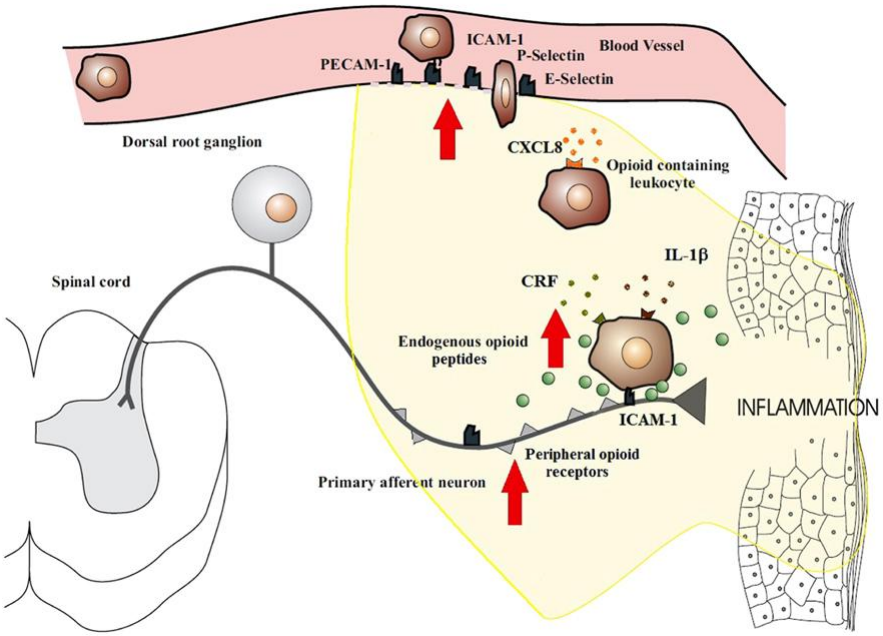

Fig. 10. Migration of opioid-containing immune cells and opioid release within inflamed tissue. Adhesion molecules facilitate endothelial transmigration of immune cells. In response to stress or releasing agents (e.g., CRF, IL-1, CXCL8), the immune cells secrete opioid peptides. Opioid peptides or exogenous opioids bind to opioid receptors on primary afferent neurons, leading to analgesia. Copyright © 2013 Iwaszkiewicz, Schneider and Hua (*56*).

Noteworthy, central and peripheral mechanisms of endogenous opioid analgesia are interconnected, particularly in the early stages of inflammation (*66*), whereas at later stages the peripheral opioid antinociception played an an increased role. (*67*).

Targeting peripheral endogenous opioid receptors to avoid central side-effects. Several attempts were conducted to specifically deliver morphine to peripheral opioid receptors, thus avoiding the side effects associated with the over-excitation of the central opioid receptors. With this aim, a serie of hydrophilic analogues of morphine were synthesized, among which 14-O-methylmorphine-6-O-sulfate (14-O-MeM6SU) exhibits peripheral antinociception in rat and mouse inflammatory pain models, without displaying central adverse effects (*68, 69*). S. González-Rodríguez et. al. reported another peripherally restricted opioid formulation, by covalently linking morphine to hyperbranched polyglycerol (PG-M). Due to the high-molecular weight and the hydrophilicity of this conjugate, morphine release was restricted to the injured tissue and blood-brain-barrier permeation was hampered which allowed to avoid central side effects of morphine(*70*).

Moreover, studies have shown that macrophages and polymorphonuclear leukocytes at the inflammation site could secrete a variety of products on exposure to different stimuli. These include enzymes from lysosomes that capable of hydrolyzing a wide variety of both natural and synthetic substrates, including simple and complex polysaccharides, oligopeptides, polypeptides, phosphate esters, lipids, and so forth (*71, 72*).

III. OPIOID PEPTIDES FOR DRUG DEVELOPMENT

Peptide drugs are recognized for being highly specific with low off-target toxicity and, most

importantly, they present a remarkable efficiency. Given their attractive pharmacological profile and intrinsic properties, peptides represent an excellent starting point for the design of novel therapeutics and their specificity has been seen to translate into excellent safety, tolerability, and efficacy profiles in humans (*73*).

In some cases, distinct differences have been demonstrated for opioid peptide ligands in comparison with their nonpeptide counterparts. Indeed, *in vivo* studies revealed that the high specificity of peptide ligands for opioid receptors could minimize off-target side effects compared to small molecule ligands (*74, 75*). However, these endogenous opioid peptides are often not directly suitable for use as convenient therapeutics because of their intrinsic weaknesses, including poor chemical and physical stability, and a short circulating plasma half-life. In this respect, it was reported that extremely high quantities (120 to 200 µg) of enkephalins are required to induce analgesia even when microinjected into rat cerebral ventricles (*76*) and brain (*77*), due to brain enzymatic activity. It was also reported that enkephalins half-life in plasma ranged from few (*78*) seconds to 2-3 minutes (*79*). These important limitations have to be seriously taken in account for their use as medicines.

Thus, a range of attempts has been proposed to improve the proteolytic stability of these neuropeptides for improving their analgesic activity. These attempts include the chemical modification of peptides (enkephalin analogs), the synthesis of prodrugs, the use of enzyme inhibitors and the development of novel drug delivery systems.

1. Enkephalin analogues

• Incorporation of non-proteinogenic amino acids

Since the first sequencing of endogenous opioid pentapeptides, extensive researches were conducted concerning the chemical modification on enkephalins structure in order to enhance their resistance to metabolization (*80*). For this purpose, thousands of enkephalin analogues have been synthesized since then (*81*). These approaches include the incorporation of nonproteinogenic amino acids such as D-amino acids (*82*), the cyclization (*83*), the glycosylation (*84*), and the alteration of the amide bond (*85*).

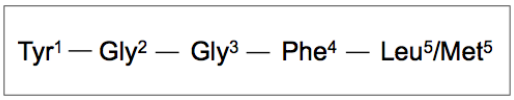

Fig. 11. Structure of Leu (or Met) enkephalins.

The fundamental building blocks of peptides and proteins are natural L-amino acids. L-amino acids and their D-amino acids enantiomers, shares identical chemical and physical properties, except their ability to rotate plane-polarized light (in opposite directions). Unlike L-amino acids, D-amino acids rarely act as the substrates of endogenous proteases. The replacement of L-amino acid by its D-enantiomer represents therefore a very useful tool to prevent proteolytic degradation. With regard to this stereochemical advantage, a series of enkephalin analogs containing D-amino acid(s) have been synthesized and studied. It is important to note that for enkephalins, the preservation of the structure and configuration on Tyr^1, Gly^3, and Phe^4 is essential to preserve peptide's biological activity (*77, 86, 87*). Thus, much more latitude is allowed at the remaining two positions (Gly^2 and Met/Leu^5). In this context, Pert *et al.* designed the substitution of glycine in the second position by D-alanine in Met-enkephalin and in addition, a C-terminal amidation. The resulting analogue ([$D\text{-}Ala^2$]-Met-enkephalin

amide, DALA) considerably increased the *in vivo* agonist potency of Met-Enkephalin (*88*). This was the first significant step forward in synthesizing an *in vivo* potent enkephalin derivative. However, its analgesic activity has been emphasized only after intracerebroventricular (i.cv.) administration. No activity was observed after intravenous (i.v.) administration. The hexapeptide Leu-enkephalin analogue dalargin ([D-Ala^2, Leu^5]-enkephalyl-Arg), also showed good blood stability (*81*). Like DALA, dalargin only induced analgesic effects after i.cv. injection. No pharmacological activity was, indeed, observed after its systemic administration (*89*). It has to be noted that the replacement of D-alanine by D-methionine (*90, 91*) or D-norleucine at position 2 increased peptide stability. These analogues were actually more resistant to metabolization than those with D-alanine. However, substitution by basic (D-lysine) or aromatic (D-phenylalanine) amino acids reduced peptides' activity. A real breakthrough was achieved when proline residue was introduced in position 5 (*92*). These proline analogues were the first systemically (intravenously and subcutaneously) active enkephalin derivatives. Interestingly, the substitution of methionine in position 5 with its D-isomer or with D-proline did not increase the efficacy, if comparing them to the most active proline enkephalin-analogues i.e. to [D-Ala^2, Phe^5]- enkephalin amide (coded as GYKI-14 238). This analogue was found to be 80-times more efficient than morphine when i.cv. injected and about twice more potent if administrated intravenously both in mice and rats (*88, 91, 93*). Analogs such as [D-Ala^2, MePhe-Met (O)-ol^5]-enkephalin (FK-33824) (*94*) and [D-Thr^2, Thz-$NH_2{}^5$]-enkephalin (*95*) have also been found to be excellent analgesics. For instance, FK-33824 was tested clinically in human volunteers. However, because of its serious side effects, clinical trials had to be stopped. Receptor selectivity could also be manipulated in this way. DAMGO ([D-Ala^2, N-MePhe^4, Gly-ol]-enkephalin, μ-opioid spscific ligand) and DADLE ([D-Ala^2, D-Leu^5]-Enkephalin, δ-opioid spscific ligand) are two successful example of this strategy.

- **Cyclization**

The small, linear pentapeptide enkephalins are flexible molecules and their biologically active conformation may only be realized through their complexation with the corresponding receptor. In this way, cyclization of enkephalins represents an important route to chemically modulate peptide structure and activity, in order to promote enzymatic stability and to maintain the peptide drug structure in a rigid conformation that can promote receptor binding. Actually, the reduction in conformational freedom by cyclization may result in higher receptor-binding affinities (*96*). In general, the stability of the cyclic analogues were remarkably higher than the corresponding native peptides, due to the lack of both carboxyl and amino termini (*97*). Unfortunately, *in vivo*, the development of these peptides into viable clinical candidates has been limited by their lack of enzymatic stability and undesirable physicochemical properties.

Therefore, the cyclic prodrug strategy (**Fig. 12**) was employed to create cyclic peptide prodrugs that would overcome these problems, while maintaining the biological activity. This strategy has three main objectives: (i) to enhance membrane permeation, (ii) to increase metabolic stability towards exo- and endopeptidases, and (iii) to promote rapid prodrug bioconversion.

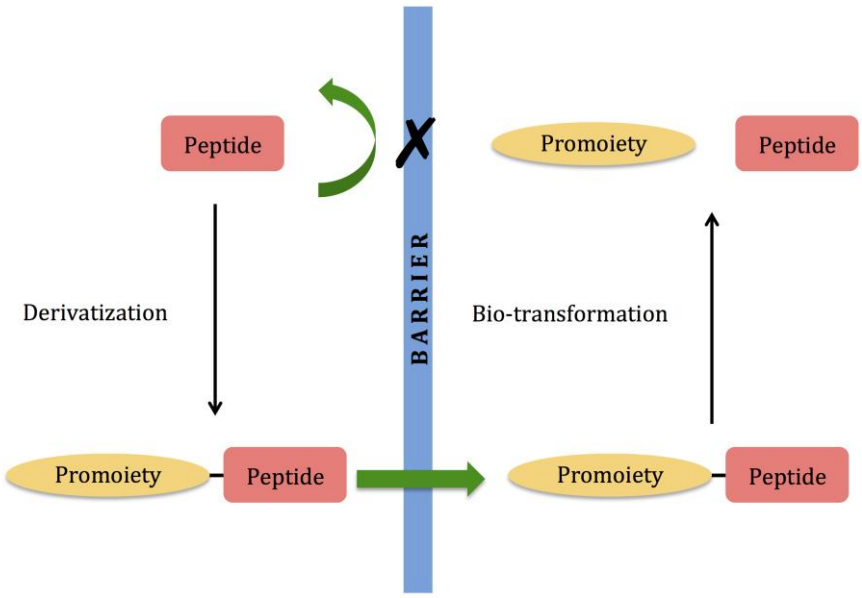

Fig. 12. A schematic illustration of prodrug concept. The linkage of a promoiety to the peptide can increase its lipophilicity, resulting enhanced permeability through biological barriers.

In this context, cyclic peptide prodrugs were designed to further increase the metabolic stability of DADLE towards peptidases. This approach was accomplished through the cyclisation of the N- and C-termini of the peptide. The cyclic design resulted in DADLE prodrugs with greater stability against exo- and endopeptidases (*98, 99*). In fact, the group of Ronald T. Borchardt has synthesized a series of esterase-sensitive cyclic prodrugs of enkephalin and DADLE with different promoiety linkers, i.e., acyloxyalkoxy (AOA) (*100, 101*), coumarinic acid (CA), phenylpropionic acid (PPA), or oxymethyl-modified coumarinic acid (OMCA) linkers (**Fig. 13**) (*98, 102*). These cyclic prodrugs exhibited high lipophilicity and low hydrogen bonding potential, which are the favorable physicochemical characteristics for optimal transcellular permeation (*103*). During this route of permeation, the prodrugs travel through the cells membrane, and then, released *in vitro* and *in vivo* the parent active peptide via esterase-sensitive pathway. However, these prodrugs were also proved to be substrate for efflux transporters P-glycoprotein (Pgp) (expressed on luminal membranes of the endothelium blood vessel) which thus restricted their blood-brain-barrier (BBB) permeation (*104, 105*).

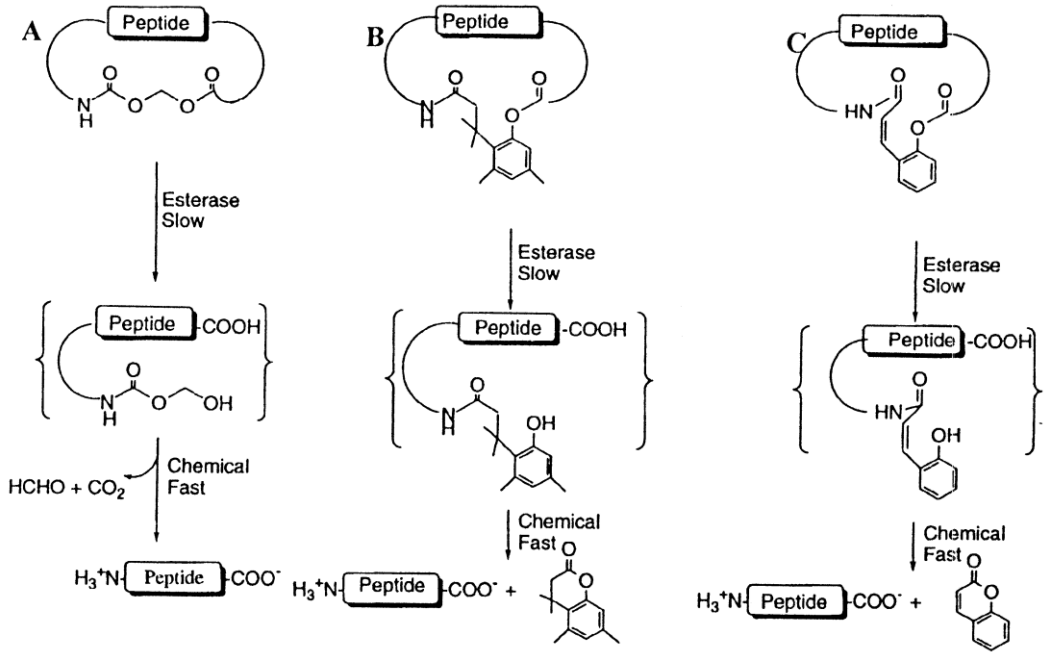

Fig. 13. Cyclic prodrug strategies of opioid peptides. (A) Acyloxyalkoxy-based prodrug; (B) phenylpropionic acid-based prodrug; (C) coumarinic acid-based prodrug. Copyright © 1999 Elsevier Science B.V. Used with permission.

- **Others**

Replacement of the amide bond(s) by thiomethylene ether linkage or thioamide can also lead to enkephalin analogues with increased stability in serum (*85, 106*). However, the amide bond replacement led to a loss of selectivity and efficiency towards δ-opioid receptors in comparison with their parent compounds (*107*). On the other hand, **Glycosylation** strategy, which consists in coupling a glycosyl units to opioid peptides, was also adopted in order to prevent peptide metabolisation and to improve the BBB translocation (*108*). However, the linkage of β-D-glucose to Met-enkephalin analogue peptide resulted in a decrease of opioid receptors binding and a total inactivity *in vivo*. (*109*).

2. Enzyme inhibitors

As mentioned above, enkephalins are substrates of peptidases which hydrolyse them in inactive fragments. The aminopeptidases N (APN) [EC 3.4.11.2], for instance, cleave the N-terminal Tyr^1-Gly^2 bond, while neutral endopeptidases (NEP) [EC 3.4.24.11] or angiotensin converting enzymes (ACE) cleave the Gly^3-Phe^4 bond. In addition, a dipeptidyl peptidase III (DPP III) [EC 3.4.14.4] cleaves the Gly^2-Gly^3 bond, whereas the carboxypeptidase A [EC 3.4.17.1] cleaves the Phe^4-Leu^5 (or -Met^5) bond (**Fig. 14**) (*110, 111*).

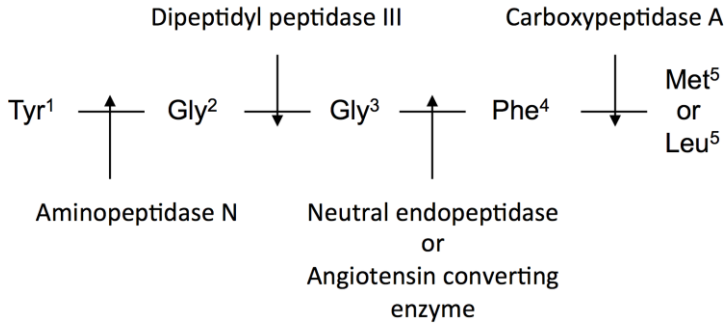

Fig. 14. Inactivation of endogenous enkephalins by various enzymes.

Therefore, a novel approach to prolong the anti-nociceptive activity of enkephalins was proposed by using enkephalinases inhibitors. In general, once released within the extracellular space following prolonged depolarization of the neuronal membrane, enkephalins activate the opioid receptors before being quickly removed from the synaptic cleft and degraded by enkephalinases. Thus, the inhibition of these enkephalin-degrading enzymes may result in an extended duration of action of enkephalins, thus prolonging their anti-nociception effect. Biological studies showed that thiorphan, a NEP inhibitor (*112*) or bestatin, an APN inhibitor (*113*) could only partially prevent enkephalin catabolism, whereas their combination resulted in a better reduction of peptide degradation leading to a higher analgesic response (*113*). It is important to note that the degradation of enkephalins is induced by the concomitant action of APN, NEP and DPP III enkephalinases, and especially by APN and NEP. Hence, inhibition with only one inhibitor didn't show improvements in anti-nociceptive responses (*114, 115*). The development of dual or multiple inhibitors of enkephalinases (*110*) was then tested thereafter. The enkephalinases inhibitors have been classified as illustrated in **Fig. 15** according to their respective substrates.

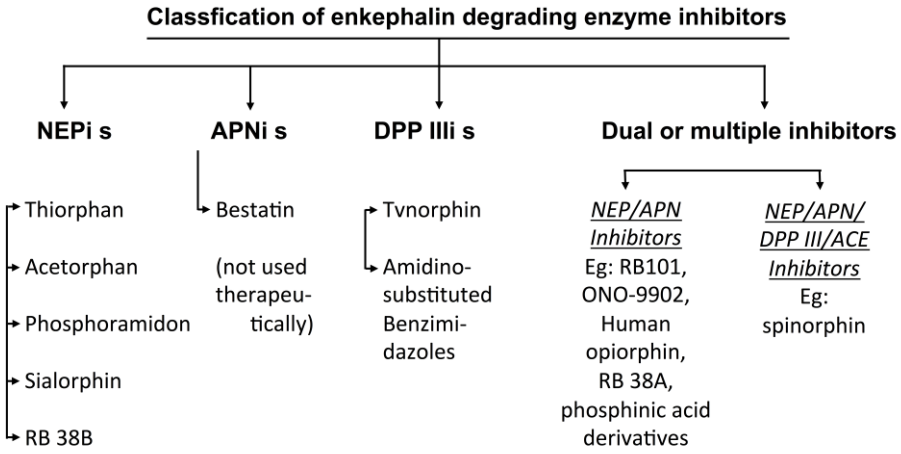

Fig. 15. Classification of enkephalin degrading enzyme inhibitors. (*110*)

In order to improve analgesic potency, highly potent inhibitors of multiple enkephalinases, able to coordinate the catalytic zinc ion of metallopeptidases, were also designed. Indeed, enkephalin-degrading enzymes such as aminopeptidases, enkephalinase, dipeptidylaminopeptidases, belong to the family of metallopeptidases. These peptidases cleave their substrate (the enkephalin) in a single step involving solvent molecule (water) and a catalytic metal ion such as Zinc. In order to inhibit these

metallopeptidases, zinc-chelating agents were built by introduction of hydroxamate group, able to coordinate metallopeptidases active zinc site (*116, 117*), therefore blocking their metabolic activity. Compounds such as kelatorphan (*118*) or RB-38A are two examples of such inhibitors, which exhibited an analgesic potency significantly higher than that of bestatin/thiorphan combination *in vivo*. Based on this concept, a large number of bidentate-containing inhibitors with nanomolar affinities for both APN and NEP have been synthesized. However, *in vivo*, these compounds could not cross the blood-brain-barrier after systemic administration, because of their high hydrophilic properties. But, a promising orally administered ONO-9902 enkephalinase inhibitor was shown to produce significant effects in cases of visceral pain. Subsequently, a series of lipophilic "dual prodrug inhibitors", able to block two different enzymes and crossing the BBB were developed, such as RB101 (*119, 120*). These dual compounds were made up by the association through a disulfide bond of β-amino thiol, a potent inhibitor of APN, with a mercaptoacylamino ester, a potent NEP inhibitor. RB101 was shown to cross the BBB after i.v. administration and could generate the release of APN and NEP inhibitors after disulfide bond cleavage by cerebral reductases. Then, once chelating the metallopeptidases in the brain, both APN and NEP inhibitors contributed to the increase of enkephalins level, thus inducing a prolonged anti-nociceptive effect. However, the duration of the action was short. On the other hand, the oral administration of RB-101 led to the absence of any pharmacological activity, probably due to precipitation within the gut. RB 120, a structural analogue of RB 101, has been synthesized subsequently, and showed strong analgesic effects in mice and rats after oral administration (*121*). Another promising dual enkephalinase inhibitor PL265 which acts by inhibiting APN and NEP, was developed by Bernard P. Roques et al. It is a prodrug with cleavable carbamate as N-terminal protection and can be slowly transformed in plasma into its active metabolite (PL254), which inhibit both APN and NEP (*122*). Administrated orally, this inhibitor allowed an increase of the local concentration of enkephalins, thus triggering a local and sustainable pain relief. PL265 completed a phase Ia single ascending dose and demonstrated good safety. The compound is currently being evaluated in a phase Ib multiple dose escalation for neuropathic pain at Pharmaleads (*123, 124*). A new series of dual aminophosphinic inhibitors of the two enkephalin-catabolizing enzymes has also been designed (*125, 126*). Among them, RB3007 presented all the antinociceptive properties of RB101 but with a significant increase in the duration of action after systemic administration (i.p., i.v., or p.o.).

In this way, Enkephalin-degrading enzyme inhibitors are high beneficial since they allow the increase of enkephalins concentrations, thus producing a potent analgesic activity without the opioid-like side effects. It was also reported that high-dose dual enkephalinase inhibitors therapy didn't result in respiratory depression, emesis, constipation, sedation, tolerance or dependence (*127*). However, the problems with this approach center on the lack of biochemical selectivity towards the peptidase involved in enkephalins metabolism. It should be stressed that enkephalins are not the only substrates of NEP and APN, and the possible involvement of these enzymes in other peptidergic pathways that have not been characterized cannot be excluded (*128, 129*).

3. Gene therapy

Gene therapy represents another potential approach for chronic pain treatment. It introduces genetic materials (DNA or RNA) for the over-expression of endogenous analgesic or anti-inflammatory compounds, or to inhibit genetic transcription of nociceptive proteins. As mentioned before, opioid peptides play an essential role in the control of pain. They are derived from the protein precursor,

such as proenkephalin (ProEnk) or pro-opiomelanocortin (POMC), which in turn is encoded by the corresponding Preproenkephalin (PPE) or Preproopiomelanocortin (PPOMC) genes. Gene therapy was applied to these neuropeptides precursor genes by cloning their complementary DNA (cDNA) fragments to import the coding sequence in host cells to express those specific neuropeptides. In that respect, PPE cDNA- or PPOMC cDNA-coated gold microcarriers (1.5 to 2.0 μm) were injected into the bladder wall of adult female rats using gene gun technique to suppress the nociceptive response on bladder hyperactivity induced by intravesical acetic acid or capsaicin. These data suggested that the PPE gene increased expression of enkephalins in bladder which resulted in the suppression nociceptive responses (*130, 131*). Despite these encouraging results, the progress of gene gun in clinics is challenged due to its limited efficiency to transfect larger and deeper areas, and because of its high cost (*132*).

Viral-mediated gene transfer is more commonly used for pain alleviation (*133*). Viral vectors include adenovirus (AdV), adeno-associated virus (AAV), retrovirus, and herpes simplex virus (HSV) vectors. HSV vectors represent an obvious candidate for the delivery of opioids to primary afferents (**Fig. 16**). Indeed, HSV infections naturally begin in peripheral tissues, travels along sensory nerve fibers and hides out indefinitely in ganglia aligned near the brain and *spinal cord* (*134*). Moreover, as approximately half of the HSV genome is not essential for its replication in cell cultures (*135*), numerous viral genes can be replaced with multiple or large therapeutic transgenes. In addition, unlike with other viral vectors, the potential risks of viral integration into host genome are avoided, which reduces the possibility of mutagenic events (*136-138*). The first HSV vector-based gene therapy that has been reported with analgesic properties was a replication-competent vector. It was derived from attenuated viruses which were genetically modified, in order to express PPE. This viral vector inducted an increase of enkephalin peptides which were released from transduced neurons(*139*). J. M. Antunes Bras et. al. demonstrated that the inoculation of the viral vector into the footpad resulted in a strong expression of preproenkephalin mRNA in the dorsal root ganglion. Increased levels of radioimmunoassayable Met-enkephalin-like material was also detected in the dorsal root ganglion and in the dorsal horn of the spinal cord (*140*). Moreover, this gene therapy approach encoding PPE has been tested and shown to be effective for treating inflammatory, neuropathic, and visceral pain in various rat models (*141-146*). This strategy has been pushed into phase I clinical trial, showing that this treatment was well tolerated (*139, 147*). However, the phase II study did not meet its primary objective of reducing pain in subjects with severe intractable cancer pain.

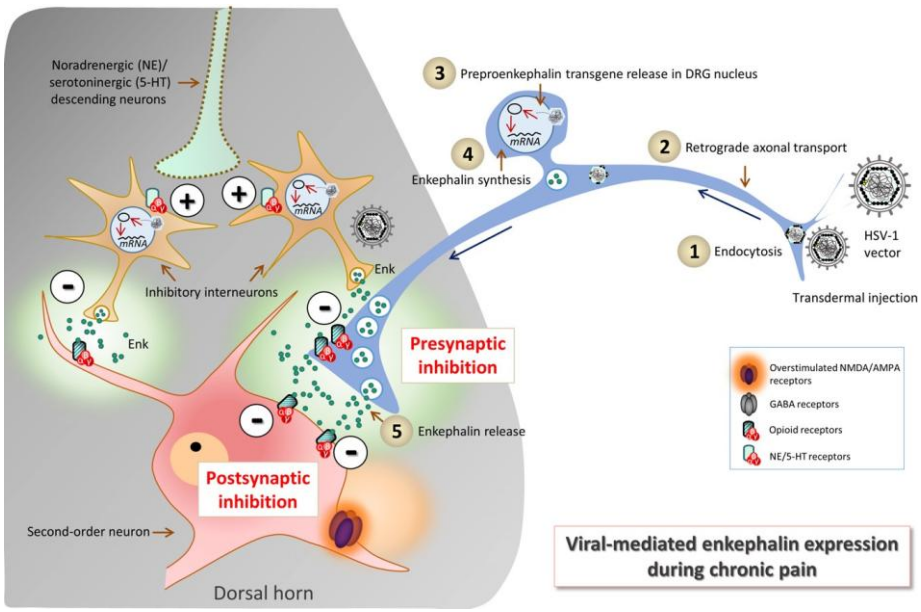

Fig. 16. HSV-mediated enkephalin (Enk) expression in chronic pain conditions. (1) Intradermally injected HSV particles are taken up into sensory nerve endings. (2) The viral nucleocapsid is retrogradely transported to the neuronal perikaryon in the dorsal root ganglion (DRG). (3) The DNA delivered by the HSV vector remains in the nucleus of the host cell and is transcribed by the host transcription machinery. (4) The synthesized Enk is transported to the presynaptic terminals of primary nociceptive afferents, where it is released (5). This Enk can activate opioid receptors that are found presynaptically on the terminals of primary nociceptive afferents. HSV vectors can also spread transsynaptically from neuron to neuron and can induce expression of Enk in other neurons of the CNS. Copyright © 2016 Elsevier Inc. (*148*)

4. Nanomedicine

Recently, application of nanotechnology in drug delivery has attracted great attention. It allowed the development of nanoparticle-based drug formulations (nanomedicines) able to deliver drugs to specific tissues and provide controlled release. This targeted and sustained drug delivery may decrease the drug related toxicity and increase patient's compliance with less frequent drug administrations. Nanomedicines are, on the other hand, very useful to increase drug stability, aqueous solubility, absorption and bioavailability.

In the past few decades, considerable attention has been focused on the development of novel drug delivery systems for peptide drugs in order to protect them from enzymatic degradation and to carry the transported peptides to the site of action.

As mentioned before, a majority of the opioid receptors exists in the central nervous system. However, the accessibility of the administered neuropeptides to their receptors in the brain is insurmountably restricted by the blood-brain-barrier (BBB), which is a highly selective semi-permeable hurdle that separates the blood circulation from the brain. The same type of barrier exists also in the spinal cord and is called the blood-spinal cord barrier (BSCB)(*149*). The BBB controls the CNS homeostasis, allows the proper neuronal function, as well as, the protection of the neural tissue from toxins and pathogens. The presence of tight junctions between adjacent endothelial cells forms the most tight cell-to-cell connection. There are several natural transport routes by which molecules can cross the BBB or the BSCB (Fig. 17). Small water-soluble molecules simply diffuse through the tight junctions when small lipid soluble substances, like alcohol and steroid hormones,

penetrate transcellularly. However, with regard to the other essential molecules for CNS, they take specific transport routes such as transport proteins (carriers), specific receptor-mediated or vesicular mechanisms (adsorptive transcytosis) to cross the BBB (*150*). Highly hydrophilic molecules, such as the neuropeptides with molecular weights often exceeding 500 Da, are not able to cross the BBB using these natural transport routes. Thus, the conception of drug delivery systems protecting the neuropeptides from degradation and allowing them to reach the opioid receptors located in the nervous system is a challenging goal. Indeed, despite numerous attempts, only few nanoparticulate drug delivery systems could be applied to enkephalins or enkephalin derivatives as reported below.

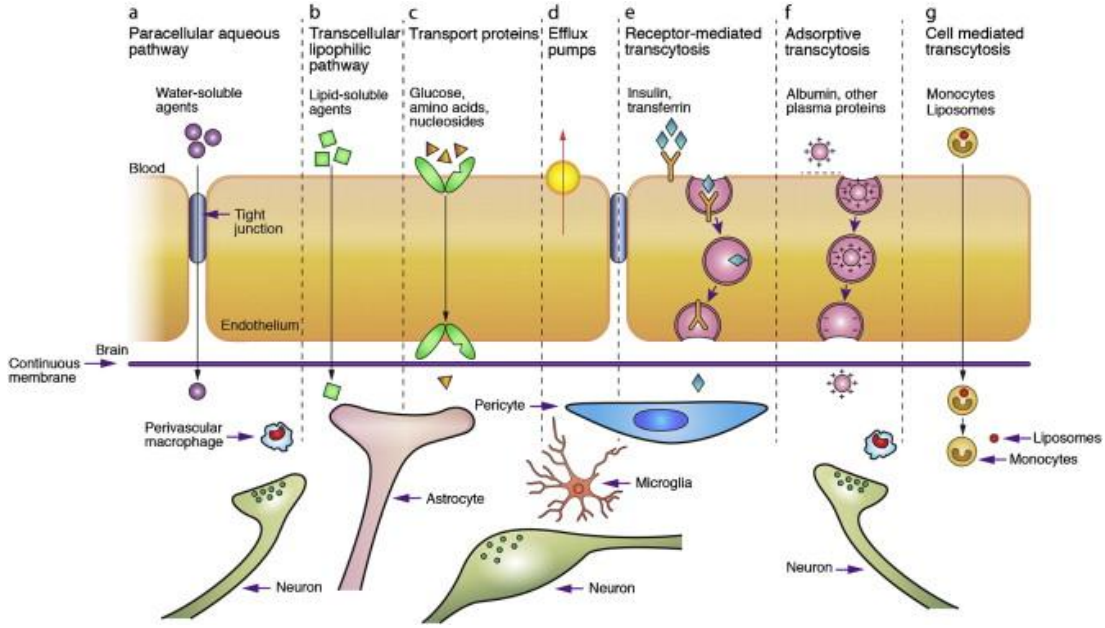

Fig. 17. Transport routes across the BBB.

Poly (butylcyanoacrylate) (PBCA) nanoparticles (NPs) were the first polymer-based nanoparticle system used to deliver drugs to the CNS (*151-155*). In these first studies, dalargin (Tyr-D-Ala-Gly-Phe-Leu-Arg), a synthetic analog of enkephalin, was incorporated onto the surface of NPs before coating with polysorbate 80. *In vivo* studies demonstrated that dalargin-loaded PBCA particles exhibited an anti-nociceptive effect (*152, 156*). More extended studies showed that polysorbate 80 (also known as Tween 80) appeared to enhance the CNS penetration of systemically-delivered polymer nanoparticles (*153, 157, 158*). Concerning the mechanism of action, Kreuter et al. hypothesized that apolipoproteins B and E were involved in the mediation of polysorbate 80-coated PBCA NPs transport across the BBB. Polysorbate 80-coated NPs could, indeed, adsorb these apolipoproteins from the blood circulation after iv injection and subsequently ressemble lipoprotein particles to undergo endocytosis by brain capillary endothelial cells (receptor-mediated endocytosis) (*155, 159, 160*). This mechanism is, however, still controversial (*161*). Of note, the potential toxicity associated with polysorbate 80-coated PBCA nanoparticles is one of the important concerns remaining with this approach (*162*) since polysorbate 80 was shown to induce BBB disturbance following i.v. injection (*163, 164*).

Among all polymers, poly(lactic-co-glycolic acid) (PLGA) was the most widely-applied in biology and biomedicine fields. Indeed, these biocompatible and biodegradable polymers decompose inside the body in non-toxic natural byproducts such as water and carbon dioxide. These biomaterials were approved by the FDA for clinical use in humans (*165*), and have been extensively envisaged for the

vectorization of drugs, proteins and various other macromolecules such as DNA, RNA and peptides. In that respect, among neuropeptides, only Dalargin was incorporated into PLGA or PEGylated PLGA NPs (*166*). However, no *in vivo* studies have been reported so far.

Chitosan is another interesting polymer that has been extensively used in medical application. It is either partially or fully deacetylated chitin, giving the chitosan nanoparticles a positive charge. This mucoadhesive biocompatible polymer was approved by the U.S. FDA for dietary use and wound dressing applications (*167*). However, positively charged chitosan is only soluble in acidic conditions. On the contrary, Trimethyl chitosan (TMC) is a water soluble positively charged quaternized chitosan derivative, devoid of toxicity and presenting the same mucoadhesive properties than chitosan. LENK-loaded TMC nanoparticles has been designed for brain delivery of LENK via the nasal route (*168*). This readily accessible route of administration is of great interest for delivering hydrophilic drugs to the brain, along the olfactory and trigeminal nerve pathways. Indeed, it is known that nasal mucosa has a highly vascularized epithelium, a porous and easily accessible endothelial membrane and a large surface area for rapid drug absorption. As a cationic ligand, TMC was supposed to facilitate the active transport of nanoparticles via absorption-mediated transcytosis through the BBB. Enhanced brain uptake of LENK, as well as, significant improved antinociceptive effect were observed with this nanoformulation.

The group of I. F. Uchegbu has proposed a strategy for Leu-enkephalin (LENK) brain delivery via oral route. For this purpose, they developed palmitic LENK prodrug nanofibers coated with chitosan amphiphile polymer (GCPQ). The oral route administration of this nanoparticle-prodrug formulation increased the brain drug levels by 67% and significantly increased LENK's antinociceptive activity (*169*). In that respect, this technology increased the upper gastrointestinal drug residence time due to the adherence of GCPQ NPs to the gastrointestinal mucosa. Once absorbed into the blood the prodrug is bioconverted to LENK by plasma and liver esterases (*170-172*). Of note, a nanoformulation of native LENK coated by chitosan polymer (LENK-GCPQ) exhibited similar brain levels of LENK, while the pharmacodynamic activity was shorter in duration. These results are quite surprising since the bioavailability of nanoparticles after oral administration remains in general very low. And since 2012, there was no follow-up concerning this approach.

The use of liposomes as drug carriers for transdermal delivery of Leu-Enkephalin (LENK) using iontophoretic transport was also investigated by Ajay K. Banga et. al. The experiments were conducted under pH conditions corresponding to LENK isoelectric point and were performed using human cadaver skin (*173, 174*). This preliminary *ex vivo* study indicated that the liposomal formulation prolonged the protection of the LENK from degradation which occured into the skin by proteolytic enzymes. However, once released from the liposomes during transdermal transport, the neuropeptide underwent rapid degradation within the skin.

Reference

1. C. J. Woolf, What is this thing called pain? *The Journal of Clinical Investigation* **120**, 3742-3744 (2010).
2. M. J. Millan, The induction of pain: an integrative review. *Progress in Neurobiology* **57**, 1-164 (1999).
3. I. Tavares, I. Martins, in *Gene Therapy - Tools and Potential Applications*. (2013), chap. Chapter 28.

4. B. Heppelmann, K. Messlinger, W. F. Neiss, R. F. Schmidt, Fine sensory innervation of the knee joint capsule by group III and group IV nerve fibers in the cat. *Journal of Comparative Neurology* **351**, 415-428 (1995).
5. A. E. Olesen, T. Andresen, C. Staahl, A. M. Drewes, Human Experimental Pain Models for Assessing the Therapeutic Efficacy of Analgesic Drugs. *Pharmacological Reviews* **64**, 722 (2012).
6. R. Milner, C. Doherty, in *Nerves and Nerve Injuries*, R. S. Tubbs, E. Rizk, M. M. Shoja, M. Loukas, N. Barbaro, R. J. Spinner, Eds. (Academic Press, San Diego, 2015), pp. 3-22.
7. M. S. Gold, G. F. Gebhart, Nociceptor sensitization in pain pathogenesis. *Nature Medicine* **16**, 1248 (2010).
8. C. Sherrington, The Integrative Action of the Nervous System. *The Journal of Nervous and Mental Disease* **34**, 801-802 (1907).
9. *2. Mechanisms of Pain*. National Research Council (US) Committee on Recognition and Alleviation of Pain in Laboratory Animals. Recognition and Alleviation of Pain in Laboratory Animals. (Washington (DC): National Academies Press (US), 2009).
10. C. J. Woolf, G. J. Bennett, M. Doherty, R. Dubner, B. Kidd, M. Koltzenburg, R. Lipton, J. D. Loeser, R. Payne, E. Torebjork, Towards a mechanism-based classification of pain? *PAIN* **77**, 227-229 (1998).
11. Focus on pain. *Nature Neuroscience* **17**, 145 (2014).
12. S. Lolignier, N. Eijkelkamp, J. N. Wood, Mechanical allodynia. *Pflügers Archiv - European Journal of Physiology* **467**, 133-139 (2015).
13. K. P. Grichnik, F. M. Ferrante, The difference between acute and chronic pain. *Mt Sinai J Med* **58**, 217-220 (1991).
14. D. Julius, A. I. Basbaum, Molecular mechanisms of nociception. *Nature* **413**, 203 (2001).
15. K. M. Smith-Edwards, J. J. DeBerry, J. L. Saloman, B. M. Davis, C. J. Woodbury, Profound alteration in cutaneous primary afferent activity produced by inflammatory mediators. *eLife* **5**, e20527 (2016).
16. Y. Zuo, N. M. Perkins, D. J. Tracey, C. L. Geczy, Inflammation and hyperalgesia induced by nerve injury in the rat: a key role of mast cells. *Pain* **105**, 467-479 (2003).
17. X. Zhang, J. Huang, P. A. McNaughton, NGF rapidly increases membrane expression of TRPV1 heat-gated ion channels. *The EMBO journal* **24**, 4211-4223 (2005).
18. F. Maingret, B. Coste, F. Padilla, N. Clerc, M. Crest, S. M. Korogod, P. Delmas, Inflammatory mediators increase Nav1.9 current and excitability in nociceptors through a coincident detection mechanism. *The Journal of general physiology* **131**, 211-225 (2008).
19. E. Brodin, L. Olgart, Neurobiology : General considerations – from acute to chronic pain. *Conference Proceedings*, (2015).
20. L. Terenius, Stereospecific Interaction Between Narcotic Analgesics and a Synaptic Plasma Membrane Fraction of Rat Cerebral Cortex. *Acta Pharmacologica et Toxicologica* **32**, 317-320 (1973).
21. C. B. Pert, S. H. Snyder, Opiate Receptor: Demonstration in Nervous Tissue. *Science* **179**, 1011 (1973).
22. E. J. Simon, J. M. Hiller, I. Edelman, Stereospecific Binding of the Potent Narcotic Analgesic [(3)H]Etorphine to Rat-Brain Homogenate. *Proceedings of the National Academy of Sciences of the United States of America* **70**, 1947-1949 (1973).

23. W. R. Martin, C. G. Eades, J. A. Thompson, R. E. Huppler, P. E. Gilbert, The effects of morphine- and nalorphine- like drugs in the nondependent and morphine-dependent chronic spinal dog. *Journal of Pharmacology and Experimental Therapeutics* **197**, 517 (1976).
24. J. A. H. Lord, A. A. Waterfield, J. Hughes, H. W. Kosterlitz, Endogenous opioid peptides: multiple agonists and receptors. *Nature* **267**, 495 (1977).
25. B. L. Kieffer, Recent advances in molecular recognition and signal transduction of active peptides: Receptors for opioid peptides. *Cellular and Molecular Neurobiology* **15**, 615-635 (1995).
26. B. L. Kieffer, K. Befort, C. Gaveriaux-Ruff, C. G. Hirth, The delta-opioid receptor: isolation of a cDNA by expression cloning and pharmacological characterization. *Proceedings of the National Academy of Sciences of the United States of America* **89**, 12048-12052 (1992).
27. M. Satoh, M. Minami, Molecular pharmacology of the opioid receptors. *Pharmacology & therapeutics* **68**, 343-364 (1995).
28. J. Hughes, T. W. Smith, H. W. Kosterlitz, L. A. Fothergill, B. A. Morgan, H. R. Morris, Identification of two related pentapeptides from the brain with potent opiate agonist activity. *Nature* **258**, 577 (1975).
29. B. M. Cox, A. Goldstein, C. H. Hi, Opioid activity of a peptide, beta-lipotropin-(61-91), derived from beta-lipotropin. *Proceedings of the National Academy of Sciences of the United States of America* **73**, 1821-1823 (1976).
30. A. Goldstein, S. Tachibana, L. I. Lowney, M. Hunkapiller, L. Hood, Dynorphin-(1-13), an extraordinarily potent opioid peptide. *Proceedings of the National Academy of Sciences of the United States of America* **76**, 6666-6670 (1979).
31. J.-L. Butour, C. Moisand, H. Mazarguil, C. Mollereau, J.-C. Meunier, Recognition and activation of the opioid receptor-like ORL1 receptor by nociceptin, nociceptin analogs and opioids. *European Journal of Pharmacology* **321**, 97-103 (1997).
32. R. Al-Hasani, M. R. Bruchas, Molecular Mechanisms of Opioid Receptor-Dependent Signaling and Behavior. *Anesthesiology* **115**, 1363-1381 (2011).
33. M. Filizola, L. A. Devi, Grand opening of structure-guided design for novel opioids. *Trends in Pharmacological Sciences* **34**, 6-12 (2013).
34. K. Sriram, P. A. Insel, G Protein-Coupled Receptors as Targets for Approved Drugs: How Many Targets and How Many Drugs? *Molecular Pharmacology* **93**, 251 (2018).
35. C. Stein, M. Schäfer, H. Machelska, Attacking pain at its source: new perspectives on opioids. *Nature Medicine* **9**, 1003-1008 (2003).
36. C. Stein, M. J. Millan, T. S. Shippenberg, K. Peter, A. Herz, Peripheral opioid receptors mediating antinociception in inflammation. Evidence for involvement of mu, delta and kappa receptors. *Journal of Pharmacology and Experimental Therapeutics* **248**, 1269 (1989).
37. C. Zollner, C. Stein, Opioids. *Handb Exp Pharmacol*, 31-63 (2007).
38. M. Sobczak, M. Sałaga, M. A. Storr, J. Fichna, Physiology, signaling, and pharmacology of opioid receptors and their ligands in the gastrointestinal tract: current concepts and future perspectives. *Journal of Gastroenterology* **49**, 24-45 (2014).
39. L. Terenius, A. Wahlström, Search for an Endogenous Ligand for the Opiate Receptor. *Acta Physiologica Scandinavica* **94**, 74-81 (1975).
40. J. Hughes, Isolation of an endogenous compound from the brain with pharmacological properties similar to morphine. *Brain Research* **88**, 295-308 (1975).

41. J. Hughes, T. Smith, B. Morgan, L. Fothergill, Purification and properties of enkephalin — The possible endogenous ligand for the morphine receptor. *Life Sciences* **16**, 1753-1758 (1975).
42. A. F. Bradbury, D. G. Smyth, C. R. Snell, N. J. M. Birdsall, E. C. Hulme, C fragment of lipotropin has a high affinity for brain opiate receptors. *Nature* **260**, 793 (1976).
43. A. Goldstein, W. Fischli, L. I. Lowney, M. Hunkapiller, L. Hood, Porcine pituitary dynorphin: complete amino acid sequence of the biologically active heptadecapeptide. *Proceedings of the National Academy of Sciences of the United States of America* **78**, 7219-7223 (1981).
44. V. Höllt, Multiple endogenous opioid peptides. *Trends in Neurosciences* **6**, 24-26 (1983).
45. J. Anna, F. Jakub, J. Tomasz, Opioid Receptors and their Ligands. *Current Topics in Medicinal Chemistry* **4**, 1-17 (2004).
46. J. C. Froehlich, Opioid peptides. *Alcohol Health Res World* **21**, 132-136 (1997).
47. J. Hughes, H. W. Kosterlitz, T. W. Smith, THE DISTRIBUTION OF METHIONINE-ENKEPHALIN AND LEUCINE-ENKEPHALIN IN THE BRAIN AND PERIPHERAL TISSUES. *British Journal of Pharmacology* **120**, 428-436 (2011).
48. C. Stein, Opioid Receptors. *Annual Review of Medicine* **67**, 433-451 (2016).
49. C. Stein, J. D. Clark, U. Oh, M. R. Vasko, G. L. Wilcox, A. C. Overland, T. W. Vanderah, R. H. Spencer, Peripheral mechanisms of pain and analgesia. *Brain Research Reviews* **60**, 90-113 (2009).
50. C. Zöllner, S. A. Mousa, O. Fischer, H. L. Rittner, M. Shaqura, A. Brack, M. Shakibaei, W. Binder, F. Urban, C. Stein, M. Schäfer, Chronic morphine use does not induce peripheral tolerance in a rat model of inflammatory pain. *The Journal of Clinical Investigation* **118**, 1065-1073 (2008).
51. A. E. Takemori, P. S. Portoghese, Evidence for the interaction of morphine with kappa and delta opioid receptors to induce analgesia in beta-funaltrexamine-treated mice. *Journal of Pharmacology and Experimental Therapeutics* **243**, 91 (1987).
52. S. Hua, P. J. Cabot, Pain—novel targets and new technologies. *Frontiers in Pharmacology* **5**, 211 (2014).
53. C. Stein, A. H. Hassan, R. Przewłocki, C. Gramsch, K. Peter, A. Herz, Opioids from immunocytes interact with receptors on sensory nerves to inhibit nociception in inflammation. *Proceedings of the National Academy of Sciences* **87**, 5935-5939 (1990).
54. C. Stein, H. Machelska, Modulation of Peripheral Sensory Neurons by the Immune System: Implications for Pain Therapy. *Pharmacological Reviews* **63**, 860 (2011).
55. C. Stein, M. J. Millan, A. Yassouridis, A. Herz, Antinociceptive effects of μ- and κ-agonists in inflammation are enhanced by a peripheral opioid receptor-specific mechanism. *European Journal of Pharmacology* **155**, 255-264 (1988).
56. K. Iwaszkiewicz, J. Schneider, S. Hua, Targeting peripheral opioid receptors to promote analgesic and anti-inflammatory actions. *Frontiers in Pharmacology* **4**, (2013).
57. E. M. Jutkiewicz, RB101-mediated Protection of Endogenous Opioids: Potential Therapeutic Utility? *CNS Drug Reviews* **13**, 192-205 (2007).
58. J. E. Linley, K. Rose, L. Ooi, N. Gamper, Understanding inflammatory pain: ion channels contributing to acute and chronic nociception. *Pflügers Archiv - European Journal of Physiology* **459**, 657-669 (2010).
59. J.-M. Zhang, J. An, Cytokines, Inflammation and Pain. *International anesthesiology clinics* **45**, 27-37 (2007).

60. C. M. Cahill, A. Morinville, C. Hoffert, D. O'Donnell, A. Beaudet, Up-regulation and trafficking of δ opioid receptor in a model of chronic inflammation: implications for pain control. *Pain* **101**, 199-208 (2003).
61. C. Zöllner, M. A. Shaqura, C. P. Bopaiah, S. Mousa, C. Stein, M. Schäfer, Painful Inflammation-Induced Increase in μ-Opioid Receptor Binding and G-Protein Coupling in Primary Afferent Neurons. *Molecular Pharmacology* **64**, 202 (2003).
62. I. Antonijevic, S. A. Mousa, M. Schafer, C. Stein, Perineurial defect and peripheral opioid analgesia in inflammation. *The Journal of Neuroscience* **15**, 165 (1995).
63. M. D. Heike L. Rittner, P. D. S. Amasheh, M. D. R. Moshourab, P. D. D. Hackel, P. D. R.-S. Yamdeu, P. D. Shaaban A. Mousa, M. D. M. Fromm, M. D. C. Stein, M. D. A. Brack, Modulation of Tight Junction Proteins in the Perineurium to Facilitate Peripheral Opioid Analgesia. *Anesthesiology* **116**, 1323-1334 (2012).
64. D. Labuz, M. Ö. Celik, A. Zimmer, H. Machelska, Distinct roles of exogenous opioid agonists and endogenous opioid peptides in the peripheral control of neuropathy-triggered heat pain. *Scientific Reports* **6**, 32799 (2016).
65. M. Busch-Dienstfertig, C. Stein, Opioid receptors and opioid peptide-producing leukocytes in inflammatory pain – Basic and therapeutic aspects. *Brain, Behavior, and Immunity* **24**, 683-694 (2010).
66. K. S. Iwaszkiewicz, J. J. Schneider, S. Hua, Targeting peripheral opioid receptors to promote analgesic and anti-inflammatory actions. *Frontiers in pharmacology* **4**, 132-132 (2013).
67. H. Machelska, J. K. Schopohl, S. A. Mousa, D. Labuz, M. Schäfer, C. Stein, Different mechanisms of intrinsic pain inhibition in early and late inflammation. *Journal of Neuroimmunology* **141**, 30-39 (2003).
68. E. Lacko, A. Varadi, R. Rapavi, F. Zador, P. Riba, S. Benyhe, A. Borsodi, S. Hosztafi, J. Timar, B. Noszal, S. Furst, M. Al-Khrasani, A Novel μ-Opioid Receptor Ligand with High In Vitro and In Vivo Agonist Efficacy. *Current Medicinal Chemistry* **19**, 4699-4707 (2012).
69. E. Lackó, P. Riba, Z. Giricz, A. Váradi, L. Cornic, M. Balogh, K. Király, K. Csekő, S. A. Mousa, S. Hosztafi, M. Schäfer, Z. S. Zádori, Z. Helyes, P. Ferdinandy, S. Fürst, M. Al-Khrasani, New Morphine Analogs Produce Peripheral Antinociception within a Certain Dose Range of Their Systemic Administration. *Journal of Pharmacology and Experimental Therapeutics* **359**, 171 (2016).
70. S. González-Rodríguez, M. A. Quadir, S. Gupta, K. A. Walker, X. Zhang, V. Spahn, D. Labuz, A. Rodriguez-Gaztelumendi, M. Schmelz, J. Joseph, M. K. Parr, H. Machelska, R. Haag, C. Stein, Polyglycerol-opioid conjugate produces analgesia devoid of side effects. *eLife* **6**, e27081 (2017).
71. I. M. Goldstein, Lysosomal hydrolases and inflammation: mechanisms of enzyme release from polymorphonuclear leukocytes. *Journal of Endodontics* **3**, 329-333 (1977).
72. J. Schnyder, M. Baggiolini, Secretion of lysosomal hydrolases by stimulated and nonstimulated macrophages. *The Journal of experimental medicine* **148**, 435-450 (1978).
73. K. Fosgerau, T. Hoffmann, Peptide therapeutics: current status and future directions. *Drug Discovery Today* **20**, 122-128 (2015).
74. J. V. Aldrich, J. P. McLaughlin, Opioid Peptides: Potential for Drug Development. *Drug discovery today. Technologies* **9**, e23-e31 (2012).
75. J. E. Zadina, M. R. Nilges, J. Morgenweck, X. Zhang, L. Hackler, M. B. Fasold, Endomorphin analog analgesics with reduced abuse liability, respiratory depression, motor

impairment, tolerance, and glial activation relative to morphine. *Neuropharmacology* **105**, 215-227 (2016).

76. J. D. Belluzzi, N. Grant, V. Garsky, D. Sarantakis, C. D. Wise, L. Stein, Analgesia induced in vivo by central administration of enkephalin in rat. *Nature* **260**, 625 (1976).
77. J.-K. Chang, B. T. W. Fong, A. Pert, C. B. Pert, Opiate receptor affinities and behavioral effects of enkephalin: Structure-activity relationship of ten synthetic peptide analogues. *Life Sciences* **18**, 1473-1481 (1976).
78. A. Dupont, L. Cusan, M. Garon, G. Alvarado-Urbina, F. Labrie, Extremely rapid degradation of [3H] methionine-enkephalin by various rat tissues in vivo and in vitro. *Life Sciences* **21**, 907-914 (1977).
79. J. M. Hambrook, B. A. Morgan, M. J. Rance, C. F. C. Smith, Mode of deactivation of the enkephalins by rat and human plasma and rat brain homogenates. *Nature* **262**, 782 (1976).
80. M. Fujino, S. Shinagawa, K. Kawai, H. Ishii, Tetrapeptide acyl-hydrazide analogs of enkephalin. *The Science of Nature* **66**, 625-626 (1979).
81. N. Pencheva, J. Pospišek, L. Hauzerova, T. Barth, P. Milanov, Activity profiles of dalargin and its analogues in μ-, δ- and κ-opioid receptor selective bioassays. *British Journal of Pharmacology* **128**, 569-576 (1999).
82. D. H. Coy, A. J. Kastin, A. V. Schally, O. Morin, N. G. Caron, F. Labrie, J. M. Walker, R. Fertel, G. G. Berntson, C. A. Sandman, Synthesis and opioid activities of stereoisomers and other D-amino acid analogs of methionine-enkephalin. *Biochemical and Biophysical Research Communications* **73**, 632-638 (1976).
83. J. DiMaio, P. W. Schiller, A cyclic enkephalin analog with high in vitro opiate activity. *Proceedings of the National Academy of Sciences of the United States of America* **77**, 7162-7166 (1980).
84. K. A. Witt, T. P. Davis, CNS drug delivery: Opioid peptides and the blood-brain barrier. *The AAPS Journal* **8**, E76-E88 (2006).
85. D. E. Benovitz, A. F. Spatola, Enkephalin pseudopeptides: Resistance to in vitro proteolytic degradation afforded by amide bond replacements extends to remote sites. *Peptides* **6**, 257-261 (1985).
86. J. S. Morley, Structure-Activity Relationships of Enkephalin-Like Peptides. *Annual Review of Pharmacology and Toxicology* **20**, 81-110 (1980).
87. J. I. Székely, Z. Dunai-Kovács, E. Miglécz, A. Z. Rónai, I. Berzétei, in *Opiate Receptors and the Neurochemical Correlates of Pain*. (Pergamon, 1980), pp. 79-92.
88. C. B. Pert, A. Pert, J. K. Chang, B. T. Fong, (D-Ala2)-Met-enkephalinamide: a potent, long-lasting synthetic pentapeptide analgesic. *Science* **194**, 330 (1976).
89. E. I. Kalenikova, O. F. Dmitrieva, N. V. Korobov, S. V. Zhukovsky, V. A. Tischenko, V. A. Vinogradov, Pharmacokinetics of dalargine. *Voprosy Meditsinskoi Khimii* **34**, 75-83 (1988).
90. K. M. Sivanandaiah, S. Gurusiddappa, D. C. Gowda, New analogues of leucine-methionine-enkephalin. *Journal of Biosciences* **13**, 181-187 (1988).
91. S. Bajusz, A. Z. Rónai, J. I. Székely, L. Gráf, Z. Dunai-Kovács, I. Berzétei, A superactive antinociceptive pentapeptide, (D‐Met2,Pro5)‐enkephalinamide. *FEBS Letters* **76**, 91-92 (1977).
92. S. Bajusz, A. Z. Ronai, J. I. Szekely, Z. Dunai-Kovacs, I. Berzetei, L. Graf, Enkephalin analogs with enhanced opiate activity. *Acta Biochim Biophys Acad Sci Hung* **11**, 305-309 (1976).

93. J. I. Székely, A. Z. Rónai, Z. Dunai-Kovács, E. Miglécz, I. Berzétri, S. Bajusz, L. Gráf, (D-MET2, PRO5)-enkephalinamide: a potent morphine-like analgesic. *European Journal of Pharmacology* **43**, 293-294 (1977).
94. D. Roemer, H. H. Buescher, R. C. Hill, J. Pless, W. Bauer, F. Cardinaux, A. Closse, D. Hauser, R. Huguenin, A synthetic enkephalin analogue with prolonged parenteral and oral analgesic activity. *Nature* **268**, 547 (1977).
95. D. Yamashiro, L.-f. Tseng, C. H. Li, [D-Thr2, Thz5]- and [D-Met2, Thz5]-enkephalinamides: Potent analgesics by intravenous injection. *Biochemical and Biophysical Research Communications* **78**, 1124-1129 (1977).
96. G. Luca, M. Rossella De, C. Lucia, Chemical Modifications Designed to Improve Peptide Stability: Incorporation of Non-Natural Amino Acids, Pseudo-Peptide Bonds, and Cyclization. *Current Pharmaceutical Design* **16**, 3185-3203 (2010).
97. S. H. Joo, Cyclic Peptides as Therapeutic Agents and Biochemical Tools. *Biomolecules & Therapeutics* **20**, 19-26 (2012).
98. R. T. Borchardt, Optimizing oral absorption of peptides using prodrug strategies. *Journal of Controlled Release* **62**, 231-238 (1999).
99. G. M. Pauletti, S. Gangwar, G. T. Knipp, M. M. Nerurkar, F. W. Okumu, K. Tamura, T. J. Siahaan, R. T. Borchardt, Structural requirements for intestinal absorption of peptide drugs. *Journal of Controlled Release* **41**, 3-17 (1996).
100. A. Bak, O. S. Gudmundsson, S. Gangwar, G. J. Friis, T. J. Siahaan, R. T. Borchardt, Synthesis and evaluation of the physicochemical properties of esterase‐sensitive cyclic prodrugs of opioid peptides using an (acyloxy)alkoxy linker. *The Journal of Peptide Research* **53**, 393-402 (2003).
101. O. S. Gudmundsson, D. G. Vander Velde, S. D. S. Jois, A. Bak, T. J. Siahaan, R. T. Borchardt, The effect of conformation of the acyloxyalkoxy‐based cyclic prodrugs of opioid peptides on their membrane permeability. *The Journal of Peptide Research* **53**, 403-413 (2003).
102. B. Wang, W. Wang, H. Zhang, D. Shan, K. Nimkar, O. Gudmundsson, S. Gangwar, T. Siahaan, R. T. Borchardt, Synthesis and evaluation of the physicochemical properties of esterase‐sensitive cyclic prodrugs of opioid peptides using coumarinic acid and phenylpropionic acid linkers. *The Journal of Peptide Research* **53**, 370-382 (2003).
103. P. S. Burton, R. A. Conradi, N. F. H. Ho, A. R. Hilgers, R. T. Borchardt, How Structural Features Influence the Biomembrane Permeability of Peptides. *Journal of Pharmaceutical Sciences* **85**, 1336-1340 (1996).
104. A. Bak, O. S. Gudmundsson, G. J. Friis, T. J. Siahaan, R. T. Borchardt, Acyloxyalkoxy-based cyclic prodrugs of opioid peptides: evaluation of the chemical and enzymatic stability as well as their transport properties across Caco-2 cell monolayers. *Pharm Res* **16**, 24-29 (1999).
105. H. Ouyang, T. E. Andersen, W. Chen, R. Nofsinger, B. Steffansen, R. T. Borchardt, A comparison of the effects of p-glycoprotein inhibitors on the blood–brain barrier permeation of cyclic prodrugs of an opioid peptide (DADLE). *Journal of Pharmaceutical Sciences* **98**, 2227-2236 (2009).
106. D. B. Sherman, A. F. Spatola, W. S. Wire, T. F. Burks, T. M. D. Nguyen, P. W. Schiller, Biological activities of cyclic enkephalin pseudopeptides containing thioamides as amide bond replacements. *Biochemical and Biophysical Research Communications* **162**, 1126-1132 (1989).

107. J. V. Edwards, A. F. Spatola, C. Lemieux, P. W. Schiller, In vitro activity profiles of cyclic and linear enkephalin pseudopeptide analogs. *Biochemical and Biophysical Research Communications* **136**, 730-736 (1986).
108. Y. Li, M. R. Lefever, D. Muthu, J. M. Bidlack, E. J. Bilsky, R. Polt, Opioid glycopeptide analgesics derived from endogenous enkephalins and endorphins. *Future Medicinal Chemistry* **4**, 205-226 (2012).
109. S. V. Moradi, W. M. Hussein, P. Varamini, P. Simerska, I. Toth, Glycosylation, an effective synthetic strategy to improve the bioavailability of therapeutic peptides. *Chemical Science* **7**, 2492-2500 (2016).
110. V. Thanawala, V. J. Kadam, R. Ghosh, Enkephalinase Inhibitors: Potential Agents for the Management of Pain. *Current Drug Targets* **9**, 887-894 (2008).
111. M. Miura, M. Yoshikawa, M. Watanabe, S. Takahashi, J. Ajimi, K. Ito, M. Ito, M. Kawaguchi, H. Kobayashi, T. Suzuki, Increase in antinociceptive effect of [leu5]enkephalin after intrathecal administration of mixture of three peptidase inhibitors. *Tokai J Exp Clin Med* **38**, 62-70 (2013).
112. B. P. Roques, M. C. Fournié-Zaluski, E. Soroca, J. M. Lecomte, B. Malfroy, C. Llorens, J. C. Schwartz, The enkephalinase inhibitor thiorphan shows antinociceptive activity in mice. *Nature* **288**, 286 (1980).
113. P. Chaillet, H. Marçais-Collado, J. Costentin, C.-C. Yi, S. De La Baume, J.-C. Schwartz, Inhibition of enkepha,in metabolism by, and antinociceptive activity of, bestatin, an aminopeptidase inhibitor. *European Journal of Pharmacology* **86**, 329-336 (1983).
114. S. Bourgoin, D. Le Bars, F. Artaud, A. M. Clot, R. Bouboutou, M. C. Fournie-Zaluski, B. P. Roques, M. Hamon, F. Cesselin, Effects of kelatorphan and other peptidase inhibitors on the in vitro and in vivo release of methionine-enkephalin-like material from the rat spinal cord. *Journal of Pharmacology and Experimental Therapeutics* **238**, 360 (1986).
115. J. C. Willer, A. Roby, M. Ernst, The enkephalinase inhibitor, GB 52, does not affect nociceptive flexion reflexes nor pain sensation in humans. *Neuropharmacology* **25**, 819-822 (1986).
116. B. P. Roques, F. Noble, V. Daugé, M. C. Fournié-Zaluski, A. Beaumont, Neutral endopeptidase 24.11: structure, inhibition, and experimental and clinical pharmacology. *Pharmacological Reviews* **45**, 87 (1993).
117. M.-C. Fournie-Zaluski, R. Perdrisot, G. Gacel, J.-P. Swerts, B. P. Roques, J.-C. Schwartz, Inhibitory potency of various peptides on enkephalinase activity from mouse striatum. *Biochemical and Biophysical Research Communications* **91**, 130-135 (1979).
118. M.-C. Fournie-Zaluski, P. Chaillet, R. Bouboutou, A. Coulaud, P. Cherot, G. Waksman, J. Costentin, B. P. Roques, Analgesic effects of kelatorphan, a new highly potent inhibitor of multiple enkephalin degrading enzymes. *European Journal of Pharmacology* **102**, 525-528 (1984).
119. F. Noble, J. M. Soleilhac, E. Soroca-Lucas, S. Turcaud, M. C. Fournie-Zaluski, B. P. Roques, Inhibition of the enkephalin-metabolizing enzymes by the first systemically active mixed inhibitor prodrug RB 101 induces potent analgesic responses in mice and rats. *Journal of Pharmacology and Experimental Therapeutics* **261**, 181 (1992).
120. F. Noble, S. Turcaud, M.-C. Fournié-Zaluski, B. P. Roques, Repeated systemic administration of the mixed inhibitor of enkephalin-degrading enzymes, RB101, does not induce either antinociceptive tolerance or cross-tolerance with morphine. *European Journal of Pharmacology* **223**, 83-89 (1992).

121. F. Noble, C. Smadja, O. Valverde, R. Maldonado, P. Coric, S. Turcaud, M.-C. Fournié-Zaluski, B. P. Roques, Pain-suppressive effects on various nociceptive stimuli (thermal, chemical, electrical and inflammatory) of the first orally active enkephalin-metabolizing enzyme inhibitor RB 120. *PAIN* **73**, 383-391 (1997).
122. E. Bonnard, H. Poras, X. Nadal, R. Maldonado, M.-C. Fournié-Zaluski, B. P. Roques, Long-lasting oral analgesic effects of N-protected aminophosphinic dual ENKephalinase inhibitors (DENKIs) in peripherally controlled pain. *Pharmacology research & perspectives* **3**, e00116-e00116 (2015).
123. E. Bonnard, H. Poras, M.-C. Fournié-Zaluski, B. P. Roques, Preventive and alleviative effects of the dual enkephalinase inhibitor (Denki) PL265 in a murine model of neuropathic pain. *European Journal of Pharmacology* **788**, 176-182 (2016).
124. S. González-Rodríguez, H. Poras, L. Menéndez, A. Lastra, T. Ouimet, M.-C. Fournié-Zaluski, B. P. Roques, A. Baamonde, Synergistic combinations of the dual enkephalinase inhibitor PL265 given orally with various analgesic compounds acting on different targets, in a murine model of cancer-induced bone pain. *Scandinavian Journal of Pain* **14**, 25-38 (2017).
125. H. Chen, F. Noble, P. Coric, M.-C. Fournie-Zaluski, B. P. Roques, Aminophosphinic inhibitors as transition state analogues of enkephalin-degrading enzymes: A class of central analgesics. *Proceedings of the National Academy of Sciences* **95**, 12028 (1998).
126. H. Chen, F. Noble, A. Mothé, H. Meudal, P. Coric, S. Danascimento, B. P. Roques, P. George, M.-C. Fournié-Zaluski, Phosphinic Derivatives as New Dual Enkephalin-Degrading Enzyme Inhibitors: Synthesis, Biological Properties, and Antinociceptive Activities. *Journal of Medicinal Chemistry* **43**, 1398-1408 (2000).
127. B. P. Roques, M.-C. Fournié-Zaluski, M. Wurm, Inhibiting the breakdown of endogenous opioids and cannabinoids to alleviate pain. *Nature Reviews Drug Discovery* **11**, 292-310 (2012).
128. D. J. Campbell, Long-term neprilysin inhibition — implications for ARNIs. *Nature Reviews Cardiology* **14**, 171-186 (2016).
129. J.-C. Schwartz, J. Costentin, J.-M. Lecomte, Pharmacology of enkephalinase inhibitors. *Trends in Pharmacological Sciences* **6**, 472-476 (1985).
130. Y.-C. Chuang, L. C. Yang, P.-H. Chiang, H.-Y. Kang, W.-L. Ma, P. C. Wu, F. DeMiguel, M. B. Chancellor, N. Yoshimura, Gene gun particle encoding preproenkephalin cDNA produces analgesia against capsaicin-induced bladder pain in rats. *Urology* **65**, 804-810 (2005).
131. Y.-C. Chuang, A. K. Chou, P. C. Wu, P.-H. Chiang, T. J. Yu, L. C. Yang, N. Yoshimura, M. B. Chancellor, Gene Therapy for Bladder Pain With Gene Gun Particle Encoding Pro-Opiomelanocortin cDNA. *The Journal of Urology* **170**, 2044-2048 (2003).
132. L. Huang, D. Liu, E. Wagner, *Nonviral vectors for gene therapy : physical methods and medical translation*. Advances in Genetics (Academic Press, 2015), vol. 89.
133. D. K. Cope, W. R. Lariviere, Gene Therapy and Chronic Pain. *TheScientificWorldJOURNAL* **6**, 1066-1074 (2006).
134. O. O. Koyuncu, I. B. Hogue, L. W. Enquist, Virus infections in the nervous system. *Cell host & microbe* **13**, 379-393 (2013).
135. R. Manservigi, R. Argnani, P. Marconi, HSV Recombinant Vectors for Gene Therapy. *The open virology journal* **4**, 123-156 (2010).
136. D. C. Bloom, N. V. Giordani, D. L. Kwiatkowski, Epigenetic regulation of latent HSV-1 gene expression. *Biochimica et Biophysica Acta (BBA) - Gene Regulatory Mechanisms* **1799**, 246-256 (2010).

137. F. Catez, C. Picard, K. Held, S. Gross, A. Rousseau, D. Theil, N. Sawtell, M. Labetoulle, P. Lomonte, HSV-1 Genome Subnuclear Positioning and Associations with Host-Cell PML-NBs and Centromeres Regulate LAT Locus Transcription during Latency in Neurons. *PLOS Pathogens* **8**, e1002852 (2012).
138. C. Marwick, FDA halts gene therapy trials after leukaemia case in France. *BMJ (Clinical research ed.)* **326**, 181-181 (2003).
139. D. Wolfe, M. Mata, D. J. Fink, A human trial of HSV-mediated gene transfer for the treatment of chronic pain. *Gene therapy* **16**, 455-460 (2009).
140. J. M. Antunes Bras, A. L. Epstein, S. Bourgoin, M. Hamon, F. Cesselin, M. Pohl, Herpes Simplex Virus 1-Mediated Transfer of Preproenkephalin A in Rat Dorsal Root Ganglia. *Journal of Neurochemistry* **70**, 1299-1303 (1998).
141. S. P. Wilson, D. C. Yeomans, M. A. Bender, Y. Lu, W. F. Goins, J. C. Glorioso, Antihyperalgesic effects of infection with a preproenkephalin-encoding herpes virus. *Proceedings of the National Academy of Sciences* **96**, 3211 (1999).
142. J. Braz, C. Beaufour, A. Coutaux, A. L. Epstein, F. Cesselin, M. Hamon, M. Pohl, Therapeutic Efficacy in Experimental Polyarthritis of Viral-Driven Enkephalin Overproduction in Sensory Neurons. *The Journal of Neuroscience* **21**, 7881 (2001).
143. J. R. Goss, M. Mata, W. F. Goins, H. H. Wu, J. C. Glorioso, D. J. Fink, Antinociceptive effect of a genomic herpes simplex virus-based vector expressing human proenkephalin in rat dorsal root ganglion. *Gene Therapy* **8**, 551 (2001).
144. Y. Lu, T. A. McNearney, W. Lin, S. P. Wilson, D. C. Yeomans, K. N. Westlund, Treatment of Inflamed Pancreas with Enkephalin Encoding HSV-1 Recombinant Vector Reduces Inflammatory Damage and Behavioral Sequelae. *Molecular Therapy* **15**, 1812-1819 (2007).
145. H. Yang, T. A. McNearney, R. Chu, Y. Lu, Y. Ren, D. C. Yeomans, S. P. Wilson, K. N. Westlund, Enkephalin-encoding herpes simplex virus-1 decreases inflammation and hotplate sensitivity in a chronic pancreatitis model. *Molecular Pain* **4**, 8 (2008).
146. H. Yokoyama, K. Sasaki, M. E. Franks, W. F. Goins, J. R. Goss, W. C. de Groat, J. C. Glorioso, M. B. Chancellor, N. Yoshimura, Gene Therapy for Bladder Overactivity and Nociception with Herpes Simplex Virus Vectors Expressing Preproenkephalin. *Human Gene Therapy* **20**, 63-71 (2009).
147. D. J. Fink, J. Wechuck, M. Mata, J. C. Glorioso, J. Goss, D. Krisky, D. Wolfe, Gene therapy for pain: results of a phase I clinical trial. *Annals of neurology* **70**, 207-212 (2011).
148. C. Kibaly, H. H. Loh, P. Y. Law, in *International Review of Cell and Molecular Biology*, K. W. Jeon, L. Galluzzi, Eds. (Academic Press, 2016), vol. 327, pp. 89-161.
149. R. Daneman, A. Prat, The blood-brain barrier. *Cold Spring Harbor perspectives in biology* **7**, a020412-a020412.
150. Y. Chen, L. Liu, Modern methods for delivery of drugs across the blood–brain barrier. *Advanced Drug Delivery Reviews* **64**, 640-665 (2012).
151. P. Couvreur, P. Tulkenst, M. Roland, A. Trouet, P. Speiser, Nanocapsules: A new type of lysosomotropic carrier. *FEBS Letters* **84**, 323-326 (1977).
152. J. Kreuter, R. N. Alyautdin, D. A. Kharkevich, A. A. Ivanov, Passage of peptides through the blood-brain barrier with colloidal polymer particles (nanoparticles). *Brain Research* **674**, 171-174 (1995).
153. J. Kreuter, P. Ramge, V. Petrov, S. Hamm, S. E. Gelperina, B. Engelhardt, R. Alyautdin, H. von Briesen, D. J. Begley, Direct Evidence That Polysorbate-80-Coated Poly(Butylcyanoacrylate) Nanoparticles Deliver Drugs to the CNS via Specific Mechanisms

Requiring Prior Binding of Drug to the Nanoparticles. *Pharmaceutical Research* **20**, 409-416 (2003).

154. J. Kreuter, Nanoparticulate Systems in Drug Delivery and Targeting. *Journal of Drug Targeting* **3**, 171-173 (1995).
155. J. Kreuter, Nanoparticulate systems for brain delivery of drugs. *Advanced Drug Delivery Reviews* **47**, 65-81 (2001).
156. R. Alyautdin, D. Gothier, V. Petrov, K. Da, J. Kreuter, *Analgesic activity of the hexapeptide dalargin adsorbed on the surface of polysorbate 80-coated poly (butyl cyanoacrylate) nanoparticles*. (1995), vol. 41.
157. U. Schroeder, H. Schroeder, B. A. Sabel, Body distribution of 3HH-labelled dalargin bound to poly(butyl cyanoacrylate) nanoparticles after I.V. injections to mice. *Life Sciences* **66**, 495-502 (2000).
158. J. Kreuter, Influence of the Surface Properties on Nanoparticle-Mediated Transport of Drugs to the Brain. *Journal of Nanoscience and Nanotechnology* **4**, 484-488 (2004).
159. R. N. Alyaudtin, A. Reichel, R. Löbenberg, P. Ramge, J. Kreuter, D. J. Begley, Interaction of Poly(butylcyanoacrylate) Nanoparticles with the Blood-Brain Barrier in vivo and in vitro. *Journal of Drug Targeting* **9**, 209-221 (2001).
160. J. Kreuter, D. Shamenkov, V. Petrov, P. Ramge, K. Cychutek, C. Koch-Brandt, R. Alyautdin, Apolipoprotein-mediated Transport of Nanoparticle-bound Drugs Across the Blood-Brain Barrier. *Journal of Drug Targeting* **10**, 317-325 (2002).
161. J.-C. Olivier, Drug Transport to Brain with Targeted Nanoparticles. *NeuroRx* **2**, 108-119 (2005).
162. J.-C. Olivier, L. Fenart, R. Chauvet, C. Pariat, R. Cecchelli, W. Couet, Indirect Evidence that Drug Brain Targeting Using Polysorbate 80-Coated Polybutylcyanoacrylate Nanoparticles Is Related to Toxicity. *Pharmaceutical Research* **16**, 1836-1842 (1999).
163. M. N. Azmin, J. F. B. Stuart, A. T. Florence, The distribution and elimination of methotrexate in mouse blood and brain after concurrent administration of polysorbate 80. *Cancer Chemotherapy and Pharmacology* **14**, 238-242 (1985).
164. P. Calvo, B. Gouritin, H. Chacun, D. Desmaele, J. D'Angelo, J. P. Noel, D. Georgin, E. Fattal, J. P. Andreux, P. Couvreur, Long-circulating PEGylated polycyanoacrylate nanoparticles as new drug carrier for brain delivery. *Pharm Res* **18**, 1157-1166 (2001).
165. A. Roointan, S. Kianpour, F. Memari, M. Gandomani, S. M. Gheibi Hayat, S. Mohammadi-Samani, Poly(lactic-co-glycolic acid): The most ardent and flexible candidate in biomedicine! *International Journal of Polymeric Materials and Polymeric Biomaterials* **67**, 1028-1049 (2018).
166. Y. Chen, F. Wang, H. A. E. Benson, Effect of formulation factors on incorporation of the hydrophilic peptide dalargin into PLGA and mPEG-PLGA nanoparticles. *Peptide Science* **90**, 644-650 (2008).
167. A. M. Mohammed, T. J. Syeda, M. K. Wasan, K. E. Wasan, An Overview of Chitosan Nanoparticles and Its Application in Non-Parenteral Drug Delivery. *Pharmaceutics* **9**, (2017).
168. M. Kumar, R. S. Pandey, K. C. Patra, S. K. Jain, M. L. Soni, J. S. Dangi, J. Madan, Evaluation of neuropeptide loaded trimethyl chitosan nanoparticles for nose to brain delivery. *International Journal of Biological Macromolecules* **61**, 189-195 (2013).
169. A. Lalatsa, V. Lee, J. P. Malkinson, M. Zloh, A. G. Schätzlein, I. F. Uchegbu, A Prodrug Nanoparticle Approach for the Oral Delivery of a Hydrophilic Peptide, Leucine5-enkephalin, to the Brain. *Molecular Pharmaceutics* **9**, 1665-1680 (2012).

170. A. Lalatsa, N. L. Garrett, T. Ferrarelli, J. Moger, A. G. Schätzlein, I. F. Uchegbu, Delivery of Peptides to the Blood and Brain after Oral Uptake of Quaternary Ammonium Palmitoyl Glycol Chitosan Nanoparticles. *Molecular Pharmaceutics* **9**, 1764-1774 (2012).
171. A. Lalatsa, A. G. Schatzlein, I. F. Uchegbu, Strategies To Deliver Peptide Drugs to the Brain. *Molecular Pharmaceutics* **11**, 1081-1093 (2014).
172. A. Siew, H. Le, M. Thiovolet, P. Gellert, A. Schatzlein, I. Uchegbu, Enhanced Oral Absorption of Hydrophobic and Hydrophilic Drugs Using Quaternary Ammonium Palmitoyl Glycol Chitosan Nanoparticles. *Molecular Pharmaceutics* **9**, 14-28 (2012).
173. N. B. Vutla, G. V. Betageri, A. K. Banga, Transdermal lontophoretic Delivery of Enkephalin Formulated in Liposomes. *Journal of Pharmaceutical Sciences* **85**, 5-8 (1996).
174. V. Betageri G, B. Vutla N, K. Banga A, Liposomal Formulation and Characterization of the Opioid Peptide Leucine Enkephalin. *Pharmacy and Pharmacology Communications* **3**, 587-591 (2011).

Squalenoylation:

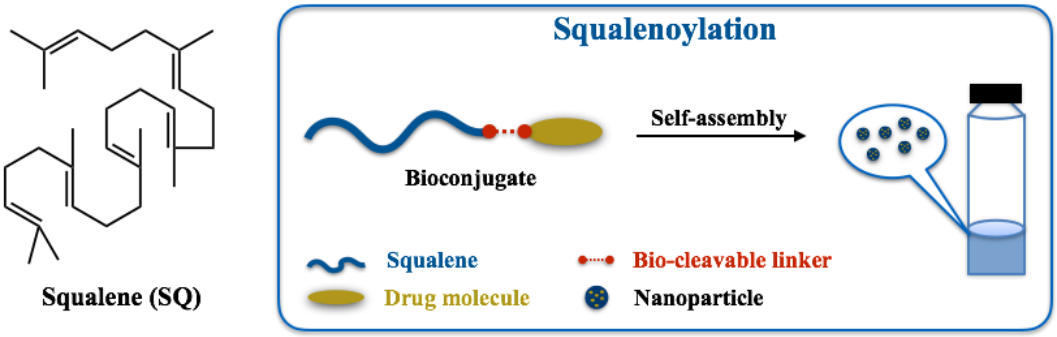

Squalenoylation technology, an innovative and original concept, allows the formation of a wide range of drug molecules as nanoparticles in order to increase their bioavailability and pharmacological efficacy.

Squalenoylation involves the linkage of squalene to therapeutic agents, in order to create squalene based bioconjugates (or prodrugs) which have the ability to form nanoparticles. Compared with other nanocarries, squalenoylation represents a novel technology with numerous advantages: 1) significant high drug loading; 2) free of the "burst" release; 3) enhanced drug concentration within targeted tissues.

Review article:

Design, Preparation and Characterization of Modular Squalene-based Nanosystems for Controlled Drug Release

Published in ***Current Topics in Medicinal Chemistry***, 2017 Jul 19

Jiao Feng, Sinda Lepetre-Mouelhi*, Patrick Couvreur

Institut Galien Paris-Sud, UMR CNRS 8612, Université Paris-Sud, Université Paris Saclay, 5 Rue J.B. Clément, 92296, Châtenay-Malabry Cedex, France

*To whom correspondence should be addressed: sinda.lepetre@u-psud.fr.

ABSTRACT OF THE ARTICLE

This article reviews the innovative and original concept the “squalenoylation”, a technology allowing the formulation of a wide range of drug molecules (both hydrophilic and lipophilic) as nanoparticles. The "squalenoylation" approach is based on the covalent linkage between the squalene, a natural and biocompatible lipid belonging to the terpenoid family, and a drug, in order to increase its pharmacological efficacy. Fundamentally, the dynamically folded conformation of squalene triggers the resulting squalene-drug bioconjugates to self-assemble as nanoparticles of 100–300 nm. In general, these nanoparticles showed long blood circulation times after intravenous administration and improved pharmacological activity with reduced side effects and toxicity. This flexible and generic technique opens exciting perspectives in the drug delivery field.

Keywords: Squalenoylation, Prodrug, Nanoassemblies, Drug loading, Oncology, Intracellular infections, Neurological disorders

1. INTRODUCTION

The use of nanotechnology in drug delivery has gained great attention in recent years. Nanocarriers can be used to increase drug stability and solubility, deliver drug to specific site in the body and thus minimize the side effects. The concept of nanocarrier was inspired by the idea of the "magic bullet", proposed by Paul Ehrlich at the beginning of 20th century (*1*). However, it was only until the 1970s that the first nanoparticles were developed by professor Peter Speiser and his colleagues (*2*). Nanocarriers have been extensively studied since then. So far, different kinds of nanocarriers have been explored, such as nanoparticles, liposomes, polymersomes, micelles, dendrimers, ultrasmall iron oxide nanoparticles (USPIO) etc. However, despite the impressive progress made in the design of various nanoparticles, only a few nanoparticle-based medicines have reached the market. In other words, currently available nanoparticle technologies have not been able to improve the activity of a great number of drugs. This is probably due to the following reasons: (i) Poor drug loading (the ratio of the transported drug to the total material), which usually does not exceed 5%. As a result, a great quantity of carrier materials needs to be administrated in order to reach a pharmacologically active concentration of the drugs, which in turn may generate toxicity and undesirable side-effects and (ii) "Burst" release of the drug immediately after intravenous administration, generally corresponding to the release of the drug fraction which is simply adsorbed (or anchored) at the surface of the nanocarrier. As a consequence, a significant fraction of the drug will be released before reaching the pharmacological target in the body, resulting in lower activity and more side effects.

Among these colloidal systems, lipid-drug conjugates (LDC) nanoparticles have exhibited considerable advantages in some cases because of their high drug payload. They have been shown to prolong drug release, decrease toxicity, improve pharmacokinetic properties, and increase the therapeutic index of the corresponding drugs (*3*). There have been some reports of LDC that already reached clinical trials (*4, 5*). In this context, Couvreur et al. have developed a novel lipid-drug conjugate nanoparticle platform based on squalene (*6*).

Squalene is a natural endogenous lipid belonging to the terpenoid family. It is an intermediate metabolite in the synthesis of cholesterol, structurally similar to beta-carotene. It is widespread in nature and with reasonable amounts found in shark liver oil, olive oil, wheat germ oil and rice bran oil. It received its name because of its occurrence in shark liver oil (Squalus spp.) (*7*). In human body, squalene is produced in the liver and the skin, transported by very low density lipoproteins (VLDL) and low density lipoprotein (LDL) in the blood, and then secreted in large quantities by the sebaceous glands (*8, 9*). It is well tolerated after exogenous administration, whether parenterally or orally, and its high oral absorption (>60%) may be used to increase the oral bioavailability of some drugs. Additionally, squalene has been extensively used as excipient in several pharmaceutical formulations for oral and parenteral administration, but it has never been used as covalent partner for drug delivery and targeting purposes before the introduction of the "squalenoylation" by Couvreur's group (*6*).

Squalenoylation involves the linkage of squalene to therapeutic agents, in order to create squalene based bioconjugates (or prodrugs) which have the ability to form nanoparticles. Since prodrugs are bioreversible derivatives that undergo an enzymatic and/or a chemical transformation *in vivo* to release the active drug, bio-cleavable linkages, such as direct ester or amide bond, have been used between squalene and the drug. It should be noted that sometimes, for chemical incompatibility reasons or steric hindrance, the synthesis of bioconjugates required the intercalation of a spacer

between the ester or amide bond and the squalene. Thus, the synthesis of various squalene-drug conjugates involves first the functionalization of one of the terminal double bond of the squalene into acid, amino or hydroxyl group, as seen in **Fig. 1**, to allow further conjugation with therapeutic molecules.

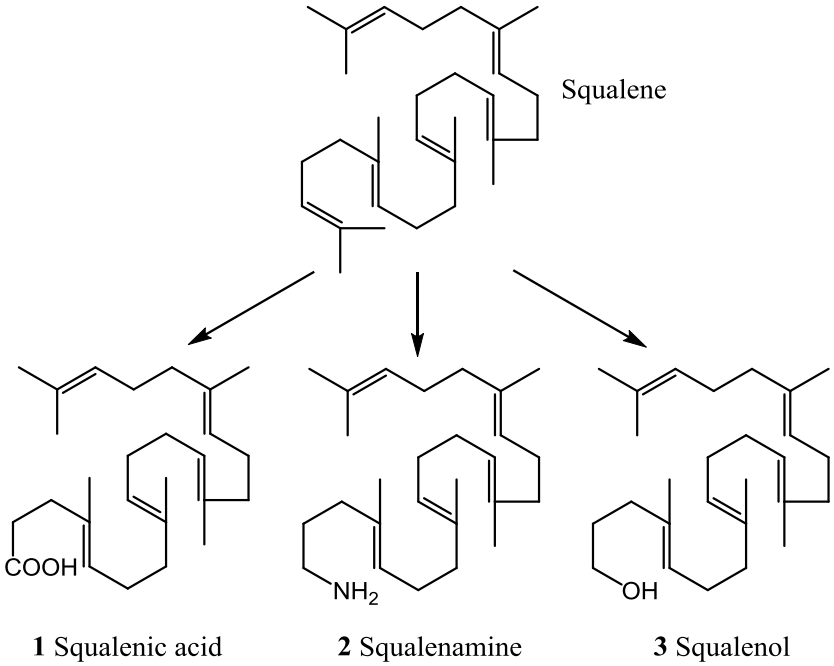

Fig. 1. Chemical structures of squalene and squalene derivatives.

Owing to the rigid structural property of squalene, the resulting squalene-drug conjugates may self-assemble in aqueous media without the use of any surfactant into compacted nanoparticles with high drug loading. The nanoparticle conformation allows protecting drug molecules from degradation/metabolization, which results in greater plasmatic half-life, when a controlled and prolonged release of the drug may also be obtained. Unlike polymer nanoparticles or liposome nanoformulations which encapsulate by physical means the active principles into their matrices, the squalene-drug conjugates nanoparticles employ a chemical encapsulation approach, thus avoiding the "burst" release (*6*). Moreover, these nanosystems facilitated drug's passage through biomembranes due to the lipophilic properties of squalene, resulting in an enhanced drug concentration within targeted tissues and cells and generating dramatic increase in drug pharmacological activity. This article aims to give an overview of recent advances in the development of squalene-based nanoparticles, a generic platform for the discovery of new nanomedicines.

2. SQUALENE-BASED BIOCONJUGATES WITH HYDROPHILIC DRUGS

2.1. Squalene-nucleoside analogue prodrugs

Nucleosides are endogenous compounds involved in the synthesis of DNA and RNA. Nucleoside analogues are chemically modified molecules that were developed to mimic their physiological counterparts in terms of cellular uptake, cellular metabolism and incorporation into newly synthesized DNA and RNA, for instance in order to inhibit DNA chain elongation. Some nucleoside analogues can also interact with and inhibit the enzymes involved in the synthesis of DNA and RNA, including

DNA or RNA polymerases, kinases, pyrimidine and purine nucleoside phosphorylase and DNA methyltransferases (*10*), etc. All these effects may lead to inhibition of cell division or viral replication. Thus nucleoside analogues have great potential in the treatment of cancer (such as cytarabine, gemcitabine, mercaptopurine), viral infection (such as didanosine, zalcitabine), rheumatologic diseases (such as azathioprine, allpurinol) and even bacterial infections (such as trimethoprim).

However, these compounds face various limitations that restrict their use. They have a short plasma half-life, undergo rapid intracellular and extracellular metabolism, and have a poor permeability across biological membranes due to their hydrophilicity. On the other hand, most of them display severe side effects because of lack of specificity and they induce resistance to treatments of cancer and infectious diseases. Squalenoylation of these hydrophilic molecules were proposed and developed to increase their therapeutic index and decrease above-mentioned side effects (*11*).

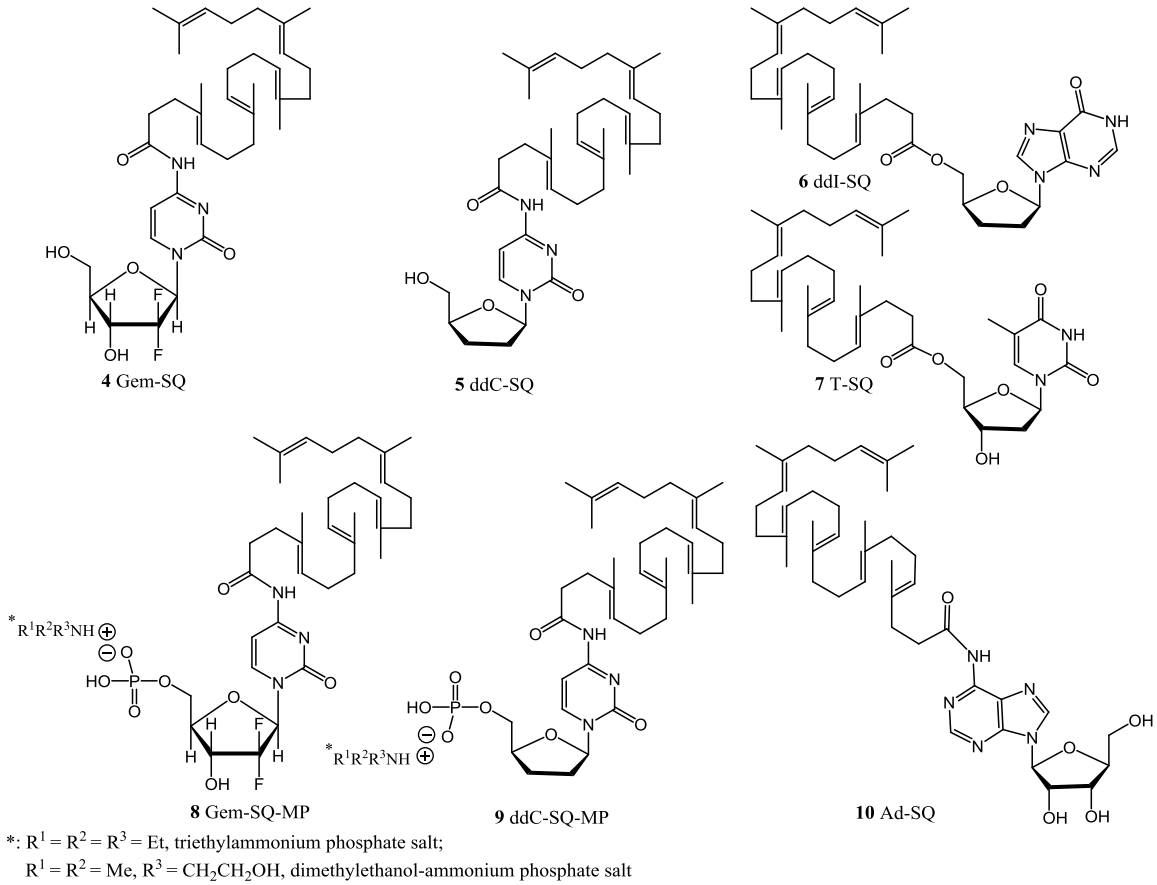

Fig. 2. Chemical structures of squalene-nucleoside (T-SQ: thymidine-squalene; Ad-SQ: adenosine-squalene), squalene-nucleoside analogue (Gem-SQ: gemcitabine-squalene; ddC-SQ: 2′,3′-dideoxycytidine-squalene; ddI-SQ: 2′,3′-dideoxyinosine-squalene) and squalene-nucleoside analogue monophosphate (Gem-SQ-MP: gemcitabine-squalene monophosphate; ddC-SQ-MP: 2′,3′-dideoxycytidine-squalene monophosphate) conjugates.

2.1.1. Squalene-Gemcitabine prodrugs

Concerning cancer treatment, “squalenoylation” was first applied to the delivery of nucleoside analogues such as gemcitabine (dFdC) in order to inhibit DNA replication in cancer cells (*6*).

Gemcitabine has been demonstrated to be active against a wide range of solid tumors, including colon, lung, pancreatic, breast, bladder, and ovarian cancers (*12, 13*). However, this molecule is rapidly metabolized in the body by deoxycytidine deaminase into the chemotherapeutically inactive uracil derivative (*14, 15*), resulting in a short plasma half-life (1.5 h). Another concern is the drug resistance due to nucleoside transporter down regulation or to deoxycytidine kinase (dCK) deficiency.

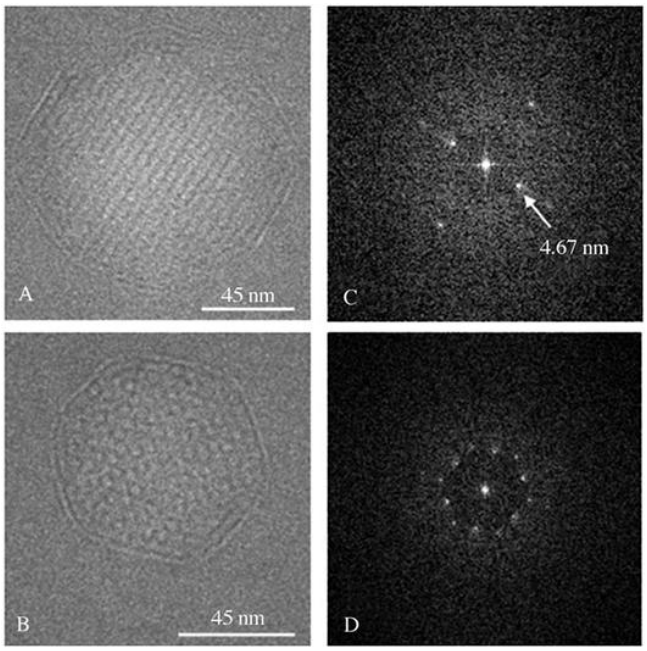

Fig. 3. Cryo-TEM images of Gem-SQ NAs. The supramolecular organization is clearly visible. NAs of hexagonal shape **(A** and **B)** are surrounded by an external shell and display an internal structure. The Fourier trans-forms of **(A)** and **(B)** assessed by ImageJ software reveal a hexagonal symmetry **(D)** between columns with a 4.67-nm periodicity **(C)**. Figures adapted with permission from [16]. © 2008 John Wiley & Sons.

Squalenoylation of gemcitabine was achieved by covalent coupling of the squalene derivative, squalenic acid, with gemcitabine. In order to protect gemcitabine from deamination, squalenic acid was linked onto the amino group of the nucleoside heterocycle through an amide bond (**Fig. 2**). The resulting gemcitabine-squalene (Gem-SQ) bioconjugates could self-organize as homogeneous nanoassemblies (NAs) with average diameter of 130 nm in aqueous solutions and with a unimodal size distribution (*6*). The use of surfactant is not necessary to provide colloidal stability of Gem-SQ NAs. The internal structure of Gem-SQ nanoparticles, using cryogenic transmission electron microscopy (cryo-TEM) and small angle X-ray scattering (SAXS), revealed an inverse hexagonal structure, with a lattice parameter of 87.7 Å, which was the first report of hexagonal-type organization with squalene derivative (**Fig. 3**). The aqueous cores of close-packed cylinders were ringed by hydrophilic gemcitabine molecules linked to squalene chains (*16, 17*). The gemcitabine loading was 41%, which is much higher than when gemcitabine was encapsulated in more conventional nanoparticles (i.e., liposomes or polymer nanoparticles). When entrapped into NAs, gemcitabine was protected from deamination after incubation in plasma (80% of the Gem-SQ remained intact after 24 h). *In vitro*, it was found that Gem-SQ was hydrolyzed and free gemcitabine released after incubation with cathepsin B and D, two lysosomal enzymes responsible for degrading amide-bearing drugs.

Gem-SQ NAs were found to be 6- to 8-fold more cytotoxic than gemcitabine free on MCK-7 and KB3-1 cells, respectively (*6*). Because, as discussed before, the induction of resistance represents an important limitation in gemcitabine treatment, murine resistant leukemia L1210 10K cells (deficiency

in deoxycytidine kinase responsible for gemcitabine phosphorylation) and human leukemia resistant cell line CEM/ARAC8C (nucleoside transporter-deficient cell line) were chosen to test the efficacy of Gem-SQ NAs. The greater cytotoxicity of Gem-SQ NAs on these two cell lines indicated ability of these nanoparticles to overcome cellular resistance (*18*), which was explained, in the L1210 10K cell line, by the slow release of gemcitabine from the NAs, avoiding to overflow the low intracellular enzymatic activity of deoxycytidine kinase. Moreover, the protection of gemcitabine from deamination under NAs formulation also contributed to this potent effect. On the other hand, the higher cytotoxicity of Gem-SQ NAs on CEM/ARAC8C cells, in comparison with gemcitabine free, was probably due to their difference of cellular uptake pathway. The uptake of the latter is nucleoside transporter dependent, while for Gem-SQ NAs, passive diffusion constitutes the main cell penetration corridor. In more details and as shown in **Fig. 4**, it was observed that Gem-SQ monomers were first released from the NAs once associated with extracellular proteins, and then diffused toward the cell plasma membrane where they accumulated in large quantities. Gem-SQ molecules then distributed between cell plasma membrane and the intracellular membranes. Finally, Gem-SQ bioconjugates underwent enzymatic cleavage by cathepsins B and D on the amide bond, and free gemcitabine was released, allowing the expression of biological activity after triphosphorylation by dCK (*19*, *20*). Thus, in the case of Gem-SQ NAs, the deficiency of nucleoside transporter in CEM/ARAC8C cells didn't affect the penetration of gemcitabine inside cells and didn't abolish anticancer activity. All these results showed that SQdFdC NAs were able to bypass various types of resistance mechanisms in leukemia cells, resulting in greater cytotoxicity compared to the gemcitabine free.

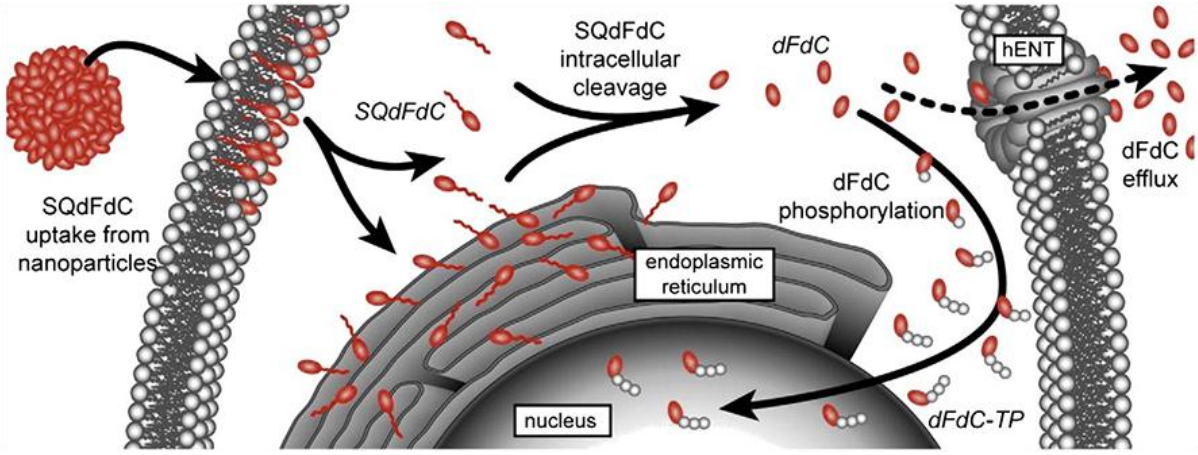

Fig. 4. Intracellular metabolization pathway of Gem-SQ. Gem-SQ monomers are firstly released from the NAs mediated by extracellular proteins, followed by diffusing toward the cell membrane. The Gem-SQ molecules are then distributed between cell membrane and the intracellular membranes. Afterward, free gemcitabine is released after the cleavage of the amide bond between squalene and gemcitabine, which is either phosphated into the biological active dFdC-TP, or pumped out of the cell through equilibrative membrane transporters. Adapted with permission from [20], © 2010 Elsevier.

Gem-SQ NAs also exhibited superior *in vivo* anticancer activity on a mouse aggressive metastatic leukemia model grafted by intravenous injection of L1210 wt cells (*18*). Interestingly, groups treated with Gem-SQ NAs showed higher survival rates than those treated with free gemcitabine. Almost half of the mice (~43%) survived after treatment with Gem-SQ NAs (15 mg/kg eq. gemcitabine) (**Fig. 5**). The anticancer activity of Gem-SQ NAs was then compared with gemcitabine at maximum tolerated doses (MTD, 4×20mg for Gem-SQ NAs versus 4×100mg in the case of free gemcitabine) in L1210 wt bearing mice (*21*). Gem-SQ NAs were much more efficient than gemcitabine at MTD, leading to

75% long-term survivors.

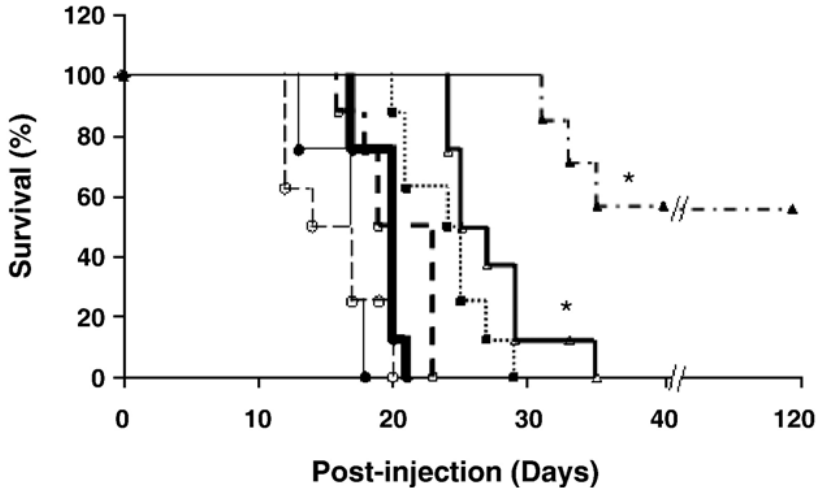

Fig. 5. Survival of the mice after treatment of Gem or Gem-SQ. Untreated (—), SQ NAs (– –), SQ + Gem 5 mg/kg (▬▬), Gem 5 mg/kg (— —), Gem-SQ NAs equivalent to 5 mg/kg Gem (▬), Gem 15 mg/kg (····), Gem-SQ NAs equivalent to 15 mg/kg Gem (— · —), n = 7–8. *Kaplan–Meier test was significant for the L1210 wt leukemia bearing mice at both 5 mg/kg and 15 mg/kg ($P < 0.05$) doses. Figures adapted with permission from [18]. © 2007 Elsevier.

Because gemcitabine is the main chemotherapeutic agent for the treatment of pancreatic cancer which represents the fourth commonest cause of cancer-related death in western countries (*22*), Gem-SQ NAs were also tested on experimental model of pancreatic cancer (*23*). Thus the anticancer activity of Gem-SQ NAs was evaluated on pancreatic cancer cell lines *in vitro*. In comparison with free gemcitabine, Gem-SQ NAs exerted higher antiproliferative and cytotoxic effects against Capan1 and BxPc3 sensitive cell lines and Panc1 resistant cell lines. In addition, Gem-SQ NAs were found to demonstrate higher inhibition of tumor growth in both Panc1 and Capan1 subcutaneous tumor models. To be closer to clinical situation, a Panc1 orthotopic mouse model was also considered to test the anticancer activity of Gem-SQ NAs comparatively to gemcitabine. It was observed that Gem-SQ NAs inhibited the growth of primary tumors by 68%, which was 36% higher than after treatment with free gemcitabine. Additionally, comparatively to gemcitabine free, Gem-SQ NAs led to longer survival of mice bearing primary pancreatic tumor. These results correlated with a higher induction of cellular apoptosis as determined by TUNEL analysis and caspase-3 staining, and a higher reduction of the proliferation maker Ki67 in the tumor tissue after Gem-SQ NAs treatment.

Pharmacokinetics study of Gem-SQ NAs after intravenous injection showed controlled and prolonged release of gemcitabine. It considerably increased plasma half-life and mean residence time compared with free gemcitabine. Additionally, the linkage of gemcitabine to squalenic acid on its amino group noticeably delayed the metabolism of gemcitabine into its inactive difluorodeoxyuridine metabolite (dFdU), compared with free gemcitabine. Moreover, the elimination of radiolabeled Gem-SQ NAs was considerably lower compared with the free drug, as indicated by the lower radioactivity counts found in urine and kidneys. Gem-SQ NAs also underwent considerably higher distribution to the organs of the reticuloendothelial system (RES), such as liver and spleen, which are the major metastatic organs of leukemia (*24*). The pharmacokinetic and biodistribution insights may also explain the higher efficacy of Gem-SQ NAs against experimental leukemia.

All these studies have demonstrated that squalenoylation of gemcitabine, favorably modified *in*

vivo the pharmacokinetics, metabolism, and biodistribution of this compound. The squalenoyl NAs of gemcitabine acted as a reservoir of gemcitabine due to its modified distribution compared with free gemcitabine while minimizing the rapid exposure of the drug to deamination.

Interestingly, Gem-SQ NAs may be combined with other drug molecules to design so-called "multidrug" nanoparticles with pluripotent pharmacological activity. This has been recently performed by co-nanoprecipitation of isocombretastatin A-4 (isoCA4) with Gem-SQ. It was observed that by combining antiangiogenic (i.e., isocombretastatine) and cytostatic (i.e., gemcitabine) compounds in the same nanocomposite, both colon carcinoma cells and endothelial cells could be simultaneously affected. Such "multidrug" NAs resulted in better *in vivo* anticancer activity than after treatment with both compounds administered separately in preclinical model of human colon cancer (*25*). Nevertheless, multidrug nanoparticles based on the co-nanoprecipitation of squalenoylated gemcitabine and sunitinib, a tyrosine-kinase inhibitor, didn't exhibit improved efficacy comparatively to the physical mixture of individual monodrug NAs on MIA PaCa-2 pancreatic cancer cells. However, it didn't exclude therapeutic improvement in dynamic conditions *in vivo* (*26*).

Chemical modification of Gem-SQ NAs surface was conducted in order to ensure their effective distribution in the brain after convection-enhanced delivery (CED). For this purpose, pegylated Gem-SQ NAs (Gem-SQ-PEG NAs) were obtained after co-nanoprecipitation of PEG-SQ and Gem-SQ bioconjugates. The Gem-SQ pegylation enhanced the NAs distribution both in healthy and tumor-bearing brains after CED which increased the survival of rats bearing RG2 glioma (*27*).

2.1.2. Squalene-ddI and -ddC prodrugs

The concept of squalenoylation was also applied to antiviral nucleoside analogues, such as ddC (2′-3′-dideoxycytidine) and ddI (2′,3′-dideoxyinosine). The chemical conjugation of squalenic acid and ddC was also achieved onto the amino group of the nucleobase through an amide bond, while ester bond was chosen to link the squalenic acid onto the 5′-nucleoside hydroxyl group of the dideoxyfuranose moiety of ddI. As control, thymidine was also coupled with squalenic acid on its 5'-hydroxy position through an ester bond (Fig. 2). All ddC-SQ, ddI-SQ and thymidine-squalene (T-SQ) could self-organize in water as nanoassemblies with a size in the range of 100 to 250 nm and homogeneous size distribution (polydispersity index of 0.2 maximum) (*6*). It was observed by SAXS that both thymidine and ddI derivatives self-organized as lamellar phases, when Cryo-TEM images showed spherical nanoparticles. On the contrary, ddC-SQ NAs displayed an inverse bicontinuous cubic organization, made by a bilayer lying on a periodic minimal surface (*17*). As Gem-SQ, ddI-SQ NAs and ddC-SQ NAs also possessed high drug loading, ie., 38% and 36%, respectively.

The antiviral activities of ddC-SQ and ddI-SQ NAs were tested on HIV-1-infected lymphocytes compared with corresponding free ddI and ddC. Both ddI-SQ NAs and ddC-SQ NAs were found to be 2- to 3- times as potent as the corresponding parent molecules in their ability to inhibit viral replication and they were shown to be quite 2 fold more selective. In order to increase the efficiency of the NAs, ddC-SQ bioconjugates were co-nanoprecipitated with pegylated cholesterol (chol-PEG). The resulting NAs were obtained with smaller size of around 70 nm. These NAs showed higher anti-HIV activity, however with an increased cytotoxicity. In the case of HIV-1 strains resistant to ddI and/or ddC (HIV-1-144 and HIV-1-146), the squalenoylated derivatives also exhibited higher antiviral activity than the free drugs (*6, 28*). The enhanced anti-HIV activity of ddI-SQ NAs could be explained by the higher intracellular concentrations of dideoxyadenosine triphosphate (ddA-TP), the active metabolite of ddI, after HIV-infected cells were treated with ddI-SQ NAs (*28*).

2.1.3. Monophosphate Squalene-Gemcitabine and Squalene-ddC prodrugs

As mentioned above, following entering into cells, the nucleoside analogues should be converted firstly into monophosphate derivatives and finally into active triphosphate form by cellular kinases. It is important to note that the monophosphorylation represents the rate-limiting step for the phamacological activity to occur. Direct delivery of nucleoside monophosphate offers an alternative to skip this rate-limiting step (*29*). However, the high polarity of monophosphate nucleosides restricts their penetration into cells.

Therefore, trialkylammonium salts of Gem-SQ monophosphate (Gem-SQ-MP) and ddC-SQ monophosphate (ddC-SQ-MP) bioconjugates were then designed and synthesized by phosphorylating respectively the 5′-hydroxy free group of Gem-SQ and ddC-SQ (Fig. 2) to increase the cellular uptake of nucleoside monophosphate.

The Gem-SQ-MP molecules self-assembled in water into very homogeneous nanoparticles of 153 nm, displaying unilamellar liposome like structures. The phosphorylated NAs displayed considerably lower IC50 values (6.7 nM) on L1210 wt leukemia cell line and improved anticancer activity, comparatively to SQdFdC nanoassemblies (*30*). This strategy also showed the potency to reverse the drug-resistant phenotype of pancreatic adenocarcinoma caused by the deficiencies in drug transport/drug activation (*31*).

Concerning ddC-SQ-MP bioconjugates, they also self-assembled in water to give nanoparticles (109 nm). These NAs were then tested *in vitro* on HIV-1-infected peripheral blood mononuclear cells for their antiviral activity. They were found to be just as active as ddC but with an increased selectivity index due to a reduced cell toxicity (*30*). This approach could be of great interest to by-pass resistance phenomena due to deficiency in intracellular deoxycytidine kinase and to eliminate viral sanctuaries in HIV-infected patients.

2.2. Squalene-nucleoside prodrugs

Nucleosides and nucleotides are involved in different physiological processes in the body. In particular, purine nucleotides and nucleosides play an important role in the regulation of the development and plasticity of nervous system (*32*). Adenosine is an endogenous nucleoside which should act as a potent endogenous neuroprotectant during ischemic stroke by slowing down neuronal metabolism and enhancing cerebral blood flow, and by acting as an intra- and intercellular messenger (*33, 34*). Adenosine has also many potential other therapeutic applications among which multiple sclerosis, and spinal cord injury treatment. However, rapid metabolization (half-life of adenosine in blood is 10 sec) and poor permeability through the blood-brain-barrier (BBB) of adenosine dramatically restrict the clinical applications of this molecule.

Therefore, the conjugation of adenosine to elongated squalenic acid (by one isoprene unit) has been considered in order to improve its pharmaceutical profile. The coupling of the squalene derivative onto the amino group of adenosine nucleobase through an amide bond was intended to protect the fragile adenosine from metabolization. The corresponding nanoassemblies were obtained with highly monodisperse size distribution (PdI less than 0.15) and with a mean diameter of around 120 nm. The drug loading reached 37 %. Structural studies of Ad-SQ NAs using SAXS and cryo-TEM revealed a sponge-like-phase in which the inner aqueous channels could provide a favorable accessibility for enzymes to ensure the prodrug activation and the adenosine release (*35*).

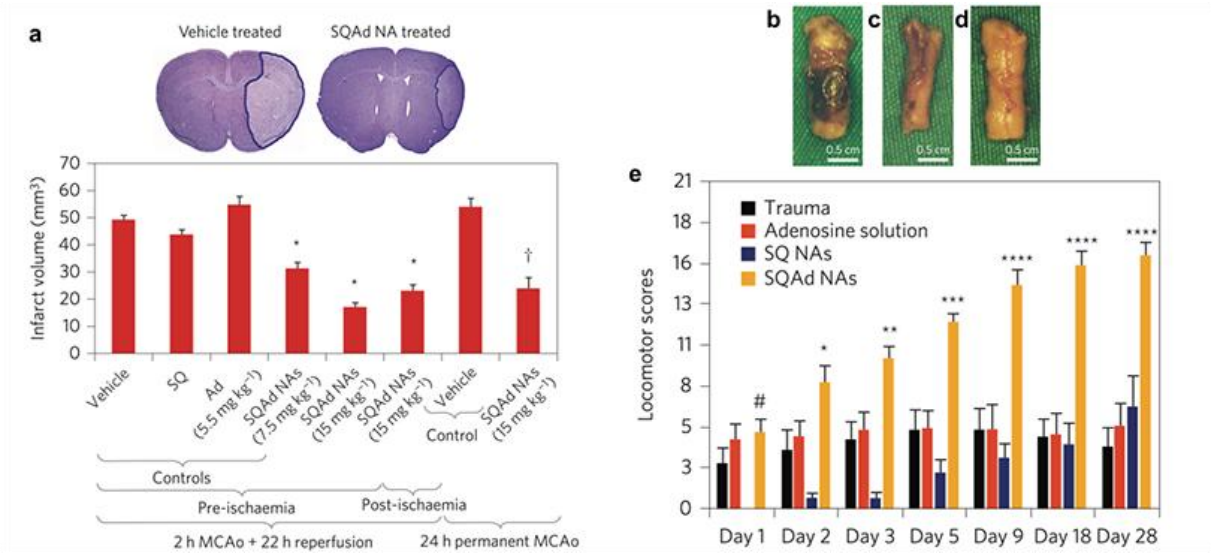

Fig. 6. Systemic administration of Ad-SQ nanoassemblies (NAs) provides significant neuroprotection both in a mouse model of cerebral ischaemia (a) and a model of spinal cord injury in rats (b-e). (a). Ischaemic volumes in control and treated mice subjected to transient (2 h MCAo and 22 h reperfusion) and permanent (24 h MCAo) focal cerebral ischaemia were identified by reduced Nissl staining under a light microscope (magnification×10, insets) (data are presented as mean (mm3) ± s.d., N = 6 animals per group; † and * indicate $P < 0.05$ compared to respective controls). Intravenous administration of 7.5 mg kg−1 or 15 mg kg−1 SQAd nanoassemblies just before ischaemia or 2 h post-ischaemia significantly decreased the infarct volume compared with control groups that received vehicle (dextrose 5%), adenosine-unconjugated SQ nanoassemblies (9.45 mg kg−1) or free adenosine (5.5 mg kg−1). A significant therapeutic effect was also observed when SQAd nanoassemblies were administered 2 h post-ischaemia in the permanent MCAo model. **(b-d)** After 72 h, the SQAd nanoassemblies-injected animals showed the absence of visible traumatic area on the cord **(d)** compared with the trauma group **(b)** and the adenosine treated group **(c)**. **e** After 24 h, 48 h and 72 h and up to 28 days post-trauma, the animals were functionally graded using the Basso, Beattie and Bresnahan grading scale (data presented as mean ± s.e.m., #, not significant, *$P < 0.05$, **$P < 0.01$, ***$P < 0.001$, ****$P < 0.0001$). Figures adapted with permission from [36]. © 2014 Nature.

It was reported that pre- or post-ischemic intravenous bolus administration of Ad-SQ NAs dose-dependently decrease the infarct volume in mice subjected to 2 h of middle cerebral artery occlusion (MCAo) and 22 h of reperfusion (**Fig. 6.a**). It was also shown that after intravenous injection, Ad-SQ NAs exhibited longer blood retention versus adenosine free (*36, 37*), allowing a prolonged interaction with the neurovascular unit which resulted in the improvement of the brain microcirculation, allowing a more efficient reperfusion and a better neuroprotective effect. Using hCMEC/D3 cell line, a well-recognized BBB model, the transport mechanism of Ad-SQ NAs across the blood-brain-barrier (BBB) was revealed. It showed that the NAs were firstly endocytosed as intact nanostructures via an energy-dependent pathway involving the LDL receptors. Then, the prodrugs were hydrolyzed inside the cells before adenosine free was exocytosed towards the baso-lateral compartment of the cell insert model (*38*).

Moreover, in spinal cord injury in Sprague–Dawley rats that undergo a T9 contusion injury, it was shown that the injection of Ad-SQ NAs (5 min post-injury), could provide neuroprotection through peripheral and central effects (*39, 40*). Indeed, as illustrated in **Fig. 6.b-d**, the Ad-SQ NAs could avoid the occurrence of visible traumatic area on spinal cord after T9 contusion injury. All animals receiving Ad-SQ NAs showed a good motor recovery of the paralyzed hindlimbs what adenosine free could not (**Fig. 6.e**). This study further confirmed the extended neuroprotective potency of this

nanomedicine.

All these results open new exciting perspectives for the treatment of severe neurological diseases where tissue ischaemia and/or trauma are involved.

2.3. Squalene-β-lactam antibiotics prodrugs

Intracellular infection poses a great challenge in antibiotic therapy. Indeed, several facultative and obligate intracellular bacteria can enter and multiply within phagocytic cells, where they are shielded from host defenses and antimicrobial therapy (*41*). In fact, many antibiotics show poor activity on intracellular bacteria, either because of their rapid metabolization into inactive agents, or their restricted penetration into cells, or because they induce low intracellular retention and subtherapeutic concentration in infected intracellular compartments. Thus, the use of nanomedicine provides an alternative solution to selectively carry the antibiotics into infected cells (*42*).

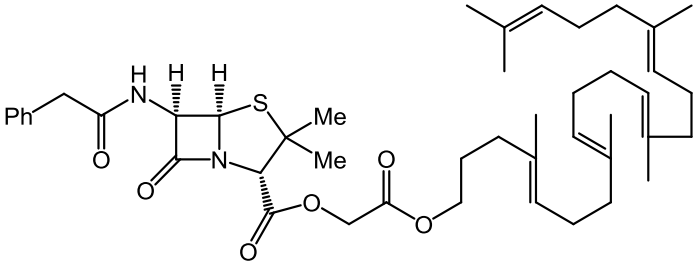

11 PNG-SQ with non-sensitive linker

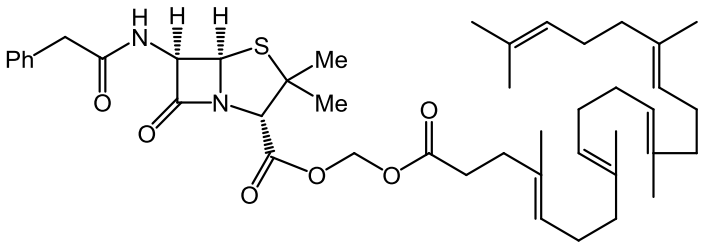

12 PNG-SQ with sensitive linker

Fig. 7. Chemical structures of PNG-SQ with non-sensitive linker and sensitive linker.

Coupling squalene to the carboxylate function of penicillin G (PNG) has been achieved by using both sensitive and non-sensitive linkers located between the squalene hydrophobic chain and the penicillin G (**Fig. 7**). Both linkers were attached to the PNG through an ester bond. In the first PNG-SQ bioconjugate, the ester bond was less hydrolyzable than in the second. The two bioconjugates were able to form NAs yielding impressive antibiotic loading (44 wt %). Their average diameter was around 150 nm with a very low polydispersity index (~0.1) and Cryo-TEM analysis indicated a spherical and regular shape of the nanoparticles. X-ray diffraction studies by SAXS and wide-angle X-ray scattering (WAXS) highlighted that PNG-SQ NAs did not display any supramolecular organization (absence of any crystal structure).

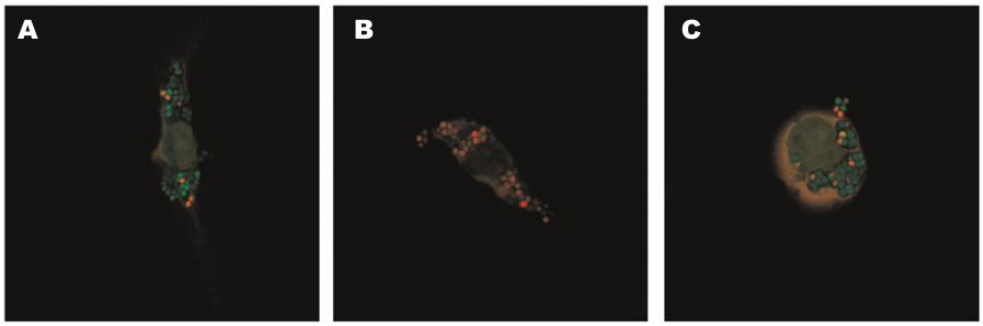

Fig. 8. Confocal fluorescence microscopy images of viable bacteria in J774 cells. J774 cells were **A)** non-treated; **B)** pretreated with SQ-Pen G NPs with sensitive linker; **C)** pretreated with Pen G, then infected with S. aureus and fixed with paraformaldehyde, permeabilized with 0.2% Triton X-100, and double-labeled with propidium iodide and Syto9 (LIVE/DEAD BacLight kit). Viable S. aureus cells are stained in green, while red signals represent dead bacteria. Figures adapted with permission from [43]. © 2012 ACS.

The minimum inhibitory concentration (MIC) for proliferation of bacteria of free PNG and PNG-SQ NAs was evaluated in several bacterial strains. As expected, PNG-SQsens (with sensitive bond) had lower MIC than PNG-SQ with non-sensitive bond because of its lower stability. The cell capture of both PNG-SQ and PNG-SQsens NAs by macrophages was studied, using J774 cell line (a murine macrophage model) when NAs were tagged with fluorescent BODIPY-cholesterol. The strong intracellular fluorescent signal and absence of fluorescence signal at the cell surface indicated that most of the PNG-SQsens NAs were internalized inside the cells rather than localized onto the cell surface. The intracellular bactericidal effect of NAs was then evaluated on S. aureus ATCC 55585 strain sensitive to PNG. PNG-SQsens NAs were found to be more efficient in killing intracellular bacteria than free PNG which diffused insufficiently into the cells (**Fig. 8**). This clearly suggested that NAs improved PNG cell penetration. Moreover, the higher antibacterial effect observed with PNG-SQ NAs using the sensitive linker (versus NAs with the non-sensitive linker) was explained by a more efficient release of PNG into the cells (*43*).

2.4. Squalene-doxorubicin prodrugs

Doxorubicin is one of the leading anticancer drugs in the treatment of a wide range of cancers, including many types of carcinoma (solid tumors), hematological malignancies (leukaemia, lymphoma) and soft tissue sarcomas. The mechanisms by which doxorubicin acts in the cancer cell include: (i) intercalation into DNA and inhibition of macromolecular biosynthesis and (ii) generation of free radicals that cause damage to DNA, cellular membranes and proteins. But, the clinical efficacy of doxorubicin is also hindered by acute and subacute adverse effects, mainly cardiotoxicity and myelosuppression (*44*, *45*).

Various nanocarriers have been developed in order to reduce the adverse effect of doxorubicin, including liposomes, dendrimers, micelles, solid-lipid, and polymer nanoparticles. Among these nanocarriers, only doxorubicin liposomes reached the market (Myocet, Doxil, PEGylated Caelyx) and are the first FDA-approved nano-drugs. Despite liposome formulation contributed to decrease doxorubicin cardiotoxicity, it generated some other side effects like "hand-foot" syndrome which affects the quality of life of the patients. Noteworthy, all these commercially available liposomes have only moderate doxorubicin loading. In order to increase drug payload, squalenic acid was coupled on doxorubicin via ester bond in order to obtain C-14 ester derivatives (squalenoyl doxorubicin, Dox-SQ)

(**Fig. 9A**). This linkage allowed the formation of NAs of 130 nm mean diameter, without the use of PEG or any other surfactant and showed an impressive drug payload (i.e., 57%). Surprisingly, Dox-SQ NAs displayed an original "loop-train" structure (**Fig. 9B, 9C**) never observed before, which may explain their long-circulating ability in the blood stream after intravenous injection, since elongated nanoparticle structures are less prone of capture by the macrophages of the mononuclear phagocyte system (MPS) (*46*).

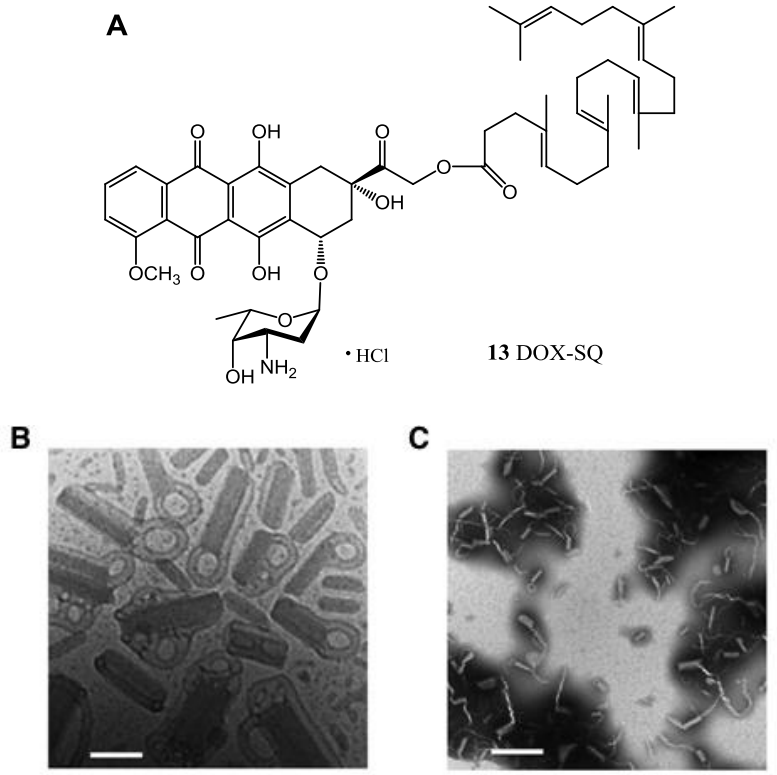

Fig. 9. (A) Chemical structure of Dox-SQ. (B) Cryo-TEM appearance of the Dox-SQ NAs. (Scale bar, 100 nm) **(C) TEM appearance of the Dox-SQ NAs.** (Scale bar, 500 nm) Figures adapted with permission from [47]. © 2014 PNAS.

The antitumor efficacy of these NAs has been investigated on two resistant human pancreatic (MiaPaCa-2) and murine lung (M109) carcinomas. The *in vitro* experiments showed a very fast uptake of Dox-SQ NAs into MiaPaCa-2 cells (5-min postincubation) and a greater internalization of the drug via active endocytosis, resulting in higher cell apoptosis than after incubation with free doxorubicin. Furthermore, *in vivo* experiments have shown that, comparatively to doxorubicin free, the Dox-SQ NAs greatly improved the anticancer efficacy on both experimental models. In particular, the growth of M109 lung tumors was inhibited by 90% after treatment with Dox-SQ NAs versus only 3% with free Doxorubicin when inhibition was 95% in MiaPaCa-2 pancreatic tumor xenografts versus 29% with doxorubicin free in the same model (Fig. 10 A-D). Toxicological studies indicated that the MTD of Dox-SQ NAs was five times higher than that of free doxorubicin and also that these NAs did not cause any apparent cardiac toxicities such as those induced by the drug free (Fig. 10 E-H). In a nutshell, the increase of the antitumor activity and the decrease of the cardiac toxicity of Dox-SQ NAs was explained by their prolonged systemic circulation time, their enhanced accumulation within tumor tissue and the reduction of drug concentration in the heart (*47*). Thus, squalenoylation of the Doxorubicin remarkably improved the doxorubicin's therapeutic index without using biocompatible transporter material.

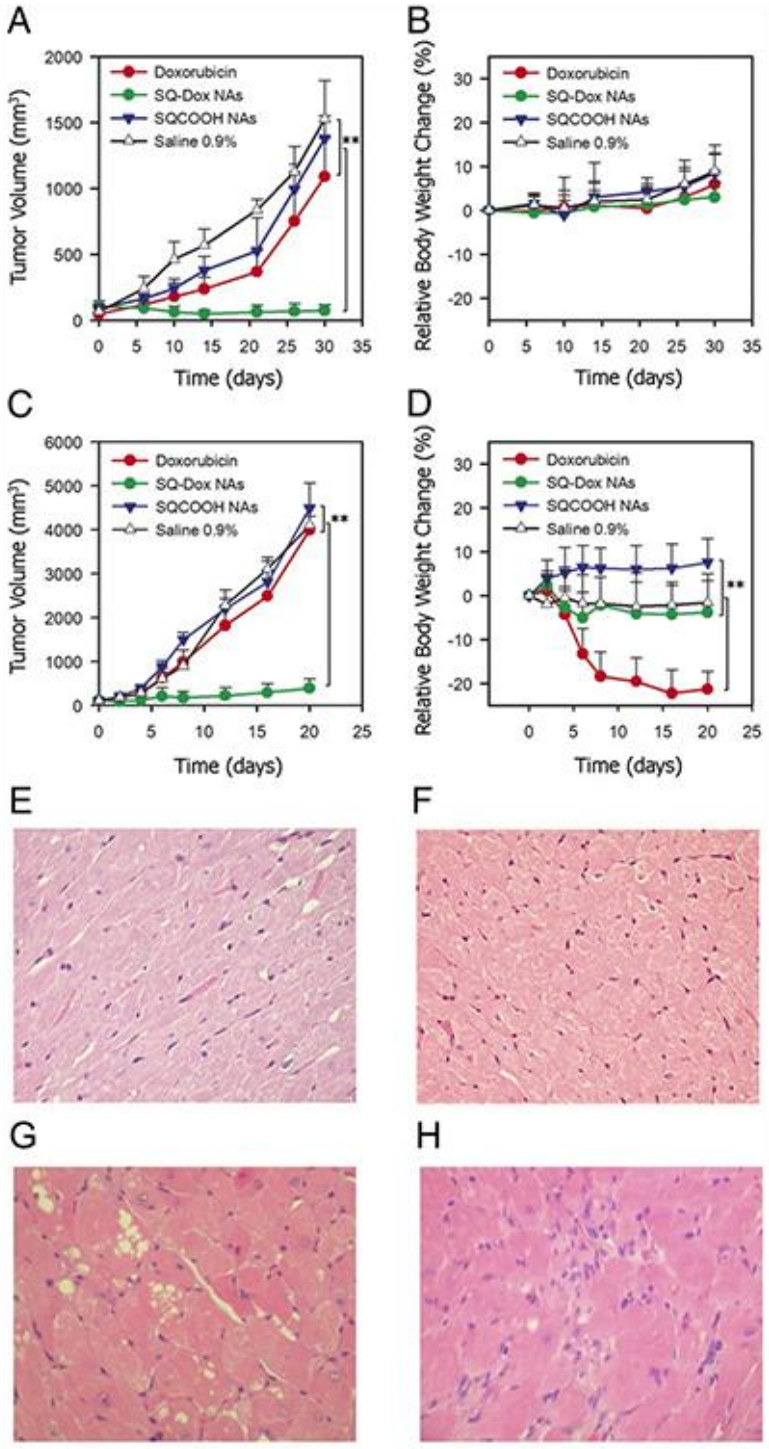

Fig. 10. Tumor growth inhibition by DOX-SQ NAs and the body-weight changes of mice bearing MiaPaCa-2 (A and B) or M109 (C and D) tumors (n = 10, **P < 0.01). Cardiotoxicity of (E) Saline-treated rat showing myocardium without any lesions (no ventricle focal inflammatory cell). (F) DOX-SQ NAs-treated rat (dose: 1 mg·kg·wk equivalent doxorubicin, during 11 wk) showing myocardium without any lesions. (G) Doxorubicin-treated rat (dose: 1 mg·kg·wk, during 11 wk) showing infiltration with ventricle hypercellularity. (H) DOX-SQ NAs-treated rat (dose: 2 mg·kg·wk equivalent doxorubicin, during 11 wk) showing myocardium without any lesion, only a slight incidence of minimal myocardiopathology was observed. Figures adapted with permission from [47]. © 2014 PNAS.

3. SQUALENE-BASED BIOCONJUGATES WITH POORLY HYDROPHILIC DRUGS

3.1. Squalene-paclitaxel prodrugs

The squalenoylation concept was also applied on taxoid compounds, such as paclitaxel (PTX), a drug with poor solubility. PTX is one of the most important chemotherapeutic agents, which is clinically used to treat ovarian, lung, pancreatic, breast and other cancers, as well as Kaposi's sarcoma. The mechanism of action of PTX involves promoting assembly of tubules into stable microtubules and interfering the normal depolymerization of microtubules during cell division. On the basis of this action, the cell cycle is arrested in the late G2/M phase, which is the main toxic mechanism of PTX (*48*). Although PTX shows great efficacy as anticancer agent, its very low aqueous solubility needs the development of specific formulations for intravenous administration. Practically, the formulation for clinical use consists in a PTX emulsion in a 50:50 mixture of absolute ethanol and Cremophor EL and is diluted with buffer prior to intravenous administration to the patient. However, the use of Cremophor is associated with a series of adverse effects, such as hypersensitivity reactions, abnormal lipoprotein patterns, hyperlipidaemia, neuropathy, peripheral neurotoxicity, etc. (*49*).

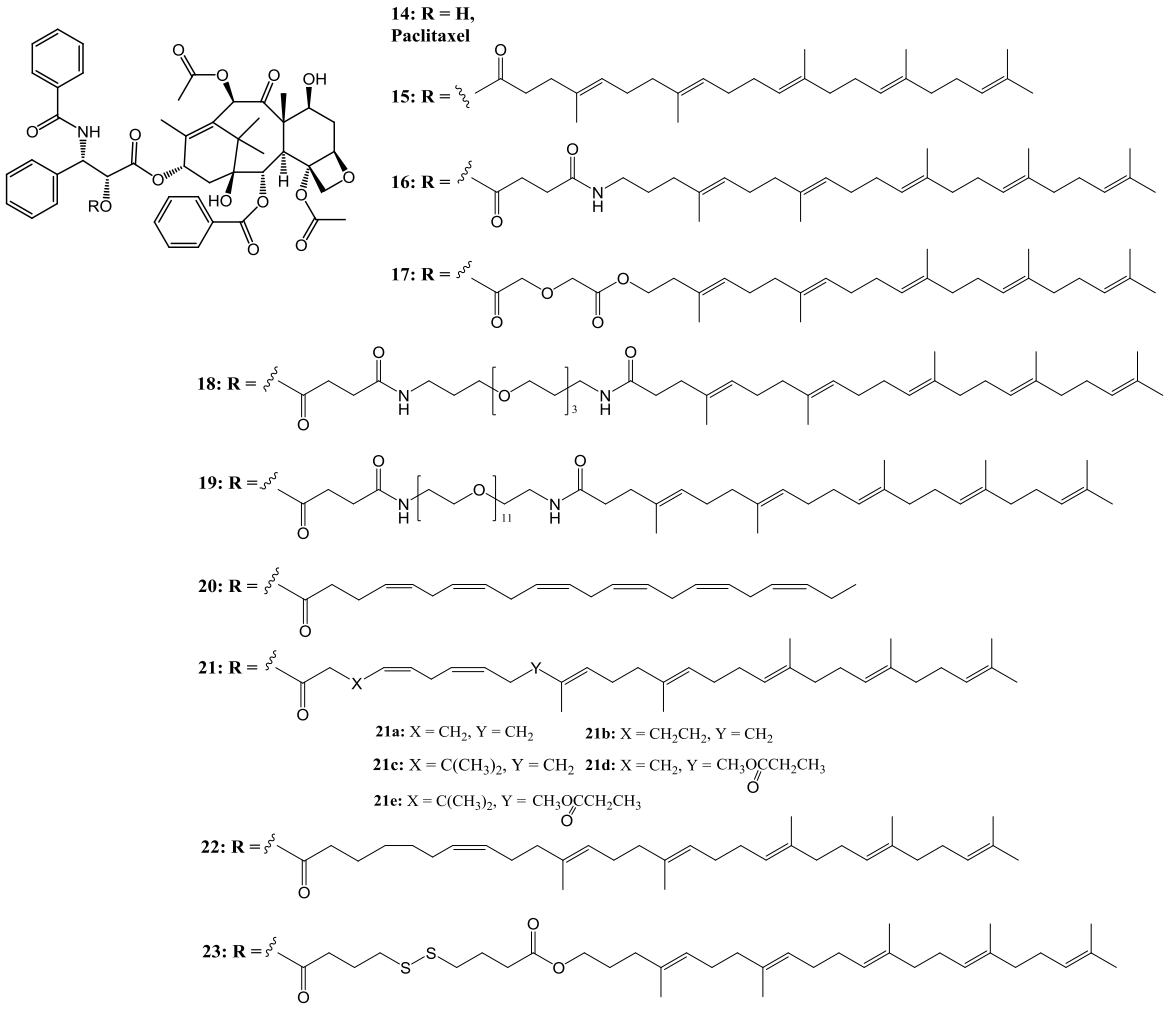

Fig. 11. Chemical structures of the reported squalenol paclitaxel prodrugs: (14) PTX; **(15)** PTX-SQ with

ester limker; **(16)** PTX-SQ with succinate ester linker; **(17)** PTX-SQ with diglycolate ester linker; **(18)**, **(19)** PTX-SQ with succinate ester-PEG linker; **(20)** DHA-PTX prodrug; **(21)**, **(22)** DHA-SQ hybrid paclitaxel prodrug; **(23)** PTX-SQ with disulfide-containing linker. Adapted from [51, 52, 53].

To circumvent these limitations, PTX has been conjugated to squalene in order to design a less toxic nanoformulation for intravenous administration. Thus, squalenic acid were coupled on the 2′-OH of PTX using either a direct ester bond or intercalating various spacers such as succinate ester, diglycolate ester, or succinate ester-PEG (*50*) in order to modulate the hydrophobicity of the prodrugs (**Fig. 11**). All those bioconjugates were able to form NAs in aqueous solution with drug payload ranging from 45% to 69%, which was considerably higher than when PTX was encapsulated in liposomes or polymer nanoparticles. These NAs were found to be remarkably stable in water but the diglycolate linkage was observed to be more susceptible to hydrolysis in serum than the succinate linkage. Because microtubules are the main target of PTX, which promotes the assembly of tubules and suppresses microtubule dynamics, a test based on microtubule bundle formation was carried out on HT-29 and KB-31 cancer cell lines. The pharmacological activity of the PTX-SQ bioconjugates with simple ester bond appeared with 50 times higher doses than PTX free which suggested that only a small fraction of PTX was released from PTX-SQ NAs and could generate the formation of microtubule bundle (**Fig. 12**).

Similarly, PTX-SQ NAs with different linkers showed a decreased cytotoxicity in comparison with free PTX toward M109 cancer cell line in the following order of activity: diglycolate linker, succinyl linker, and PEG linker. Actually, a close correlation was observed between the PTX-SQ prodrug cytotoxicities and their linkage stabilities. Indeed, diglycolate linker was the most susceptible to hydrolysis among the other linkers and displayed highest cytotoxicity (*50*). Clearly, the anticancer activity of PTX-SQ NAs was found much lower than PTX free on various experimental models *in vivo* (unpublished results). It is hypothesized that the very strong lipophilicity of PTX-SQ bioconjugates hinders enzymatic access, necessary for triggering the drug release. Apparently, the use of specific hydrophilic linkers was not sufficient for improving the anticancer activity of PTX-SQ.

A quite similar approach has been reported previously with docosahexaenoic acid–PTX (DHA-PTX) prodrugs, made by covalently conjugating the essential fatty acid DHA to the 2'-OH position of the PTX molecule (**Fig. 11**). DHA-PTX, when incorporated into lipid vehicles such as liposomes, oil emulsions or micelles, was shown to be very efficient prodrugs that even reached the phase III clinical trial for the treatment of metastatic malignant melanoma (*5*). Thus, a new series of squalene PTX prodrugs were designed in which a 1,4-cis, cis pentadiene unit was incorporated between the PTX and the squalene chain. The bioconjugates differed mainly by the number of bonds between the ester linkage (on the 2'-hydroxy position of the PTX) and the diene with two or three methylene groups respectively. Such new bioconjugates were expected to take advantage of the potent release of the free drug observed with DHA-PTX, while preserving the capacity to form NAs inherent to squalene bioconjugates (*51*). This study first showed that the introduction of such linkers did not disrupt the self-organizing capabilities of the squalene derivatives, and NAs of 90-150 nm could be obtained. *In vitro*, these PTX-SQ NAs displayed notable cytotoxicity on several tumor cell lines, including lung cell line A549, colon cell line HT-29, or nasopharyngeal epidermoid cell line KB 3.1. Especially, the cis, cis-squalenyl-deca-5, 8-dienoate prodrugs showed improved activity over PTX-SQ prodrugs (with a simple ester bond), highlighting the favorable effect of the dienic linker. Then, the antitumor efficacy of these NAs has been studied *in vivo* on human lung (A549) carcinoma xenograft model in mice: the NAs demonstrated comparable antitumor efficacy than the parent drug, but with lower subacute toxicity as seen by measuring body weight loss.

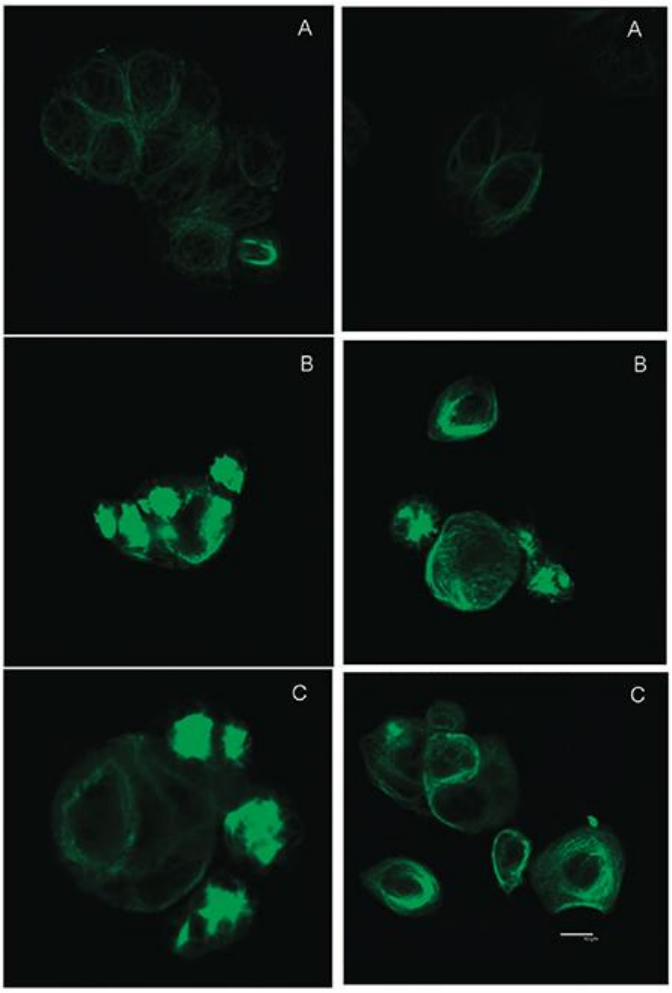

Fig. 12. Microtubule bundle formation induced by paclitaxel and PTX-SQ with simple ester bond (15 in Fig. 11) in cultured HT-29 cells (left) and KB-31 (right). Cells were incubated with FITC antitubulin antibody after exposure to paclitaxel 100 nM (panel **B)** and compound 1 at 5 μM (panel **C)** for 14 h. Panel **A**, control (solvent). Figures adapted with permission from [50]. © 2010 ACS.

Stella Borrelli and coworkers synthesized another kind of PTX-SQ prodrug, with disulfide-containing linkage (*52*). The obtained compound was effectively able to form NAs and to release the parent drugs *in vitro*. Immuno-fluorescence assay revealed that those bioconjugates entered A549 cells and stained microtubule bundles. But, *in vitro* cytotoxicity study showed that the disulfide-containing PTX-SQ derivatives displayed similar biological activity than the free drugs.

3.2. Squalene-curcumin prodrugs

Curcumin is a natural compound extracted from turmeric, with pleiotropic activities including antioxidant, anti-inflammatory, antitumor, and neuroprotective. Moreover, it shows therapeutic potential against parasites, such as Leishmania responsible of Leishmaniasis. However, the phamocological applications of curcumin are severely restricted by its very low aqueous solubility, short half-life, poor absorption and extremely low bioavailability.

To enhance the therapeutic efficacy of curcumin, the squalenoylation strategy was applied. Monosqualenoyl-curcumin and bis-squalenoylcurcumin were synthesized by coupling the squalenic acid to the free phenol group(s) of the curcumin. The resulting bioconjugates could spontaneously

form NAs in 5% dextrose solution, with sizes around 100 nm (*53*).

Both monosqualenoylcurcumin and bis-squalenoylcurcumin NAs showed improved activities against promastigotes and axenic amastigotes but not against intramacrophagic forms.

4. SQUALENE-BASED BIOCONJUGATES WITH MACROMOLECULES

4.1. Squalene-siRNA prodrugs

Small interfering RNA (siRNA), have gained increasing attention due to their unique ability to specifically interfere with mRNA gene expression by base-pairing with complementary nucleotide sequences within mRNA, degrading it after transcription and inhibiting the expression of target proteins (*54*). Thus, siRNA holds great promise as potential therapeutic agent by inhibiting disease-causing genes. Compared with conventional small molecules, siRNA show high specificity and activity. However, as a polyanionic macromolecule, siRNAs poorly diffuse across biological membranes and insufficiently penetrate intracellularly, owing to low affinity for negatively charged cell membranes. Moreover, *in vivo*, naked siRNAs are very unstable in the biological fluids due to their degradation by nucleases, renal clearance and elimination by reticuloendothelial system (RES) (*55*).

Thus, there is an urgent need to develop competent systems for the delivery of siRNA. So far, a wide range of approaches including viral vectors as well as nonviral delivery systems have been proposed to enhance nucleic acids bioavailability and pharmacodynamic activity (*56*). However, the safety of viral vectors is doubtful because of possible random recombination, oncogenic potential and immunogenicity. Thus, cation-based nanoplexes have been designed as a non-viral alternatives to improve oligonucleotides stability and cellular uptake (*57*).

Nevertheless, some important limitations remain, such as strong interactions with proteins after intravenous injection and intrinsic toxicity due to polycationic charges (*58, 59*). Thus, the conjugation of oligonucleotides with neutral lipids like cholesterol, squalene or fatty acids represents another alternative (*60*) to ensure the safe delivery of oligonucleotides through membranes and to improve their efficacy (*61*).

There are several positions for ligand conjugation to oligonucleotides, at the 5′- or 3′-ends or on the entire backbone structure (*62*). Generally, the conjugation occurs at the 5′- or 3′-ends. Since siRNA has two complementary strands (sense and antisense), there are four terminal ends as potential conjugation sites. Because the antisense siRNA strand needs to be incorporated into an effector complex or RISC complex before recognition of the homologous mRNA, this strand should not be chemically modified for steric reasons. On the contrary, the inactive sense strand can be used for chemical conjugation (*61*).

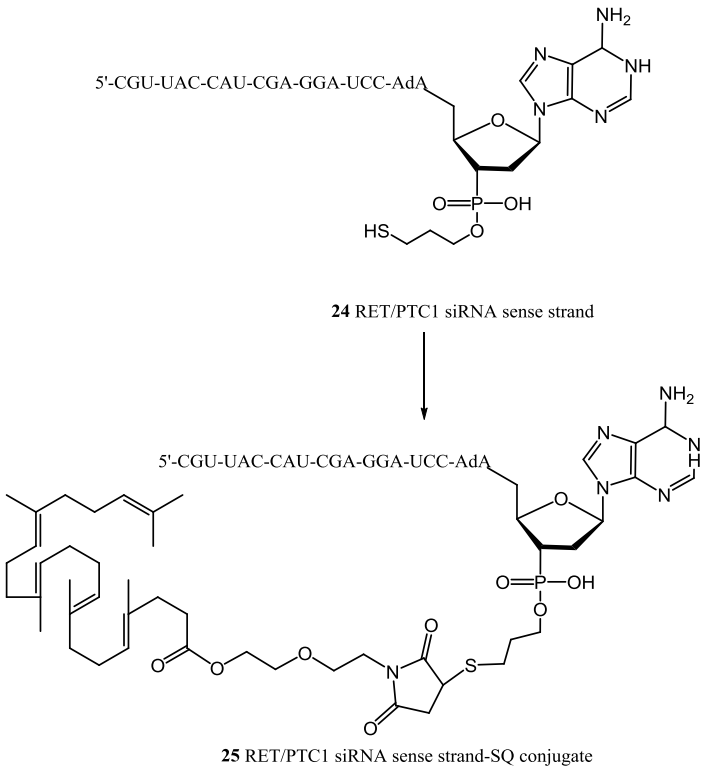

Fig. 13. Chemical structures of the siRNA sense strand and RET/PTC1 siRNA-SQ sense strand conjugate. Adapted from [63].

Thus, for squalene conjugation, 3′-end of the siRNA sense strand was chosen (**Fig. 13**) (*61*). Taking advantage of 3-mercaptopropyl phosphate group which was introduced at the 3′-end of the sense strand of each siRNA sequence during manufacturing on solid support, the more efficient conjugation was achieved by using maleimide group as thiol acceptor. For this purpose, squalene maleimide was first considered. In order to facilitate the accessibility of the maleimide functional group towards the modified SiRNA sense strand, a small ether linker was introduced between the maleimide group and the SQ group.

As thyroid papillary carcinoma (PTC) is often associated with RET gene rearrangements that generate RET/PTC fusion oncogene, a siRNA complementary to RET/PTC mRNA was used. Specifically, RET/PTC1 siRNA was used in this study because RET/PTC1 oncogene is one of the most frequent variant with RET/PTC3. Then, once the bioconjugate RET/PTC1 siRNA-SQ sense strand was synthesized, it was then hybridized with the antisense strand to form the duplex. The bioconjugates could then self-assemble in water into spherical NAs with a size of around 170 nm as measured by laser light scattering.

Compared with naked RET/PTC1 siRNA, RET/PTC1 siRNA-SQ NAs clearly improved the nucleic acid stability in serum. After intravenous injection, using RET/PTC1 xenograft mouse models, siRNA-SQ NAs were showed to inhibit tumor growth as well as oncogene and oncoprotein expression (*63, 64*). Similar studies with RET/PTC 3 siRNA-SQ NAs have confirmed these results (*65*).

Squalene based technology was also applied to prostate cancer (PCa), the most common neoplasia in men. SiRNA against TMPRSS2-ERG fusion oncogene which is found in 50% of patients, was recently squalenoylated using the same approach as mentioned above. The resulting siRNA TMPRSS2-ERG-SQ NAs showed improved therapeutic effectiveness against Pca, compatatively to

siRNA free (*66*, *67*).

Thus, squalenoylation offers a new non-cationic platform for the administration and transport of therapeutic siRNA.

4.2. Squalene-fondaparinux complex

Fondaparinux (Fpx) is the first-line anticoagulant in the treatment of short- and medium-term thromboembolic disease. Although molecular weight of fondaparinux (1728 Da) is much lower than low molecular weight heparin, this molecule has a very low bioavailability by oral route due to hydrophilic and polyanionic character. In addition, fondaparinux is instable in the acidic medium of the stomach and it undergoes fast enzymatic degradation. For those reasons, it is only administrated via subcutaneous route. Few strategies have been proposed to allow oral administration of Fpx, like Fpx-based emulsions, but the preparation methods are complicated, need heating, involve numerous excipients, and in fine, the drug loading is very low (less than 5%). As squalene is well known for its high oral bioavailability (more than 60%), its use could be very profitable to face all these disadvantages and may open a new way for the oral delivery of poorly bioavailable drugs.

It was experienced that the conjugation of squalene to Fpx was highly complicated and resulted in the loss of Fpx anticoagulant properties. Therefore, an ion-pair association between squalene and Fpx has been considered through the synthesis of monovalent (trimethyl ammonium chloride salt, SQ+) and bivalent (1,20-bis-trimethylammonium dimethanesulfonate salt, SQ++) cationic squalene derivatives before complexation polyanionic Fpx. SQ-Fpx NAs gave monodisperse and stable NAs with a mean diameter in the range of 120-150 nm. To note, SQ+-Fpx NAs showed a higher stability and encapsulation efficiency than SQ++-Fpx NAs. The encapsulation efficiencies were around 80% and the Fpx loadings reached 39 wt.%. Cryo-TEM and SAXS revealed spherical multilamellar "onion-type" nanoparticles which structure probably consisting in layers of SQ+ interacting with hydrated layers of Fpx. Presumably, both SQ+-SQ+ hydrophobic interactions and Fpx-SQ+ electrostatic interactions played a role in maintaining the cohesion of the nanoassemblies. *In vivo* experiments on rats showed that a small fraction of Fpx was absorbed after oral feeding of Fpx-SQ NAs. Nanoparticles were found to be completely disaggregated in the blood circulation, free Fpx being released from NAs in this compartment. Fpx NAs increased the plasmatic concentrations of Fpx in a dose-dependent manner but their oral bioavailability remained, however, very low (around 0.3%). Nevertheless, it has to be noted that maximal plasma concentration of Fpx observed after oral administration was close to the required plasma concentration in venous thromboembolism treatment. Furthermore, the Fpx oral bioavailability could be seriously increased (up to with 9%) when NAs were inserted in gastroresistant capsules (*68*).

5. SQUALENE-BASED BIOCONJUGATES WITH CONTRAST AGENTS

Magnetic resonance imaging (MRI) is one of the most powerful and widely used techniques for non-invasive diagnosis of diseases. It is based on the difference of relaxation times of protons (longitudinal T1 and transverse T2) and water concentration in normal and abnormal tissues. The intensity of the signal is modified by the presence of contrast agents (CAs) such as gadolinium chelates (mainly affecting T1 relaxation) using specific MRI sequences. This technique permits exploration of opaque organisms in 3D.

Among CAs, gadolinium (Gd^{3+})-based CAs are the most commonly used in clinics because of their ability to improve the contrast in MRI scans between normal and abnormal tissues. However, the lack of specificity of most CAs generate insufficient relaxivities for certain applications so that high doses of CAs are generally required in order to generate a local alteration of the water intensity signal which may induce toxicity in patients. Thus, squalenoylation of Gd^{3+} complex was explored to increase the relaxivity by guiding Gd^{3+} specifically within the tumor.

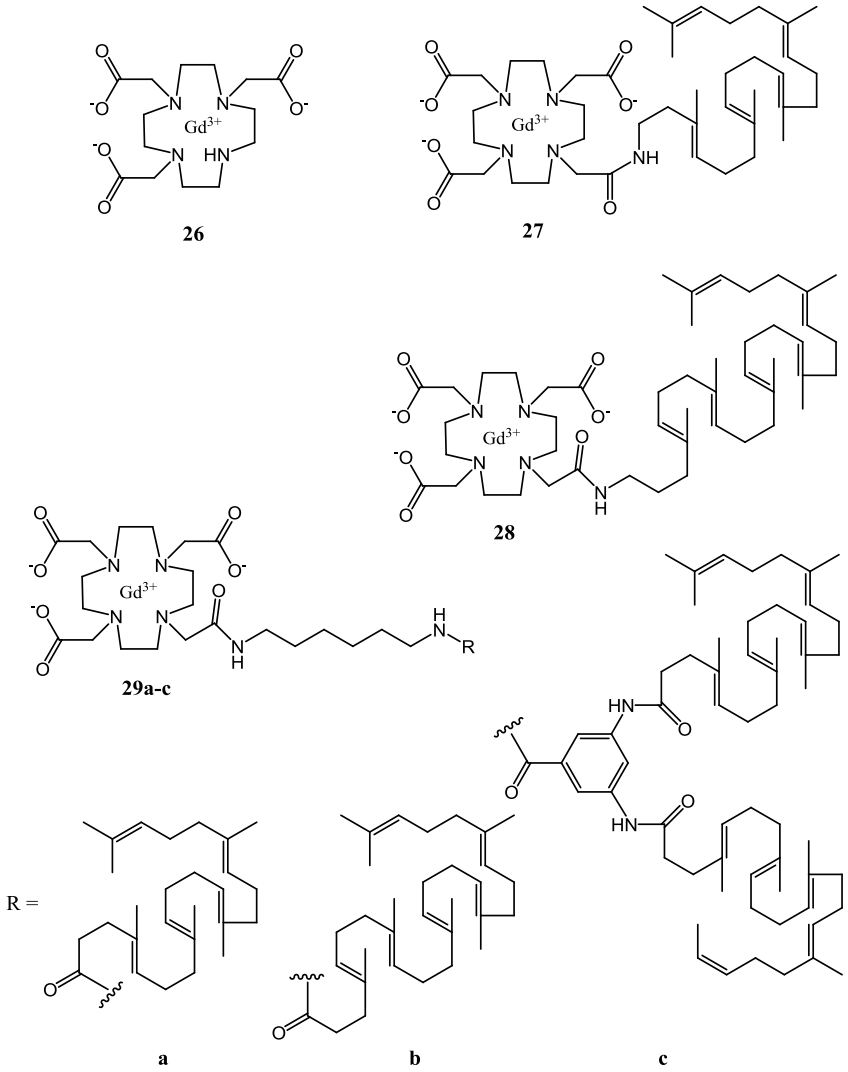

Fig. 14. Structure of DO_3A 26 and SQ-Gd^{3+}complexes 27–29. Adapted from [69].

A family of Gd^{3+} chelates-squalene derivatives was obtained by covalent coupling of the secondary amino group of the cyclen belonging to DOTA [1,4,7,10-tetrakis (carboxymethyl)-1,4,7,10-tetraazacyclododecane] to amino squalene derivatives using various linkers (**Fig. 14**). All of these Gd3+ chelates-squalene derivatives had the ability to self-assemble into micelles (8 to 30 nm for 27-29b compounds) or liposome-like (spherical to elliptical shape) structures (80-120 nm for 29c compound) with good Gd^{3+} payload (10-17 wt.%). The relaxivities of supramolecular CA were greatly enhanced (r1 = 15–22.1 mM-1 s-1 at 20 MHz and 15.6–20.4 mM-1 s-1 at 60 MHz and 310 K), which were about 5 times higher than clinically used Gd-DOTA (r1 = 3.5 and 3.1 mM-1 s-1, at 20 and 60 MHz and 310 K). Thus, squalenoylation of Gd3+ chelates provides a platform to conceive CAs with a greater degree of relaxivity efficacy (*69*).

Co-nanoprecipitation of Gem-SQ (4) and SQ-Gd^{3+} (27) were also performed to design nanoparticles with both imaging functionality and anticancer effect. The internal structure of Gem-SQ/SQ-Gd^{3+} NAs, revealed by electron microscopy after freeze-fracture (FFEM) and SAXS, an inverted bicontinuous cubic structure, with a lattice parameter of 100 Å. This novel nanoparticles showed high relaxivity (r1 = 20.1 mM-1s-1at 20 MHz) and significant cytotoxicity on MIA PaCa-2 pancreatic cancer cells, with potential applications in theranostics (i.e., medicines combining therapeutic and diagnostic capabilities).

Squalene-based NAs consisting of ultrasmall superparamagnetic iron oxide particles (USPIO) encapsulated into a series of squalenoylated anticancer compounds (i.e., Gem-SQ, PTX-SQ, cisplatine-SQ, DOX-SQ) are another example of nanocomposite for theranostic applications (*70, 71*). These nanomagnetite/squalenoyl antitumor prodrugs showed very good magnetic responsiveness and anticancer activity.

CONCLUSION

Since its first application in 2006, squalenoylation nanotechnology has showed great potential for the delivery of various therapeutic agents in a safer and more efficient manner. These nanomedicines represent a new concept with numerous advantages in comparison with the conventional nanocarriers, incl. absence of "burst release", high drug loading and biocompatibility. Their *in vivo* applications generally show high ability to act like a reservoir by protecting drugs from rapid degradation/metabolization, allowing to increase the drug plasma half-life, and to progressively release the drug inside the cell. In addition, they facilitate drugs to cross biological membranes, thus increasing drug concentration within the target cells or tissue. Proofs of this concept have been done with drugs presenting different physicochemical characteristics, like small hydrophilic or lipophilic molecules, and charged macromolecules. In general, the squalenoylation favorably modifies the pharmacokinetic profile and biodistribution of the carried drug, allowing its intravenous administration as nanoparticles and increasing its therapeutic index. This innovation has a versatile and generic character and has been awarded as the "European Inventor Award 2013".

LIST OF ABBREVIATIONS

Ad-SQ	adenosine-squalene
BBB	blood-brain-barrier
CAs	contrast agents
CED	convection-enhanced delivery
CNS	central nervous system
cryo-TEM	cryogenic transmission electron microscopy
dCK	deoxycytidine kinase
ddA-TP	dideoxyadenosine triphosphate
ddC	2′,3′-dideoxycytidine
ddC-SQ	2′,3′-dideoxycytidine-squalene
ddC-SQ-MP	2′,3′-dideoxycytidine-squalene monophosphate
ddI	2′,3′-dideoxyinosine
ddI-SQ	2′,3′-dideoxyinosine-squalene
DHA	docosahexaenoic acid

DOTA	1,4,7,10-tetrakis(carboxymethyl)-1,4,7,10-tetraazacyclododecane
DOX-SQ	doxorubicin-squalene
FFEM	electron microscopy after freeze-fracture
Fpx	fondaparinux
Gem-SQ	gemcitabine-squalene
Gem-SQ-MP	gemcitabine-squalene monophosphate
isoCA-4	isocombretastatin A-4
LDC	lipid-drug conjugates
LDL	low density lipoproteins
MCAo	middle cerebral artery occlusion
MIC	minimum inhibitory concentration
MRI	magnetic resonance imaging
MPS	mononuclear phagocyte system
MTC	maximum tolerated concentration
MTD	maximum tolerance doses
NAs	nanoassemblies
PCa	prostate cancer
PEG	polyethylene glycol
PNG	penicillin G
PNG-SQ	penicillin G-squalene
PNG-SQsens	penicillin G-squalene with sensitive bond
PTX	paclitaxel
RES	reticuloendothelial system
SAXS	small angle X-ray scattering
T-SQ	thymidine-squalene
USPIO	ultrasmall superparamagnetic iron oxide particles
VLDL	very low density lipoproteins
WAXS	wide-angle X-ray scattering

CONFLICT OF INTEREST

The authors declare no financial interest.

ACKNOWLEDGEMENTS

Some results described in this review were financed by the European Research Council under the European Community's Seventh Framework Programme FP7/2007-2013 Grand Agreement No. 249835. CNRS and Université Paris-Sud are also acknowledged for financial support. Jiao FENG received a scholarship from China Scholarship Council (CSC).

REFERENCES

1. K. Strebhardt, A. Ullrich, Paul ehrlich's magic bullet concept: 100 years of progress. *Nature reviews. Cancer* **8**, 473-480 (2008).
2. J. Kreuter, Nanoparticles--a historical perspective. *International journal of pharmaceutics* **331**, 1-10 (2007).

3. C. Olbrich, A. Gessner, O. Kayser, R. H. Muller, Lipid-drug-conjugate (ldc) nanoparticles as novel carrier system for the hydrophilic antitrypanosomal drug diminazenediaceturate. *Journal of drug targeting* **10**, 387-396 (2002).
4. S. Dueland *et al.*, Intravenous administration of cp-4055 (elacyt) in patients with solid tumours. A phase i study. *Acta oncologica (Stockholm, Sweden)* **48**, 137-145 (2009).
5. A. Y. Bedikian *et al.*, Phase 3 study of docosahexaenoic acid-paclitaxel versus dacarbazine in patients with metastatic malignant melanoma. *Annals of oncology : official journal of the European Society for Medical Oncology / ESMO* **22**, 787-793 (2011).
6. P. Couvreur *et al.*, Squalenoyl nanomedicines as potential therapeutics. *Nano letters* **6**, 2544-2548 (2006).
7. G. S. Kelly, Squalene and its potential clinical uses. *Alternative medicine review : a journal of clinical therapeutic* **4**, 29-36 (1999).
8. P. P. Simonen, H. Gylling, T. A. Miettinen, The distribution of squalene and non-cholesterol sterols in lipoproteins in type 2 diabetes. *Atherosclerosis* **194**, 222-229 (2007).
9. L. H. Reddy, P. Couvreur, Squalene: A natural triterpene for use in disease management and therapy. *Advanced drug delivery reviews* **61**, 1412-1426 (2009).
10. L. P. Jordheim, D. Durantel, F. Zoulim, C. Dumontet, Advances in the development of nucleoside and nucleotide analogues for cancer and viral diseases. *Nature reviews. Drug discovery* **12**, 447-464 (2013).
11. D. Desmaele, R. Gref, P. Couvreur, Squalenoylation: A generic platform for nanoparticular drug delivery. *Journal of controlled release : official journal of the Controlled Release Society* **161**, 609-618 (2012).
12. D. F. Roychowdhury, C. A. Cassidy, P. Peterson, M. Arning, A report on serious pulmonary toxicity associated with gemcitabine-based therapy. *Investigational new drugs* **20**, 311-315 (2002).
13. L. W. Hertel *et al.*, Evaluation of the antitumor activity of gemcitabine (2',2'-difluoro-2'-deoxycytidine). *Cancer research* **50**, 4417-4422 (1990).
14. V. Heinemann *et al.*, Cellular elimination of 2',2'-difluorodeoxycytidine 5'-triphosphate: A mechanism of self-potentiation. *Cancer research* **52**, 533-539 (1992).
15. D. Y. Bouffard, J. Laliberte, R. L. Momparler, Kinetic studies on 2',2'-difluorodeoxycytidine (gemcitabine) with purified human deoxycytidine kinase and cytidine deaminase. *Biochemical pharmacology* **45**, 1857-1861 (1993).
16. P. Couvreur *et al.*, Discovery of new hexagonal supramolecular nanostructures formed by squalenoylation of an anticancer nucleoside analogue. *Small (Weinheim an der Bergstrasse, Germany)* **4**, 247-253 (2008).
17. E. Lepeltier *et al.*, Self-assembly of squalene-based nucleolipids: Relating the chemical structure of the bioconjugates to the architecture of the nanoparticles. *Langmuir : the ACS journal of surfaces and colloids* **29**, 14795-14803 (2013).
18. L. H. Reddy *et al.*, A new nanomedicine of gemcitabine displays enhanced anticancer activity in sensitive and resistant leukemia types. *Journal of controlled release : official journal of the Controlled Release Society* **124**, 20-27 (2007).
19. L. Bildstein *et al.*, Extracellular-protein-enhanced cellular uptake of squalenoyl gemcitabine from nanoassemblies. *Soft Matter* **6**, 5570-5580 (2010).
20. L. Bildstein *et al.*, Transmembrane diffusion of gemcitabine by a nanoparticulate squalenoyl prodrug: An original drug delivery pathway. *Journal of controlled release : official journal of the Controlled Release Society* **147**, 163-170 (2010).

21. L. H. Reddy *et al.*, Preclinical toxicology (subacute and acute) and efficacy of a new squalenoyl gemcitabine anticancer nanomedicine. *The Journal of pharmacology and experimental therapeutics* **325**, 484-490 (2008).
22. D. Hariharan, A. Saied, H. M. Kocher, Analysis of mortality rates for pancreatic cancer across the world. *HPB : the official journal of the International Hepato Pancreato Biliary Association* **10**, 58-62 (2008).
23. S. Rejiba *et al.*, Squalenoyl gemcitabine nanomedicine overcomes the low efficacy of gemcitabine therapy in pancreatic cancer. *Nanomedicine : nanotechnology, biology, and medicine* **7**, 841-849 (2011).
24. L. H. Reddy *et al.*, Squalenoylation favorably modifies the in vivo pharmacokinetics and biodistribution of gemcitabine in mice. *Drug metabolism and disposition: the biological fate of chemicals* **36**, 1570-1577 (2008).
25. A. Maksimenko *et al.*, Therapeutic modalities of squalenoyl nanocomposites in colon cancer: An ongoing search for improved efficacy. *ACS nano* **8**, 2018-2032 (2014).
26. S. Mura *et al.*, In vitro investigation of multidrug nanoparticles for combined therapy with gemcitabine and a tyrosine kinase inhibitor: Together is not better.
27. A. Gaudin *et al.*, Pegylated squalenoyl-gemcitabine nanoparticles for the treatment of glioblastoma.
28. H. Hillaireau *et al.*, Anti-hiv efficacy and biodistribution of nucleoside reverse transcriptase inhibitors delivered as squalenoylated prodrug nanoassemblies. *Biomaterials* **34**, 4831-4838 (2013).
29. F. Puech *et al.*, Intracellular delivery of nucleoside monophosphates through a reductase-mediated activation process. *Antiviral research* **22**, 155-174 (1993).
30. J. Caron *et al.*, Squalenoyl nucleoside monophosphate nanoassemblies: New prodrug strategy for the delivery of nucleotide analogues. *Bioorganic & medicinal chemistry letters* **20**, 2761-2764 (2010).
31. A. Maksimenko, J. Caron, J. Mougin, D. Desmaele, P. Couvreur, Gemcitabine-based therapy for pancreatic cancer using the squalenoyl nucleoside monophosphate nanoassemblies.
32. J. T. Neary, M. P. Rathbone, F. Cattabeni, M. P. Abbracchio, G. Burnstock, Trophic actions of extracellular nucleotides and nucleosides on glial and neuronal cells. *Trends in neurosciences* **19**, 13-18 (1996).
33. T. V. Dunwiddie, S. A. Masino, The role and regulation of adenosine in the central nervous system. *Annual review of neuroscience* **24**, 31-55 (2001).
34. B. B. Fredholm, J. F. Chen, R. A. Cunha, P. Svenningsson, J. M. Vaugeois, Adenosine and brain function. *International review of neurobiology* **63**, 191-270 (2005).
35. E. Lepeltier *et al.*, Influence of the nanoprecipitation conditions on the supramolecular structure of squalenoyled nanoparticles.
36. A. Gaudin *et al.*, Squalenoyl adenosine nanoparticles provide neuroprotection after stroke and spinal cord injury. *Nature nanotechnology* **9**, 1054-1062 (2014).
37. A. Gaudin *et al.*, Pharmacokinetics, biodistribution and metabolism of squalenoyl adenosine nanoparticles in mice using dual radio-labeling and radio-hplc analysis.
38. A. Gaudin *et al.*, Transport mechanisms of squalenoyl-adenosine nanoparticles across the blood–brain barrier. *Chemistry of Materials* **27**, 3636-3647 (2015).
39. I. Paterniti *et al.*, Selective adenosine a2a receptor agonists and antagonists protect against spinal cord injury through peripheral and central effects. *Journal of neuroinflammation* **8**, 31 (2011).

40. D. O. Okonkwo *et al.*, A comparison of adenosine a2a agonism and methylprednisolone in attenuating neuronal damage and improving functional outcome after experimental traumatic spinal cord injury in rabbits. *Journal of neurosurgery. Spine* **4**, 64-70 (2006).
41. T. Laskay, G. van Zandbergen, W. Solbach, Neutrophil granulocytes--trojan horses for leishmania major and other intracellular microbes? *Trends in microbiology* **11**, 210-214 (2003).
42. N. Abed, P. Couvreur, Nanocarriers for antibiotics: A promising solution to treat intracellular bacterial infections. *International journal of antimicrobial agents* **43**, 485-496 (2014).
43. N. Sémiramoth *et al.*, Self-assembled squalenoylated penicillin bioconjugates: An original approach for the treatment of intracellular infections. *ACS Nano* **6**, 3820-3831 (2012).
44. C. F. Thorn *et al.*, Doxorubicin pathways: Pharmacodynamics and adverse effects. *Pharmacogenetics and genomics* **21**, 440-446 (2011).
45. E. H. Herman, A. N. el-Hage, V. J. Ferrans, B. Ardalan, Comparison of the severity of the chronic cardiotoxicity produced by doxorubicin in normotensive and hypertensive rats. *Toxicology and applied pharmacology* **78**, 202-214 (1985).
46. Y. Geng *et al.*, Shape effects of filaments versus spherical particles in flow and drug delivery. *Nature nanotechnology* **2**, 249-255 (2007).
47. A. Maksimenko *et al.*, A unique squalenoylated and nonpegylated doxorubicin nanomedicine with systemic long-circulating properties and anticancer activity. *Proceedings of the National Academy of Sciences of the United States of America* **111**, E217-226 (2014).
48. E. K. Rowinsky, R. C. Donehower, Paclitaxel (taxol). *The New England journal of medicine* **332**, 1004-1014 (1995).
49. A. J. ten Tije, J. Verweij, W. J. Loos, A. Sparreboom, Pharmacological effects of formulation vehicles : Implications for cancer chemotherapy. *Clinical pharmacokinetics* **42**, 665-685 (2003).
50. F. Dosio *et al.*, Novel nanoassemblies composed of squalenoyl-paclitaxel derivatives: Synthesis, characterization, and biological evaluation. *Bioconjugate chemistry* **21**, 1349-1361 (2010).
51. J. Caron *et al.*, Improving the antitumor activity of squalenoyl-paclitaxel conjugate nanoassemblies by manipulating the linker between paclitaxel and squalene. *Advanced healthcare materials* **2**, 172-185 (2013).
52. S. Borrelli *et al.*, New class of squalene-based releasable nanoassemblies of paclitaxel, podophyllotoxin, camptothecin and epothilone a. *European journal of medicinal chemistry* **85**, 179-190 (2014).
53. Z. Cheikh-Ali *et al.*, "Squalenoylcurcumin" nanoassemblies as water-dispersible drug candidates with antileishmanial activity.
54. J. K. Lam, M. Y. Chow, Y. Zhang, S. W. Leung, Sirna versus mirna as therapeutics for gene silencing. *Molecular therapy. Nucleic acids* **4**, e252 (2015).
55. R. Juliano, J. Bauman, H. Kang, X. Ming, Biological barriers to therapy with antisense and sirna oligonucleotides. *Molecular pharmaceutics* **6**, 686-695 (2009).
56. C.-f. Xu, J. Wang, Delivery systems for sirna drug development in cancer therapy. *Asian Journal of Pharmaceutical Sciences* **10**, 1-12 (2015).
57. J. Wang, Z. Lu, M. G. Wientjes, J. L. Au, Delivery of sirna therapeutics: Barriers and carriers. *The AAPS journal* **12**, 492-503 (2010).

58. L. Parhamifar, A. K. Larsen, A. C. Hunter, T. L. Andresen, S. M. Moghimi, Polycation cytotoxicity: A delicate matter for nucleic acid therapy-focus on polyethylenimine. *Soft Matter* **6**, 4001-4009 (2010).
59. W. T. Kuo, H. Y. Huang, Y. Y. Huang, Intracellular trafficking, metabolism and toxicity of current gene carriers. *Current drug metabolism* **10**, 885-894 (2009).
60. R. L. Juliano, The delivery of therapeutic oligonucleotides. *Nucleic acids research* **44**, 6518-6548 (2016).
61. M. Raouane, D. Desmaele, G. Urbinati, L. Massaad-Massade, P. Couvreur, Lipid conjugated oligonucleotides: A useful strategy for delivery. *Bioconjugate chemistry* **23**, 1091-1104 (2012).
62. J. Winkler, Oligonucleotide conjugates for therapeutic applications. *Therapeutic delivery* **4**, 791-809 (2013).
63. M. Raouane *et al.*, Synthesis, characterization, and in vivo delivery of sirna-squalene nanoparticles targeting fusion oncogene in papillary thyroid carcinoma. *Journal of medicinal chemistry* **54**, 4067-4076 (2011).
64. H. M. Ali *et al.*, Effects of silencing the ret/ptc1 oncogene in papillary thyroid carcinoma by sirna-squalene nanoparticles with and without fusogenic companion gala-cholesterol. *Thyroid : official journal of the American Thyroid Association* **24**, 327-338 (2014).
65. H. M. Ali *et al.*, Effects of sirna on ret/ptc3 junction oncogene in papillary thyroid carcinoma: From molecular and cellular studies to preclinical investigations. *PloS one* **9**, e95964 (2014).
66. G. Urbinati *et al.*, Antineoplastic effects of sirna against tmprss2-erg junction oncogene in prostate cancer.
67. G. Urbinati *et al.*, Knocking down tmprss2-erg fusion oncogene by sirna could be an alternative treatment to flutamide.
68. B. Ralay-Ranaivo *et al.*, Novel self assembling nanoparticles for the oral administration of fondaparinux: Synthesis, characterization and in vivo evaluation. *Journal of controlled release : official journal of the Controlled Release Society* **194**, 323-331 (2014).
69. M. Othman *et al.*, Synthesis and physicochemical characterization of new squalenoyl amphiphilic gadolinium complexes as nanoparticle contrast agents. *Organic & biomolecular chemistry* **9**, 4367-4386 (2011).
70. J. L. Arias *et al.*, Squalene based nanocomposites: A new platform for the design of multifunctional pharmaceutical theragnostics. *ACS nano* **5**, 1513-1521 (2011).
71. J. L. Arias, L. H. Reddy, P. Couvreur, Magnetoresponsive squalenoyl gemcitabine composite nanoparticles for cancer active targeting. *Langmuir : the ACS journal of surfaces and colloids* **24**, 7512-7519 (2008).

Squalenoylated Leu-enkephalin Nanomedicine

Squalenoylated Leu-enkephalin Nanomedicine:

As mentioned in the previous section, squalenoylation has showed great potential for the delivery of various therapeutic agents in a safer and more efficient manner. This new nanotechnology exhibits numbrous advantages in comparison with the conventional nanocarriers, including absence of "burst release", high drug loading and biocompatibility. Therefore, we propose to couple Leu-enkephalin with squalene to give the Leu-enkephalin-squalene bioconjugates. We hypothesized that these bioconjugates can form nanoparticles, which could protect the peptides from rapid degradation during circulation.

Research article:

A new painkiller nanomedicine to bypass the blood-brain-barrier and the use of morphine

Science Advances under review

Jiao FENG[1], Sinda LEPETRE-MOUELHI[1], Anne GAUTIER[1,3], Simona MURA[1], Catherine CAILLEAU[1], François COUDORE[2], Michel HAMON[3], Patrick COUVREUR[1]*

[1] Institut Galien Paris-Sud, UMR8612, Univ. Paris-Sud, Université Paris-Saclay, Châtenay-Malabry 92290, France
[2] Laboratoire de Neuropharmacologie, INSERM UMRS 1178, Univ. Paris-Sud, Université Paris-Saclay, Châtenay-Malabry 92290, France
[3] Centre de Psychiatrie et Neurosciences, INSERM UMR 894, Université Paris Descartes, 75014 Paris, France

*To whom correspondence should be addressed: *patrick.couvreur@u-psud.fr*.

ABSTRACT OF THE ARTICLE

The clinical use of endogenous neuropeptides has historically been limited due to pharmacokinetic issues, including plasma stability and blood-brain-barrier permeability. In this study, we show for the first time, that the rapidly metabolized Leu-enkephalin (LENK) neuropeptide may become pharmacologically efficient owing to a simple conjugation with the lipid squalene (SQ). LENK neuropeptide was included into nanoparticles (NPs) by conjugation to squalene using three different chemical linkers, i.e., dioxycarbonyl, diglycolate, and amide bond. This new squalene-based nanoformulation prevented rapid plasma degradation of LENK and conferred to the released neuropeptide a significant anti-hyperalgesic effect in a carrageenan-induced paw edema model in rats (Hargreaves test) which lasted longer than after treatment with morphine. Pretreatment with opioid receptor antagonists such as naloxone (brain-permeant) and naloxone methiodide (brain-impermeant) reversed the nanoparticles induced anti-hyperalgesia, indicating that the LENK-SQ NPs acted through peripherally located opioid receptors. Moreover, the biodistribution of DiD-fluorescently labeled LENK-SQ NPs showed a strong accumulation of the fluorescence within the inflamed paw, while no signal could be detected in the brain, confirming the peripheral effect of LENK-SQ NPs. This study represents a novel nanomedicine approach, allowing the specific delivery of LENK neuropeptide into inflamed tissues for pain control.

Keywords: Nanomedicine, Leu-Enkephalin, Squalene, Prodrug, Bioconjugate, Hyperalgesia, Inflammatory Pain, Opioid receptors, Peripheral effect, Rat

INTRODUCTION

Pain represents an important global health challenge for many reasons, including high prevalence, serious associated sequelae and the relative lack of efficient treatment , especially for neuropathic pain alleviation. Pain relevant disorders such as arthritis, cancer and pathological changes in nervous system are highly prevalent and bring great inconvenience and distress to the patients (*1*). Chronic pain has a significant impact not only on the patients themselves, but also on the broader community and economy. By activating μ-opioid receptors, the most powerful and widely used painkillers in current clinical practice are morphine and the related synthetic opioids. But morphinic treatments are associated with severe side effects, such as respiratory depression and addiction linked to the development of opioid tolerance and dependence (*2*). According to CDC/NCHS, National Vital Statistics System (*3*), every day, more than 115 people in the United States die after overdosing on opioids. The misuse of and addiction to opioids, especially morphine, represents a serious national crisis in the US (and probably also in other countries) that affects public health, as well as, social and economic welfare. This highlights the need to urgently find new painkillers. In this context, endogenous neuropeptides, such as enkephalin, remain an attractive option. Enkephalins activate both μ- and δ-opioid receptors, but with a ten-fold higher affinity towards δ-opioid receptors (*4*). Compared with μ-opioid receptor agonists, δ-opioid receptor ligands are believed to have a much lower abuse potential (*5*), as well as, reduced respiratory (*6*), gastrointestinal (*7*) and cognitive (*8*) impairments. However, enkephalins have historically been limited because of pharmacokinetic issues, and rapid plasma metabolization.

To date, the two main approaches to enhance the analgesic activity of opioid peptides relied on (i) the increase of the stability of endogenous peptides using enkephalinase inhibitors, or (ii) the chemical synthesis of exogenous peptides with enhanced lipophilicity and degradation resistance. However, due to insufficient enzymatic specificity, the enkephalinase inhibitors are often endowed with poorly tolerated side effects (*9*). In addition, the derivatization of peptides often ends-up with biologically inactive compounds, and the same applies to neuropeptides covalently linked to transport vectors for crossing the blood-brain-barrier (BBB) (*10*). This explains why none of the research efforts performed since decades ago has resulted in marketed medicines.

On the other hand, although nanoparticulate drug delivery systems represent an efficient approach for protecting drug molecules from rapid metabolization, only few were applied to enkephalins and enkephalin derivatives. In a primary study, Kreuter et al. (*11*) showed that intravenously injected dalargin-loaded polybutylcyanoacrylate nanoparticles coated with a non-ionic surfactant, induced time- and dose- dependent antinociceptive effects. In subsequent studies, positively charged nanocarriers were also used for the delivery of opiate-related drugs and peptides into the brain (*12-15*). Nevertheless, these approaches have met with limited success because, in general, the amount of nanoparticles able to cross the BBB remains very low (less than 1% of the injected dose) (*16*). In addition, the toxicity and elimination of nanoparticles from the brain parenchyma remain a major issue and this is especially true for the above mentioned cationic nanodrugs.

Thus, the design of safe analgesic nanoformulations able to restrict their activity peripherally and to optimize drug concentration at the site of injury may overcome these issues. Another advantage of targeting peripheral opioid receptors is to prevent and reverse the effects of multiple excitatory agents expressed in damaged tissue (*17*).

We report here a very simple and easy way to use the currently unusable LENK as analgesic drug following intravenous injection. To this goal, a new nanoformulation was achieved which proved capable of precise and efficient delivery of LENK for pain control. Practically, LENK was conjugated to squalene, a natural and biocompatible lipid, through various chemical linkers, resulting in a library of LENK lipidic prodrugs, which allowed the controlled release of the peptide. As shown previously with anticancer compounds (*18*), the linkage of LENK with squalene triggered the spontaneous self-assembly of the bioconjugates into LENK-squalene nanoparticles (LENK-SQ NPs) in water, which was attributed to the dynamically folded conformation of the natural lipid. The analgesic effect of these LENK-SQ NPs was evaluated on carrageenan-induced pain model using a thermal nociception test (Hargreaves) to assess hyperalgesia. Pain sensitivity was rated in response to a hot stimulus on the inflamed hind paw of rats. In addition, the *in vivo* biodistribution of NPs was investigated in mice using *in vivo* fluorescence imaging for assessing the ability of the LENK-SQ NPs to target the inflamed tissue. Finally, a toxicological study was also performed to ensure these NPs safety.

RESULTS

Synthesis of LENK-SQ conjugates

In this study, various squalenoyl-Leu-enkephalin (LENK-SQ) conjugates were designed with different linkers using bioconjugation (**Fig. 1**). Conjugation of squalene to LENK was performed by exploiting 2 sites: C-terminal acid and N-terminal amine. In order to modulate the release kinetics of LENK from NPs, three linkers were used with different sensitivity to hydrolysis in the following order: dioxycarbonyl (LENK-SQ-Diox also called “sensitive bound”) > diglycolic (LENK-SQ-Dig) > amide (LENK-SQ-Am).

Practically, the squalenic acid was coupled to C-terminal LENK using a dioxycarbonyl linker (LENK-SQ-Diox, conjugate 1) or squalenol was conjugated to N-terminal LENK through a diglycolic spacer (LENK-SQ-Dig, conjugate 2). Starting from squalenic acid, it was also possible to perform the linkage to N-terminal LENK using a simple amide bond (LENK-SQ-Am, conjugate 3).

The LENK-SQ-Diox conjugate was synthesized by alkylation of the carboxylate function of the peptide with the chloromethyl ester of squalenic acid, which was prepared upon treatment of squalenic acid with chloromethyl chlorosulfate. In order to avoid N-terminal conjugation, Fmoc strategy was first adopted for the protection of the primary amino group of LENK, but due to early release of the peptide from Fmoc-LENK-SQ during the deprotection step, this approach was abandoned in favor of Alloc (allyloxycarbonyl) strategy. Thus, the LENK was protected with an Alloc group on its N-terminal amine prior to react with the chloromethyl ester of squalenic acid. Subsequent deprotection of Alloc-LENK-SQ under neutral conditions was then achieved by catalytic transfer hydrogenation method using triethylsilane and 10% Pd-C (*19*), affording pure LENK-SQ-Diox in 9.5% yield.

The LENK-SQ-Dig prodrug with 2′-diglycolate spacer was synthesized by reaction of the squalenol with diglycolic anhydride before reaction with the condensing agent and LENK, resulting in 69% yield. The oxa moiety of the linker was intended to enhance the susceptibility to hydrolysis by increasing the distance between LENK and squalene and so the accessibility to the linkage.

Direct conjugation between LENK and squalenic acid via single amide bond was achieved by acid activation using ethyl chloroformate, affording LENK-SQ-Am in 73% yield.

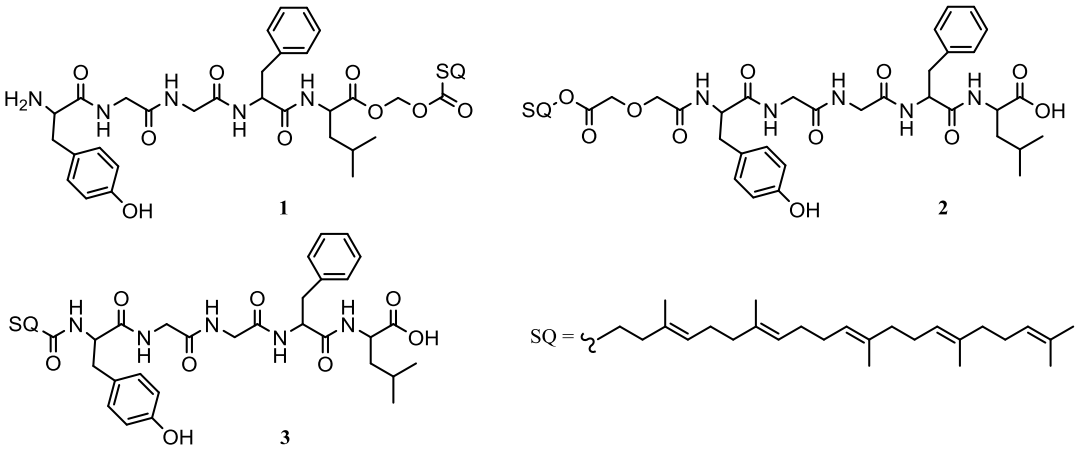

Fig. 1. Chemical structures of the bioconjugates. (1) Leu-Enkephalin-squalene with dioxycarbonyl linker (LENK-SQ-Diox), **(2)** Leu-Enkephalin-squalene with diglycolic linker (LENK-SQ-Dig), and **(3)** Leu-Enkephalin-squalene with amide linker (LENK-SQ-Am).

Preparation and characterization of LENK-SQ NPs

All bioconjugates showed the capability to self-assemble as NPs in aqueous solution after nanoprecipitation from LENK-SQ ethanolic solutions. When measured by DLS, the size of the NPs varied from 60 to 120 nm, depending on the linkage between squalene and enkephalin (**Fig. 2**). The difference in NPs zeta potential was related to the nature of the exposed amino acids onto the NPs surface. Indeed, in case of the LENK-SQ-Diox bioconjugate, the squalene conjugation on the C-terminus LENK peptide let its N-terminus site free (primary amino group), leading to a net positive charge. On the contrary, the zeta potential became negative when the conjugation with SQ was performed on the N-terminus LENK peptide (LENK-SQ-Dig and LENK-SQ-Am). Drug loadings (**Fig. 2)** ranged between 53% and 60% which was much higher than in conventional nanoparticles or liposomes which amounted to a maximum of 5% (*20*, *21*). **Fig. 2** shows representative cryogenic transmission electron microscopy (cryo-TEM) images of the LENK-SQ NPs at concentrations of 4 mg/mL in Milli-Q water. They displayed spherical and monodisperse structures with sizes ranging from 50 nm to 100 nm. The slight discrepancy between DLS and Cryo-TEM size measurements could be attributed to the known hydrodynamic radius-related differences (*22*). The sizes and the surface charges of the LENK-SQ NPs were found to be quite stable at +4°C (**Fig. S6**).

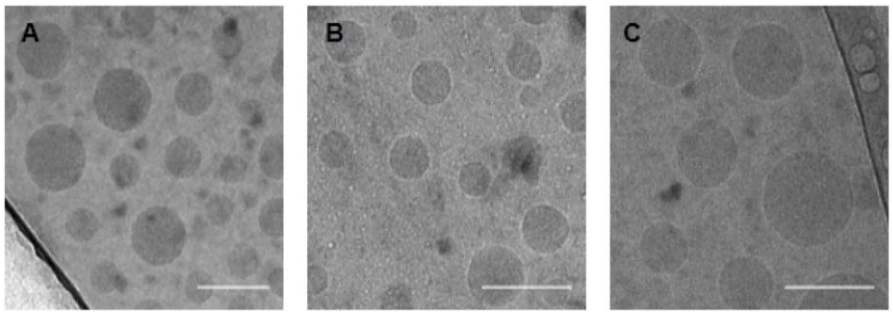

Compounds	Size (nm)	PDI	Zeta potential (mV)	Drug loading (%)
LENK-SQ-Diox	120±6	0.25±0.01	+33±4	57.38
LENK-SQ-Dig	75±11	0.13±0.05	-35±7	53.41
LENK-SQ-Am	122±22	0.08±0.01	-31±10	59.22

Fig. 2. NPs characterization. Representative Cryo-TEM images showing the formation of NPs from different bioconjugates: **(A)** LENK-SQ-Diox NPs, **(B)** LENK-SQ-Dig NPs, and **(C)** LENK-SQ-Am NPs. Scale bars = 100 nm. Physicochemical characteristics of NPs (ie. size, polydispersity index (PDI), zeta potential and % drug loading) are shown in the table.

In vitro release of LENK from NPs in serum

The incubation of LENK-SQ-Diox in serum resulted in a decrease of the bioconjugate, which correlated well with the release of the peptide (**Fig. 3A)**. The concentration of the bioconjugate decreased gradually till 7h, while LENK-SQ-Diox NPs progressively released the free LENK peptide. The peptide was then slowly degraded by the peptidases of the serum but still lasted beyond 10 h post-incubation (**Fig. 3A**). The incubation of LENK-SQ-Dig in serum resulted in a decrease of the bioconjugate until completely disappearance at 2 h, but no presence of free peptide was detected. The RP-HPLC analyses, however, highlighted a slow release of the peptide still attached to its linker. This release reached a maximum at 45 min followed by progressive degradation of the peptide-linker fragment which could still be detected over 10h (**Fig. 3B**). On the contrary, LENK-SQ-Am remained stable in serum, without significant decrease during 48 h, and no peptide was released in the course of the experiment (**Fig. 3C**). It was observed that the degradation of LENK free was very fast (half-life 2 min), whereas the LENK-SQ bioconjugate was unaffected during the course of the experiment (60 min) (**Fig. S7**).

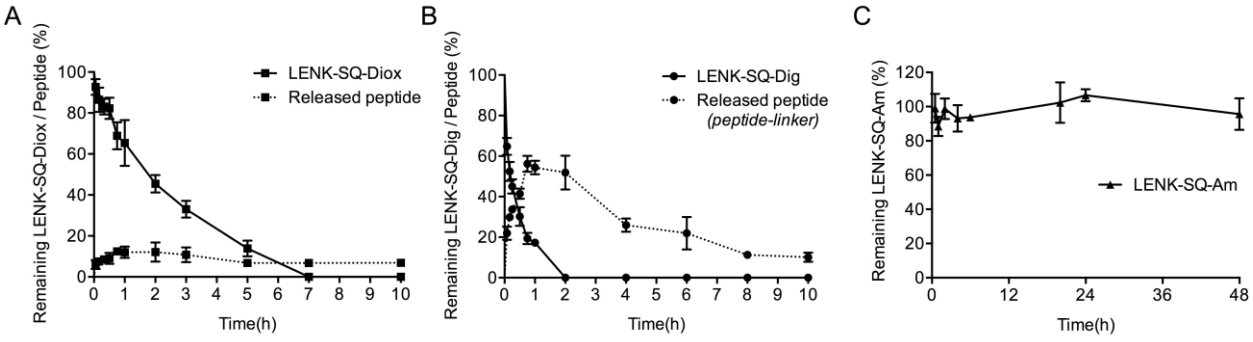

Fig. 3. *In vitro* bioconversion of LENK-SQ bioconjugates into LENK in the presence of serum. (A) LENK-SQ with dioxycarbonyl linker **(B)** LENK-SQ with diglycolic linker **(C)** LENK-SQ with amide bond. Solid lines

and dashed lines represent the bioconjugates and the released peptides, respectively.

Analgesic efficacy of LENK-SQ NPs

The anti-hyperalgesic effect of LENK-SQ NPs was determined in a carrageenan-induced paw edema model in rats. Baseline measurements of paw withdrawal latencies (PWL) were made prior to carrageenan injection using Hargreaves test (*23*) and presented a mean value ± SEM (n = 8) of 6.65 ± 0.37 s. Then, thermal sensitivities were evaluated 3 h after carrageenan injection into the right hind paw, which corresponded to the peak inflammatory response. Anti-hyperalgesic effects were assessed using the same test at various times after acute administration of the different drug treatments at this 3 h inflammation peak (**Fig. 4**).

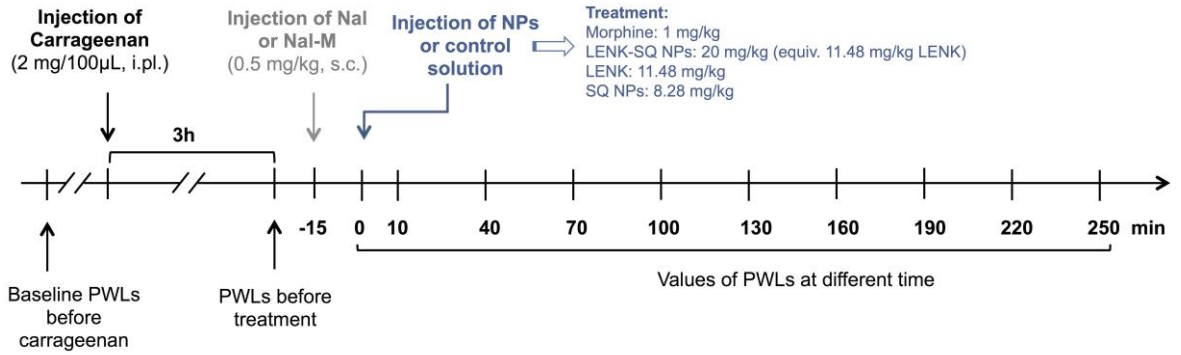

Fig. 4. Experimental design for algesimetry. The antinociceptive effect of NPs was tested in a pathophysiological context induced by an intraplantar carrageenan injection (2% in saline, 100 µL). Involvement of central or peripheral opioid receptors was performed using a brain-permeant opioid antagonist naloxone (Nal) and a brain-impermeant opioid receptor antagonist naloxone methiodide (Nal-M). NPs suspensions or control solutions were injected intravenously with a dose volume of 10 mL/kg during 30 s. Hargreaves test was performed 10 min after NPs administration and then every 30 min till 250 min. The dose of LENK-SQ NPs 20 mg/kg was equiv. to 11.48 mg/kg LENK and to 8.28 mg/kg SQ NPs, and corresponded to 20.66 mmol/kg for both LENK-SQ and LENK.

Effect of intraplantar λ-carrageenan injection on thermal sensitivity. Intraplantar injection of λ-carrageenan into the right hind paw induced a local inflammatory response characterized by marked edema, hyperthermia, and hyperalgesia restricted to the injected right hind paw. Thermal hypersensitivity was developed in all the rats with a mean decrease of 52.48% of PWL compared to the basal PWLs in naïve rats. ($P < 0.001$; see **Fig. 5**).

Effect of morphine on thermal hyperalgesia. The acute treatment with 1 mg/kg morphine (**Fig. 5A**) reduced the thermal hyperalgesia as shown by the resulting significant increase in PWLs. Indeed, 10 min post-morphine injection, the PWL reached 12.87 ± 1.38 s, while it remained at 3.05 ± 0.20 s after treatment with a control dextrose solution (**Fig. 5A**). However, morphine anti-hyperalgesic pharmacological activity disappeared rapidly and no longer significant effect was observed as soon as 100 min post-morphine administration (**Fig. 5A**).

Effect of LENK-SQ NPs on thermal hyperalgesia. The anti-hyperalgesic effect of LENK-SQ NPs with the 3 different linkers was evaluated during 4 h after their administration (**Fig. 5C-H**). All injected rats with LENK-SQ NPs displayed significant reduction of thermal hyperalgesia, as expressed by a dramatic increase of respective AUC values in comparison with λ-carrageenan-treated rats injected with either the free LENK peptide or the blank SQ NPs **(Fig. 5D, F, H)**. In particular, the

anti-hyperalgesic activity was significant at all time points from 10 min to 130 min in rats injected with LENK-SQ Diox NPs or LENK-SQ Am NPs (**Fig. 5C, G**). As shown in **Fig. 5E**, LENK-SQ-dig NPs also displayed a significant anti-hyperalgesic effect, with a maximum increase in PWL maintained from 10 min to 130 min post-injection, and a progressive decline down to baseline at 220 min. Interestingly, maximal PWL values reached after administration of LENK-SQ NPs in λ-carrageenan-treated rats corresponded to basal PWL values measured in control naïve rats, before λ-carrageenan treatment (**Fig. 5C, E, G**), indicating a pure anti-hyperalgesic action of these nanoparticles. In contrast, morphine injection in λ-carrageenan-treated rats resulted in PWL values twice as high as those found in control naïve rats (**Fig. 5A**), as expected of not only an anti-hyperalgesic effect but also the well established analgesic effect of the opiate agonist. In addition, blank SQ NPs (without the LENK) did not demonstrate any anti-hyperalgesic activity (**Fig. 5**), which indicated that the analgesic response to LENK-SQ NPs administration resulted from the release of LENK peptide.

Effects of opioid receptor blockade using naloxone and naloxone methiodide. In order to ascertain the involvement of central or peripheral opioid receptors during the anti-hyperalgesic effect of LENK-SQ NPs, naloxone (Nal, brain-permeant opioid receptor antagonist) or naloxone methiodide (Nal-M, brain-impermeant opioid receptor antagonist) (*24*) were subcutaneously injected 15 min prior to the injection of morphine or NPs (**Fig. 4**). Pre-administration of the non-selective *opioid receptor antagonist Nal* (0.5 mg/kg s.c.) abolished the amplitude and the duration of the anti-hyperalgesic effect of morphine (PWL 3.20 ± 0.59 s vs 12.87 ± 1.38 s at 10 min) and decreased the corresponding AUC value by 81% in comparison with the morphine group (**Fig. 5B**). The peripheral opioid receptor antagonist, Nal-M, was markedly less effective since it reduced the morphine's effect by only 13%. (**Fig. 5A** and **5B**). Interestingly, pre-administration of either Nal or its quaternary derivative Nal-M, abrogated the anti-hyperalgesic effect of the three LENK-SQ NPs (**Fig. 5C-H**). Indeed, Nal pre-treatment caused a reduction of 66%, 105% or 73% of the AUC values compared to these found in rats injected with LENK-SQ-Diox, LENK-SQ-Dig and LENK-SQ-Am NPs alone, respectively. The corresponding reductions in AUC values with Nal-M reached 81%, 99% and 96%, respectively, indicating that the selective blockade of peripheral opioid receptors only was enough to abrogate the anti-hyperalgesic effects of LENK-SQ NPs.

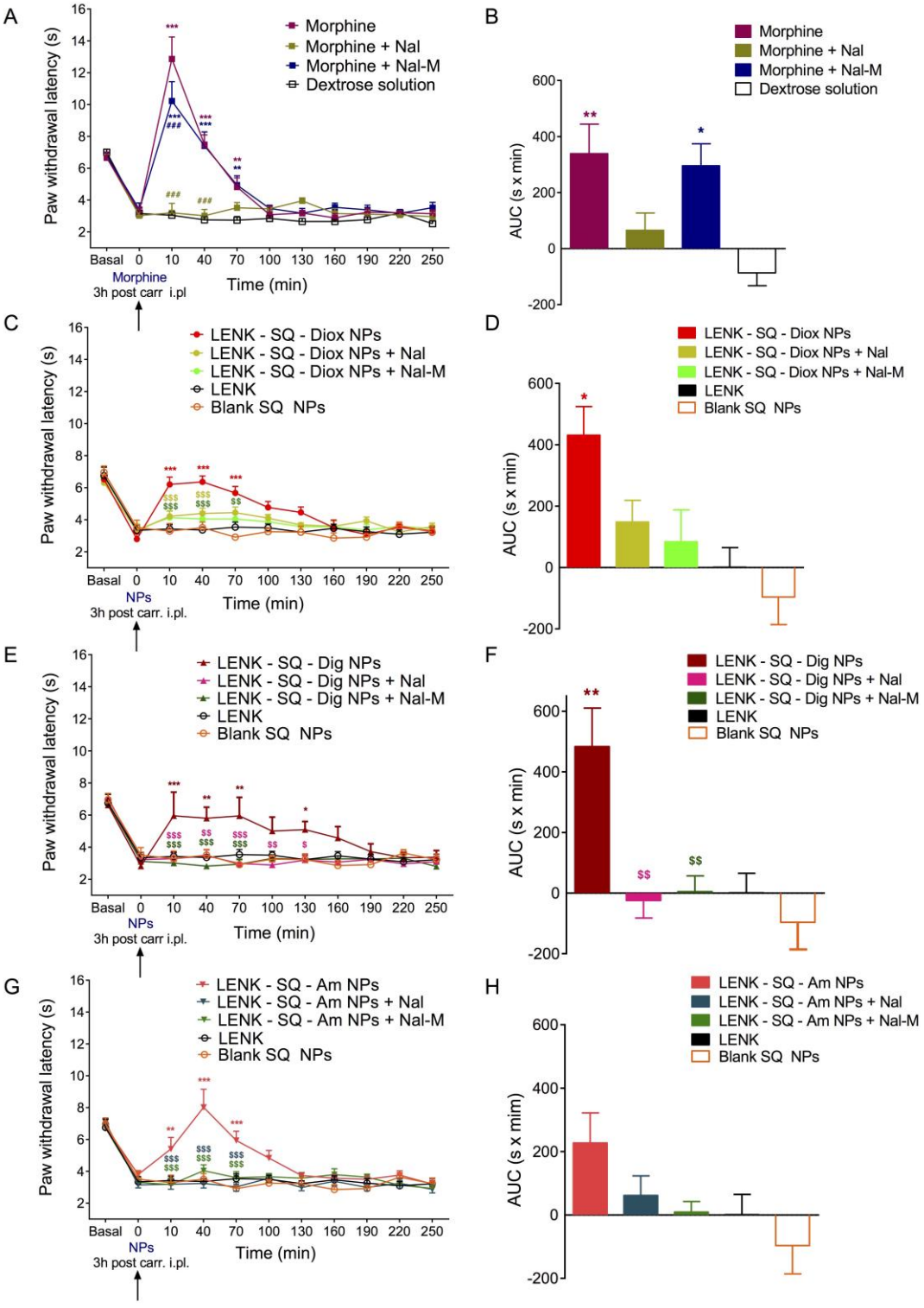

Fig. 5. Anti-hyperalgesic effects of acute treatment with Morphine (A, B), LENK-SQ-Diox NPs (C, D), LENK-SQ-Dig NPs (E, F) and LENK-SQ-Am NPs (G, H) in λ-carrageenan-induced inflammatory pain injected rats. Administration of morphine, LENK-SQ NPs, Nal, Nal-M, LENK, blank SQ NPs or dextrose solution (vehicle) was performed (arrow, 0 on abscissa) 3 h after λ-carrageenan injection into the right hind paw. Morphine **(A)**, LENK-SQ-Diox NPs **(C)**, LENK-SQ-Dig NPs **(E)** and LENK-SQ-Am NPs **(G)** induced an increase in paw withdrawal latency (in seconds, mean ± SEM of independent determinations in 5-9 animals per group) in the Hargreaves test. *, #, $ P<0.05, **, ##, $$ P<0.01, ***, ###, $$$ P<0.001 (*: compared to dextrose solution or LENK solution, #: compared to morphine; $: compared to LENK-SQ NPs. Two-way

Anova with repeated measures, Bonferroni post test.). Nal or Nal-M was administered 15 min prior to morphine or LENK-SQ NPs injection. Basal on abscissa: control (naïve) rats (prior to λ-carrageenan injection). **B, D, F** and **H**: Bars are the mean ± SEM of AUCs (second x minute) of the cumulative durations derived from the time course changes **(A, C, E** and **G)** in paw withdrawal latency after the various treatments. *, $ P<0.05, **, $$ P<0.01, ***, $$$ P<0.001, one way Anova, Tukey post test, *: compared to dextrose (vehicle) or LENK solution, $: compared with LENK-SQ NPs.

Biodistribution of LENK-SQ NPs

The *in vivo* biodistribution of LENK-SQ-Am NPs was assessed after intravenous injection of DiD-fluorescently labeled LENK-SQ-Am NPs in a murine λ-*carrageenan*-induced *paw* edema model (right hind paw). The fluorescence in tissues was monitored up to 24h, non-invasively, from the abdomen side using an IVIS Lumina (**Fig. 6**). Mice injected with saline into the paw were used as non-inflamed control. The real-time *in vivo* imaging showed, in comparison with the healthy paw, an increase by 2-3 times of the average radiant efficiency within the inflamed paw after iv injection of fluorescent LENK-SQ-Am NPs (**Fig. 6A, D, F**). In a control experiment, when the λ-carrageenan administered *mice* were intravenously injected with a single DiD solution, no significant accumulation of fluorescence was observed in the inflamed paw (**Fig. 6C, F**). In another control experiment, mice were injected locally with saline in the hind paw and intravenously treated with fluorescent LENK-SQ NPs. No significant accumulation of fluorescence at hind paw level was also observed under this condition (**Fig. 6B, E**) showing that the accumulation of fluorescence in the λ-carrageenan-inflamed paw was not due to the local hind paw injection *per se*. In an additional experiment, it was shown that the incubation in serum of LENK-SQ NPs containing the fluorescent dye (DiD) and a fluorescent quencher (DiR) resulted in the progressive appearance of fluorescence, the dynamics of which indicating a relatively slow dissociation of LENK-SQ nanoparticles in serum: 20% after 5 min and 50% after 30 min. This suggested that under our *in vivo* conditions, a significant proportion of intact NPs could reach the inflamed tissue (**Fig. S8**).

Finally, in a separate experiment, 4 h after the intravenous injection of fluorescent NPs or DiD solution, animals were euthanized and transcardially perfused with 40 mL of saline to remove the fluorescence from the blood. After collection of tissues, a strong *ex vivo* fluorescence signal was again observed in the inflamed paw, but also in the liver, the spleen and the lungs, whereas no detectable accumulation of fluorescence occurred in the brain of the animals (**Fig. S9**).

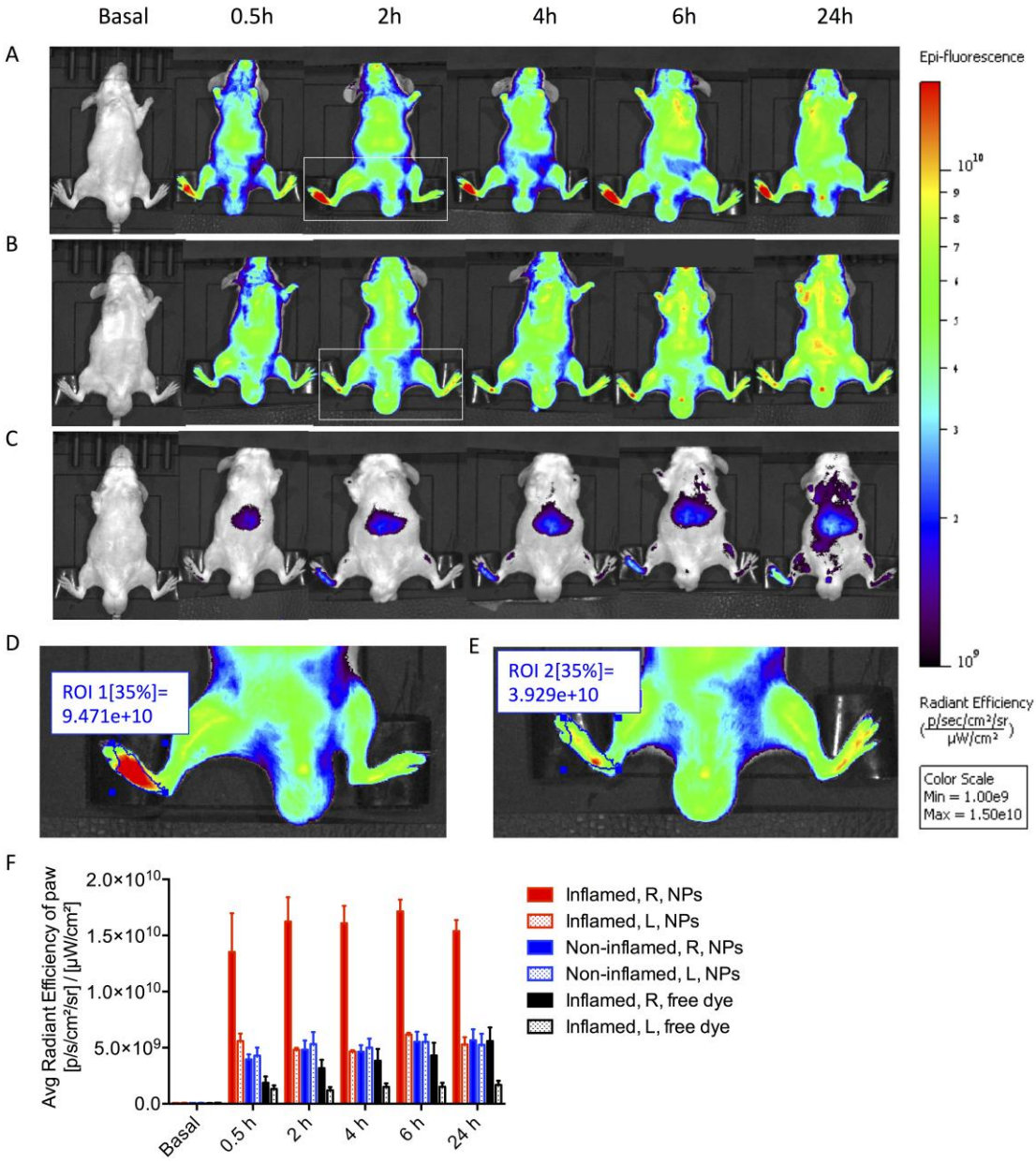

Fig. 6. IVIS® Lumina scan of mice and of their organs after intravenous administration of fluorescent LENK-SQ-Am NPs or control fluorescent dye solution (ventral view). (A) Biodistribution of fluorescent LENK-SQ-Am NPs in mice with inflamed right hind paw. (B) Biodistribution of fluorescent LENK-SQ-Am NPs in mice with non-inflamed hind paw (saline only injected into the right hind paw). (C) Biodistribution of free dye in mice with inflamed right paw. (D) Zoom of group A at 2 h. (E) Zoom of group B at 2 h. (F) Quantitative analysis of the paws with the same region of interest (ROI). R= right hind paw and L= left hind paw.

Toxicity study

The overall toxicity of LENK-SQ NPs was investigated 24 h and 48 h after their intravenous administration (20 mg/kg) in rats and compared to control animals injected with 5% dextrose solution. The levels of aspartate transaminase (AST) (**Fig. S10A**) and alanine transaminase (ALT) (**Fig. S10B**) were not increased in the LENK-SQ NPs group, indicating no toxicity towards the liver which was confirmed by histological analysis of this tissue at 24h and 48 h (**Fig S10C-F**). The observations of

the spleen (**Fig. S10G-J**), the kidneys (**Fig. S10K-N**), the lungs (**Fig. S10O-R**) and the heart (**Fig. S10S-V**) didn't show any morphological damage after LENK-SQ NPs administration, too. Together, these results show that the LENK-SQ NPs may be considered as safe upon systemic intravenous administration at the therapeutic dose of 20 mg/kg.

DISCUSSION

Peptides and proteins have great potential as therapeutic macromolecules. However, their use in the clinical practice is generally hampered by poor serum stability and rapid metabolization (*25*). In this context, the «squalenoylation» technology should be of great interest as we showed here, for the first time, that it allows the delivery of therapeutic amounts of LENK neuropeptide for efficient pain control. The so-called squalenoylation approach, which refers to the linkage of a drug to the squalene, has already been proposed for small molecules, mainly for anticancer compounds, like gemcitabine, doxorubicine or cis-platin (*26*) or for the other molecules, like adenosine, ddI or ddC (*27*). Nevertheless, the conjugation of a peptide to squalene has been an innovative, rather tricky achievement for the following reasons: (i) peptides are unstable biomolecules, and their chemical engineering is not easy, (ii) peptides are hydrophilic molecules, whereas squalene is a lipid, insoluble in water. This makes the chemical reaction rather uncertain and (iii) the chemical modification of a peptide often results in a loss of its pharmacological activity. The chemical approach used in the present study has overcome all these complications, allowing the design of a small library of innovative enkephalin-squalene bioconjugates with a preserved pharmacological activity. For the synthesis of these bioconjugates, we took advantage of the remarkable dynamically folded conformation of squalene to chemically conjugate this natural lipid with the neuropeptide using different linkers. Although it is well known that the N-terminal of LENK is required for binding to opioid receptors (*28*), the conjugation on N-terminal was also achieved, based on the fact that the amide bond is susceptible to be cleaved by overexpressed peptidases within inflammation site (*29*). Thus, the resulting LENK-SQ prodrugs were synthesized with either direct amide bond, diglycolic or dioxycarbonyl linker in order to investigate the possible influence of the linkage stability on the peptide release. It was expected that LENK-SQ-Diox released faster than LENK-SQ-Dig, and LENK -SQ-Am was supposed to trigger the slower release as reported in the literature (*30*). Both LENK-SQ-Am and LENK-SQ-Dig, were obtained in good yields (around 70%). The third one with dioxycarbonyl linker led to a lower yield due to an additional step for removal of the alloc group, followed by two successive purifications.

The LENK-SQ bioconjugates were then formulated as nanoparticles in dextrose solution (2 mg/mL) with impressively high drug payload (i.e. 53 to 59%), using simple nanoprecipitation technique without the aid of any surfactant. It is noteworthy that such drug payload was dramatically higher than into liposomes (*20*) or PLGA (*21*) enkephalin-loaded nanoparticles (respectively 0.4% and 4.75 % drug loading), which might explain why the latter two nanoformulations had never been used for *in vivo* pharmacological studies. The size of the NPs varied from 61 nm to 112 nm, depending on the peptide and the conjugation site (**Fig. 2**). The NPs displayed spherical and monodisperse structures with net positive or negative surface charge (**Fig. 2**), which could be attributed to the free terminal function of the peptide depending on the bioconjugation mode. Indeed, free N-terminal amine function led to a net positive surface charge while free C-terminal acid function resulted in a net negative surface charge.

In order to ascertain that free LENK peptide could be released from the LENK-SQ nanoparticles, we tested the chemical stability of the different linkers (i.e., direct amide or dioxycarbonyl or diglycolate spacers) after incubation of the LENK-SQ NPs with mouse serum (**Fig. 3**). Corresponding experiments clearly showed that LENK peptide was released from LENK-SQ-Diox and LENK-SQ-Dig but not from LENK-SQ-Am (**Fig. 3**). In the case of LENK-SQ-Diox and LENK-SQ-Dig, the release of the respective LENK and LENK-linker fragment was followed by a progressive degradation of the peptide, due to serum enkephalinases (**Fig. 3A** and **3B**). Of note, in the case of the LENK-SQ-Diox bioconjugate, both the LENK and the squalene moieties were each linked through an ester bond to the dioxycarbonyl linker. In the case of the LENK-SQ-Dig bioconjugate, the diglycolate linker was attached on one side to squalene by an ester bond and on the other side to the LENK through an amide bond when in the LENK-SQ-Am bioconjugate a direct amide bond connected the LENK to the SQ moiety. The absence of release of LENK from LENK-SQ-Am was not surprising given that, generally, amide bond is chemically and enzymatically more stable than ester bond (*31, 32*). Furthermore, it is well known that N-terminal modification of linear peptides increases the peptidase resistance, which is the case for LENK-SQ-Am and LENK-SQ-Dig (*33*). Finally, as mouse serum is particularly rich in esterases, it was expected that the release of LENK from LENK-SQ NPs mainly resulted from enzymatic hydrolysis of ester bond (*31*). Despite these *in vitro* data showing that depending on the type of linker, whether or not the LENK peptide was released, all the 3 conjugates were recruited for anti-hyperalgesia experiments. It was expected that the more aggressive *in vivo* enzymatic content, particularly rich in proteolytic enzymes at the inflammation site, will contribute to the release of LENK from all the bioconjugates (*29*). Indeed, the presence of high concentrations of proteolytic enzymes like chymotrypsin, cathepsin D and other proteases in inflammatory exudates has been reported which also indicates their important role in the inflammatory process (*29*).

Then, anti-hyperalgesic properties of LENK-SQ NPs were evaluated using an animal model of inflammatory hyperalgesia that mimics human clinical pain conditions (*34*). The anti-hyperalgesic activity was assessed after a single intravenous administration of the different LENK-SQ NPs in the λ-carrageenan-induced inflammatory paw model using Hargreaves test. All LENK-SQ NPs displayed a significant anti-hyperalgesic effect on inflamed hind paw. The anti-hyperalgesic effect was less intense than after morphine treatment, but nanoparticles evidenced a much longer lasting effect. Surprisingly, LENK-SQ-Am NPs, which was expected to release the peptide slower in comparison with the other two NPs, exhibited a stronger effect with a shorter duration, probably because the enzymatic serum capability is not predictive of the enzymatic ecosystem in the inflamed paw. LENK-SQ-Dig NPs and LENK-SQ-Diox NPs had nearly the same anti-hyperalgesic profile with prolonged effect, resulting in a significantly higher AUC than morphine and LENK-SQ-Am NPs. In particular, the LENK-SQ-Dig NPs showed an anti-hyperalgesic effect which lasted twice as long as morphine. In addition, as expected for an analgesic compound, PWL values after morphine treatment in λ-carrageenan-treated rats exceeded basal values in naïve healthy rats, whereas, in contrast, under the conditions used here, PWL values after LENK-SQ NPs just reached these basal values (**Fig. 5**). This would suggest that LENK nanoparticles are devoid of analgesic properties but are especially potent to counteract hyperalgesia in chronic pain suffering subjects. However, further studies are required to assess this hypothesis.

Pretreatment with Nal (a prototypical opioid antagonist) prevented the increase in PWL evoked by LENK-SQ NPs as well as morphine, indicating that the anti-hyperalgesic effect of all these compounds was mediated by opioid receptors. On the other hand, pretreatment with Nal-M (which does not cross the BBB, (*24*)) only marginally decreased the anti-hyperalgesic effect of morphine,

suggesting that the drug acted mainly through central and, to a lesser extent, peripheral opioid receptors. In contrast, Nal-M pretreatment abolished the anti-hyperalgesic effect of LENK-SQ NPs, which clearly demonstrated that all three LENK-SQ NPs acted exclusively through peripherally located opioid receptors.

In order to investigate the ability of LENK-SQ NPs to address the peptide towards the inflamed tissue, biodistribution studies were performed using *in vivo* fluorescence imaging in a mouse carrageenan-induced paw edema model. Our data clearly highlighted the ability of the nanoparticles to gain access to the peripheral inflamed tissue. Indeed, intravenous injection of fluorescent DiD-labeled LENK-SQ NPs in inflammation-bearing mice resulted in a dramatic increase of fluorescence within the inflamed hind paw, up to a level 3-fold higher than in the contralateral non-inflamed paw or in the paw of mice treated with saline only (instead of λ-carrageenan). The very low accumulation of fluorescence in the non-inflamed paw and in the brain confirmed that the anti-hyperalgesic effect resulted from the targeting of LENK-SQ NPs toward peripheral opioid receptors in inflamed tissue, rather than central opioid receptors. It is likely that the LENK-SQ distributed within the inflamed area as nanoparticles rather than in a single LENK-SQ molecular form. Indeed, whole body imaging of Fig. 6 shows strong fluorescence in the inflamed paw, which was not the case when the fluorescent dye was injected as a free compound. In addition, after incubation of LENK-SQ NPs in serum, a significant proportion of NPs remained intact (**Fig. S8**).

Finally, safety of LENK-SQ NPs after i.v. injection was confirmed by normal levels of transaminases as well as normal histology of vital organs.

Thus, the novelty of the approach resulted from the unexpected ability of the peptidic nanoparticles to target the small area of the body where inflammation and nociception are occurring. As this resulted in an effective pain alleviation, which lasted even longer than with morphine and avoided any diffusion into the CNS, such properties of LENK-SQ NPs might open novel perspectives for pain management.

CONCLUSION

Based on the bioconjugation of LENK to squalene, we describe here a new nano-formulation capable of precise and efficient delivery of LENK for pain control associated with inflammatory events. Our data demonstrated that the anti-hyperalgesic activity of LENK-SQ NPs took place at the level of peripheral opioid receptors. The experimental approach to make these nanoparticles is simple and easy (i.e., it doesn't require any complicated nanoparticle surface functionalization), which should facilitate further pharmaceutical development and clinical translation. Although further studies are needed to more precisely determine how dosage, administration frequency and timing of treatment with LENK-SQ may affect the clinical outcome, this study opens a new exciting perspective for an efficient treatment of intense pain, which evades from the severe side effects associated with morphine or related synthetic opioids. Finally, due to the versatility of the approach, the application to this delivery system to other therapeutic peptide molecules may be reasonably envisioned.

MATERIALS AND METHODS

Materials

All the chemicals used were of analytical grade. Squalene (SQ), diglycolic anhydride, ethyl chloroformate, chloromethyl chlorosulfate, ammonium acetate, n-Bu_4NHSO_4, triethylsilane, triethylamine, were purchased from Sigma-Aldrich, France. Pd-C was obtained from Alfa Aesar, France and DiD (1,1'-dioctadecyl-3,3,3',3'-tetramethylindodicarbocyan-ine, 4-chlorobenzenesulfonate salt) from PromoKine, Germany. Roti®-Histofix 4 % (formaldehyde) was provided by Roth, Germany.

All the drugs used were of analytical grade. Morphine sulfate salt pentahydrate, λ-carrageenan, naloxone hydrochloride (Nal, μ, δ, κ opioid-receptor antagonist), naloxone methiodide (Nal-M, a nonspecific opioid receptor antagonist that does not cross the BBB) were purchased from Sigma-Aldrich (Saint-Quentin Fallavier), France. Ketamine and xylazine were purchased from Centravet (Maisons-Alfort), France.

Leucine enkephalin (LENK) and Alloc-Leucine enkephalin were purchased from Ontores Biotechnologies (Zhejiang), China.

General information on chemicals

Analytical thin-layer chromatography was performed on Merck silica gel 60F254 glass pre-coated plates (0.25 mm layer). Column chromatography was performed on Merck silica gel 60 (230-400 mesh ASTM). HPLC water was purified using a Milli-Q system (Millipore, France). Tetrahydrofuran (THF) was distilled from sodium/benzophenone ketyl. Dimethylformamide (DMF), dichloromethane (DCM), and pyridine were dried on calcium hydride (CaH_2) prior to distillation under an argon atmosphere. Methanol (MeOH) was dried over magnesium and distilled. All reactions involving air- or water-sensitive compounds were routinely conducted in glassware which was flame-dried under a positive pressure of nitrogen. HPLC grade acetonitrile (ACN), MeOH, ethanol (EtOH) and ethyl acetate (AcOEt) were provided by Carlo Erba (Rodano, Italy).

Synthesis of the Leu-enkephalin-squalene bioconjugate with dioxycarbonyl linker (LENK-SQ-Diox).

1,1′,2-tris-norsqualenic acid chloromethyl ester. 1,1′,2-tris-norsqualenic acid was synthesized by oxidation of 1,1′,2-tris-norsqualenic aldehyde by Jone's reagent as previously reported (*35, 36*). To a solution of 1,1′,2-tris-norsqualenic acid (400 mg, 1 mmol) and n-Bu_4NHSO_4 (34 mg, 0.1 mmol) in DCM (2 mL) was added a solution of $KHCO_3$ (300 mg, 3.0 mmol) in water (2 mL). The reaction mixture was vigorously stirred, and chloromethyl chlorosulfate (185 mg, 1.15 mmol) was added dropwise. After stirring for 1 h, DCM (10 mL) was added to extract the product. The organic phase was separated, washed with brine, dried over magnesium sulfate, and concentrated under reduced pressure to afford a pale yellow oil which was used in the following step without further purification.

Alloc-Leu-enkephalin-squalene(AllocLENK-SQ-Diox). The 1,1′, 2-tris-norsqualenic acid chloromethyl ester (200 mg, 0.445 mmol) was added into a mixture of Alloc-LENK (285 mg, 0.445 mmol) and $NaHCO_3$ (37 mg, 0.4 mmol) in 3 mL DMF. The reaction mixture was stirred at 40 ºC under argon for 4 days. The final reaction mixture was concentrated *in vacuo*, and the residue was purified by flash column chromatography on silica gel DCM /EtOH (100:0 to 97:3) to afford the title

compound as a yellow oil (168 mg, 40% yield).

Leu-enkephalin-squalene (LENK-SQ-Diox). To a stirred solution of Alloc-LENK-SQ (110 mg, 0.1 mmol) and 10% Pd-C (20% by weight of Alloc-LENK-SQ-Diox) in MeOH (11 mL) was added dropwise neat triethylsilane (TES) (1215 mg, 10 mmol) under argon. When the reaction was completed, the mixture was filtered through celite to remove the Pd-C, and the residual TES and solvent were removed by evaporation. The residue was first purified by flash column chromatography on silica gel with DCM/EtOH (90/10). The resulting product was dissolved in 200 µL of ethanol prior to undergo a second purification by semi-preparative reverse-phase HPLC (RP-HPLC) system (Waters, Ma 01757, USA) on a uptisphere C18 column (100 × 21.2 mm, pore size=5 µm) (Interchim, California, USA) to get the pure product (23 mg; 23% yield). HPLC was then performed using a gradient elution with the mobile phase composed of an ammonium acetate buffer (20 mM) and ACN. Elution was carried out at a flow rate of 21 mL/min for 10 min with the linear gradient from 10% to 100% of ACN, then the system was held at 100% of ACN with isocratic flow during 10 min. Temperature was set at 30°C and UV detection was monitored at 280 nm and 257 nm. The retention time was 15 min, and the total yield of the pure product, after coupling and deprotection steps, corresponded to 9.5%.

Synthesis of the Leu-enkephalin-Squalene Bioconjugate with diglycolic linker (LENK-SQ-Dig).

1,1′,2-tris-norsqualenol was synthesized from squalene via 1,1′,2-tris-norsqualenic aldehyde according to previously reported methods (*35*, *36*). To a solution of 1,1′,2-tris-norsqualenol (200 mg, 0.52 mmol) in 3 mL of dry pyridine was added diglycolic anhydride (150 mg, 1.29 mmol). The reaction was stirred overnight at room temperature. The solvent was removed and the residue was extracted with DCM from dilute hydrochloric acid and brine. Conversion to the squalene-diglycolic acid, monitored by TLC, was approximately 100%. The resultant product was dried under vacuum, and used in the following step without further purification. To a solution of squalene-diglycolic acid (50 mg, 0.1 mmol) and triethylamine (TEA) (12 mg, 0.12 mmol) in 1 mL of anhydrous THF was added the ethyl chloroformate (10.8 mg, 0.1 mmol) under argon at 0°C. The reaction was stirred during 1 h at room temperature and a solution of LENK (55 mg, 0.1 mmol) in 1 mL anhydrous DMF was added. The mixture was maintained at 40°C during 2 days with stirring under argon. The solvents were removed *in vacuo* and the crude product was purified using silica gel chromatography (purified with gradient eluent DCM/EtOH: 100/0 to 90/10). Then ammonium salt was eliminated by simple filtration on silica using EtOH/AcOEt (40/60) as solvents. The pure bioconjugate was obtained with 69% of yield.

Synthesis of the Leu-enkephalin-Squalene Bioconjugate with amide linker (LENK-SQ-Am).

1,1′,2-Tris-nor-squalenic acid (100 mg, 0.25 mmol) and TEA (34.79 mg, 0.3 mmol) were dissolved in 1.5 mL of anhydrous THF under argon and ethyl chloroformate (27 mg, 0.25 mmol) was added to the mixture at 0°C. The reaction was allowed to warm at room temperature and kept under stirring for 1 h. A solution of LENK (138 mg, 0.25 mmol) in 1.5 mL of anhydrous DMF was then added to the reaction and the mixture was kept under stirring for 2 days. The solvents were removed *in vacuo* and the crude product was purified twice using silica gel chromatography (purification with gradient eluent DCM/EtOH: 100/0 to 90/10 and then simple filtration with EtOH/AcOEt: 40/60 to remove the ammonium salt). The pure bioconjugate was obtained with 73% of yield.

Preparation and characterization of Leu-enkephalin-Squalene nanoparticles

Preparation of nanoparticles. LENK-SQ NPs were prepared using the nanoprecipitation methodology. Briefly, the LENK-SQ bioconjugate (ie. LENK-SQ-Diox, LENK-SQ-Dig or LENK-SQ-Am) was dissolved in EtOH (8 mg/mL) and added dropwise under stirring (500 rpm) into a 5% aqueous dextrose solution (volume ratio EtOH: dextrose solution = 1:4). The solution became spontaneously turbid with a tyndall effect, indicating the formation of the nanoparticles. Ethanol was then completely evaporated using a Rotavapor® (80 rpm, 30°C, 30 mbar) to obtain an aqueous suspension of pure LENK-SQ NPs (final concentration 2 mg/mL). Blank SQ NPs (LENK-free NPs) were prepared by the same method as described above by adding dropwise an ethanolic solution of squalenic acid into 5% aqueous dextrose solution. Fluorescent LENK-SQ NPs were also obtained by the same procedure, except that the fluorescent probe DiD was solubilized in the ethanolic phase together with the LENK-SQ-Am bioconjugate (ratio DiD/LENK-SQ-Am was 4% wt), before addition to the dextrose solution. Fluorescent quenched LENK-SQ NPs were also prepared by the same way using DiR as a fluorescent quencher (ratio DiD/DiR/LENK-SQ-Am was 2/2/100 wt). The peptide drug loadings into the NPs were expressed as percentage (%), calculated from the ratio between LENK peptide Mw and LENK-SQ bioconjugate Mw. The LENK-SQ nanoparticles were regularly observed by cryo-TEM. All the NPs were freshly prepared and used within 2 h (conservation at 4 °C) before *in vivo* experiments.

Dynamic Light Scattering (DLS) Measurements. The mean particle size, polydispersity index (PDI) and zeta potential were primarily evaluated by DLS (Nano ZS, Malvern; 173° scattering angle at 25 °C). The measurements were performed in triplicate following appropriate dilution of the nanoparticles in water (DLS) or in 0.1 mM KCl (zeta potential). The results represent the mean and standard deviation of three repeated sample preparations or more.

Cryo-TEM. The morphology of the LENK-SQ NPs was investigated by Cryo-TEM. NPs were vitrified using a chamber designed and set up in the laboratory where both humidity and temperature could be controlled. 4 µL solution of LENK-SQ NPs (4 mg/mL in Milli-Q water) was deposited onto a perforated carbon film mounted on a 200 mesh electron microscopy grid. The homemade carbon film holes dimensions were about 2 mm in diameter. Most of the drop was removed with a blotting filter paper and the residual thin films remaining within the holes were quick-frozen by plunging them in liquid ethane cooled with liquid N_2. The specimen was then transferred, using liquid N_2, to a cryo-specimen holder and observed using a JEOL FEG-2010 electron microscope. Micrographs were recorded at 200 kV under low-dose conditions at a magnification of 40 000 on SO-163 Kodak films. Micrographs were digitized using a film scanner (Super Coolscan 8000 ED, Nikon), and analyses were made using the ImageJ software.

***In vitro* LENK release from NPs in serum**

Frozen serum of male SWISS mice (900 µL) was quickly thawed and then pre-incubated at 37 °C for 30 min before the addition of 300 µL LENK-SQ-Dig NPs or LENK-SQ-Am NPs (2 mg/mL). In the case of LENK-SQ-Diox NPs, diluted serum (30% in 5% dextrose solution) was used for the release study. At various time intervals, aliquots (80 µL) were collected and added into 320 µL ACN to denature and precipitate the enzymes and proteins of the serum, in order to remove them after centrifugation (3000 g for 15 min). To quantify the residual LENK-SQ bioconjugate and the released LENK, the resulting supernatants (150 µL) were evaporated to dryness at 40°C under nitrogen flow, and then solubilized in 150 µL of Milli-Q water. Free peptide quantification was performed using RP-HPLC on a Uptisphere Strategy C18HQ column (4.6 x 100 mm, 5 µm, Interchim), a 1525 Binary LC Pump (Waters, a 2707 Auto-sampler (Waters) and a 2998 PDA detector (Waters). The HPLC was

carried out using a gradient elution with the mobile phase composed of 5 mM ammonium acetate in milli-Q water (phase A) and 5 mM ammonium acetate in ACN (phase B). Elution was carried out at a flow rate of 1 mL/min for 13 min with the linear gradient from 10% to 100% of B; then, the system was held at 100% of B with isocratic flow during 10 min. Temperature was set at 35°C and UV detection was monitored at 257 nm. The detection limit of the HPLC technique was 0.39 µg/mL for the peptide. This method exhibited linearity (R^2=0.99998) over the assayed concentration range (0.39-200 µg/ml) and demonstrated good precision with relative standard deviation (RSD) being all less than 2.01%. The accuracy corresponded to 96 ± 5%.

General information on *in vivo* study

Animals. Adult male Sprague-Dawley rats (200-220 g on arrival, 280-300 g at the time of experiments) and adult male Swiss mice (18-20 g on arrival, 22-25 g at the time of experiments) were purchased from Janvier Labs (France) for algesimetry tests and biodistribution respectively. They were housed in a standard controlled environment (22 ± 1 °C, 60% relative humidity, 12:12 h light-dark cycle, lights on at 8:00 a.m.) with food and water available *ad libitum*, without any handling for at least 1 week before being used for experiments. In all cases, experiments were performed in conformity with the guidelines of the Committee for Research and Ethical Issues of the International Association for the Study of Pain (IASP) (*37*) and approved by the Animal Care Committee of the University Paris-Sud in accordance with the principles of laboratory animal care and the European legislation 2010/63/EU. All efforts were made to reduce animal numbers and minimize their suffering, as defined in the specific agreement (registered under #7493-2016102520355414).

Carrageenan-induced paw edema model. Since the demonstration that indomethacin reduces inflammation caused by intraplantar injection of □-carrageenan, this acute model is widely accepted for screening compounds with anti-inflammatory potentialities (*38*). λ-Carrageenan was dissolved in physiological saline (NaCl, 0.9%) just prior to injection. Rats or mice received a single intraplantar injection of λ-carrageenan solution in the plantar region of the right hind paw (*23*, *39*) in order to induce inflammation. The injected λ-carrageenan dose corresponded to 100 µL (2% solution w/v) for rat, and 20 µL (3% solution w/v) for mice. Inflammation reached its maximum 3 h after λ-carrageenan injection. Thermal nociceptive test was then performed on the ipsilateral inflamed hind paw.

Nociceptive behavioral study in rats

Thermal Nociceptive test. Hypersensitivity to thermal nociceptive stimuli was assessed using the Hargreaves test (*23*). Rats were placed individually in an open Plexiglas cylindrical chamber (20 cm in diameter, 35 cm high) on a 3 mm thick transparent glass floor, and allowed to habituate for at least 20 min before testing. A moveable radiant heat source (Model 7370, Ugo Basile plantar test, Italy) was positioned under the glass floor directly beneath the plantar surface of the right hind paw and the time (in seconds) that elapsed from switching on the radiant heat until paw withdrawal was measured automatically. A cut-off time of 20 s was established to prevent tissue damage. Each trial was repeated 3 times with 5 min intervals for basal threshold and 2 times spaced of 2 min after NPs treatments at 3 h after λ-carrageenan injection. The average of paw withdrawal latencies (PWL) was calculated and expressed as mean values ± SEM. (standard error of mean).

Experimental design for algesimetry test. Basal responses to thermal stimuli were obtained on the day before the λ-carrageenan injection. On the basis of previous studies, acute pharmacological

treatments were performed 3 h post-carrageenan injection, which corresponded to the peak inflammatory response.

The efficacy of these treatments on thermal hyperalgesia was evaluated by measurement of paw withdrawal latencies (PWL) using Hargreaves test at regular time intervals after drug or vehicle administration, first at 10 min and then each 30 min during a period of 4 h (**Fig. 4**).

Acute pharmacological treatments. Morphine and LENK were dissolved in dextrose 5%, whereas Nal and Nal-M were dissolved in physiological saline (NaCl, 0.9%). All these drugs and NPs suspensions were prepared just before administration. All acute treatments were performed at 3 h after λ-carrageenan intraplantar injection according to **Fig. 4**. Nal and Nal-M were injected subcutaneously (s.c.) whereas the intravenous (i.v.) route in the tail vein was used for LENK-SQ NPs, LENK and their controls. The antagonist (Nal or Nal-M) was administered 15 min before the agonist (morphine or tested NPs). A single dose of morphine (1 mg/kg), Nal (0.5 mg/kg) and Nal-M (0.5 mg/kg) was administered based on literature data (*40*). A single i.v. dose of LENK-SQ NPs (20 mg/kg, equivalent to 11.48 mg/kg of LENK) or control unconjugated SQ NPs (8.28 mg/kg) was used, based on maximal volume of LENK-SQ NPs that could be injected.

Biodistribution study in mice

In vivo imaging biodistribution studies were performed after i.v. injection of fluorescent LENK-SQ-Am NPs (250 µL, 2 mg/mL containing 4% DiD) or control fluorescent DiD solution (250 µL, 80 µg/mL in 5% dextrose solution) in shaved mice bearing λ-carrageenan-induced inflammation. In parallel, control non-inflamed shaved mice (injected with 20 µL saline into the right hind paw, instead of λ-carrageenan), received also injection of fluorescent LENK-SQ NPs. The biodistribution of the NPs was recorded at 0.5, 2, 4, 6 and 24 h after excitation at 640 nm and emission in the 695–775 nm filter respectively, using IVIS Lumina LT serie III system (Caliper, Life science). During imaging, the mice were kept on the imaging stage under anesthesia with 2% isoflurane gas in oxygen flow (1 L/min) and were imaged in ventral position. Images and measures of fluorescence signals were acquired and analyzed with Living Imaging®. To measure photon radiance, regions of interest (ROI, threshold of 35%) were selected on the paw of the mice and average radiant efficiency values were used for quantification. Threshold of ROI for the inflamed paw was then pasted on the non-inflamed paw to compare the radiance with the same region.

In a separate experiment, fluorescent LENK-SQ NPs injected mice were deeply anesthetized with a mixture of ketamine (100 mg/kg, i.p.) and xylazine (10 mg/kg, i.p.) before euthanisia by transcardiac perfusion of 40 ml saline (8 mL/min), until the fluid exiting the right atrium was entirely clear. Then, liver, spleen, kidneys, heart, lungs, brain, and inflamed right hind paw were excised and immediately imaged with the imager. The fluorescence emitted was quantified with Living Image software over the ROI (threshold of 20%).

Toxicity study in rats

Adult male Sprague-Dawley rats were injected with either LENK-SQ-Am NPs (20 mg/kg) or dextrose 5% (N = 3 animals per group). At 24, or 48 hours post-injection, the animals were anaesthetized under anesthesia with 2% isoflurane gas in oxygen flow (1 L/min) and blood was collected from tail blood vessels by anticoagulant (heparin, 500UI/mL) treated syringes. The blood samples were centrifuged at 1000g for 15 minutes and the plasma was collected and stored at -20°C before analysis. The AST and ALT levels in plasma were analyzed by Cerba Vet, France.

In a separate experiment, 24, or 48 hours post-injection, rats were deeply anesthetized by Doletal. Liver, kidneys, spleen, heart, and lungs were then excised, fixed by 4% formaldehyde, paraffin-embedded, and cut into 5 µm thick sections. Haematoxylin and eosin staining was performed on all the organs for analysis of the morphology (Zeiss).

Statistical analyses

All values are expressed as means ± SEM. and statistical analyses were made with GraphPad prism 6 software (San Diego, CA, USA). A two-way analysis of variance (Anova) was used with or without repeated measures as appropriate (see Materials and Methods and legends to figures). The comparison between groups was performed using the Bonferroni post hoc test. A one-way analysis of variance (Anova) followed by a tukey post test was used to compare 3 or more groups in bars of AUC. Areas under curves (AUC) were calculated using the trapezoidal rule. For all analyses, statistical significance was set at $P \leq 0.05$.

LIST OF ABBREVIATIONS

ACN	= acetonitrile
AcOEt	= ethyl acetate
ALT	= aspartate transaminase
AST	= alanine transaminase
AUC	= area under the curve
Cryo-TEM	= cryogenic transmission electron microscopy
DCM	= dichloromethane
DMF	= dimethylformamide
DLS	= dynamic light scattering
EPR	= enhanced permeation and retention
EtOH	= ethanol
LDC	= lipid-drug conjugates
LENK	= Leu-enkephalin
LENK-SQ	= Leu-enkephalin-squalene
LENK-SQ-Diox	= Leu-enkephalin-squalene with dioxycarbonyl linker
LENK-SQ-Dig	= Leu-enkephalin-squalene with diglycolic linker
LENK-SQ-Am	= Leu-enkephalin-squalene with amide linker
MeOH	= methanol
Nal	= naloxone
Nal-M	= naloxone methiodide
NPs	= nanoparticles
PDI	= polydispersity index
PWL	= paw withdrawal latency
SQ	= squalene
TES	= triethylsilane
THF	= tetrahydrofuran

SUPPLEMENTARY MATERIALS

REFERENCES

1. D. S. Goldberg, S. J. McGee, Pain as a global public health priority. *BMC Public Health* **11**, 770 (2011).
2. B. L. Kieffer, C. Gavériaux-Ruff, Exploring the opioid system by gene knockout. *Progress in Neurobiology* **66**, 285-306 (2002).
3. J. M. Adams, Increasing naloxone awareness and use: The role of health care practitioners. *JAMA* **319**, 2073-2074 (2018).
4. J. Anna, F. Jakub, J. Tomasz, Opioid Receptors and their Ligands. *Current Topics in Medicinal Chemistry* **4**, 1-17 (2004).
5. C. Contet, B. L. Kieffer, K. Befort, Mu opioid receptor: a gateway to drug addiction. *Current Opinion in Neurobiology* **14**, 370-378 (2004).
6. J. A. Kiritsy-Roy, L. Marson, G. R. Van Loon, Sympathoadrenal, cardiovascular and blood gas responses to highly selective mu and delta opioid peptides. *Journal of Pharmacology and Experimental Therapeutics* **251**, 1096-1103 (1989).
7. A. Tavani, P. Petrillo, A. La Regina, M. Sbacchi, Role of peripheral mu, delta and kappa opioid receptors in opioid-induced inhibition of gastrointestinal transit in rats. *Journal of Pharmacology and Experimental Therapeutics* **254**, 91-97 (1990).
8. L. Dykstra, A. L. Granger, R. M. Allen, X. Zhang, K. C. Rice, Antinociceptive effects of the selective delta opioid agonist SNC80 alone and in combination with mu opioids in the squirrel monkey titration procedure. *Psychopharmacology* **163**, 420-429 (2002).
9. D. J. Campbell, Long-term neprilysin inhibition — implications for ARNIs. *Nature Reviews Cardiology* **14**, 171-186 (2016).
10. D. Goodwin, P. Simerska, I. Toth, Peptides As Therapeutics with Enhanced Bioactivity. *Current Medicinal Chemistry* **19**, 4451-4461 (2012).
11. J. Kreuter, V. E. Petrov, D. A. Kharkevich, R. N. Alyautdin, Influence of the type of surfactant on the analgesic effects induced by the peptide dalargin after its delivery across the blood–brain barrier using surfactant-coated nanoparticles. *Journal of Controlled Release* **49**, 81-87 (1997).
12. C. Yung-Chu, H. Wen-Yuan, L. Wen-Fu, Z. Ding-Tai, Effects of surface modification of PLGA-PEG-PLGA nanoparticles on loperamide delivery efficiency across the blood–brain barrier. *Journal of Biomaterials Applications* **27**, 909-922 (2011).

13. A. Lalatsa, A. G. Schätzlein, N. L. Garrett, J. Moger, M. Briggs, L. Godfrey, A. Iannitelli, J. Freeman, I. F. Uchegbu, Chitosan amphiphile coating of peptide nanofibres reduces liver uptake and delivers the peptide to the brain on intravenous administration. *Journal of Controlled Release* **197**, 87-96 (2015).
14. M. Popov, I. Abu Hammad, T. Bachar, S. Grinberg, C. Linder, D. Stepensky, E. Heldman, Delivery of analgesic peptides to the brain by nano-sized bolaamphiphilic vesicles made of monolayer membranes. *European Journal of Pharmaceutics and Biopharmaceutics* **85**, 381-389 (2013).
15. A. Lalatsa, V. Lee, J. P. Malkinson, M. Zloh, A. G. Schätzlein, I. F. Uchegbu, A Prodrug Nanoparticle Approach for the Oral Delivery of a Hydrophilic Peptide, Leucine5-enkephalin, to the Brain. *Molecular Pharmaceutics* **9**, 1665-1680 (2012).
16. S. Wohlfart, S. Gelperina, J. Kreuter, Transport of drugs across the blood–brain barrier by nanoparticles. *Journal of Controlled Release* **161**, 264-273 (2012).
17. C. Stein, M. Schäfer, H. Machelska, Attacking pain at its source: new perspectives on opioids. *Nature Medicine* **9**, 1003-1008 (2003).
18. A. Maksimenko, F. Dosio, J. Mougin, A. Ferrero, S. Wack, L. H. Reddy, A. A. Weyn, E. Lepeltier, C. Bourgaux, B. Stella, L. Cattel, P. Couvreur, A unique squalenoylated and nonpegylated doxorubicin nanomedicine with systemic long-circulating properties and anticancer activity. *Proc Natl Acad Sci U S A* **111**, E217-226 (2014).
19. P. K. Mandal, J. S. McMurray, Pd−C-Induced Catalytic Transfer Hydrogenation with Triethylsilane. *The Journal of Organic Chemistry* **72**, 6599-6601 (2007).
20. G. V. Betageri, N. B. Vutla, A. K. Banga, Liposomal Formulation and Characterization of the Opioid Peptide Leucine Enkephalin. *Pharmacy and Pharmacology Communications* **3**, 587-591 (2011).
21. Y. Chen, F. Wang, H. A. E. Benson, Effect of formulation factors on incorporation of the hydrophilic peptide dalargin into PLGA and mPEG-PLGA nanoparticles. *Peptide Science* **90**, 644-650 (2008).
22. V. S. Chernyshev, R. Rachamadugu, Y. H. Tseng, D. M. Belnap, Y. Jia, K. J. Branch, A. E. Butterfield, L. F. Pease, P. S. Bernard, M. Skliar, Size and shape characterization of hydrated and desiccated exosomes. *Analytical and Bioanalytical Chemistry* **407**, 3285-3301 (2015).
23. K. Hargreaves, R. Dubner, F. Brown, C. Flores, J. Joris, A new and sensitive method for measuring thermal nociception in cutaneous hyperalgesia. *Pain* **32**, 77-88 (1988).
24. K. M. Buller, A. S. Hamlin, P. B. Osborne, Dissection of peripheral and central endogenous opioid modulation of systemic interleukin-1β responses using c-fos expression in the rat brain. *Neuropharmacology* **49**, 230-242 (2005).
25. A. K. Sato, M. Viswanathan, R. B. Kent, C. R. Wood, Therapeutic peptides: technological advances driving peptides into development. *Current Opinion in Biotechnology* **17**, 638-642 (2006).
26. P. Couvreur, B. Stella, L. H. Reddy, H. Hillaireau, C. Dubernet, D. Desmaële, S. Lepêtre-Mouelhi, F. Rocco, N. Dereuddre-Bosquet, P. Clayette, V. Rosilio, V. Marsaud, J.-M. Renoir, L. Cattel, Squalenoyl Nanomedicines as Potential Therapeutics. *Nano Letters* **6**, 2544-2548 (2006).
27. A. Gaudin, M. Yemisci, H. Eroglu, S. Lepetre-Mouelhi, O. F. Turkoglu, B. Dönmez-Demir, S. Caban, M. F. Sargon, S. Garcia-Argote, G. Pieters, O. Loreau, B. Rousseau, O. Tagit, N. Hildebrandt, Y. Le Dantec, J. Mougin, S. Valetti, H. Chacun, V. Nicolas, D. Desmaële, K.

Andrieux, Y. Capan, T. Dalkara, P. Couvreur, Squalenoyl adenosine nanoparticles provide neuroprotection after stroke and spinal cord injury. *Nature Nanotechnology* **9**, 1054 (2014).
28. H. H. Büscher, R. C. Hill, D. RÖMer, F. Cardinaux, A. Closse, D. Hauser, J. Pless, Evidence for analgesic activity of enkephalin in the mouse. *Nature* **261**, 423-425 (1976).
29. A. H. M. Viswanatha Swamy, P. A. Patil, Effect of Some Clinically Used Proteolytic Enzymes on Inflammation in Rats. *Indian Journal of Pharmaceutical Sciences* **70**, 114-117 (2008).
30. N. Sémiramoth, C. D. Meo, F. Zouhiri, F. Saïd-Hassane, S. Valetti, R. Gorges, V. Nicolas, J. H. Poupaert, S. Chollet-Martin, D. Desmaële, R. Gref, P. Couvreur, Self-Assembled Squalenoylated Penicillin Bioconjugates: An Original Approach for the Treatment of Intracellular Infections. *ACS Nano* **6**, 3820-3831 (2012).
31. M. F. Simões, E. Valente, M. J. R. Gómez, E. Anes, L. Constantino, Lipophilic pyrazinoic acid amide and ester prodrugs: Stability, activation and activity against M. tuberculosis. *European Journal of Pharmaceutical Sciences* **37**, 257-263 (2009).
32. P. T. Wong, S. K. Choi, Mechanisms of Drug Release in Nanotherapeutic Delivery Systems. *Chemical Reviews* **115**, 3388-3432 (2015).
33. R. Oliyai, Prodrugs of peptides and peptidomimetics for improved formulation and delivery. *Advanced Drug Delivery Reviews* **19**, 275-286 (1996).
34. E. Burma Nicole, H. Leduc‐Pessah, Y. Fan Churmy, T. Trang, Animal models of chronic pain: Advances and challenges for clinical translation. *Journal of Neuroscience Research* **95**, 1242-1256 (2016).
35. E. E. van Tamelen, T. J. Curphey, The selective in vitro oxidation of the terminal double bonds in squalene. *Tetrahedron Letters* **3**, 121-124 (1962).
36. C. Skarbek, L. L. Lesueur, H. Chapuis, A. Deroussent, C. Pioche−Durieu, A. Daville, J. Caron, M. Rivard, T. Martens, J.-R. Bertrand, E. Le Cam, G. Vassal, P. Couvreur, D. Desmaele, A. Paci, Preactivated Oxazaphosphorines Designed for Isophosphoramide Mustard Delivery as Bulk Form or Nanoassemblies: Synthesis and Proof of Concept. *Journal of Medicinal Chemistry* **58**, 705-717 (2015).
37. M. Zimmermann, Ethical guidelines for investigations of experimental pain in conscious animals. *Pain* **16**, 109-110 (1983).
38. C. A. Winter, E. A. Risley, G. W. Nuss, Anti-inflammatory and antipyretic activities of indomethacin, 1-(p-chlorobenzoyl)-5-methoxy-2-methyl-indole-3-acetic acid. *Journal of Pharmacology and Experimental Therapeutics* **141**, 369 (1963).
39. S. T. Meller, C. P. Cummings, R. J. Traub, G. F. Gebhart, The role of nitric oxide in the development and maintenance of the hyperalgesia produced by intraplantar injection of carrageenan in the rat. *Neuroscience* **60**, 367-374 (1994).
40. H. Brasch, G. Zetler, Caerulein and morphine in a model of visceral pain. *Naunyn-Schmiedeberg's Archives of Pharmacology* **319**, 161-167 (1982).

Acknowledgements. The authors thank Valérie Domergue for animal housing and care at the Animex facility, IPSIT, Châtenay-Malabry, France. Ms. Julie Mougin (Institut Galien Paris-Sud, Châtenay-Malabry, France) and Mrs. Ghislaine Frébourg (Electron Microscopy Facility/FR 3631-CNRS‐UPMC) are acknowledged for their contribution to Cryo‐TEM. The authors warmly thank Dr. Mariana Varna-Pannerec (Institut Galien Paris-Sud, Châtenay-Malabry, France) and Dr. Delphine Courilleau (CIBLOT Plateforme, Châtenay-Malabry, France) for their help concerning histological study. Ms. Camille Dejean (BioCIS, Châtenay-Malabry, France) is acknowledged for help with the

NMR interpretations. **Funding:** JF is a fellow of the Chinese Scholarship Council (CSC). Part of this work was supported by the RBUCE-UP grant agreement (#00001002483/78) between the ERC and Université Paris-Sud, by the ERC under the Framework Program FP7/2007–2013 (Grant Agreement N°249835) and by the Centre National de la Recherche Scientifique. UMR 8612 (P. Couvreur team) is a member of the laboratory of excellence NANOSACLAY. **Author contributions:** P. Couvreur and S. Lepetre-Mouelhi were involved in planning and supervised the work. J. Feng and S. Lepetre-Mouelhi conceived and designed the bioconjugates. P. Couvreur and S. Lepetre-Mouelhi conceived and planned the experiments. J. Feng, S. Lepetre-Mouelhi and P. Couvreur developed the methodology. Others (M. Hamon and A. Gauthier developed the experimental design for algesimetry and F. Coudoré attended meetings). J. Feng carried out the experiments. Others (A. Gauthier participated in algesimetry experiments, S. Mura and C. Cailleau participated in biodistribution studies). P. Couvreur, J. Feng and S. Lepetre-Mouelhi contributed to the analysis and interpretation of the results. M. Hamon contributed to the interpretation of the results of the behavioral study. J. Feng wrote the manuscript (in consultation with S. Lepetre-Mouelhi and P. Couvreur). S. Lepetre-Mouelhi and P. Couvreur revised the manuscript. Others (M. Hamon and A. Gauthier revised the nociceptive behavioral study part. S.Mura and C. Cailleau participated in the manuscript revision). **Conflict of interest:** The authors declare that there is no conflict of interest regarding the publication of this article. **Data and materials availability:** All data needed to evaluate the conclusions in the paper are present in the paper and/or the Supplementary Materials. Additional data available from authors upon request.

Supplementary Materials for

A new painkiller nanomedicine to bypass the blood-brain-barrier and the use of morphine

Jiao FENG, Sinda LEPETRE-MOUELHI, Anne GAUTIER, Simona MURA, Catherine CAILLEAU, François COUDORE, Michel HAMON, Patrick COUVREUR*

*Correspondence to: patrick.couvreur@u-psud.fr

This PDF file includes:

Supplementary Text: IR, NMR and MS characterization of bioconjugates

IR spectra were obtained from solids or neat liquids with a PerkinElmer UATR Two spectrometer. Only significant absorptions are listed. The ^{1}H and ^{13}C NMR spectra were recorded on a Bruker ARX 400 spectrometer (400 and 100 MHz for ^{1}H and ^{13}C, respectively). Recognition of methyl, methylene, methine, and quaternary carbon nuclei in ^{13}C NMR spectra rests on the J-modulated spin-echo sequence. Mass spectra were recorded on a Bruker Esquire-LC. High resolution Mass spectra (HR-MS) were achieved with an LTQ-Orbitrap Velos Pro (Thermo Fisher Scientific) operating in positive and negative electrospray ionization.

IR, NMR and MS characterization of LENK-SQ-Diox: IR (neat, cm^{-1}): ν 3289, 2958, 2916, 2849, 1763, 1646, 1537, 1515, 1447, 1381, 1259, 1116, 1020, 982, 870, 802, 729, 700, 549, 493. ^{1}H NMR (400 MHz, MeOD) δ: 7.31-7.23 (m, 4H, $2H_{Ar\text{-}ortho}$ Phe, $2H_{Ar\text{-}meta}$ Phe), 7.18 (m, 1H, $H_{Ar\text{-}para}$ Phe), 7.04 (d, 2H, $H_{Ar\text{-}ortho}$ Tyr, *J* = 8.4 Hz), 6.71 (d, 2H, $H_{Ar\text{-}meta}$ Tyr, *J* = 8.4 Hz), 5.77 (d, 1H, O*C*H_2O, *J* = 5.6 Hz), 5.71 (d, 1H, O*C*H_2O, *J* = 5.6 Hz), 5.19–5.04 (m, 5H, *H*C=C(CH_3)), 4.65 (dd, 1H, CH Phe, *J* = 4.9 Hz, *J* = 9.6 Hz), 4.44 (m, 1H, CH Leu), 4.00-3.60 (m, 4H, 2 CH_2 Gly), 3.54 (dd, 1H, CH Tyr, *J* = 6.5 Hz, *J* = 7.6 Hz), 3.16 (dd, 1H, C*Ha*Hb Phe, *J* = 4.9 Hz, *J* = 14.0 Hz), 3.10-2.87 (m, 2H, CHa*Hb* Phe, C*Ha*Hb Tyr), 2.80 (dd, 1H, CHa*Hb* Tyr, *J* = 7.6 Hz, *J* = 13.9 Hz), 2.44 (m, 2H, CH_2-CH_2-CO SQ), 2.26 (m, 2H, CH_2-CH_2-CO SQ), 2.14-1.90 (m, 16H, 8 CH_2 SQ), 1.75-1.48 (m, 21H, CH_2 Leu, C*H*(CH_3)$_2$ Leu, 6 CH_3 SQ), 0.94 (d, 3H, CH_3 Leu, *J* = 6.2 Hz), 0.90 (d, 3H, CH_3 Leu, *J* = 6.2 Hz). ^{13}C NMR (75 MHz, MeOD) δ: 178.0 (CONH), 173.7 (CONH), 173.0 (CONH), 172.4 (CONH), 172.0 (CONH), 171.3 (CONH), 157.6 ($C_{Ar\text{-}para}$ Tyr), 138.3 (C_{Ar} Phe), 136.0 (HC=*C*(CH_3)), 135.8 (2 HC=*C*(CH_3)), 134.1 (HC=*C*(CH_3)), 132.0 (HC=*C*(CH_3)), 131.5 (2 $CH_{Ar\text{-}ortho}$ Tyr), 130.4 (2 $CH_{Ar\text{-}ortho}$ Phe), 129.5 (2 $CH_{Ar\text{-}meta}$ Phe, C_{Ar} Tyr), 127.8 ($CH_{Ar\text{-}para}$ Phe), 126.5 (H*C*=C(CH_3)), 125.7 (H*C*=C(CH_3)), 125.5 (2 H*C*=C(CH_3)), 125.4 (H*C*=C(CH_3)), 116.5 (2 $CH_{Ar\text{-}meta}$ Tyr), 80.9 (O-CH_2-O), 62.6 (CH Tyr), 55.8 (CH Phe), 52.2 (CH Leu), 43.8 (CH_2 Gly), 43.6 (CH_2 Gly), 41.0 (*C*H_2-CH(CH_3)$_2$ Leu), 40.8 (CH_2 SQ), 40.7 (2 CH_2 SQ, CH_2 Tyr), 38.7 (CH_2 Phe), 35.3 (*C*H_2-CH_2-CO), 33.8 (CH_2-*C*H_2-CO), 30.7 (CH_2 SQ), 30.4 (CH_2 SQ), 29.2 (CH_2 SQ), 27.8 (CH_2 SQ), 27.5 (CH_2 SQ), 25.9 (*C*H(CH_3)$_2$ Leu), 23.4 (CH_3 Leu), 21.9 (CH_3 Leu), 17.8 (CH_3 SQ), 16.7 (CH_3 SQ), 16.2 (CH_3 SQ), 16.1 (CH_3 SQ), 16.0 (CH_3 SQ), 14.5 (CH_3 SQ). HRMS (+ESI): *m/z* 968.6064 ($[M + H]^+$ calcd for $C_{56}H_{82}N_5O_9$: 968.6107).

IR, NMR and MS characterization of LENK-SQ-Dig: IR (neat, cm^{-1}): ν 3297, 3068, 2958, 2924, 2851, 1653, 1516, 1443, 1260, 1142, 1099, 1020, 799, 699, 583. ^{1}H NMR (400 MHz, MeOD) δ: 7.30–7.22 (m, 4H, $2H_{Ar\text{-}ortho}$ Phe, $2H_{Ar\text{-}meta}$ Phe), 7.19 (m, 1H, $H_{Ar\text{-}para}$ Phe), 7.06 (d, 2H, $H_{Ar\text{-}ortho}$ Tyr, *J* = 8.5 Hz), 6.71 (d, 2H, $H_{Ar\text{-}meta}$ Tyr, *J* = 8.5 Hz), 5.20–5.05 (m, 5H, *H*C=C(CH_3)), 4.65 (dd, 1H, CH Phe, *J* = 4.7 Hz, *J* = 9.4 Hz), 4.57 (dd, 1H, CH Tyr, *J* = 6.1 Hz, *J* = 8.3 Hz), 4,40 (m, 1H, CH Leu), 4.17-3.85 (m, 6H, 2 CH_2 Diglycolyl, CH_2-O SQ), 3.90-3.72 (m, 4H, 2 CH_2 Gly), 3.20 (dd, 1H, C*Ha*Hb Phe , *J* = 4.7 Hz, *J* = 14.0 Hz), 3.11 (dd, 1H, C*Ha*Hb Tyr, *J* = 6.1 Hz, *J* = 13.9 Hz), 3.00-2.89 (m, 2H, CHa*Hb* Phe, CHa*Hb* Tyr), 2.14-1.93 (m, 19H, 9 CH_2 SQ, C*Ha*Hb-CH_2-O SQ), 1.74 (m, 1H, CHa*Hb*-CH_2-O SQ), 1.71–1.54 (m, 21H, CH_2 Leu, C*H*(CH_3)$_2$, 6 CH_3 SQ), 0.94 (d, 3H, CH_3 Leu, *J* = 6.2 Hz), 0.91 (d, 3H, CH_3 Leu, *J* = 6.2 Hz). ^{13}C NMR (75 MHz, MeOD) δ: 176.8 (CONH), 174.2 (CONH), 173.4 (CONH), 172.2 (O-*C*O-CH_2), 172.0 (CONH), 171.3 (CONH), 157.5 ($C_{Ar\text{-}para}$ Tyr), 138.5 ($C_{Ar\ Phe}$), 135.9 (3 HC= *C*(CH_3)), 134.8 (HC=*C*(CH_3)), 132.0 (HC=*C*(CH_3)), 131.4 (2$CH_{Ar\text{-}ortho}$ Tyr), 130.4 (2$CH_{Ar\text{-}ortho}$ Phe), 129.4 (2$CH_{Ar\text{-}meta}$ Phe), 128.6 (C_{Ar} Tyr), 127.7 ($CH_{Ar\text{-}para}$ Phe), 126.3 (H*C*=C(CH_3)), 125.6 (2 H*C*=C(CH_3)), 125.5 (H*C*=C(CH_3)), 125.4 (H*C*=C(CH_3)), 116.3 (2$CH_{Ar\text{-}meta}$ Tyr), 71.5 (O-CH_2-O), 69.4 (CO-*C*H_2-O), 65.9 (CH_2-CH_2-*C*H_2-O), 56.2 (CH Tyr), 56.0 (CH Phe), 52.3 (CH Leu), 44.0 (CH_2 Gly), 43.4 (CH_2 Gly), 41.7 (*C*H_2-CH(CH_3)$_2$ Leu), 38.6 (CH_2Phe), 37.9

(CH_2 Tyr), 36.8 (*C*H_2-CH_2-CH_2-O), 29.2 (CH_2 SQ), 27.8 (2 CH_2 SQ), 27.6 (3 CH_2 SQ), 25.9 (*C*H(CH_3)$_2$ Leu, CH_3 SQ), 23.4 (CH_3 Leu), 22.0 (CH_3 Leu), 17.8 (CH_3 SQ), 16.2 (2 CH_3 SQ), 16.0 (2 CH_3 SQ). HRMS (-ESI): *m/z* 1038.61572 ([M - H]$^-$ calcd for $C_{59}H_{84}N_5O_{11}$: 1038.61618).

IR, NMR and MS characterization of LENK-SQ-Am: IR (neat, cm^{-1}): ν 3303, 2957, 2925, 2856, 1711, 1697, 1543, 1516, 1440, 1282, 1241, 1213, 828, 671. ^{1}H NMR (400 MHz, MeOD) δ: 7.31–7.22 (m, 4H, 2$H_{Ar\text{-}ortho}$ Phe, 2$H_{Ar\text{-}meta}$ Phe), 7.18 (m, 1H, $H_{Ar\text{-}para}$ Phe), 7.05 (d, 2H, $H_{Ar\text{-}ortho}$ Tyr, *J* = 8.5 Hz), 6.71 (d, 2H, $H_{Ar\text{-}meta}$ Tyr, *J* = 8.5 Hz), 5.19–5.05 (m, 5H, *H*C=C(CH_3)), 4.68 (dd, 1H, CH Phe, *J* = 4.9 Hz, *J* = 9.2 Hz), 4.50-4.39 (m, 2H, CH Tyr, CH Leu), 3.87-3.67 (m, 4H, 2 CH_2 Gly), 3.20 (dd, 1H, C*Ha*Hb Phe , *J* = 4.9 Hz, *J* = 14.0 Hz), 3.07-2.93 (m, 2H, CHa*Hb* Phe, C*Ha*Hb Tyr), 2.85 (dd, 1H, CHa*Hb* Tyr, *J* = 8.2 Hz, *J* = 13.8 Hz), 2.31 (m, 2H, CH_2-C*H*$_2$-CO), 2.18 (m, 2H, C*H*$_2$-CH_2-CO), 2.13-1.88 (m, 16H, 8 CH_2 SQ), 1.73-1.53 (m, 21H, CH_2 Leu, C*H*(CH_3)$_2$ Leu, 6 CH_3 SQ), 0.94 (d, 3H, CH_3 Leu, *J* = 6.2 Hz), 0.91 (d, 3H, CH_3 Leu, *J* = 6.2 Hz). ^{13}C NMR (75 MHz, MeOD) δ: 176.2 (CO_2H), 175.8 (CONH), 174.7 (CONH), 173.3 (CONH), 172.0 (CONH), 171.2 (CONH), 157.4 ($C_{Ar\text{-}para}$ Tyr), 138.4 ($C_{Ar\ Phe}$), 136.0 (2 HC=*C*(CH_3)), 135.8 (HC=*C*(CH_3)), 134.7 (HC=*C*(CH_3)), 132.0 (HC=*C*(CH_3)), 131.3 (2$CH_{Ar\text{-}ortho}$ Tyr), 130.4 (2$CH_{Ar\text{-}ortho}$ Phe), 129.4 (2$CH_{Ar\text{-}meta}$ Phe), 128.9 (C_{Ar} Tyr), 127.7 ($CH_{Ar\text{-}para}$ Phe), 126.2 (H*C*=C(CH_3)), 125.6 (H*C*=C(CH_3)), 125.5 (H*C*=C(CH_3)), 125.5 (2 H*C*=C(CH_3)), 116.3 (2$CH_{Ar\text{-}meta}$ Tyr), 56.9 (CH Tyr), 55.9 (CH Phe), 52.3 (CH Leu), 43.9 (CH_2 Gly), 43.3 (CH_2 Gly), 41.7 (*C*H_2-CH(CH_3)$_2$ Leu), 38.7 (CH_2Phe), 37.9 (CH_2 Tyr), 36.5 (*C*H_2-CH_2-CO), 35.8 (CH_2-*C*H_2-CO), 29.2 (3 CH_2 SQ), 27.8 (4 CH_2 SQ), 27.5 (2 CH_2 SQ), 25.9 (*C*H(CH_3)$_2$ Leu, CH_3 SQ), 23.4 (CH_3 Leu), 21.9 (CH_3 Leu), 17.7 (CH_3 SQ), 16.2 (2 CH_3 SQ), 16.1 (CH_3 SQ), 16.0 (CH_3 SQ). HRMS (-ESI): *m/z* 936.5826 ([M - H]$^-$ calcd for $C_{55}H_{78}N_5O_8$: 936.5845).

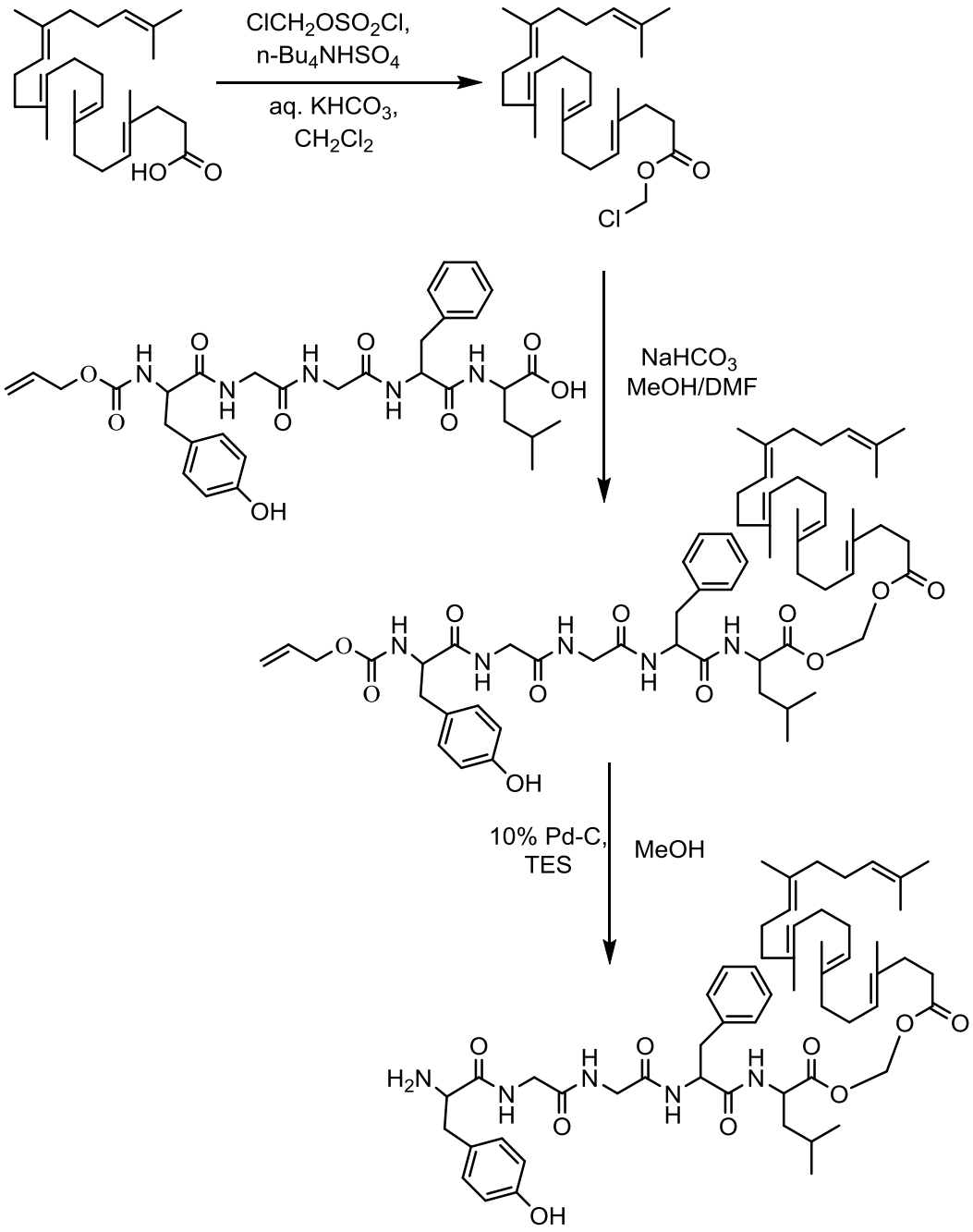

Fig. S1. Synthesis of Leu-enkephalin-squalene with dioxycarbonyl linker (LENK-SQ-Diox).

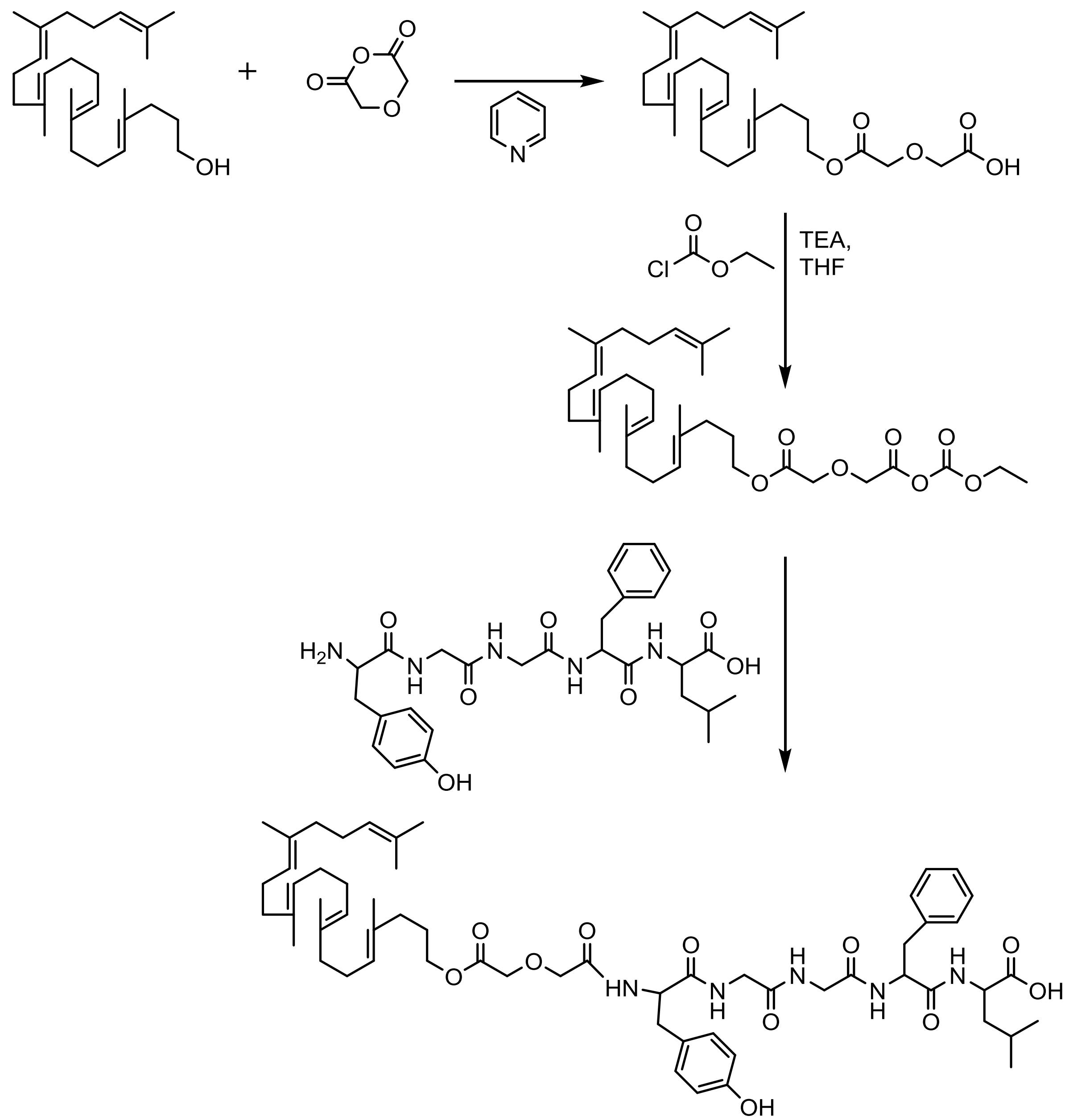

Fig. S2. Synthesis of Leu-enkephalin-squalene with diglycolic linker (LENK-SQ-Dig).

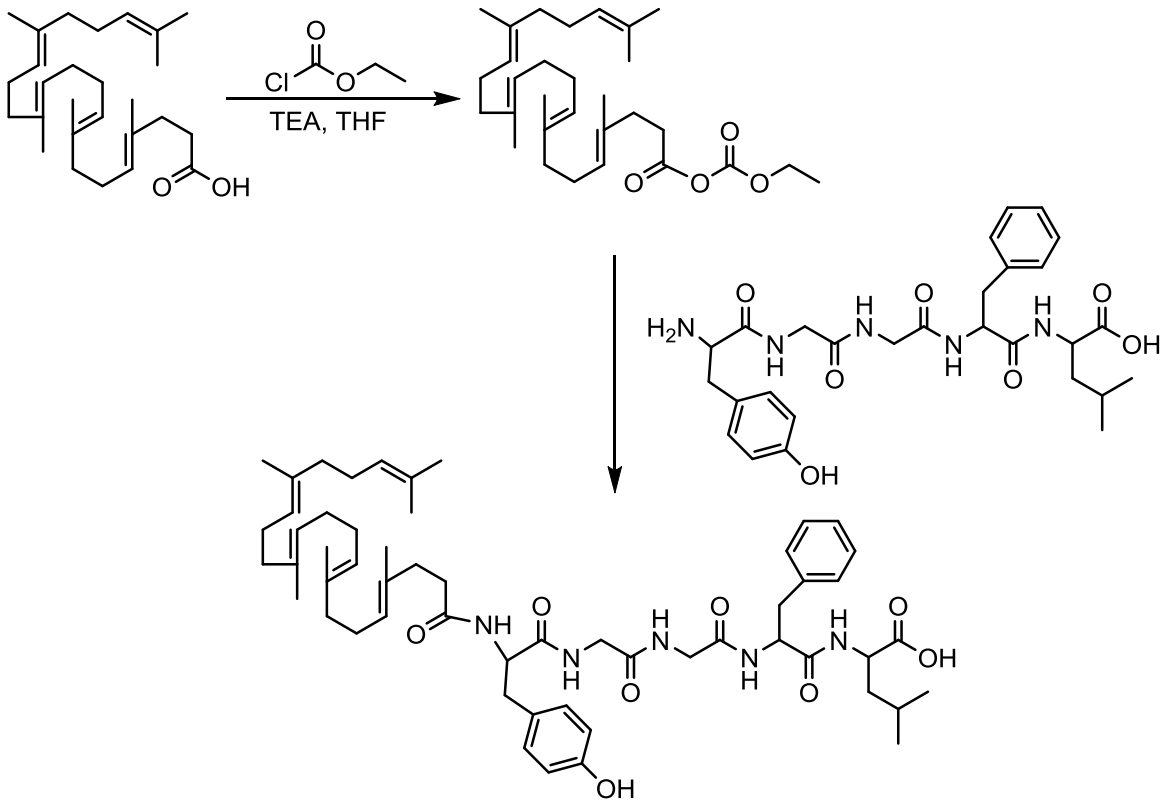

Fig. S3. Synthesis of Leu-enkephalin-squalene with amide linker (LENK-SQ-Am).

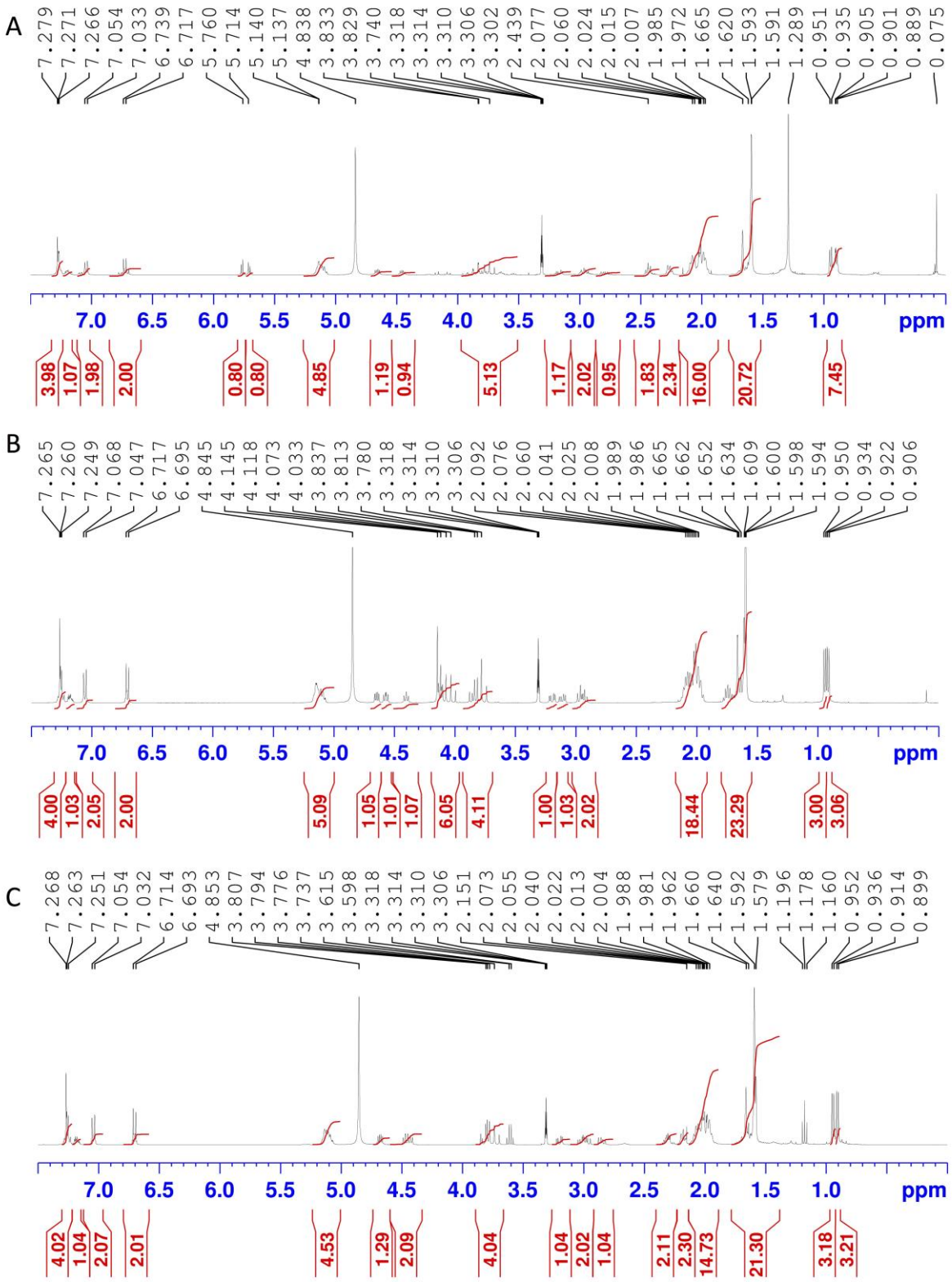

Fig. S4. ^{1}H spectrum of LENK-SQ bioconjugates. (A) LENK-SQ-Diox, **(B)** LENK-SQ-Dig, and **(C)** LENK-SQ-Am.

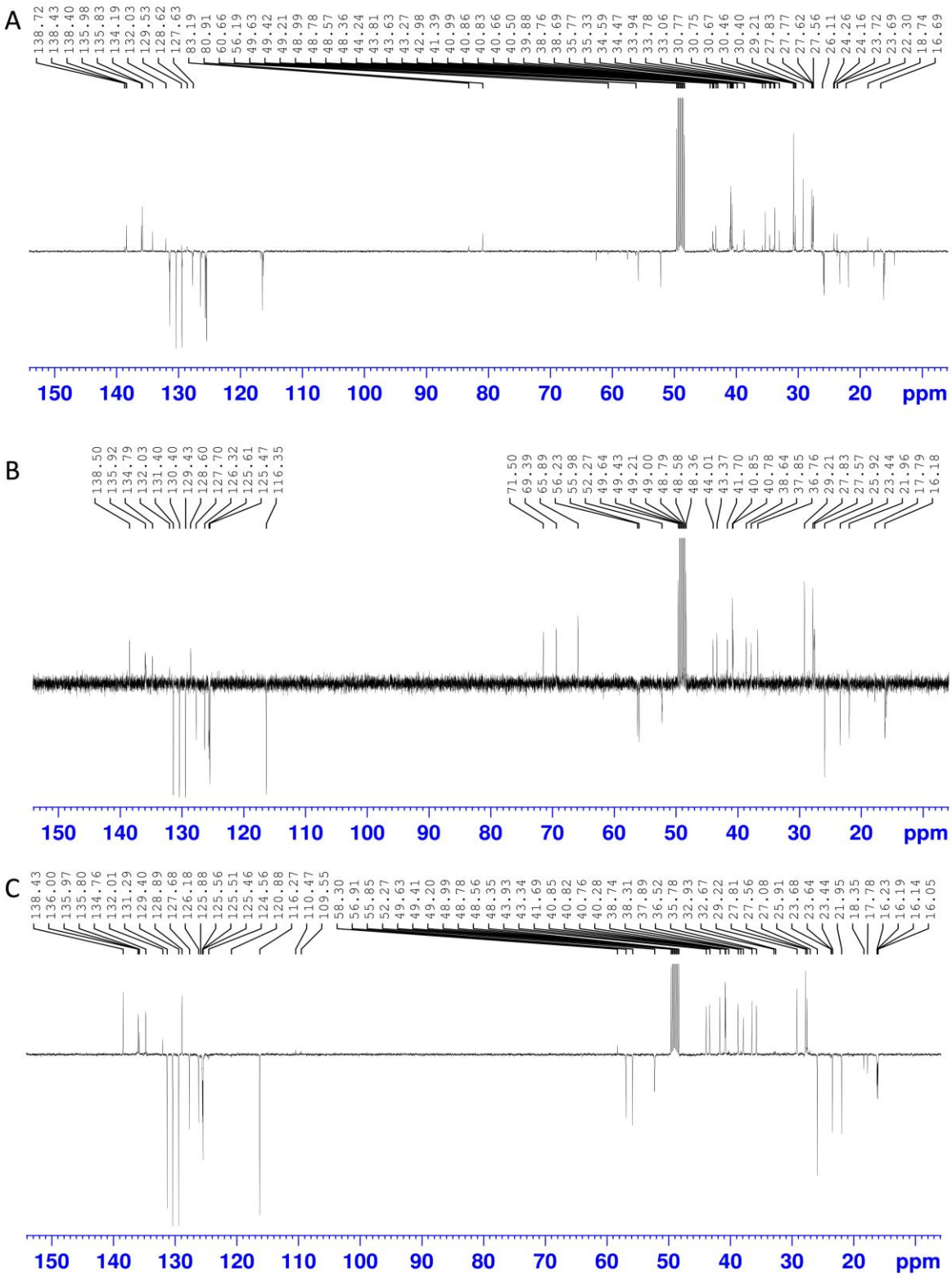

Fig. S5. ^{13}H spectrum of LENK-SQ bioconjugates. (A) LENK-SQ-Diox, **(B)** LENK-SQ-Dig, and **(C)** LENK-SQ-Am.

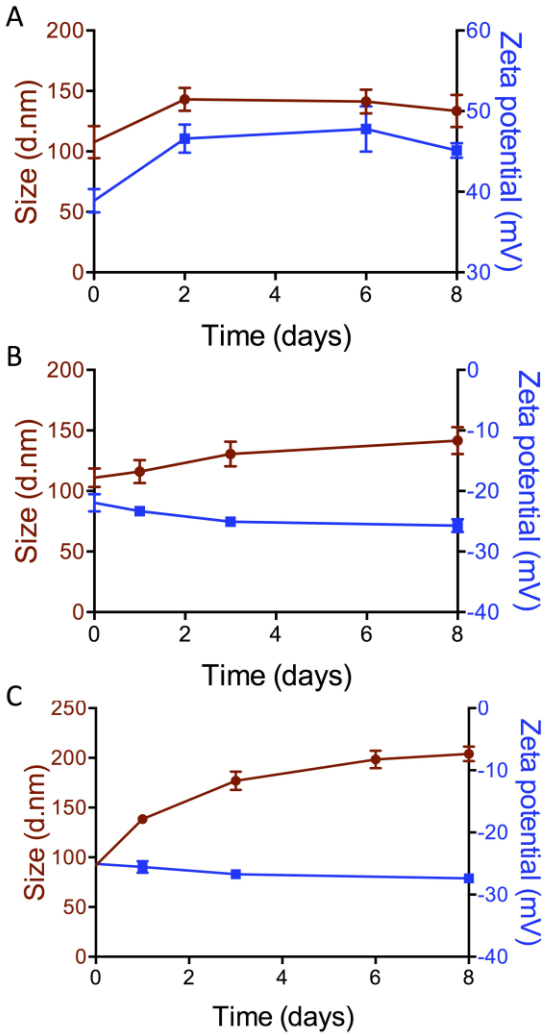

Fig. S6. Size and zeta potential of LENK-SQ NPs kept at +4°C. (A) LENK-SQ-Diox NPs, **(B)** LENK-SQ-Dig NPs and **(C)** LENK-SQ-Am NPs. Results of three independent preparations are presented as mean ± SEM.

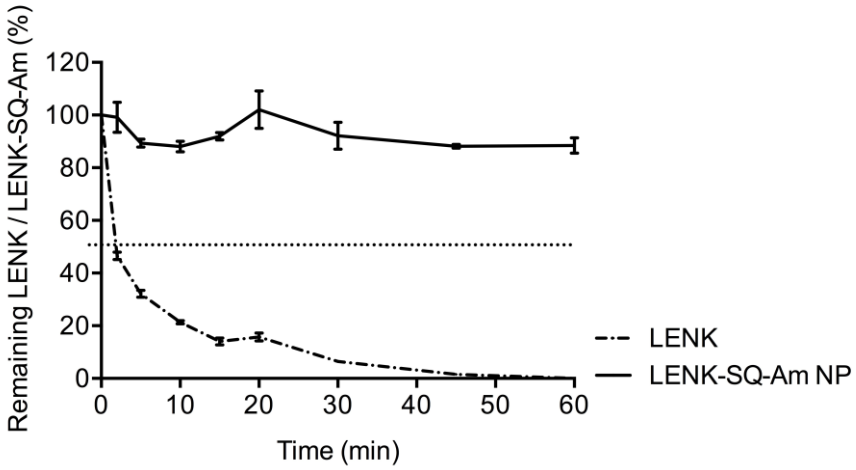

Fig. S7. Hydrolysis of LENK or LENK-SQ-Am NPs in the presence of serum. 300 µL of LENK-SQ-Am NPs (2 mg/mL, 2 mmol) or LENK (1.15 mg/mL, 2 mmol) were incubated in 900 µL mouse serum, and samples were collected at different times for HPLC analysis. The LENK-SQ bioconjugate was unaltered during the course of the experiment, whereas free LENK was rapidly metabolized.

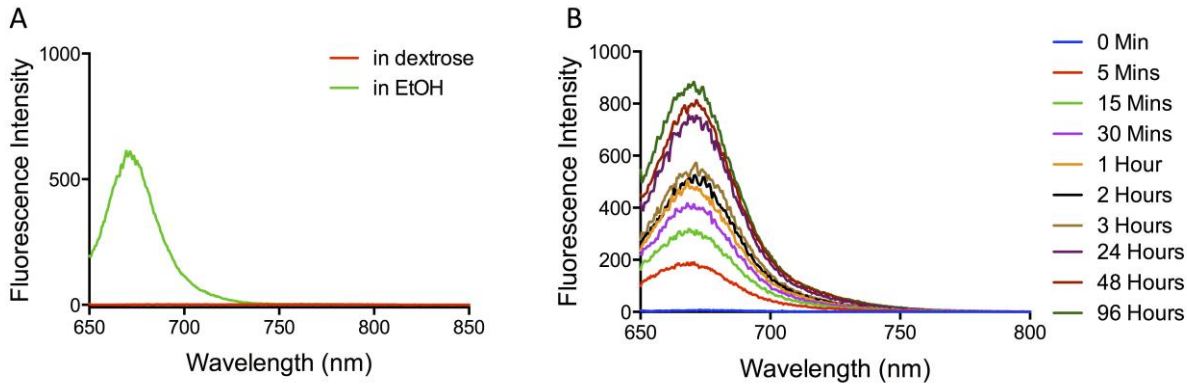

Fig. S8. *In vitro* colloidal stability of LENK-SQ-Am NPs in mouse serum. (A) Controls: When diluted in 5% dextrose LENK-SQ-Am NPs remained assembled (DiD: reporter dye; DiR: quencher). They disassembled in ethanol; **(B)** LENK-SQ-Am NPs (DiD: reporter dye; DiR: quencher) incubated in mouse serum (1:4). The fluorescence emission was measured to assess the progressive disassembly of the nanoparticles.

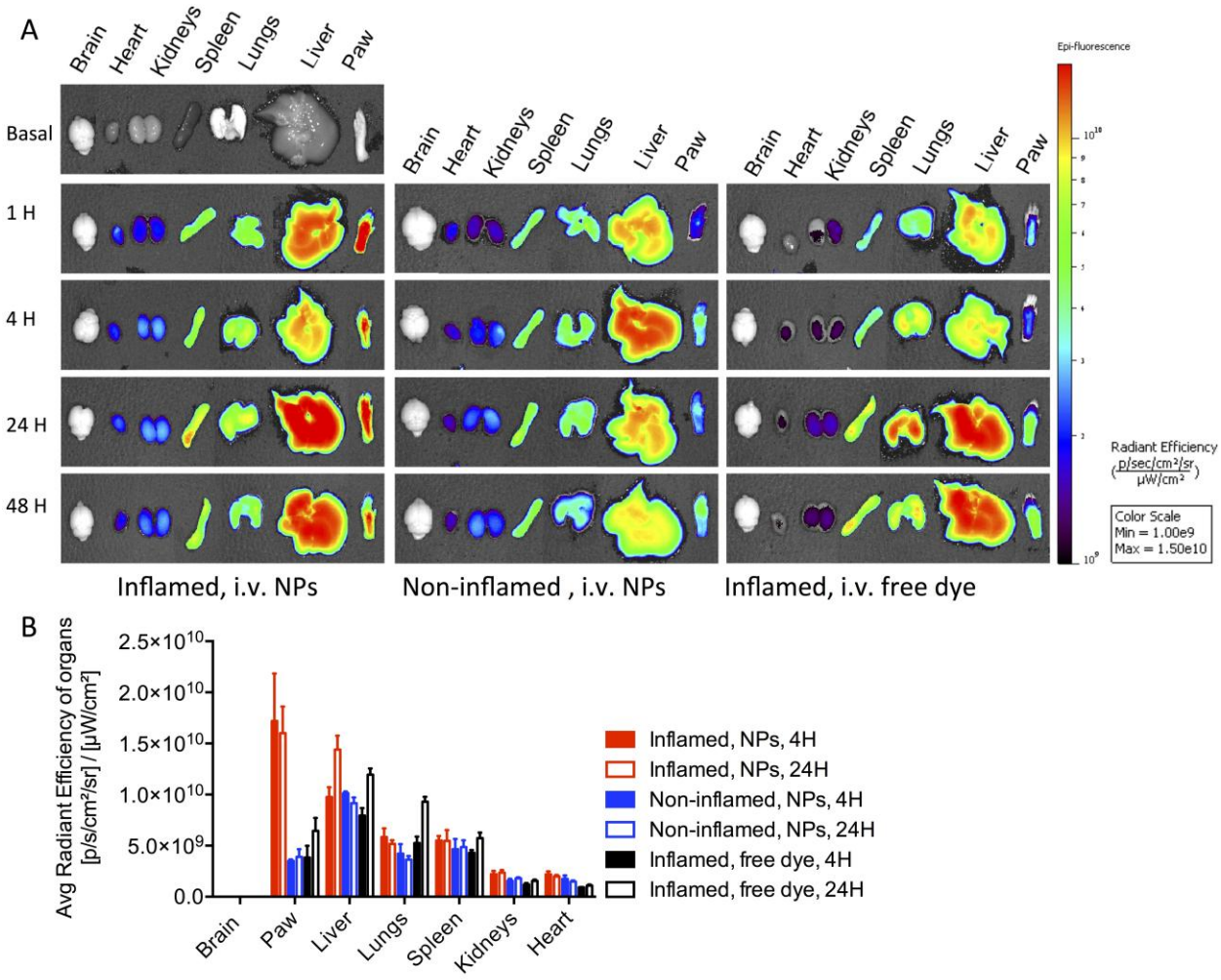

Fig. S9. Biodistribution of fluorescent LENK-SQ-Am NPs or control fluorescent dye solution in mice with or without inflamed paw. 4 h after λ-carrageenan or saline injection into the right paw, fluorescent LENK-SQ NPs or free dye were intravenously introduced into the mice. At different time points, mice were deeply anesthetized with a mixture of ketamine (100 mg/kg, i.p.) and xylazine (10 mg/kg, i.p.) before euthanasia by transcardiac perfusion of 40 ml saline (8 mL/min), until the fluid exiting the right atrium was entirely clear. Then, liver, spleen, kidneys, heart, lungs, brain, and inflamed right hind paw were excised and immediately imaged with the imager. The fluorescence emitted was quantified with Living Image software over the region of interest (ROI) with the threshold of 20%. **(A)** Ex vivo fluorescence imaging of the harvested brain, heart, kidneys, lungs, liver and paw from fluorescent NPs or free dye-injected SWISS mice. **(B)** Average radiant efficiency of these organs after 4 or 24 h injection of NPs or free dye.

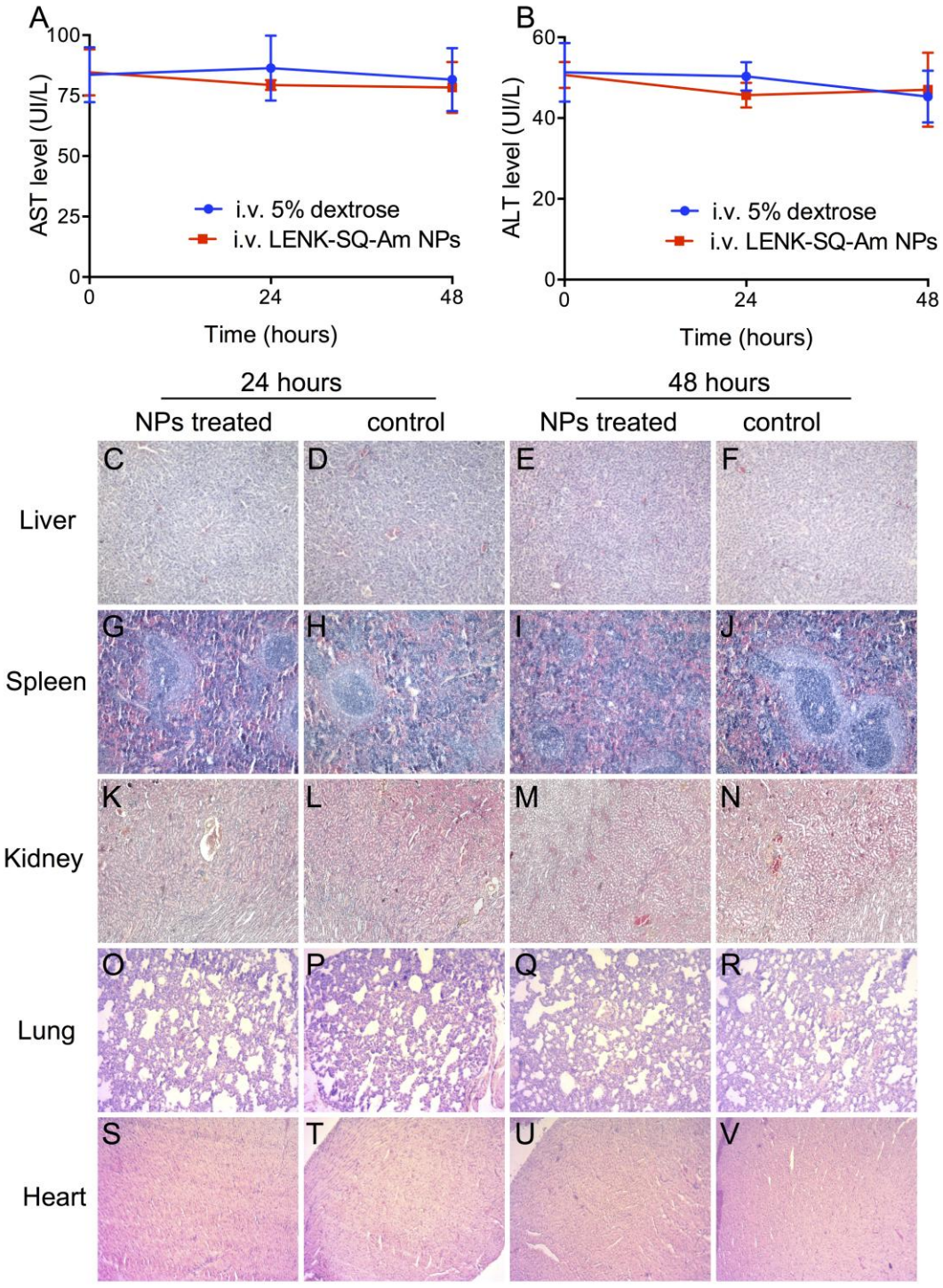

Fig. S10. Toxicity study of LENK-SQ-Am NPs upon systemic administration. LENK-SQ-Am NPs (20mg/kg) were intravenously administered in rats. The AST **(A)** and ALT **(B)** levels in plasma showed no differences compared with dextrose solution (data presented as mean UI/L ± SED, N = 3 animals per group). Histological analysis of organs after intravenous administration of LENK-SQ-Am NPs (20mg/kg) did not show any signs of cell or tissue damage at 24 h and 48h, comparatively to a control 5% dextrose solution. Liver **(C-F),** spleen **(G-J)**, kidneys **(K-N)**, lungs **(O-R)** and heart **(S-V)**. All tissue images were analyzed by microscopy at 10× magnification except for kidneys which were at 5× magnification (Zeiss).

Supplementary experiments:

Table of content

I. EXPERIMENTAL SECTION

Materials: Fluorescent probes CholEsteryl BODIPY® FL C12 and CholEsteryl BODIPY® 542/563 C11, were obtained from Life Technologies. Fmoc-Leucine enkephalin was purchased from Genecust, Luxembourg. Piperidine was obtained from Sigma-Aldrich, France.

1. Failed attempts to link squalene and LENK thrugh an ester bond

Several attempts were conducted to link LENK with squalene through direct ester bond, either by coupling SQ-COOH on the phenolic hydroxyl group of LENK (1st strategy) or SQ-OH on C-terminal acid of LENK (2nd strategy) (**Supp. Fig. 1**, **Supp. Table. 1**). But none of them could lead to an ester bond between SQ and LENK.

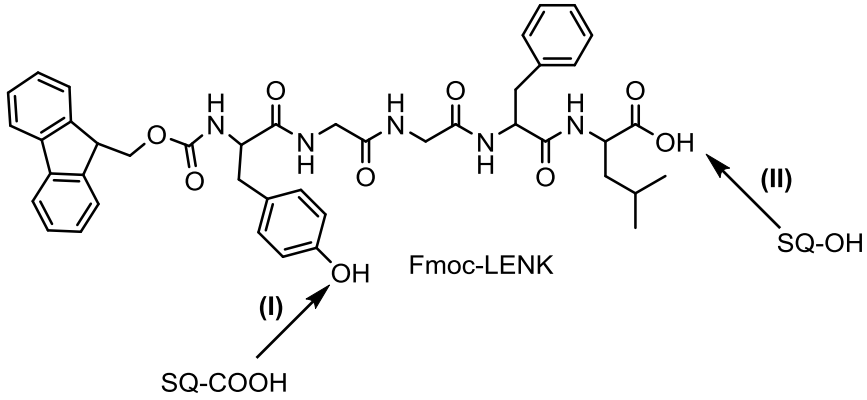

(I). 1st Strategy: Linkage to phenol group of tyrosine

Activation of SQ-COOH by:

a). N-Hydroxysuccinimide (NHS)

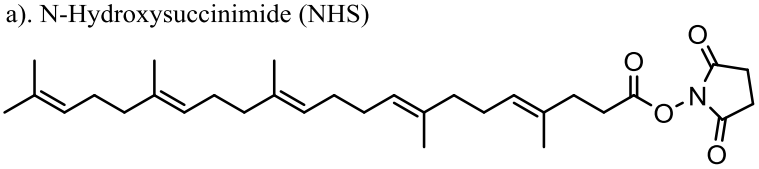

b). Oxalyl chlooride

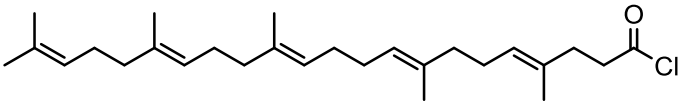

c). Methyl chloroformate

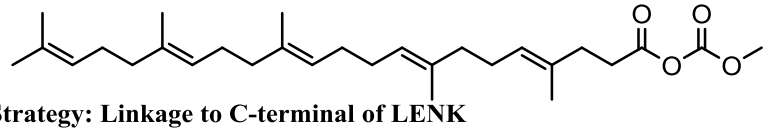

(II). 2nd Strategy: Linkage to C-terminal of LENK

Activation of LENK by: Dicyclohexylcarbodiimide (DCC)

Supp. Fig. 1. Strategies to link squalene with LENK through an ester bond.

Supp. Table 1. Strategies to link squalene with LENK through an ester bond.

Strategy 1	a). Activated by NHS	1st step: activation of squalenic acid with NHS		2nd step: bioconjugation	
		Squalenic acid	1 equiv.	SQ-NHS	2 equiv.
		NHS	2 equiv.	Fmoc-LENK	1 equiv.
		EDCI	2 equiv.	TEA	1 equiv.
		DMAP	0.025 equiv.	Dry DMF	
		DCM			
	b). Activated by oxalyl chloride	Squalenic acid	2 equiv.		
		Oxalyl chloride	6 equiv.		
		Fmoc-LENK	1 equiv.		
		Toluene			
		Dry DMF			
	c). Activated by methyl chloroformate oxalyl	Squalenic acid	2 equiv.		
		Methyl chloroformate	1.6 equiv.		
		Fmoc-LENK	1 equiv.		
		Piridine			
		Dry THF			
		TEA	1.6 equiv.		
Strategy 2	Activated by DCC	Squalenol	2 equiv.		
		Fmoc-LENK	1 equiv.		
		DCC	1 equiv.		
		PTSA	0.3 equiv.		
		Piridine			

Notes: NHS: N-hydroxysuccinimide; EDCI: 1-Ethyl-3-(3-dimethylaminopropyl)carbodiimide; DMAP: 4-Dimethylaminopyridine; DCM: dichloromethane; TEA: Triethylamine; DMF: N,N-Dimethylformamide; THF: Tetrahydrofuran; DCC: Dicyclohexylcarbodiimide; PTSA: p-Toluenesulfonic acid.

2. Failed attempts to synthesize LENK-SQ-Diox through Fmoc protection.

1,1′, 2-tris-norsqualenic acid chloromethyl ester **(2)** was added into a mixture of Fmoc-LENK and $NaHCO_3$ (37 mg, 0.4 mmol) in anhydrous DMF. After reacting at 40 °C under argon for 4 days, Fmoc-LENK-SQ **(4)** was obtained. Piperidine is an efficient agent to deprotect the Fmoc group. But in the case of Fmoc-LENK-SQ-Diox, the dioxycarbonyl linker was cleaved during the deprotection (**Supp. Fig. 2.**). It was the same with triethylamine.

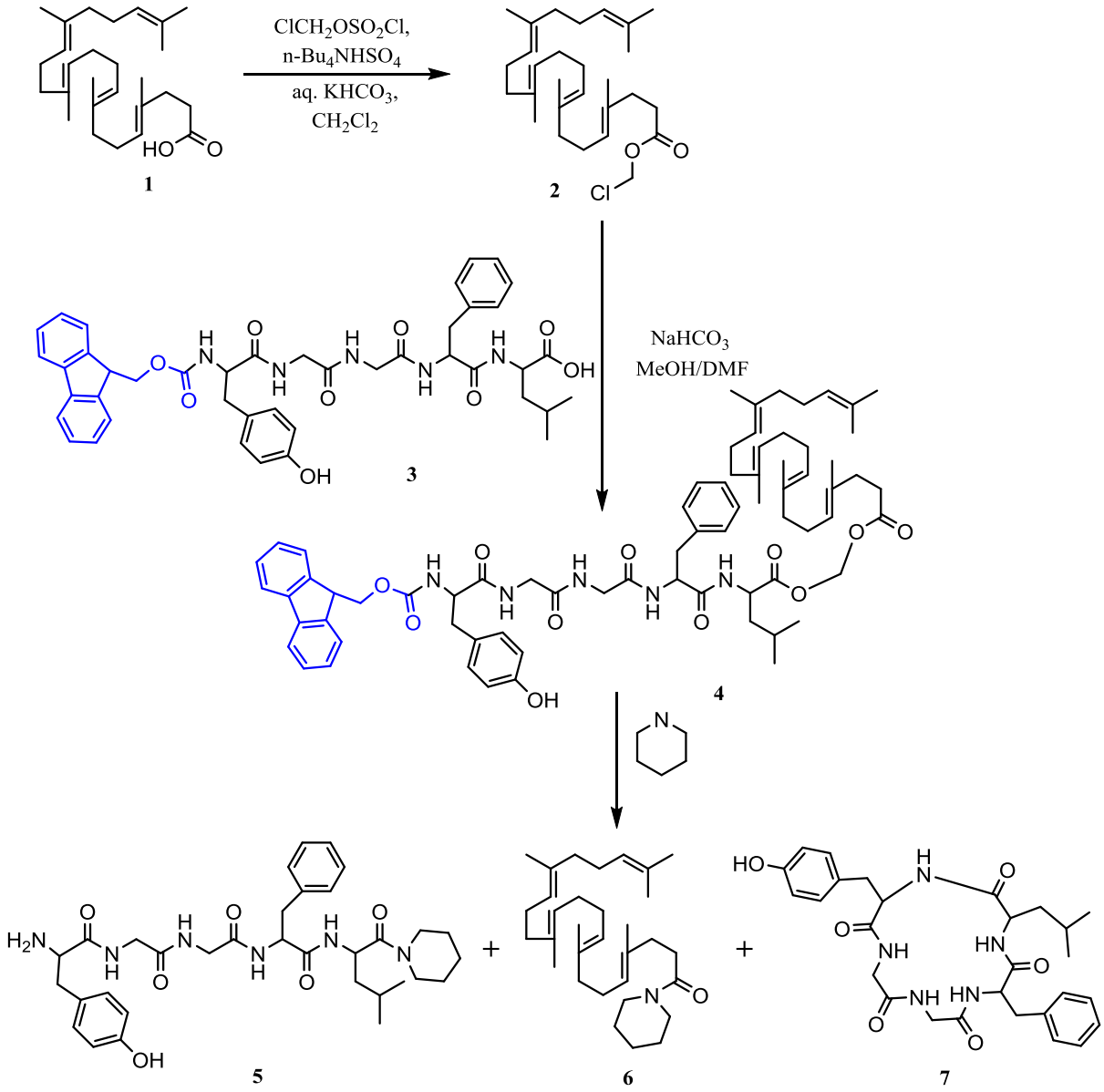

Supp. Fig. 2. Fmoc strategy failed to obtain Leu-enkepahlin-squalene wih dioxycarbonyl linker. (1) 1,1′, 2-tris-norsqualenic acd; **(2)** 1,1′, 2-tris-norsqualenic acid chloromethyl ester; **(3)** Fmoc protected LENK; **(4)** Fmoc-LENK-SQ; **(5-7)** molecules after deprotection step.

3. Failed attempts to remove the Alloc protection

Supp. Table 2. Failed strategies to remove Alloc protection

Strategy 1 (*1*)		Strategy 2 (*2*)		Strategy 3 (*3*)	
Alloc-LENK-SQ	1 equiv.	Alloc-LENK-SQ	1 equiv.	Alloc-LENK-SQ	1 equiv.
$Pd(PPh_3)_4$	0.1 equiv.	$Pd(PPh_3)_4$	0.1 equiv.	Pd-C	0.1 equiv.
Dimedone	7.5 equiv.	$PhSiH_3$	25 equiv.	TES	10 equiv.
Dry THF		Dry DCM		MeOH	
Problems: • Not totally deprotected.		Problem: • Difficulty to remove $Pd(PPh_3)_4$.		Problem: • Formation of allylamines as a side reaction.	

Notes: $Pd(PPh_3)_4$: Palladium-tetrakis(triphenylphosphine); $PhSiH_3$: Phenylsilane; Pd-C: Palladium on carbon; TES: Triethylsilane.

4. *In vitro* transcytosis study through blood-brain-barrier model

4.1. Preparation of fluorescent nanoparticles

Briefly, for the NPs with BODIPY probes, a mixture of LENK-SQ (8 mg/mL in ethanol), BODIPY® FL C12 and BODIPY® 542/563 C11 (both at 0.5 mg/mL in a mixture of ethanol and acetone (1:1)) were added dropwise into a 5% aqueous dextrose solution under magnetic stirring. The solution became spontaneously turbid with a tyndall effect, indicating the formation of the nanoparticles. The solvent was then completely evaporated using a Rotavapor® (80 rpm, 30°C, 30 mbar) to obtain an aqueous suspension of pure LENK-SQ NPs (final concentration 2 mg/mL). Keeping a constant total amount of incorporated probes at 2% with respect to the LENK-SQ, different formulations were prepared by varying the relative fraction of each probe. The size and surface charge were measured using Malvern Zetasizer Nano ZS 6.12 (173° scattering angle, 25°C).

4.2. Transcytosis of the LENK-SQ through hCMEC/D3 cellular monolayer

hCMEC/D3 cells were grown in EBM-2 medium supplemented with 5% FBS, 10 mM HEPES, 1 ng/mL bFGF, 1.4 µM hydrocortisone, 5 µg/mL acid ascorbic, 1% Chemically Defined Lipid Concentrate and 1% penicillin-streptomycin at 37 °C and 5% CO_2. Cells were passaged every 3 - 4 days by 1:4.

A total of 232500 hCMEC/D3 cells (50,000 cells/cm2) was seeded on 0.4 µm pores, 4.67 cm^2, collagen precoated PTFE membrane transwells (Corning). 1.5 mL of medium was added in the apical compartment and 2.6 mL in the baso-lateral compartment. Cells were cultivated for 7 days at 37 °C and 5% CO_2 to confluence and medium was changed after three days. In order to check the formation of tight junctions, transendothelial electrical resistance (TEER) was measured using an epithelial voltmeter (EVOM2), which should be more than 30 Ohm*cm^2.

Then, fluorescent LENK-SQ NPs (40 µg/ mL) diluted in culture medium were added to the apical compartments of the transwells, and after 4h and 6h of incubation, the media of the two compartments were withdrawn. The fluorescence intensity was measured using spectrofluorimeter. The transmembrane passage was expressed as the percentage of the fluorescence found in the baso-lateral compartment, as compared to the initial fluorescence placed in the apical compartment using a calibration curve. Transcytosis of Results were expressed as mean ± SD corresponding to three independent experiments run in duplicate.

Apical media (0.25mL) was added to 0.75mL of acetonitrile. The baso-lateral media (0.5mL) was added to 1.5mL of acetonitrile. Each medium was then centrifuged under 5000g during 15 mins in order to precipitate the proteins from the medium, the surpernatant was then collected, dried under nitrogen flow and re-solubilized in 0.25mL of H_2O for HPLC.

II. SUPPLEMENTARY RESULTS

1. Peptide quantification by HPLC

The HPLC technique exhibited linearity for LENK over the assayed concentration range (0.39-200 µg/ml) (**Supp. Fig. 3**). The linear regression analysis displayed a high correlation coefficient (R^2= 0.99998) between peak area and concentration and the detection limit of the HPLC technique was of 0.39 µg/mL for LENK. The accuracy of the technique corresponded to 96 ± 5% which is within the acceptance limit (90%-110%), hence giving a suitable recovery of LENK. Percentage of RSD

(relative standard deviation) of the LENK was found to be less than 2.01%, showing a high degree of precision and reproducibility (**Supp. Table 3**).

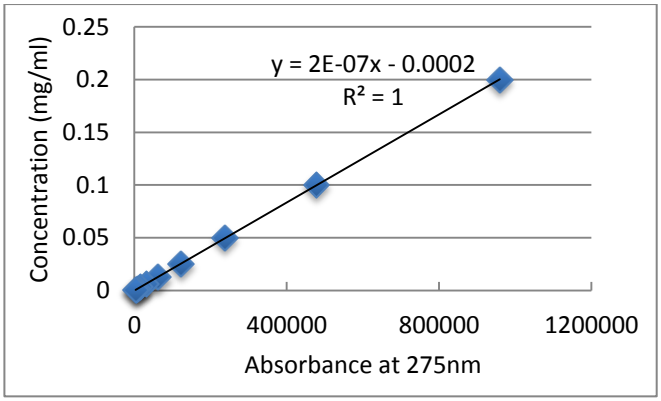

Supp. Fig. 3. Standard curve of LENK from 0.0004 to 0.2 mg/ml analysized by HPLC. The limitation of the HPLC technique for LENK is 0.0004mg/ml.

Supp. Table. 3. Accuracy and precision of HPLC technique for LENK analysis

True values (LENK) at 3 levels	Accuracy	Precision/Repeatability	
		Measured values (Mean±SD µg/mL)	RSD
125%, (71.875µg/mL)	96.41±1.39%	71.57±0.11	0.15%
75%, (43.125µg/mL)	97.23±1.41%	43.85±0.88	2.01%
25%, (14.375µg/mL)	96.87±4.95%	14.07±0.05	0.36%

The release of peptide from LENK-SQ was confirmed by HPLC Alliance 2695 coupled to a MS-TOF LCT Premier (WATERS) (**Supp. Fig. 4**). After incubation with serum, LENK-SQ-Diox NPs could release the free peptide, and the retention time for the released LENK (Mass plus H^+ was 556.27) corresponded to 7.58 mins. In the case of LENK-SQ-Dig NPs, LENK attached to its diglycolic linker was released, which corresponded to the peak at 6.90 mins, as shown in **Supp. Fig. 4B.**

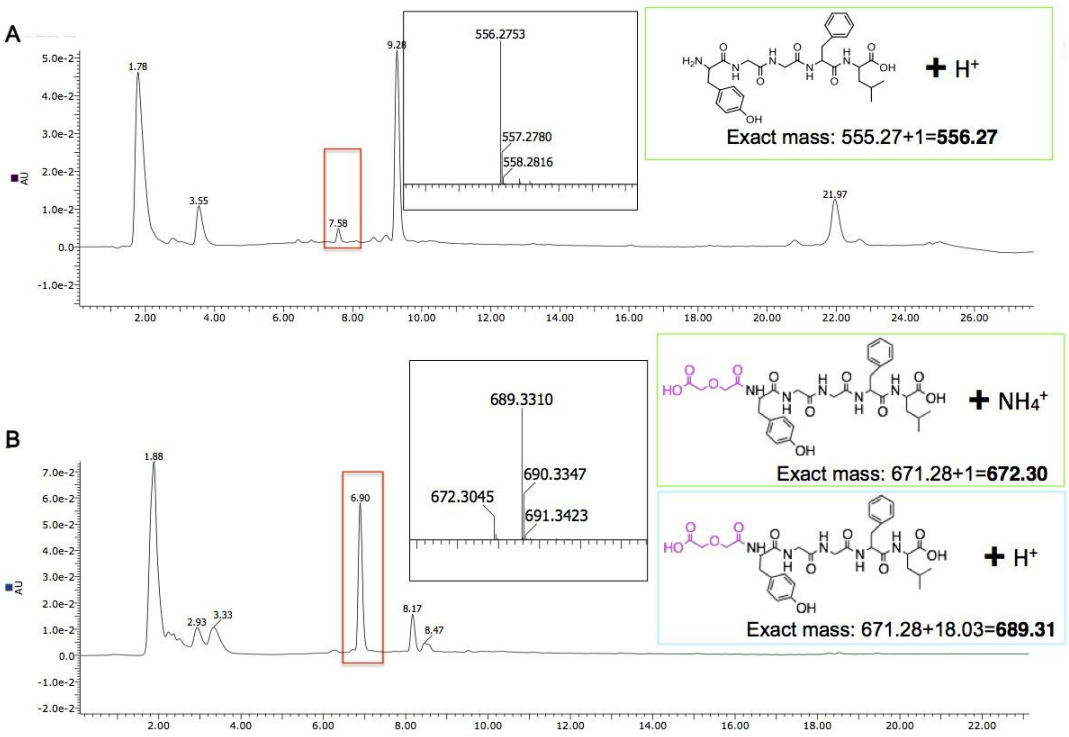

Supp. Fig. 4. Release study in mouse serum of LENK from LENK-SQ-Diox (A) or LENK-diglycolic fragment from LENK-SQ-Dig (B) by HPLC-MASS.

2. *In vitro* study of the ability of NPs to cross the blood-brain-barrier

For the transcytosis study, labeled LENK-SQ NPs with both BODIPY dyes were prepared by conanoprecipitation of the two BODIPY probes together with the LENK-SQ. The optimization of the FRET NPs was performed by varying the relative fractions of donor and acceptor dyes resulting a series of FRET NPs preparations which were characterized by fluorescence spectroscopy. Concerning intact FRET NPs, when the two dyes are close to each other, energy transfer could be observed by simultaneous donor PL intensity quenching and acceptor fluorescence intensity sensitization (**Supp. Fig. 5A**). The disassembled FRET NPs (in ethanol) and the mixtures of single-dye NPs showed only concentration-dependent donor fluorescence intensity changes (**Supp. Fig. 5B, C**), because of the variation in donor concentration fractions. This confirmed that only the intact FRET NPs showed FRET signal between BODIPY-FL and BODIPY-542/563, whereas disassembled NPs or donor-NPs/acceptor-NPs physical mixture did not provide any FRET signal. Thus, the FRET signal could be used to determine the integrity (FRET on) or disassembly (FRET off) of the NPs. Concerning FRET LENK-SQ NPs, the strongest FRET signal was obtained for the NAs with fractions of 1.6% donor and 0.4% acceptor (1.6%D/0.4%A), as determined by the strongest acceptor PL intensity under equivalent donor excitation (**Supp. Fig. 5A**). Therefore, for all following experiment, were used the 1.6%D/ 0.4%A preparation for all following experiments to investigate endocytosis and transcytosis of SQAd NAs across the BBB model. Moreover, incorporation of the BODIPY probes did not significantly alter the colloidal properties of the NPs (**Supp. Fig. 5E**).

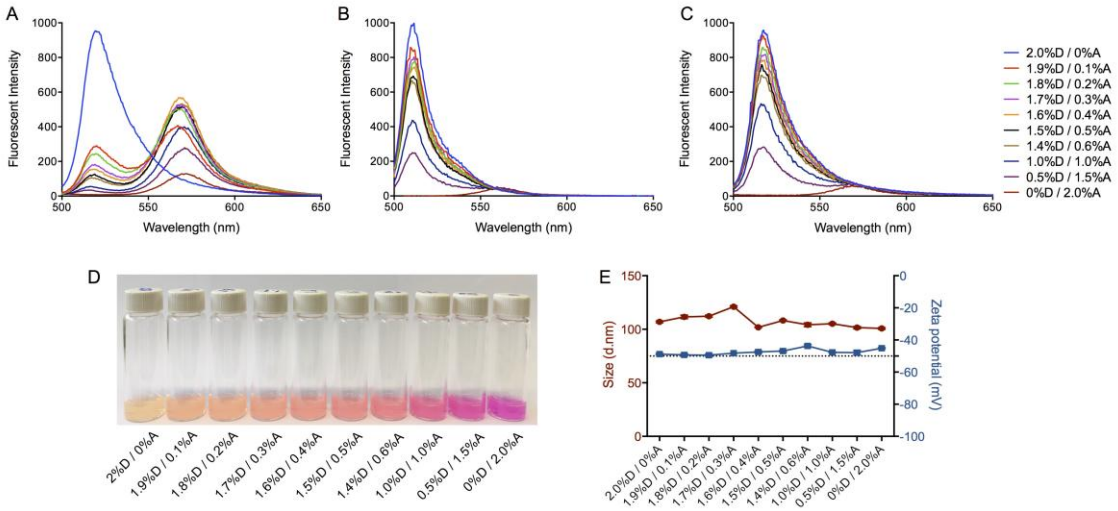

Supp. Fig. 5: Characterization of FRET LENK-SQ-Am NPs. Upon donor excitation (478 nm), FRET NPs showed a strong acceptor emission intensity increase at 570 nm and a strong donor emission intensity decrease at 515 nm compared to the single dye NPs. The strongest FRET signal was obtained with the NPs preparation of 1.6%D/0.4%A **(A).** Pictures of FRET LENK-SQ NPs preparations obtained by varying donor/acceptor concentration fractions as indicated below the images showed that the different preparations displayed various optical properties **(D).** Dillution of NPs in ethanol was used to mimic the disassembly of NPs **(B).** Measurement of the mixtures of single dye NPs at the same donor/acceptor concentration fractions did not show any FRET signals **(C).**

The passage of LENK-SQ NPs across the *in vitro* blood-brain-barrier model has been analyzed using a transwell system (**Supp. Fig. 6**). hCMEC/D3 cells were grown on a collagen-coated membrane to form the barrier. Then, the FRET NPs or fluorescent NPs (dye C11 or C12 alone) were added in the apical compartment (modeling the blood compartment), whereas the translocation toward the baso-lateral compartment (modeling the brain compartment) was measured by spectrofluorimetry. It was found that the fluorescence intensity in the baso-lateral compartment increased with time, indicating a passage of the fluorophore across the BBB after 4 and 6 hours incubation (**Supp. Fig. 7**). But neither FRET signal (**Supp. Fig. 7**) nor LENK-SQ bioconjugates (**Supp. Fig. 8**) was detected in the baso-lateral compartment.

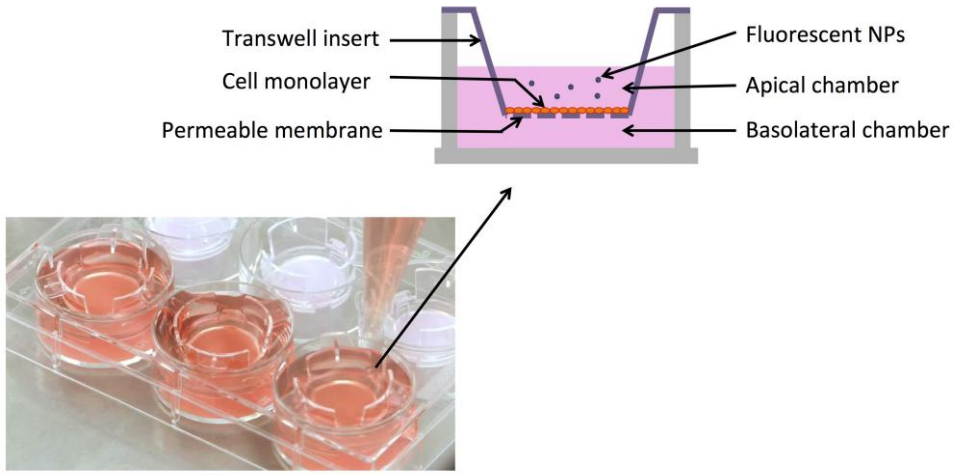

Supp. Fig. 6: Transcytosis study of NPs using transwell system. hCMEC/D3 cells grown on collagen-coated membrane filter inserts were incubated apically with fluorescent or FRET NPs.

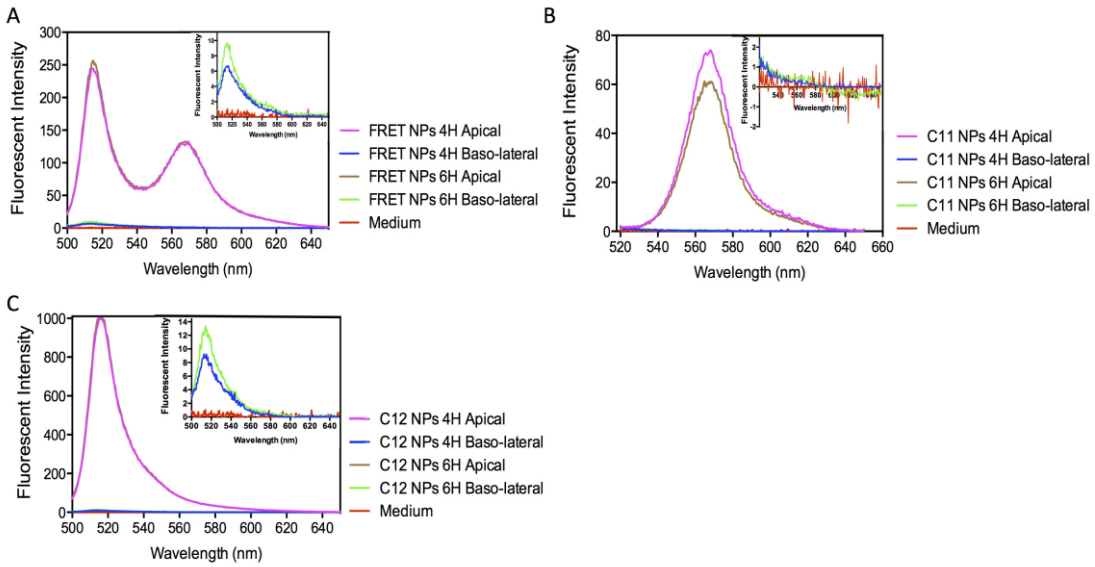

Supp. Fig. 7: Transcytosis study of fluorescent or FRET NPs using an *in vitro* model of blood-brain-barrier. hCMEC/D3 cells grown on collagen-coated membrane filter inserts were incubated apically with fluorescent or FRET NPs. **(A)** FRET NPs were added in the apical chamber and the FRET intensity in apical and basolateral was measured 4h and 6h after incubation; **(B)** Fluorescent NPs with BODIPY® 542/563 C11 (Acceptor) were added in the apical chamber and the fluorescent intensity in apical and basolateral was measured 4h and 6h after incubation; **(C)** Fluorescent NPs with BODIPY® FL C12 (Donor) were added in the apical chamber and the fluorescent intensity in apical and basolateral was measured 4h and 6h after incubation.

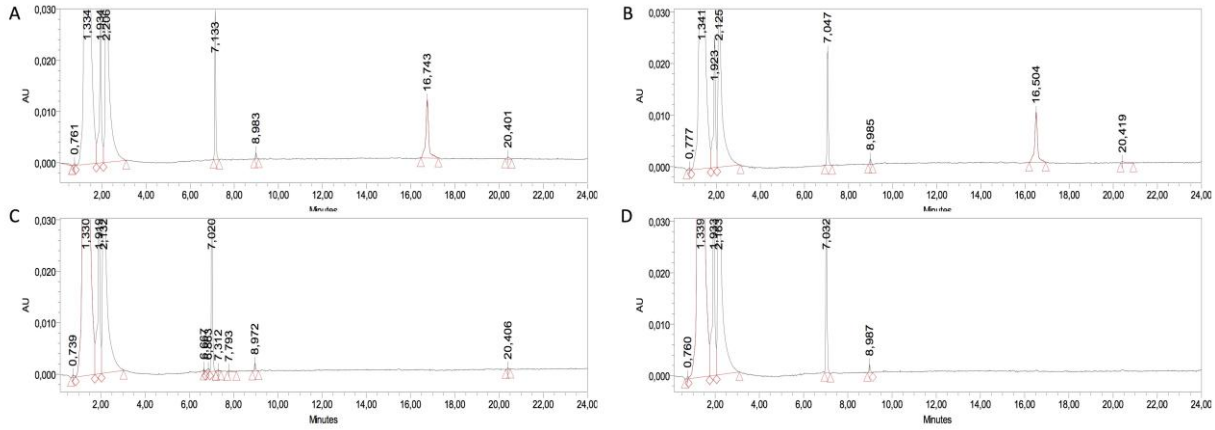

Supp. Fig. 8: Transcytosis study of NPs using an *in vitro* model of blood-brain-barrier. hCMEC/D3 cells grown on collagen-coated membrane filter inserts were incubated apically with NPs. After 4h **(A, C)** and 6h **(B, D)**, medium from apical **(A, B)** and basolateral **(C, D)** were taken and analyzed by HPLC.

3. MASS spectra of the bioconjugates

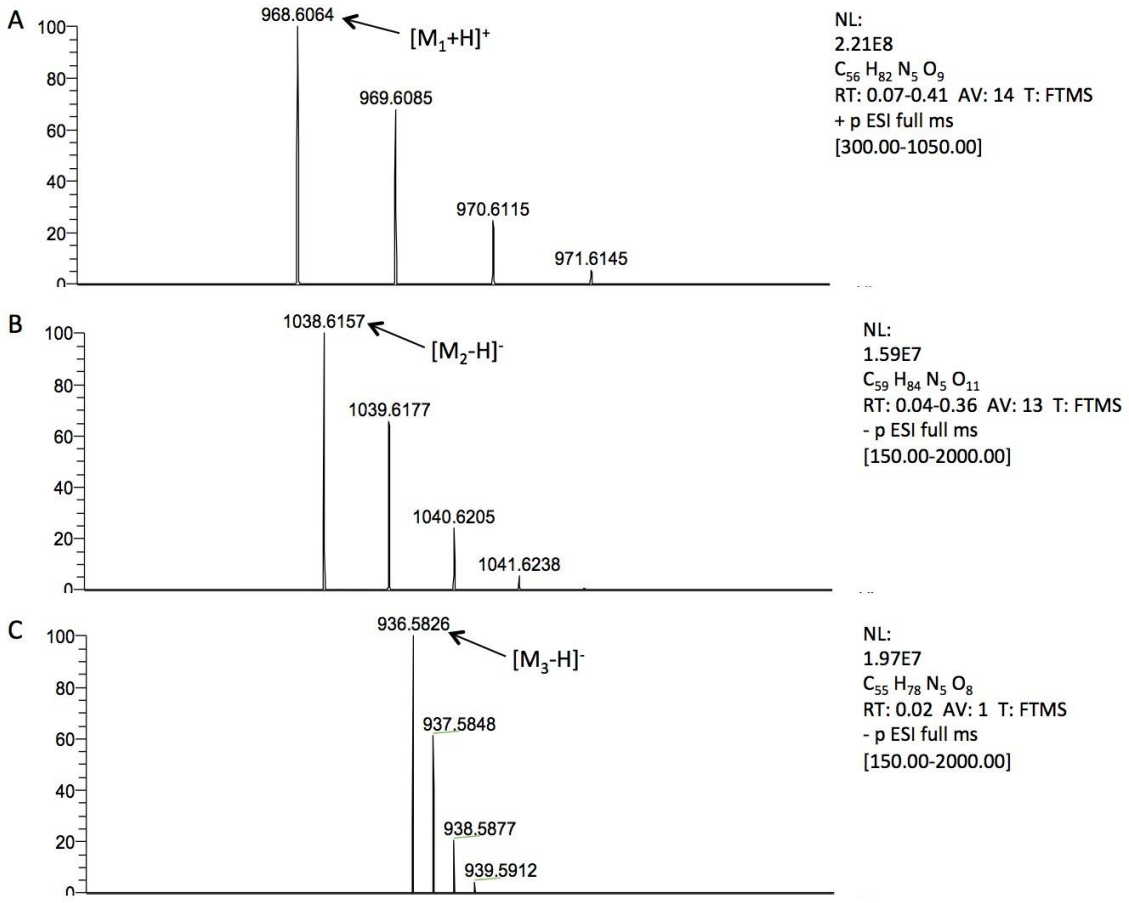

Supp. Fig. 9. Isotopic profiles of (A) LENK-SQ-Diox, (B) LENK-SQ-Dig, (C) LENK-SQ-Am.

Reference

1. H. Kunz, C. Unverzagt, The Allyloxycarbonyl (Aloc) Moiety—Conversion of an Unsuitable into a Valuable Amino Protecting Group for Peptide Synthesis. *Angewandte Chemie International Edition in English* **23**, 436-437 (1984).
2. P. Grieco, P. M. Gitu, V. J. Hruby, Preparation of 'side-chain-to-side-chain' cyclic peptides by Allyl and Alloc strategy: potential for library synthesis. *The Journal of Peptide Research* **57**, 250-256 (2004).
3. P. K. Mandal, J. S. McMurray, Pd−C-Induced Catalytic Transfer Hydrogenation with Triethylsilane. *The Journal of Organic Chemistry* **72**, 6599-6601 (2007).

General discussion

The main objective of this PhD project was to develop new nanomedicines allowing the specific delivery of Enkephalin neuropeptide into inflamed tissues for pain control, using "squalenoylation" concept. For this purpose, Leu-enkepahalin (LENK) neuropeptides were chemically linked to squalene through three different chemical linkers, i.e., dioxycarbonyl, diglycolate, and amide bond in order to obtain LENK prodrugs. These squalenoyl-LENK bioconjugates (LENK-SQ) showed the capability to form nanoparticles (NPs) using nano-precipitation technology. The potential of these NPs to releave pain has been studied using carrageenan-induced paw edema model in rats (Hargreaves test), and revealed a significant anti-hyperalgesic effect which lasted longer than after treatment with morphine. Pretreatment with opioid receptor antagonists such as naloxone (brain-permeant) and naloxone methiodide (brain-impermeant), could reverse this anti-hyperalgesia , thus indicating that the LENK-SQ NPs acted through peripheral opioid receptors. A biodistribution study was conducted in order to confirm the peripheral action of these NPs using *in vivo* fluorescence imaging. This study showed a strong accumulation of fluorescently labeled LENK-SQ NPs in the inflamed paw, and also in the liver, spleen and lungs while no fluorescent signal could be detected in the brain, confirming the peripheral effect of LENK-SQ NPs. The safety of these NPs was also checked by toxicity studies which revealed normal AST/ALT levels. In addition, histological analysis didn't show any anomaly in the organs.

The present discussion aims to interpret and describe the global input of this PhD research to the pain treatment, and to discuss the remaining challenges for the translation of LENK-SQ NPs toward the clinics.

Squalenolation of Leu-enkephalin

Our group has explored the remarkable properties of squalene to form nanoparticles when conjugated to different kinds of small molecule drugs (i.e. gemcitabine, doxorubicine, cis-platin, Penicillin G, adenosine, and so on) (*1*). It has been shown that, in general, the resulting nanomedicines displayed safer and more efficient pharmacological activity than the parent drugs. The focus of the current study was to enlarge this groundbreaking concept to opioid peptide Leu-enkephalin for efficient pain control. In this study, three different prodrugs of Leu-enkephalin were synthesized, using three different linkers between the peptide and the hydrophobic squalene, in order to modulate drug release in a specific environment such as inflammation.

At the beginning, squalene conjugation on solid-supported peptides (LENK) was envisaged. However, since trifluoroacetic acid (TFA) treatment, commonly employed for the peptide–resin cleavage, pose the risk of possible SQ degradation, a postsynthetic strategy was designed by introducing squalene moiety on already preformed peptide sequences.

Derivatives of squalene, 1,1',2-trisnorsqualenoic acid (SQ-COOH), or 1,1',2-tris-norsqualenol (SQ-OH), were recruited in order to bind enkephalin through its N-terminal amine, C-terminal acid or Phenol group of tyrosine (**Fig. 1**). A first part will be devoted to unsuccessful attempts that have not been described in the article and a second part will briefly go through the synthesis of the LENK-SQ-Diox, LENK-SQ-Dig and LENK-SQ-Am bioconjugates.

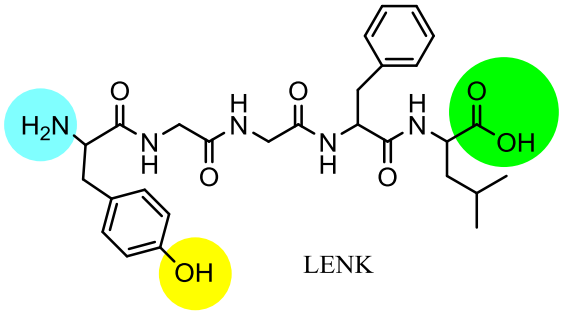

Fig. 1. Linkage sites on Leu-enkephalin.

A direct ester link has been first considered in order to couple directly SQ-COOH on the phenolic hydroxyl group of LENK (1st strategy) or SQ-OH on C-terminal acid of LENK (2nd strategy). Several attempts were conducted but none of them could lead to an ester bond between SQ and LENK. Thus, concerning the first strategy, in order to avoid additional protection/deprotection steps on C-terminal LENK, activation of SQ-COOH prior to the condensation was envisaged. Thus, SQ-COOH was activated using N-hydroxysuccinimide, oxallyl chloride or methyl chloroformate. Unfortunately, none of them could react with the phenol group of LENK. The second strategy was then adopted, using direct coupling of SQ-OH to C-terminal acid of the LENK using DCC coupling reagent, though, this strategy have proven to be unsuccessful too. Hence, direct ester link finally could not be achieved, probably due to the bulky moiety of squalene which hindered the access to the phenol group. As for the second approach, the nucleophilicity of squalenol was not enough sufficient to counteract the bulky moiety of squalene.

Regarding to synthesis of LENK-SQ-Diox, LENK-SQ-Dig and LENK-SQ-Am bioconjugates, the synthesis could be successfully achieved. Indeed, 1,1′,2-trisnorsqualenoic acid (SQ-COOH), or 1,1′,2-tris-norsqualenol (SQ-OH), were attached to LENK through its N-terminal amine or C-terminal acid. Therefore, the resulting LENK-SQ prodrugs were synthesized with either direct amide bond, diglycolic or dioxycarbonyl linker in order to investigate the possible influence of the linkage stability on the peptide release. It was expected that LENK-SQ-Diox released faster than LENK-SQ-Dig, and LENK -SQ-Am was supposed to trigger the slower release as reported in the literature (*2-4*). Both LENK-SQ-Am and LENK-SQ-Dig, were obtained in good yields (around 70%) (see article under review). However the synthesis of the bioconjugate with dioxycarbonyl linker at the C-terminal of LENK, was found particularly tricky. First of all, in order to avoid N-terminal conjugation, the primary amino group of LENK was protected before the conjugation process. In that respect, Fmoc (fluorenylmethyloxycarbonyl) strategy was first adopted for the protection of the primary amino group of LENK. Then, the Fmoc-LENK-SQ-Diox conjugate was easily synthesized by simple alkylation of the carboxylate function of the Fmoc-peptide with the chloromethyl ester of squalenic acid, which was prepared upon treatment of squalenic acid with chloromethyl chlorosulfate. However, the amine deprotection step involving the most common solution of 20% piperidine in DMF, resulted in the cleavage of the sensitive dioxycarbonyl linker. Among the byproducts, cyclized LENK, N-squalenoylpiperidine and N-Leu-enkephanoylpiperidine were identified by HPLC-MS technique. Deprotection by tertiary amine such as triethylamine was also tried but with limited success. Hence, this approach was abandoned in favor of Alloc (Allyloxycarbonyl) strategy since the deprotection step is carried out under neutral conditions. Alloc-LENK was coupled to squalene derivative following the same reaction scheme as for Fmoc-LENK leading to Alloc-LENK-SQ-Diox. The first attempt to remove the Alloc involved tetrakis(triphenylphosphine)palladium(0) in presence of dimedone. This reaction led to partial deprotection of the bioconjugate after 24h. The deprotection step was

reproduced with the same palladium complex but replacing dimedone by phenylsilane. The Alloc protecting group could be removed, however during purification step the palladium complex could not be separated from the bioconjugate. Lastly, the palladium catalysed deprotection of allyl carbamate was reproduced using this time triethylsilane as scavenger and 10% Pd/C. Though, once deprotected, amine group of LENK-SQ bioconjugate competed the nucleophilic allyl group scavenger in the trapping of the π-allyl palladium complex, resulting in N-allylation of amine function of the bioconjugate (**Fig. 2**). This secondary reaction could finally be majorly prevented by the use of high amounts of triethylsilane (TES). This step yielded only 23% of deprotected bioconjugate, due to the cleavage of the sensitive bond during purification step. Finally, the total yield of LENK-SQ-Diox corresponded to 9%.

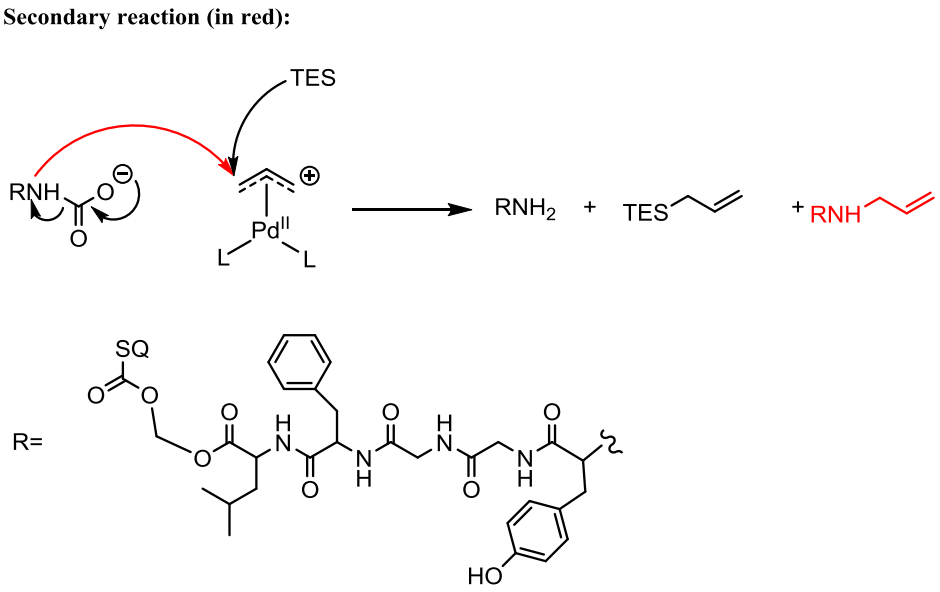

Fig. 2. The problematic sidde reaction of allylamine formation during palladium catalysed deprotection.

Given the fact that our approach was based on the covalent binding between squalene and the peptide, the peptide drug loadings into the NPs were calculated from the ratio between LENK peptide Mw and LENK-SQ bioconjugate Mw (57.38% for LENK-SQ-Diox NPs, 53.41% for LENK-SQ-Dig NPs and 59.22% for LENK-SQ-Am NPs). It is noteworthy that such drug payload was dramatically higher than into liposomes or PLGA enkephalin-loaded nanoparticles (respectively 0.4% and 4.75 % drug loading). As outlined before, high drug loading is an important feature for nanocarriers as a smaller quantity of carrier materials is administrated to reach the pharmacologically active concentration of the drugs, which in turn may decrease the associated potential toxicity (*5*). On that point, it is important to highlight that squalene is a natural and biocompatible raw material found among others in human sebum-like materials and in shark-liver oil (*6*). All LENK-SQ bioconjugates showed the ability to self-assemble in water as monodispersed spherical nanoassemblies with average diameter ranging from 75 nm to 122 nm using an easy formulation process (nanoprecipitation/solvent evaporation). The NPs exhibited positive or negative surface charge, denpending on the free terminal function of the peptide in the bioconjugates. Indeed, free N-terminal amine function led to a net positive surface charge while free C-terminal acid function resulted in a net negative surface charge. Moreover, the size and the surface charge of the LENK-SQ NPs were found to be quite stable at +4°C, even if a slight increase of the size was observed, likely due to the swelling of the particles resulting from NPs hydration, already observed previously with other squalene-based NPs (*7*).

The main limitation for systemic peptide treatment arises from the enzymatic degradation in blood

circulation. Indeed, the plasma half-life of LENK in serum corresponds to 2 minutes approximatively (Fig. S7). Concerning LENK-SQ NPs, *in vitro* release study showed that LENK peptide was released from LENK-SQ-Diox and LENK-SQ-Dig but not from LENK-SQ-Am (Fig. 3). In the case of LENK-SQ-Diox and LENK-SQ-Dig, the release of the respective LENK and LENK-linker fragment was followed by a progressive degradation of the peptide, due to serum enkephalinases. Regarding LENK-SQ-Diox bioconjugate, both LENK and squalene moieties were each linked through an ester bond to the dioxycarbonyl linker. In the case of the LENK-SQ-Dig bioconjugate, the diglycolate linker was attached on one side to squalene by an ester bond and on the other side to the LENK through an amide bond while concerning LENK-SQ-Am bioconjugate, a direct amide bond connected the LENK to the SQ moiety. This suggests that the release of LENK from LENK-SQ NPs proceeded from enzymatic hydrolysis by serum esterases. It has been previously reported (*2-4, 8*) that an amide bond is generally more resistant to hydrolysis than an ester bond. This explains why in serum, LENK-SQ-Am didn't release the peptide. Despite these *in vitro* data, all the 3 conjugates were recruited for anti-hyperalgesia experiments. As a matter of fact, it was expected that the more aggressive *in vivo* enzymatic content, particularly rich in proteolytic enzymes at the inflammation site, would contribute to the release of LENK from all the bioconjugates (*9, 10*).

Analgesic efficacy of LENK-SQ NPs

λ-carrageenan is a commonly used inflammatory irritant that stimulates the release of inflammatory and proinflammatory mediators, including histamine, bradykinin, tachykinins, reactive oxygen, and nitrogen species (*11*). It is usually used to produce short-lasting acute inflammation and hyperalgesia in animal models. In the present study, λ-carrageenan was injected subcutaneously into the *plantar* surface of the right hind paw and produced local inflammation, designated by the 5 cardinal signs: hypersensitivity, swelling, redness, heat, and loss of function. The inflammation developed hyper-sensitivity to thermal stimuli (thermal hyperalgesia) at the injected paw level. These changes became maximal 3-5 h post-λ-carrageenan injection and generally subsids within 24 hours (*12, 13*). This λ-carrageenan-induced rodent edema model has been widely accepted for screening compounds with anti-inflammatory and anti-hyperalgesic potentialities (*14*). Thus, in our study, the hypersensitivity of the rats was measured 3 hours after carrageenan administration. The treatments were then injected and hypersensitivity to a noxious stimulus (hyperalgesia) was then assessed during 4 hours using Hargreaves test and was compared to morphine used as positive control. The Hargreaves test is specifically designed to assess thermal pain sensation in rodents such as rats and mice (*15*). It measures the response of the animals (i.e. paw withdrawal latency, PWL) to infrared heat stimulus, which was applied to the plantar surface.

The results of this study showed that LENK-SQ NPs significantly increased the hindpaw withdrawal latency in rats bearing unilateral inflammation, which lasted longer than morphine, indicating marked anti-hyperalgesic efficacy. Surprisingly, LENK-SQ-Am NPs, which was expected to release the peptide slower in comparison with the other two NPs, exhibited a stronger effect with a shorter duration, probably due to enzymatic serum capability which is not predictive of the enzymatic ecosystem in the inflamed paw. LENK-SQ-Dig NPs and LENK-SQ-Diox NPs had nearly the same anti-hyperalgesic profile with prolonged effect, resulting in a significantly higher AUC (area under the curve) than morphine and LENK-SQ-Am NPs. In particular, the LENK-SQ-Dig NPs showed an anti-hyperalgesic effect, which lasted twice as long as morphine. In addition, as expected for an analgesic compound, PWL values after morphine treatment in λ-carrageenan-treated rats exceeded basal values in naïve healthy rats, whereas, in contrast, under the conditions used here, PWL values

after LENK-SQ NPs just reached these basal values. This would suggest that LENK nanoparticles are devoid of analgesic properties but are especially potent to counteract hyperalgesia in chronic pain suffering subjects. However, further studies are required to assess this hypothesis. In order to determine the involvement of central or peripheral opioid receptors during the anti-hyperalgesic effect of LENK-SQ NPs, opioid receptor antagonists naloxone or naloxone methiodide were subcutaneously injected 15 min prior to the injection of NPs or Morphine (positive control). Indeed, naloxone (NAL) is an opioid antagonist that acts upon μ, δ and κ opioid receptors while naloxone methiodide (NAL-M), the quaternary derivative of naloxone, is thought to not cross the blood-brain-barrier. Naloxone methiodide is generally used as a research tool allowing to distinguish between central and peripheral mechanisms of the LENK-SQ NPs (*16*). Pretreatment with NAL could prevent the increase in PWL evoked by LENK-SQ NPs as well as morphine, indicating that the anti-hyperalgesic effect of all these compounds was effectively mediated by opioid receptors. Nal-M, that poorly penetrates the blood-brain-barrier, antagonized the antihyperalgesic effect of the LENK-SQ NPs while it could almost not antagonize the antihyperalgesic effects of morphine. This result clearly suggested that LENK-SQ NPs acted exclusively on peripheral opioid receptors. As regards the morphine, the result was in accordance with the fact that morphine mainly acted on central opioid receptors (*17*).

Biodistribution of LENK-SQ NPs

Inflammatory responses in the peripheral play key roles in the development and persistence of many pathological pain states (*18*). Inflammation results in a dramatic change in blood vessel permeability as the capillary vasculature undergoes structural remodeling displaying fenestrations between the endothelial cells ranging from 300 nm to 4700 nm in size, thus allowing leukocyte diapedesis into the peripheral inflamed tissue (*19, 20*). Therefore, under inflammation process, when administered intravenously, nanoparticles that normally don't cross the endothelial barrier of the capillaries, can then extravasate and accumulate in the interstitial space of inflamed tissues thus allowing an increase of drug concentration locally (*21*). This targeted delivery of macromolecules or drug nanocarriers to the site of inflammation is called enhanced permeability and retention (EPR) effect (**Fig. 3**) (*22*).

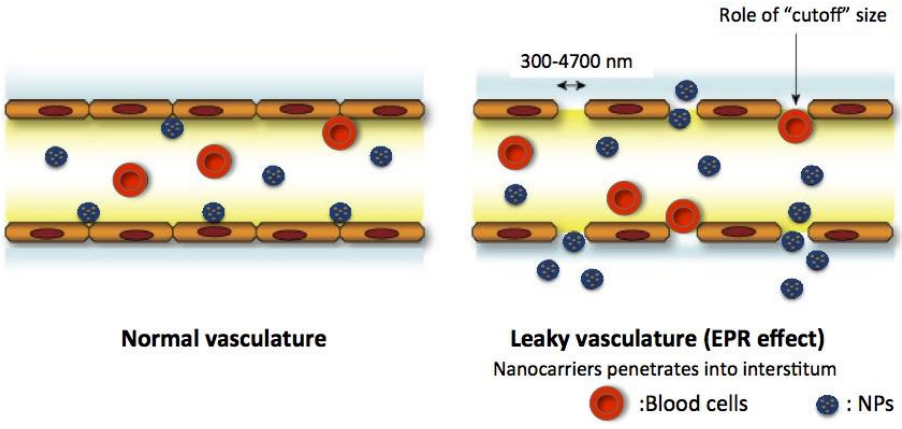

Fig. 3: EPR effect at the inflammation site. Inflammation will cause the vessel to dilate resulting in a higher blood flow. Furthermore, the contraction of endothelial cells will allow the penetration of nanoparticles into the tissue.

In order to check if LENK-SQ NPs acted peripherally within the site of inflammation, *in vivo* biodistribution study of these NPs was performed using fluorescent DiD-labeled LENK-SQ NPs.

These fluorescently labeled NPs were intravenously injected into λ-carrageenan-induced mouse edema model. This study was conducted on mice since the IVIS® Lumina scan used in our faculty was adapted to mice but not to rats. Dramatic increase of fluorescence signal was already detected in the inflamed paw 0.5 h after injection, and was 3 times more intense than in the contralateral non-inflamed paw. No difference in signal intensity was observed between this contralateral non-inflamed paw and the paw of mice injected with saline only (instead of with λ-carrageenan) and treated with fluorescently labeled NPs, which indicated that the process of subcutaneous injection *per se* didn't cause any damage to the capillary vasculature. These results clearly indicated that the accumulation of the fluorescence in the inflamed paw was due to the inflammation process induced by λ-carrageenan. By the way, injection of free DiD fluorescent dye resulted in lower fluorescence intensity in the inflamed paw, suggesting that the enhanced accumulation of fluorescence in the inflamed paw was specifically due to the nanoparticle formulation. In that respect, the LENK-SQ was distributed within the inflamed area as nanoparticles rather than in a single LENK-SQ molecular form. This was in accordance with the *in vitro* colloidal stability in serum, which showed that a significant percentage of NPs remained intact. To support the idea that intact NPs reached the inflamed tissue, fluorescent nanoparticles containing the fluorescent dye DiD together with a fluorescent quencher DiR were prepared. When intact, the nanoparticles do not emit any fluorescence (since the dye and the quencher are very close to one another). On the contrary, when the LENK-SQ NPs were disassembled in ethanol, fluorescence emission was observed due to the seperation of the dye and the quencher. Thus, when incubated within the serum, the NPs disassembled progressively, as seen from the gradual increase of the fluorescence (20% after 5 min and 50% after 30 min, see Fig. S8). This means that a significant proportion of NPs remained intact long time enough to reach the inflamed tissue. This observation was relevant with *in vivo* fluorescence imaging by Fig. 6, showing a strong fluorescence in the inflamed paw 30 minutes after injection. This clearly suggested that a significant quantity of intact LENK-SQ NPs remained intact into the blood circulation and was able to reach the site of inflammation, probably through the EPR effect. *Ex vivo* imaging was also performed on collected tissues and organs from mice injected with fluorescently labeled NPs. A strong fluorescence signal was again observed in the inflamed paw, but also in the liver, the spleen and the lungs due to the RES uptake of fluorescent nanoparticles. However, no detectable accumulation of fluorescence was noticed in the brain, confirming the peripheral effect of the LENK-SQ NPS. Based on the present study, squalene based NPs showed to be a highly promising delivery system to target inflamed tissues.

Thus, the novelty of the approach resulted from the unexpected ability of the peptide, when formulated under nanoparticular form, to reach safely and selectively the small area of the body where inflammation and nociception are occurring.

Toxicity of LENK-SQ NPs

Squalene is a natural lipid belonging to the terpenoid family which is largely widespread in nature. It is found in plants, animals and humans and is a precursor for biosynthesis of phytosterol and cholesterol. Squalene is synthesized by the liver and secreted in large quantities by the sebaceous glands in the skin (*23*, *24*). It is transported in the blood by very low density lipoproteins (VLDL) and low density lipoproteins (LDL). Furthermore, squalene is a versatile biocompatible biopolymer excipient used in numerous pharmaceutical formulations for oral and parenteral administration. At reasonable supplemental levels (0.5g/day), it is safe for prolonged administration (*25*, *26*).

Concerning LENK-SQ NPs, since they also accumulated in the liver, as mentioned above in biodistribution studies, their safety was therefore assessed. For this purpose, AST and ALT levels

were first measured. Indeed, these two liver enzymes are good markers of damage to liver cells. ALT is found primarily in the liver while AST is found in the liver, cardiac muscle, skeletal muscle, kidney, brain, pancreas, lungs, leukocytes, and erythrocytes (*27*). These enzymes are normally present at low levels in the blood. If liver cells are damaged, these enzymes leak into the blood which results in an increase in ALT and AST levels. After intravenous administration of LENK-SQ-Am NPs (20 mg/Kg) to rats, the AST and ALT levels in plasma showed no differences compared to levels of rats before injection or to the placebo control (5% dextrose solution). Moreover, the absence of toxicity was also confirmed after histological analysis of tissue organs of rats comprising liver, kidneys, spleen and lungs. Indeed, no changes in the cellular integrity or tissue morphology were observed after injection of LENK-SQ-Am NPs.

In conclusion, this research work resulted in the development of a novel nanomedicine approach allowing the specific delivery of intact Enkephalin neuropeptide into inflamed tissues and by-passing the blood-brain-barrier, for efficient pain control.

References

1. D. Desmaële, R. Gref, P. Couvreur, Squalenoylation: A generic platform for nanoparticular drug delivery. *Journal of Controlled Release* **161**, 609-618 (2012).
2. M. F. Simões, E. Valente, M. J. R. Gómez, E. Anes, L. Constantino, Lipophilic pyrazinoic acid amide and ester prodrugs: Stability, activation and activity against M. tuberculosis. *European Journal of Pharmaceutical Sciences* **37**, 257-263 (2009).
3. P. T. Wong, S. K. Choi, Mechanisms of Drug Release in Nanotherapeutic Delivery Systems. *Chemical Reviews* **115**, 3388-3432 (2015).
4. R. Oliyai, Prodrugs of peptides and peptidomimetics for improved formulation and delivery. *Advanced Drug Delivery Reviews* **19**, 275-286 (1996).
5. F. Jiao, Sinda Lepetre-Mouelhi, C. Patrick, Design, Preparation and Characterization of Modular Squalene-based Nanosystems for Controlled Drug Release. *Current Topics in Medicinal Chemistry* **17**, 2849-2865 (2017).
6. H. Sobel, Squalene in Sebum and Sebum-Like Materials**From the Department of Laboratories, Beth Israel Hospital, New York, New York. *Journal of Investigative Dermatology* **13**, 333-338 (1949).
7. D. Saha, F. Testard, I. Grillo, F. Zouhiri, D. Desmaele, A. Radulescu, S. Desert, A. Brulet, P. Couvreur, O. Spalla, The role of solvent swelling in the self-assembly of squalene based nanomedicines †. *Soft Matter* **11**, 4173 (2015).
8. A. H. M. Viswanatha Swamy, P. A. Patil, Effect of some clinically used proteolytic enzymes on inflammation in rats. *Indian journal of pharmaceutical sciences* **70**, 114-117 (2008).
9. H. L. Freedman, N. S. Taichman, J. Keystone, Inflammation and Tissue Injury II. Local Release of Lysosomal Enzymes During Mixed Bacterial Infection in the Skin of Rabbits. *Proceedings of the Society for Experimental Biology and Medicine* **125**, 1209-1213 (1967).
10. I. M. Goldstein, Lysosomal hydrolases and inflammation: mechanisms of enzyme release from polymorphonuclear leukocytes. *Journal of Endodontics* **3**, 329-333 (1977).
11. M. T. Mansouri, A. A. Hemmati, B. Naghizadeh, S. A. Mard, A. Rezaie, B. Ghorbanzadeh, A study of the mechanisms underlying the anti-inflammatory effect of ellagic acid in carrageenan-induced paw edema in rats. *Indian Journal of Pharmacology* **47**, 292-298 (2015).

12. C. A. Winter, E. A. Risley, G. W. Nuss, Carrageenin-Induced Edema in Hind Paw of the Rat as an Assay for Antiinflammatory Drugs. *Proceedings of the Society for Experimental Biology and Medicine* **111**, 544-547 (1962).
13. I. G. Otterness, P. F. Moore, in *Methods in Enzymology*. (Academic Press, 1988), vol. 162, pp. 320-327.
14. C. A. Winter, E. A. Risley, G. W. Nuss, Anti-inflammatory and antipyretic activities of indomethacin, 1-(p-chlorobenzoyl)-5-methoxy-2-methyl-indole-3-acetic acid. *Journal of Pharmacology and Experimental Therapeutics* **141**, 369 (1963).
15. K. Hargreaves, R. Dubner, F. Brown, C. Flores, J. Joris, A new and sensitive method for measuring thermal nociception in cutaneous hyperalgesia. *Pain* **32**, 77-88 (1988).
16. T. Lewanowitsch, R. J. Irvine, Naloxone and its quaternary derivative, naloxone methiodide, have differing affinities for μ, δ, and κ opioid receptors in mouse brain homogenates. *Brain Research* **964**, 302-305 (2003).
17. W. H. Oldendorf, S. Hyman, L. Braun, S. Z. Oldendorf, Blood-Brain Barrier: Penetration of Morphine, Codeine, Heroin, and Methadone after Carotid Injection. *Science* **178**, 984 (1972).
18. J.-M. Zhang, J. An, Cytokines, Inflammation and Pain. *International anesthesiology clinics* **45**, 27-37 (2007).
19. H. Hashizume, P. Baluk, S. Morikawa, J. W. McLean, G. Thurston, S. Roberge, R. K. Jain, D. M. McDonald, Openings between Defective Endothelial Cells Explain Tumor Vessel Leakiness. *The American Journal of Pathology* **156**, 1363-1380 (2000).
20. H. Nehoff, N. N. Parayath, L. Domanovitch, S. Taurin, K. Greish, Nanomedicine for drug targeting: strategies beyond the enhanced permeability and retention effect. *International Journal of Nanomedicine* **9**, 2539-2555 (2014).
21. J. M. Metselaar, G. Storm, Liposomes in the treatment of inflammatory disorders. *Expert Opinion on Drug Delivery* **2**, 465-476 (2005).
22. S. Hua, Targeting sites of inflammation: intercellular adhesion molecule-1 as a target for novel inflammatory therapies. *Frontiers in Pharmacology* **4**, 127 (2013).
23. Ovidiu Popa, Narcisa Elena Băbeanu, Ioana Popa, Sultana Niță, Cristina Elena Dinu-Pârvu, Methods for Obtaining and Determination of Squalene from Natural Sources. *BioMed Research International* **2015**, 16 (2015).
24. L. H. Reddy, P. Couvreur, Squalene: A natural triterpene for use in disease management and therapy. *Advanced Drug Delivery Reviews* **61**, 1412-1426 (2009).
25. G. S. Kelly, Squalene and its potential clinical uses. *Alternative medicine review : a journal of clinical therapeutic* **4**, 29-36 (1999).
26. H. Kamimura, N. Koga, K. Oguri, H. Yoshimura, H. Inoue, K. Sato, M. Ohkubo, *Studies on distribution, excretion and subacute toxicity of squalane in dogs*. (1989), vol. 80, pp. 269-280.
27. Parmar KS, Singh GK, Gupta GP, Pathak T, Nayak S, Evaluation of De Ritis ratio in liver-associated diseases. *International Journal of Medical Science and Public Health* **5**, 1783-1788 (2016).

General conclusion & Perspectives

This PhD research intended to address the treatment of pain disorder using squalenoylated Leu-enkephalin NPs. The main achivements of this thesis are:

1. **The preparation and characterization of the LENK-SQ NPs.** Synthesis of pure squalenoylated Leu-enkephalin bioconjugates with **1)** dioxycarbonyl linker, **2)** diglycolic linker and **3)** amide bond was successfully achieved. All bioconjugates showed the capability to self assemble in nanoparticles with sizes around 100 nm, using simple nanoprecipitation process. These NPs were found to be quite stable under 4 °C for 8 days.
2. **The *in vivo* evaluation of anti-hyperalgesic effects of the LENK-SQ NPs in carrageenan-induced paw edema model in rats.** Hyperalgesia rat model was successfully established by intraplantar injection of λ-carrageenan. All LENK-SQ NPs showed significant anti-hyperalgesic effects by activation of peripheral opioid receptors which lasted longer than morphine.
3. **The *in vivo* biodistribution study of the LENK-SQ NPs.** Fluorescently labeled LENK-SQ NPs were prepared in order to study the biodistribution of LENK-SQ-Am NPs. The real-time *in vivo* imaging showed a strong accumulation of the fluorescence within the inflamed paw, thus highlighting the release of free peptides in the inflamed tissue. Flouorescence was also observed in RES organs especially in the liver, and in the lungs. The absence of detectable fluorescence in the brain supports the peripheral action of the LENK once released from NPs at the inflammation site.
4. **The toxicity study of NPs.** Systemic administration of LENK-SQ NPs induced no damage to liver, as shown by the plasma AST or ALT levels. Histological examination of liver, heart, spleen, lungs, and kidneys didn’t show any anomaly.

Further experiments should be explored for application improvement of LENK-SQ NPs in order to get as close as possible of clinical outcome:

1. **Scaling-up the LENK-SQ bioconjugates synthesis and nanoparticles preparation.**
2. **Facilitating their manipulation by developing freeze-dryed LENK-SQ NPs easy to reconstitute into injectable form prior to administration**
3. **Defining the lowest dose required to achieve the anti-hyperalgesic effect, the administration frequency and timing treatment.**
4. **Studying the anti-hyperalgesic effect of LENK-SQ NPs on chronic pain model.**

List of Publications & Communications

Scientific Publications

1. **Jiao FENG**, Sinda LEPETRE, Anne Gautier, Simona MURA, Catherine CAILLEAU, François COUDORE, Michel Hamon, Patrick COUVREUR. A new painkiller nanomedicine to by-pass the blood-brain-barrier and the use of morphine. Science Advances. (Under review)
2. Patrick COUVREUR, **Jiao FENG**, Sinda LEPETRE. Bioconjugates of neuropeptides. Application No./Patent No.: 18306002.9 – 1109. (Under review)
3. **J. Feng**, S. Lepetre-Mouelhi, P. Couvreur, Design, preparation and characterization of modular squalene-based nanosystems for controlled drug release. Current Topics in Medicinal Chemistry 17, 2849-2865 (2017).

Scientific Communications

1. **5th Annual meeting of SFNano.** Montpellier (France), December 2018, **FENG J.** et al, A new painkiller nanomedicine to by-pass the blood-brain-barrier and the use of morphine. **(Oral presentation)**
2. **International Symposium "Drug Discovery and New Therapeutics".** Orsay (France), April 2018, **FENG J.** et al, Development of novel nano-biotechnology tools targeting opioid receptors: Squalenoylation of enkephalin peptides. **(Oral presentation)**
3. **2017 Annual Meeting & Exposition of the Controlled Release Society (CRS 2017).** Boston (US), July 2017, **FENG J.** et al, Development of novel nano-biotechnology tools targeting opioid receptors: Squalenoylation of enkephalin peptides. **(Oral presentation)**
4. **ULLA Summer school 2017.** KU Leuven, (Begium), July 2017, **FENG J.** et al, Development of novel nano-biotechnology tools targeting opioid receptors: Squalenoylation of enkephalin peptides. **(Poster)**
5. **24th Young Research Fellow Meeting in Medicinal Chemsitry.** Châtenay-Malabry (France), February 2017, **FENG J.** et al, Development of novel nano-biotechnology tools targeting opioid receptors: Squalenoylation of enkephalin peptides. (**Oral flash & Poster)**
6. **10th World Meeting on Pharmaceutics, Biopharmaceutics and Pharmaceutical Technology.** Glasgow (UK), April 2016, **FENG J.** et al, Development of novel nano-biotechnology tools targeting opioid receptors: Squalenoylation of enkephalin peptides. **(Poster)**
7. **Doc & PostDoc Day of Institut Galien.** Paris (France), July 2016, **FENG J.** et al, Development of novel nano-biotechnology tools targeting opioid receptors: Squalenoylation of enkephalin peptides. **(Oral presentation)**
8. **16ème Journées de l'Ecole Doctorale ED425**, Châtenay-Malabry (France), June 2016, **FENG J.** et al, Development of novel nano-biotechnology tools targeting opioid receptors: Squalenoylation of enkephalin peptides. **(Poster)**
9. **Doc & PostDoc Day of Institut Galien.** Paris (France), July 2015, **FENG J.** et al, Development of novel nano-biotechnology tools targeting opioid receptors: Squalenoylation of enkephalin peptides. **(Poster)**

Title: A new painkiller nanomedicine to bypass the blood-brain- and the use of morphine

Key word: Nanomedicine, Leu-Enkephalin, Squalene, Hyperalgesia, Inflammatory pain, Peripheral opioid receptors

Abstract: Enkephalin is an endogenous pentapeptide producing potent analgesia by activating opioid receptors located on central and peripheral neuronal cell membranes. However, its clinical use has historically been limited due to pharmacokinetic issues, including restricted plasma stability and blood-brain-barrier impermeability. The aim of this project is to create a new enkephalin-based nanomedicine targeting pain, using biocompatible and biodegradable materials for drug delivery and targeting purposes, such as squalene (squalenoylation nanotechnology). This nanotechnology presents a new concept with numerous advantages in comparison with the conventional nanocarriers, such as high drug loading and absence of "burst release". Here, we show for the first time, that the rapidly metabolized Leu-enkephalin (LENK) neuropeptide may become pharmacologically efficient owing to its simple conjugation with the squalene (SQ) using three different chemical linkers, i.e., dioxycarbonyl (Diox), diglycolate (Dig), or amide bond (Am). The resulting prodrugs were able to self-assemble in nanoparticles in aqueous media. This new squalene-based nanoformulation prevented rapid plasma degradation of LENK and conferred to the released neuropeptide a significant anti-hyperalgesic effect in a carrageenan-induced paw edema model in rats (Hargreaves test). It should be stressed that this effect lasted 3 times longer than morphine. Pretreatment with brain impermeant opioid receptor antagonist naloxone methiodide (Nal-M) reversed the nanoparticles induced anti-hyperalgesia, indicating that LENK-SQ NPs acted through peripherally located opioid receptors. Moreover, the biodistribution of DiD-fluorescently labeled LENK-SQ NPs showed a strong accumulation of the fluorescence within the inflamed paw as well as in the liver, spleen, and lung, while no signal could be detected in the brain, confirming the peripheral effect of LENK-SQ NPs. Toxicological studies showed that despite nanoparticles accumulation in the liver, the levels of aspartate transaminase (AST) and alanine transaminase (ALT) were not increased after i.v. injection of LENK-SQ NPs, highlighting thus their safety. This study represents a novel drug targeting approach, allowing the specific delivery of LENK neuropeptide into inflamed tissues for pain alleviation.

Université Paris-Saclay
Faculté de Pharmacie/ Institut Galien Paris-Sud - UMR CNRS 8612
5 Rue Jean-Baptiste Clément, 92290 Châtenay-Malabry, France

Titre: Développement de nanomédicaments innovants pour vaincre la douleur: une alternative à la morphine

Mots clés: Nanomédecine, Leu-Enképhaline, Squalène, Hyperalgésie, Douleur inflammatoire, Récepteurs périphériques opioïdes

Résumé: Les neuropeptides endogènes chez l'homme, tels que les enképhalines et endomorphines, ont un potentiel thérapeutique considérable dans le traitement de la douleur. Ils agissent en activant les récepteurs opioïdes qui sont très largement distribués dans le système nerveux central ainsi que dans plusieurs tissus périphériques. Ces neuropeptides présentent, cependant, un certain nombre d'inconvénients qui limitent de manière importante leur efficacité thérapeutique. Tout d'abord, en raison de leur hydrophilie, ils ne passent pas la barrière sang/système nerveux, ce qui limite leur accès aux récepteurs opioïdes. De plus, ils présentent un temps de demi-vie plasmatique relativement court du fait d'une métabolisation rapide. Enfin, pour être efficaces, ces neuropeptides devraient résister à la protéolyse dans le système circulatoire et être suffisamment hydrophobes pour traverser ces barrières hémato-nerveuses.

Le but de la thèse a consisté à créer de nouveaux nanomédicaments à base d'endorphines pour vectoriser et combattre la douleur de manière efficace. Dans ce but, a été établi une liaison chimique covalente, enzymatiquement clivable (ester ou amide), entre le squalène (SQ, un lipide naturel et biocompatible) et le neuropeptide. Ce couplage donne lieu à des prodrogues qui ont la capacité de s'auto-assembler en nanoparticules (NPs) dans l'eau sans l'aide d'un agent tensio-actif. D'une manière générale, cette technologie présente de nombreux avantages tels qu'un taux de charge élevé en principe actif, une protection efficace de celui-ci vis-à-vis de la métabolisation et l'absence de phénomène de «burst release».

Durant ce travail de thèse, nous avons pu montrer pour la première fois que les Leu-enképhalines (LENK) pouvaient devenir efficaces pharmacologiquement une fois couplées au squalène, via une liaison amide (Am), ou via un bras espaceur, tel que le dioxycarbonyl (Diox), ou le diglycolate (Dig). Les prodrogues résultant de ce couplage ont toutes montré des propriétés d'auto-assemblage en milieu aqueux. Cette nanoformulation à base de squalène a permis, d'une part de protéger la LENK de la métabolisation rapide dans le plasma et d'autre part, de lui conférer un effet anti-hyperalgésique significatif dans un modèle de douleur inflammatoire induite chez le rat par la carragénine (test de Hargreaves). Il est important de souligner que cet effet anti-hyperalgésique a duré 3 fois plus longtemps qu'avec la morphine. Un prétraitement avec un antagoniste des récepteurs opioïdes imperméable à la BHE, comme la méthylnaloxone a complètement antagonisé l'effet anti-hyperalgésique des nanoparticules de LENK-SQ, démontrant ainsi que celles-ci agissent via les récepteurs opioïdes périphériques. De plus, l'étude de biodistribution de NPs LENK-SQ fluorescentes a montré une forte accumulation des celles-ci au niveau de la patte œdémateuse, mais aussi dans le foie, la rate et les poumons alors qu'aucun signal n'a pu être détecté au niveau cérébral, ce qui confirme bien l'effet périphérique de ces nanoparticules. Enfin, des études toxicologiques ont montré que malgré l'accumulation des NPs dans le foie, les taux d'aspartate transaminase (AST) et alanine transaminase (ALT) n'ont pas augmenté garantissant ainsi l'innocuité des NPs LENK-SQ après leur injection i.v.

Cette étude représente une approche innovante et prometteuse permettant une distribution ciblée du neuropeptide endogène LENK dans les tissus œdémateux pour soulager efficacement la douleur inflammatoire.

Université Paris-Saclay
Faculté de Pharmacie/ Institut Galien Paris-Sud - UMR CNRS 8612
5 Rue Jean-Baptiste Clément, 92290 Châtenay-Malabry, France